The Contribution of Secretase Cleavage to Voltage-Gated Na^+ Channel β1-Subunit Function in Breast Cancer Cells

Alexander Haworth

PhD

University of York

Biology

September 2019

Abstract

Voltage-gated Na^+ channels (VGSCs) are complexes consisting of Na^+-conducting α-subunits and auxiliary β-subunits (β1-β4). Na^+ influx depolarises excitable tissue and VGSC mutations are common in epilepsy and arrhythmia. VGSCs are aberrantly expressed in cancer. β1 is upregulated in invasive breast cancer and enhances metastasis *in vivo*. The mechanism underlying β1-induced metastatic cell behaviour is not clear, highlighting the need for better understanding. β-subunits modulate α-subunits and induce cell adhesion. Sequential cleavage of β1 by α-/β-secretase and γ-secretase releases an intracellular domain (ICD). The impact of secretase cleavage on β1 function is unknown. The hypothesis of this study was that secretase cleavage regulates β1 function in breast cancer cells. To assess this, secretase inhibitors were used alongside expression of β1 constructs; β1-ICD and secretase-resistant (SR) β1 in MDA-MB-231 cells. The impact of secretase cleavage on β1 localisation, β1-induced Na^+ current, β1-induced cell adhesion and β1-induced cell morphology changes was assessed. β1 was expressed throughout secretory and endocytic pathways and was unaffected by γ-secretase inhibition. SRβ1 showed a similar pattern. γ-secretase inhibition increased β1-mediated cell adhesion, suggesting increased surface β1 expression, although plasma membrane β1 was undetectable. β1-induced cell morphology changes were secretase-independent, as SRβ1, but not β1-ICD, induced β1-like cell elongation. β1-induced increase of Na^+ current density was secretase-independent, as it was unchanged by γ-secretase inhibitors or expressing SRβ1. Interestingly, β1-ICD enhanced Na^+ current density, but a β1 construct lacking the ICD sequence did not, demonstrating that β1-ICD is necessary and sufficient to increase Na^+ current density. In conclusion, this study has further elucidated the function of β1 in breast cancer cells and suggests that secretase cleavage of β1 does not regulate α-subunit function or β1 spatial expression, but may regulate β1-mediated cell adhesion. Further work should focus on understanding the functional differences between β1, β1-ICD and SRβ1.

List of Contents

List of Figures

List of Tables

Acknowledgements

There are many people I'd like to acknowledge for their help over the last four years. Firstly, I'd like to thank Dr. Will Brackenbury for his insightful supervision and indispensable feedback while writing my thesis. I'd like to thank Dr. Christoph Baumann for his support and constant good humour in the face of non-fluorescent cells. Many thanks to Prof. Bob White and my thesis advisory panel members, Dr. Sangeeta Chawla and Prof. Marek Brzozowski, for their guidance and help in shaping my PhD.

I'm very grateful for the support of the Brackenbury lab members, past and present. I'd like to thank Michaela Nelson, Dr. Ming Yang and Dr. Faheem Patel for helping me get to speed in the early days and making me feel welcome. Thanks to Lauren Blackburn for making me laugh, but not for occupying my desk for two years. Thanks to Tess Leslie for her constant cheeriness in the lab and office and helping me out (multiple times) outside of work. I'd like to thank Dr. Andy James for a lot of guidance over the last year and Laura Wiggins for keeping me company in the office over the last three months. Lastly, I'd like to wish the current lab members the best of luck for their remaining time!

I'd also like to thank the past and present members of the office. Dr. Anna Simon, Dr. Stephen Hall and Dr. Iain Hartnell for keeping the office as fun as possible. Annie Smith for the daily chatter and burrito enthusiasm. Grace Cowen for the timely distractions from the thesis while I've been office-bound. Thanks to Dr. Nick Johnson for the careful "critiquing" of my figures and for preventing homelessness (alongside Dr. Jane).

Thanks to all the friends I've made in York. It was a pleasure to live with Dr. Iulia Ghermain, James Robson and Phil Brailey. Thanks to Emma Stewart and Dr. Jack Munns for the fun times and for putting up with me for three years. Added thanks to Dr. Jack for making up the numbers on the quiz team.

Lastly, I'd like to thank my family for their constant encouragement over the last seven years and their support in my upcoming unemployment!

Declaration

I declare that this thesis is a presentation of original work and I am the sole author. This work has not previously been presented for an award at this, or any other, University. All sources are acknowledged as References.

Chapter 1: Introduction

This introduction will give a detailed outline of voltage-gated Na^+ channels and their involvement in disease, before covering secretase enzymes, secretase substrates and secretase cleavage in disease, then lastly outlining the hypothesis and aims of the study.

1.1 General introduction to voltage-gated Na^+ channels

The involvement of Na^+ conductance in squid axonal membrane depolarisation was observed seventy years ago, when Hodgkin and Katz hypothesised a transient increase in inward Na^+ permeability would explain the reversable increase in membrane potential seen during an action potential and the disparity in extracellular and intracellular ionic concentrations (Hodgkin & Katz, 1949). By using Na^+-free extracellular solution, they observed the action potential was abolished, but returned after replacing with fresh extracellular solution. Conversely, increasing Na^+ concentration both increased the magnitude and the rate of onset of the action potential. Continued work in the squid giant axon further established the involvement of Na^+ conductance in axonal depolarisation as well as the involvement of an outward K^+ current, responsible for repolarisation of the membrane potential (Hodgkin & Huxley, 1952b, a, c; Hodgkin *et al.*, 1952). The existence of channels specific for Na^+ entry was later postulated following the observation that toxins capable of inhibiting action potentials inhibited Na^+ conductance specifically and not K^+ conductance (Narahashi *et al.*, 1964; Nakamura *et al.*, 1965; Hille, 1968). These toxins, namely tetrodotoxin (TTX) and saxitoxin (STX), subsequently lead to uncovering the molecular identity of voltage-gated Na^+ channels (VGSCs), after the discovery that radiolabelled TTX and STX bound a membrane protein of ~270 kDa in various excitable tissues (Agnew *et al.*, 1978; Barchi *et al.*, 1980). Expression of this novel 270 kDa protein in planar phospholipid bilayers or *Xenopus* oocytes was shown to be sufficient to reproduce a native-like Na^+ current (I_{Na}) (Talvenheimo *et al.*, 1982; Tamkun *et al.*, 1984;

Hartshorne *et al.*, 1985; Goldin *et al.*, 1986). It soon emerged there were at least two proteins in rat brain capable of conducting a voltage-sensitive I_{Na} (Noda *et al.*, 1986). This channel family has expanded to encompass nine different conducting α-subunits ($Na_v1.1$-1.9) (Goldin, 2001). The topology of the electric eel α-subunit was deduced from cDNA and it revealed four homologous domains (DI-IV) consisting of six transmembrane segments (S1-S6) (Noda *et al.*, 1984). However, the field of VGSC research expand greatly, when purification of channels from neuroblastoma cells using a scorpion toxin revealed two auxiliary subunits of 30-40 kDa (β1 and β2) bound to the larger 270 kDa α-subunit (Beneski & Catterall, 1980). Continued work focused on understanding the α-β interaction and uncovering subunit stoichiometry, which was predicted to be 1 α: 1 β1: 1 β2 (Figure 1.1) (Hartshorne & Catterall, 1981; Hartshorne *et al.*, 1982; Hartshorne & Catterall, 1984). The early observation was made that α bound to β2 pooled intracellularly, leading to the first hypothesis of β function: that β2 was required for channel localisation at the membrane (Schmidt *et al.*, 1985). The molecular identities of β1 and β2 were revealed in the 1990s, with their structure consisting of a single-pass transmembrane domain, a large extracellular domain and relatively short intracellular domain (Isom *et al.*, 1992; Isom *et al.*, 1995). Two further β-subunits, β3 (Morgan *et al.*, 2000) and β4 (Yu *et al.*, 2003), were subsequently discovered.

Initially, β-subunits were implicated in membrane trafficking of α-subunit and increased I_{Na}, from experiments performed with β1 and β2 (Isom *et al.*, 1992; Isom *et al.*, 1995; McCormick *et al.*, 1999). However, non-conducting roles for β-subunits were eventually discovered, as the extracellular immunoglobulin loop permits β-subunits to function as cell adhesion molecules (CAMs) (Srinivasan *et al.*, 1998; Malhotra *et al.*, 2000; Ratcliffe *et al.*, 2001; McEwen & Isom, 2004) and regulate various aspects of neurodevelopment (Davis *et al.*, 2004; Brackenbury *et al.*, 2008; Maschietto *et al.*, 2013).

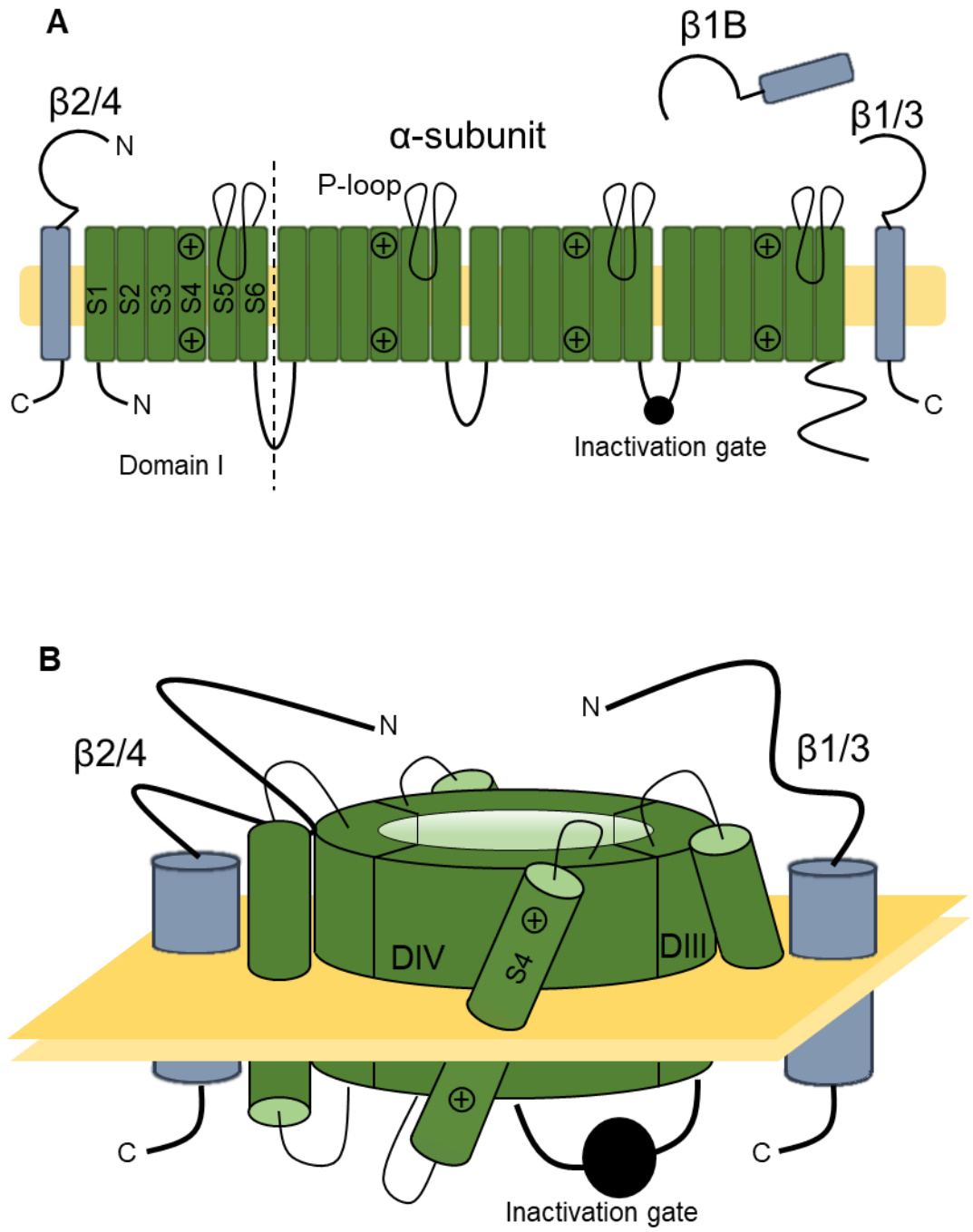

Figure 1.1 Structure of a voltage gated sodium channel (VGSC) complex

(**A**) VGSC consisting of one α-subunit, one β1 subunit and one β2 subunit (Hartshorne *et al.*, 1982). α-subunits consist of four homologous domains (DI-IV) each comprising of six transmembrane segments (S1-6) (Noda *et al.*, 1984). S4 of each domain contributes to voltage sensing, the extracellular loops between S5-S6 of each domain assemble into the pore structure, and the DIII-DIV linker functions as the inactivation gate (Yu & Catterall, 2003). (**B**) The membrane conformation of a VGSC (Yan *et al.*, 2017).

The exciting discovery that β-subunits are also substrates of secretases, the enzymes famed for their role in Alzheimer's disease and regulating intracellular signalling, further expanded the potential conducting and non-conducting function of β-subunits and added a new layer of possible VGSC regulation that has yet to be explored (Kim *et al.*, 2005; Wong *et al.*, 2005).

VGSCs are implicated in many disorders, discussed in greater detail in chapter 1.4. Mutations in α-subunits are found in disorders such as epilepsy (Catterall *et al.*, 2010), cardiac arrhythmia (Zaklyazminskaya & Dzemeshkevich, 2016) and chronic pain (Fischer & Waxman, 2010). β-subunits are similarly involved in excitability-linked disorders, such as epilepsy (Wallace *et al.*, 1998; Patino *et al.*, 2009) and nociception (Lopez-Santiago *et al.*, 2011). β-subunits have also been implicated in neurodegenerative disorders, such as β2 in multiple sclerosis and Alzheimer's disease (O'Malley *et al.*, 2009; Hu *et al.*, 2017). Surprisingly, expression of all VGSC subunits (except $Na_v1.8$) is dysregulated in various cancers (Brackenbury, 2012). *In vivo* evidence using mouse xenograft models has directly implicated β1 and $Na_v1.5$ expression in breast tumour formation (Nelson *et al.*, 2014; Nelson *et al.*, 2015b), and β4 in supressing breast tumour formation (Bon *et al.*, 2016). However, the mechanistic basis underlying VGSC function in cancer is still unclear.

1.2 VGSC α-subunits

1.2.1 Expression

Nine human VGSC α-subunits exist, $Na_v1.1$-1.5 (encoded for by *SCN1A-5A*) and $Na_v1.6$-1.9 (encoded for by *SCN8A-11A*), along with an enigmatic, voltage-insensitive, non-

inactivating α-subunit known as Na_x (encoded by *SCN7A*), which is activated instead by an elevation of extracellular Na^+ (Goldin, 2001; Matsumoto *et al.*, 2015). Na_x is expressed in circumventricular neurons and is involved in osmoregulation of cerebrospinal fluid, with Na_x-KO mice continually salt loading after dehydration (Watanabe *et al.*, 2000; Sakuta *et al.*, 2016). Na_x is expressed in a range of different cell types, including glia, dorsal root ganglion neurons and cardiomyocytes, where its function is still uncertain (Noda & Hiyama, 2015). *SCN1A-3A* and *9A* are clustered together on human chromosome 2, *SCN5A* and *10-11A* on human chromosome 3, *SCN4A* on human chromosome 17, and *SCN8A* on human chromosome 12 (Table 1.1) (Plummer & Meisler, 1999). α-subunits have distinct, albeit overlapping expression profiles. Na_v1.1-1.3 and 1.6 are expressed in the CNS (Kayano *et al.*, 1988; Lu *et al.*, 1992; Schaller *et al.*, 1995), Na_v1.4 in skeletal muscle (Wang *et al.*, 1992), Na_v1.5 in cardiac muscle (Gellens *et al.*, 1992), and Na_v1.7-1.9 in the PNS (Akopian *et al.*, 1996; Sangameswaran *et al.*, 1997; Dib-Hajj *et al.*, 1998). Despite being known as the "cardiac sodium channel," Na_v1.5 has also been detected in the brain and muscle (Wang *et al.*, 2017). CNS α-subunits display a degree of differential spatial expression themselves. Immunohistochemical analysis of rat brains demonstrated Na_v1.1 expression enriched in the brainstem, caudate and substantia nigra, whereas Na_v1.2 was enriched in the subcortical structures of the globus pallidus, thalamus and hippocampus (Gong *et al.*, 1999). Perhaps the most striking difference between CNS α-subunits, however, is in their subcellular and temporal expression. Na_v1.1, Nav1.3 and Nav1.6 are expressed in the soma, with Na_v1.1 and 1.3 also showing dendritic expression (Whitaker *et al.*, 2001). Na_v1.2, on the other hand, is expressed axonally (Whitaker *et al.*, 2001). Temporally, Na_v1.1 and Nav1.2 expression increases postnatally in rat brains, with Na_v1.1 expression decreasing after the first month to around 50 % in adults, whereas Na_v1.2 expression is maintained into adulthood (Gong *et al.*, 1999). In rat retinal ganglion cells, Na_v1.6 expression is delayed relative to Na_v1.2; Na_v1.6 eventually displaces Na_v1.2 at the axon initial segment (AIS) and nodes

Table 1.1 The expression of voltage-gated Na^+ channels in humans

	Subunit	Human gene	Chromosome	Expression	References
α-subunit	$Na_v1.1$	*SCN1A*	2	postnatal – CNS, soma	1, 2, 3
	$Na_v1.2$	*SCN2A*		postnatal – CNS, axon	1, 2, 3
	$Na_v1.3$	*SCN3A*		embryonic – CNS, soma	1, 3, 4
	$Na_v1.4$	*SCN4A*	17	postnatal - skeletal muscle	1, 5, 6
	$Na_v1.5$	*SCN5A*	3	postnatal – cardiac muscle embryonic – skeletal muscle	1, 5, 7, 8
	$Na_v1.6$	*SCN8A*	12	postnatal – CNS, soma	1, 3, 9
	$Na_v1.7$	*SCN9A*	2	postnatal – PNS	1, 10, 11
	$Na_v1.8$	*SCN10A*	3		1, 12, 13
	$Na_v1.9$	*SCN11A*			1, 13, 14
β-subunit	β1	*SCN1B*	19	postnatal – widespread	15, 16
	β1B			embryonic (persists into adulthood) – CNS, PNS, cardiac muscle, skeletal muscle	17, 18
	β2	*SCN2B*	11	postnatal – concentrated in CNS	16, 20
	β3	*SCN3B*		embryonic (persists into adulthood) – concentrated in CNS	16, 19, 20
	β4	*SCN4B*		embryonic (persists into adulthood) – widespread	16, 20

references: 1 (Plummer & Meisler, 1999), 2 (Gong *et al.*, 1999), 3 (Whitaker *et al.*, 2001), 4 (Shah *et al.*, 2001), 5 (Bailey *et al.*, 2003), 6 (Wang *et al.*, 1992), 7 (Haufe *et al.*, 2005), 8 (Gellens *et al.*, 1992), 9 (Van Wart & Matthews, 2006), 10 (Akopian *et al.*, 1996), 11 (Felts *et al.*, 1997), 12 (Akopian *et al.*, 1999), 13 (Benn *et al.*, 2001), 14 (Dib-Hajj *et al.*, 1998), 15 (Makita *et al.*, 1994a), 16 (Candenas *et al.*, 2006), 17 (Patino *et al.*, 2011), 18 (Qin *et al.*, 2003), 19 (Morgan *et al.*, 2000), 20 (Lu *et al.*, 2010)

Abbreviations: CNS: central nervous system, PNS: peripheral nervous system

of Ranvier (Van Wart & Matthews, 2006). Electrical activity and myelination appear to regulate the developmental switch of $Na_v1.2$ with $Na_v1.6$ (Kaplan *et al.*, 2001). Selective deletion of $Na_v1.6$ in cortical excitatory neurons produces viable mice with an AIS-enrichment of $Na_v1.2$ and similar action potential-generating capabilities (Katz *et al.*, 2018). A chimeric protein consisting of $Na_v1.6$ with $Na_v1.2$ N- and C-termini demonstrates $Na_v1.2$-like axonal distribution, suggesting regulatory elements in α-subunit termini dictate localisation (Lee & Goldin, 2009). The importance of postnatal $Na_v1.6$ is demonstrated by the fact that *Scn8a* null mice show progressive muscular atrophy and paralysis, and eventual juvenile lethality (Burgess *et al.*, 1995). $Na_v1.3$, on the other hand, is expressed embryonically in rats and is downregulated following birth, with almost no $Na_v1.3$ detectable by adulthood (Shah *et al.*, 2001). The requirement for electrical activity in early circuit development and the temporal differences in α-subunit expression suggest a potential role in neurodevelopment for VGSCs (Zhang & Poo, 2001). $Na_v1.6$ has a direct involvement in neurodevelopment, as I_{Na} carried by $Na_v1.6$ is required for cerebellar granule neuron neurite outgrowth, and this is dependent on β1 expression (Brackenbury *et al.*, 2010). VGSC α-subunits are also expressed in non-excitable cells. In cancer cells, α-subunits regulate migration and invasion (Brackenbury, 2012). In endothelial cells, $Na_v1.5$ potentiates migration and VEGF-mediated angiogenesis (Gosling *et al.*, 1998; Andrikopoulos *et al.*, 2011). $Na_v1.6$ expression in Schwann cells is required for synaptogenesis at neuromuscular junctions (Musarella *et al.*, 2006). $Na_v1.5$ expression in interstitial cells of Cajal generates slow wave activity in gastrointestinal (GI) smooth muscle, regulating GI motility (Strege *et al.*, 2003; Strege *et al.*, 2019).

1.2.2 Structure

α-subunits consist of ~2000 amino acids arranged into four homologous domains (DI-IV), each consisting of six transmembrane segments (S1-6) (Noda *et al.*, 1984). The

shape of a VGSC was referred to as “bell-shaped,” following the first low-resolution cryo-EM image (Sato *et al.*, 2001). This is because the domains of the α-subunit assemble around a central pore, so all four domains are in contact, with a flared cytoplasmic side. Atomic resolution was eventually managed, first of a bacterial VGSC (Payandeh *et al.*, 2011), followed by two eukaryotes structures (Shen *et al.*, 2017; Yan *et al.*, 2017). Although classically thought of as monomers, recent work has demonstrated $Na_v1.1$, Nav1.2 and Nav1.5 homodimerisation (Clatot *et al.*, 2017).

1.2.3 Activation and inactivation

α-subunits owe their voltage-sensitivity to S4 of each domain. S4 consists of repeated motifs of positively charged residues, typically arginine, that respond to a depolarisation in membrane potential (V_m) by sliding in an extracellular direction a distance of 6-8 Å through a narrow groove formed by S1-3 (the gating pore), rotating 30^o and tilting sideways (Yang *et al.*, 1996; Chanda & Bezanilla, 2002; Yarov-Yarovoy *et al.*, 2012). Charge neutralising mutations of specific S4 arginine residues to glutamate, in DI and DII of $Na_v1.2$, cause a depolarising shift in the voltage of activation (Kontis *et al.*, 1997). The idea of a moving “gating particle” has long been hypothesised, as the outward movement of positively charged S4 segments produces an observable gating current (Armstrong & Bezanilla, 1973). The pore region of the protein was identified following mutational studies of charged residues of $Na_v1.2$ until the binding site of TTX and STX was identified (Terlau *et al.*, 1991). The short α-helices (P-loops) between S5-6 of each domain assemble to form the ion selectivity filter (Heinemann *et al.*, 1992; Payandeh *et al.*, 2011). How S4 movement and pore opening is coupled is still unclear. In voltage-gated K^+ (K_v) channels, the proximal S4-5 linker moves along with S4 and might link S4 movement with downstream pore opening (Kalstrup & Blunck, 2018). In $Na_v1.5$, substituting certain asparagine residues in S6 of DIII and DIV prevents pore opening

while still allowing S4 movement, suggesting these asparagine residues are involved in coupling S4 movement to pore opening (Sheets *et al.*, 2015). Recent cryo-EM modelling of resting Na_v channels demonstrates the resting S4 position constricts the activation gate, due to interactions between S6 and the S4-S5 linker, which is overcome following activation and S4 movement (Wisedchaisri *et al.*, 2019).

Following depolarisation, VGSC activation is rapid, with a transient I_{Na} peaking then returning to baseline as the channel enters the inactivated state (Figure 1.2) (Kuhn & Greeff, 1999). Advancements in understanding the structural basis of inactivation were made after deletion of the DIII-IV linker region abolished fast inactivation (Stuhmer *et al.*, 1989). Following this, just three amino acids within the DIII-IV linker were found to be responsible for inactivation; glutamine substitution of isoleucine-1488, phenylalanine-1489 and methionine-1490 completely removed fast inactivation (West *et al.*, 1992). The DIII-IV linker is a flexible structure, proline and glycine residues flanking the IFM motif provide the hinge mechanism that allow the inactivation gate to block the pore (Kellenberger *et al.*, 1997), as supported by recent cryoEM modelling of $Na_v1.7$ (Shen *et al.*, 2019). Incomplete inactivation leads to a small subset of VGSCs conducting a persistent I_{Na} (~5 % magnitude of the transient I_{Na}), which has an important role in neuronal spike generation by maintaining the neuron in a more excitable state than if it were at rest (Muller *et al.*, 2018). This increase in neuronal excitability has implicated the persistent I_{Na} in epilepsy (Stafstrom, 2007). The mechanism of inactivation is itself voltage-dependent (Ahern, 2013). Movement of DIV:S4 is required for inactivation and recovery from inactivation, the refractory period between inactivated and closed states, during which the channel cannot be activated (Capes *et al.*, 2013). Charge neutralisation of DIV:S4 significantly hyperpolarises and delays inactivation as well as slowing recovery from inactivation (Capes *et al.*, 2013). However, S1-S3 of DIV also have an integral role

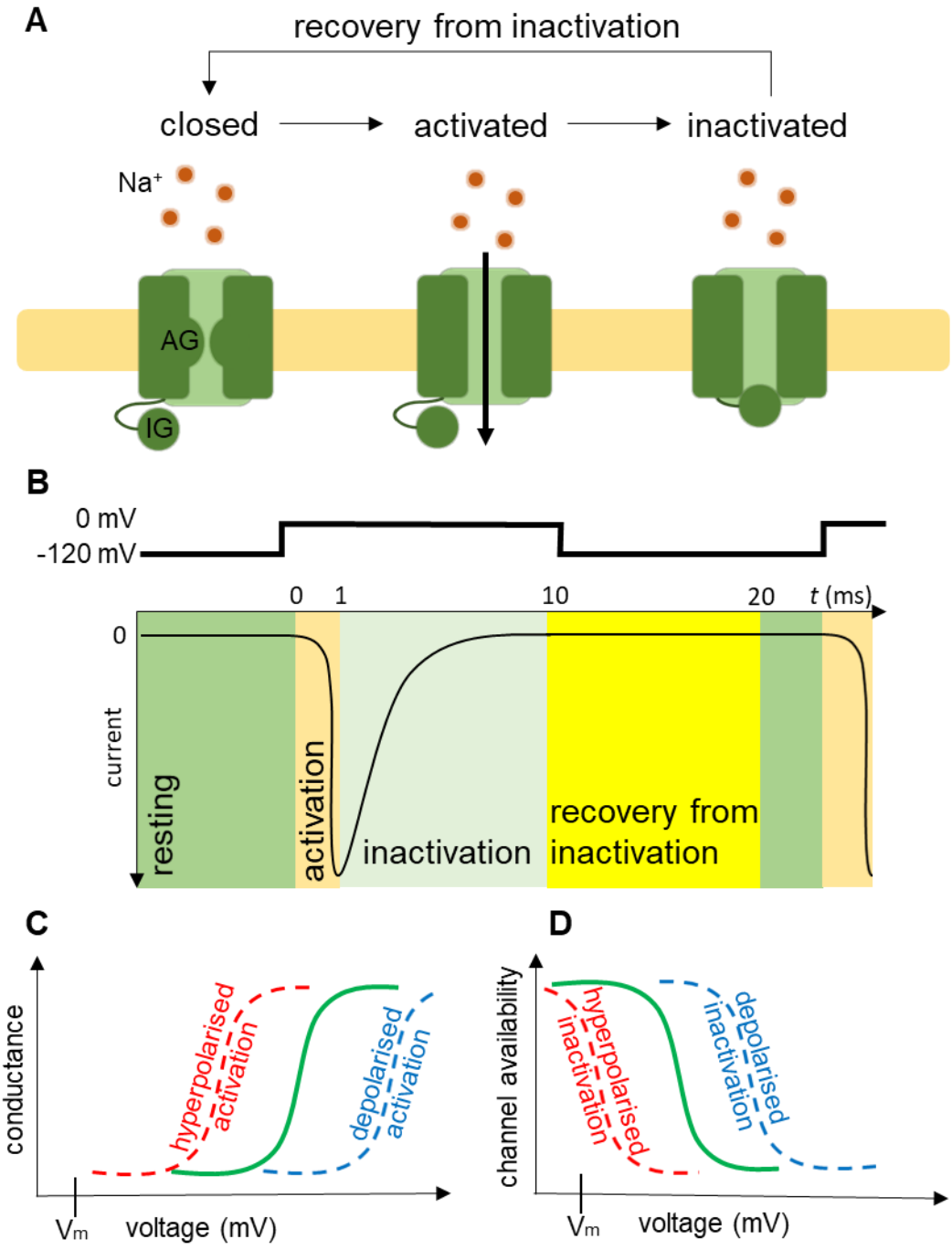

Figure 1.2 Activation and inactivation of an α-subunit

(**A**) An α-subunit in the resting/closed state is activated upon stimulation, leading to the opening of the activation gate (AG). Channels are rapidly inactivated by the inactivation gate (IG). Upon membrane repolarisation the channel enters a refractory period. Eventually the channel cycles back to the closed state after the inactivation gate relaxes. (**B**) Stimulation of the channel results in rapid activation and subsequent inactivation. The channel enters a refractory state as it recovers from inactivation before it can be activated again. (**C**) Voltage-activation relationship. Channel activation is measured by conductance and occurs at membrane potentials above resting (V_m). (**D**) Voltage-inactivation relationship. Inactivation is measured by channel availability, i.e. the inverse of inactivation.

in inactivation, demonstrated by the range of mutations found in DIV:S1-S3 that impact inactivation through impeding S4 movement (Nakajima *et al.*, 2019).Aberrant gating underlies many channelopathies. For instance, loss of channel function mutations causing depolarised activation and hyperpolarised inactivation are seen in epilepsy and paramyotonia, respectively (Struyk *et al.*, 2000; Lossin *et al.*, 2003). Likewise, gain of channel function mutations causing hyperpolarised activation, depolarised inactivation, increased persistent I_{Na} and accelerated recovery from inactivation are present in erythromelalgia, paroxysmal extreme pain disorder, sudden infantile death syndrome and long QT syndrome, respectively (Ackerman *et al.*, 2001; Rivolta *et al.*, 2001; Cummins *et al.*, 2004; Estacion *et al.*, 2008).

1.2.4 Drugs and toxins

The use of VGSC-targeting toxins and drugs has helped delineate the mechanism of VGSC activation and inactivation due to the complex range of effects they can exert. Five neurotoxin binding sites have been identified on α-subunits (Stevens *et al.*, 2011). Binding site 1 refers to the P-loops and includes TTX and STX, which directly block Na^+ conduction (Terlau *et al.*, 1991). Some toxins that act at other sites have a more specific effect on channel activation and inactivation. Such toxins do not bind at the important S4 voltage sensor or the DIII-IV inactivation gate directly however, but at other sites on the α-subunit, highlighting the structural sensitivity of the protein (Stevens *et al.*, 2011). For instance, sites 3 and 4 are found on the extracellular S1-2 and S3-4 loops. Sea anemone and scorpion α-toxins target site 3 (DIV: S3-4 loop) and inhibit channel inactivation (Rogers *et al.*, 1996). Scorpion β-toxins, acting on site 4 (DII: S1-2 and S3-4 loops), hyperpolarise the voltage of activation, reduce Na^+ conductance and trap the channel in an inactivated state (Cestele *et al.*, 2006). Lipophilic toxins that act at site 2 (e.g. veratridine and batrachotoxin) and 5 (e.g. brevetoxins and ciguatoxins) bind to S6 of

activated α-subunits, by different mechanisms, and maintain the channel in an open state, hyperpolarise activation and delay fast inactivation (Trainer *et al.*, 1994; Tikhonov & Zhorov, 2005; Du *et al.*, 2011). Antiarrhythmics, anticonvulsants and local anaesthetics also work via inhibiting VGSCs (Tikhonov & Zhorov, 2017). The binding site of antiarrhythmics and local anaesthetics is found on the intracellular side of the conducting pore (Hille, 1977). The accessibility problem of an intracellular binding site for drugs is overcome in two separate ways. Lipophilic drugs are able to access the interior of the pore via intramembranous fenestrations, regardless of the channel state, whereas less lipid soluble drugs are referred to as "use-dependent," as they rely on activation and opening of the channel to gain access to the pore (Lipkind & Fozzard, 2010; Nguyen *et al.*, 2019).

1.2.5 Post-translational modifications and interaction partners

α-subunit function is regulated by a multitude of post-transcriptional modifications, post-translational modifications and interacting partners (Figure 1.3) (Onwuli & Beltran-Alvarez, 2016). Alternative splicing of α-subunits produces a range of different splice variants (Copley, 2004). Two of the most well documented variants are the IVS5N+5 $Na_v1.1$ variant, which is implicated in febrile seizures (Schlachter *et al.*, 2009), and the neonatal $Na_v1.5$ variant ($nNa_v1.5$), which is implicated in breast cancer (Brackenbury *et al.*, 2007). Analysis of different $Na_v1.7$ splice variants found within inner hair cells of the cochlear of developing mice demonstrate a spectrum of electrophysiological properties required to produce the spontaneous action potentials necessary for cochlear maturation (Zhou *et al.*, 2019). Once translated, α-subunits are extensively glycosylated (Cohen & Barchi, 1981). ST3 β-galactoside α-1,2-sialyltransferase 4 deficient mice present an increased time to action potential peak and a decreased refractory time due to aberrant glycosylation of $Na_v1.5$ (Ednie *et al.*, 2013). Glycosylation of DRG $Na_v1.9$ is

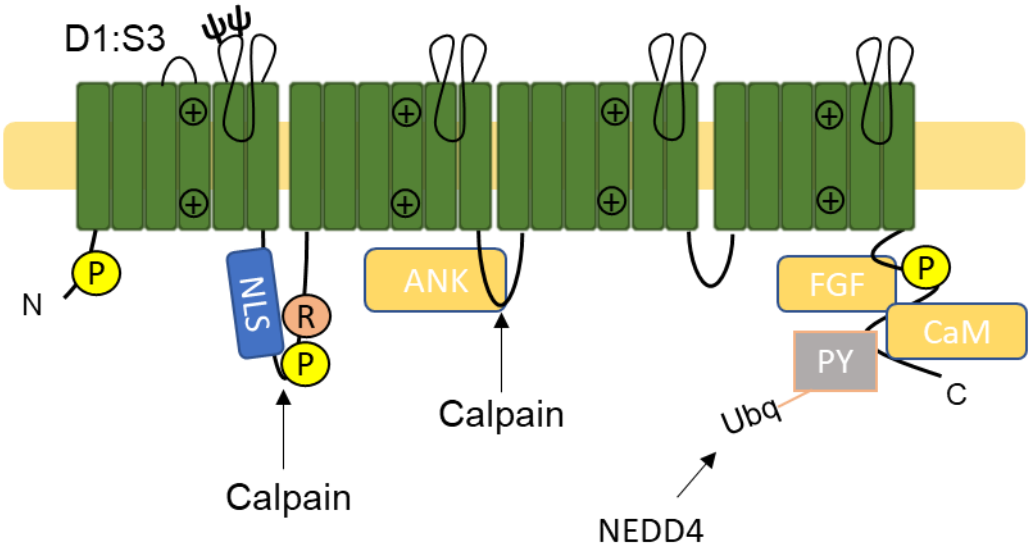

Figure 1.3 Post-translational modifications and interacting partners of VGSC α-subunits

α-subunits are extensively glycosylated (ψ) and phosphorylated (P) (Onwuli & Beltran-Alvarez, 2016). A neonatal splicing variant (D1:S3) replaces seven amino acids within D1:S3 and the S3-S4 linker of DI (Onkal *et al.*, 2008). The DI-DII linker contains a nuclear localisation signal (NLS) (Onwuli *et al.*, 2017), a calpain cleavage site (von Reyn *et al.*, 2009), phosphorylation sites and an arginine methylation site (R) (Baek *et al.*, 2014). An ankyrin binding site and another calpain cleavage site are found on the DII-III linker (Mohler *et al.*, 2004; von Reyn *et al.*, 2009). The C-terminus contains phosphorylation sites, FGF-binding site (Pablo *et al.*, 2016), calmodulin-binding site (Gardill *et al.*, 2019) and a PY domain that is ubiquitinated by NEDD4 (Rougier *et al.*, 2005).

developmentally regulated, with $Na_v1.9$ in neonatal rats showing extensive glycosylation and a concomitant hyperpolarisation in inactivation, not present in adult rats (Tyrrell *et al.*, 2001). α-subunits are also extensively phosphorylated, with phosphorylation sites concentrated in the intracellular N- and C-termini and the long DI-DII linker (Onwuli & Beltran-Alvarez, 2016). Na_v-phosphorylating kinases include PKA (Li *et al.*, 1993), PKC (Li *et al.*, 1993), CK2 (Hien *et al.*, 2014), GSK3 (James *et al.*, 2015) and MAPK (Hudmon *et al.*, 2008).

The effect of phosphorylation on different isoforms varies due to the vast number of phosphosites on each protein, 70 predicted on $Na_v1.2$ but only 28 on $Na_v1.1$ (Baek *et al.*, 2014). For example, PKA-mediated phosphorylation of $Na_v1.2$ attenuates I_{Na} (Li *et al.*, 1992), whereas PKA-mediated phosphorylation of $Na_v1.5$ enhances I_{Na} (Zhou *et al.*, 2002). Arginine methylation in the $Na_v1.2$ DI-II linker occurs in the absence of phosphorylation and enhances I_{Na}, suggesting a possible phosphorylation-methylation trade-off mechanism for $Na_v1.2$ control (Baek *et al.*, 2014). Ubiquitination of α-subunits is thought to stimulate degradation and regulate VGSC membrane expression, as Nedd4-mediated ubiquitination inhibits the Na^+ conductance of $Na_v1.2$, Nav1.5, Nav1.6, Nav1.7 and Nav1.8 (Fotia *et al.*, 2004; Rougier *et al.*, 2005; Gasser *et al.*, 2010). α-subunits are also cleaved by calpain in the DI-II and DII-III linkers (von Reyn *et al.*, 2009). The functional impact of this proteolysis is unclear as the cleaved fragments are still present at the membrane (von Reyn *et al.*, 2009). However, a nuclear-localising signal (NLS) has been discovered within the $Na_v1.5$ DI-II linker and the $Na_v1.5$ DI-II alone, when expressed in cardiac-like H9c2 cells, localises to the nucleus and activates the *SCN5A* promoter, suggesting a potential transcriptional regulatory role of α-subunit cleavage products (Onwuli *et al.*, 2017).

Many interacting proteins regulate α-subunit function. Mutations in the calmodulin binding sites in the DIII-IV linker and C-terminus prevent calmodulin binding and demonstrate reduced I_{Na} and impaired inactivation respectively (Tan *et al.*, 2002; Nof *et al.*, 2019). Ankyrin G binding, following CK2 phosphorylation, is required for AIS clustering of α-subunits (Hien *et al.*, 2014). A scaffold protein complex, including postsynaptic density-95 and zonula occludens-1, is required for $Na_v1.8$-induced I_{Na} (Pryce *et al.*, 2019). The interaction of $Na_v1.7$ with collapsing-response mediator protein 2 enhances I_{Na} in HEK293 cells (Dustrude *et al.*, 2013; Kanellopoulos *et al.*, 2018). The GPI-anchored Ig superfamily CAM contactin increases neuronal I_{Na} from $Na_v1.2$ (requiring β1 and ankyrin), $Na_v1.3$, $Na_v1.8$ and $Na_v1.9$ (McEwen *et al.*, 2004; Shah *et al.*, 2004; Rush *et al.*, 2005). Binding of intracellular FGF13 and FGF14 to α-subunit C-termini is required for correct AIS-localisation of VGSCs (Pablo *et al.*, 2016).

1.3 VGSC β-subunits

1.3.1 Expression

In humans, four transmembrane β-subunits exist (β1-β4, encoded by *SCN1B-4B*) along with a soluble β1 splice variant, known as β1B (Table 1.1) (Qin *et al.*, 2003). *SCN1B* is located on human chromosome 19, whereas *SCN2B-4B* are clustered on chromosome 11 (Makita *et al.*, 1994b; Morgan *et al.*, 2000; Lu *et al.*, 2010). Reverse transcription PCR of human tissues showed *SCN1B-4B* mRNA expression in adult brains, but only *SCN3B* and *SCN4B* mRNA are abundantly present in foetal brains (Candenas *et al.*, 2006). *SCN2B* and *SCN3B* demonstrate restricted expression to the brain, with little mRNA detected in other tissues, such as skeletal muscle, testis and the thyroid gland (Candenas *et al.*, 2006). *SCN1B* and *SCN4B*, on the other hand, show widespread

mRNA expression in adrenal glands, heart, kidney, lung, placenta, prostate, salivary gland, skeletal muscle, testis, thymus, thyroid gland, trachea and uterus; *SCN1B* expression was further detectable in bone marrow, liver, foetal liver and spleen (every tissue examined in the study) (Candenas *et al.*, 2006). *In situ* hybridisation analysis of adult rat brains demonstrate a roughly complementary expression profile of *SCN1B* and *SCN3B* mRNA, with *SCN1B* enriched in the granular and Purkinje cell layers of the cerebellum, thalamus and layers 4/5 of the neocortex, whereas *SCN3B* mRNA is most abundant in the olfactory system, basal ganglia and layers 2 and 3 of the neocortex (Morgan *et al.*, 2000). β-subunits are enriched at the AIS and nodes of Ranvier, similar to α-subunits, in neurons (Chen *et al.*, 2012; Buffington & Rasband, 2013). β1 is also localised to the growth cone in developing neurons (Brackenbury *et al.*, 2010). Not only is β-subunit expression developmentally regulated, glycosylation may also be developmentally regulated. β4 is present at the membrane in mice brains from postnatal day 0, but is only glycosylated from day 7 (Zhou *et al.*, 2012). Furthermore, deglycosylated β4 induces neurite outgrowth in Neuro2a cells more effectively than the adult, glycosylated form, suggesting a possible role in neurodevelopment for the differentially glycosylated states of β4 (Zhou *et al.*, 2012).

1.3.2 Structure

Transmembrane β-subunits are single-pass transmembrane glycoproteins, consisting of ~210 amino acids, with an extracellular V-type immunoglobulin (Ig) loop and a short intracellular C-terminus (Isom *et al.*, 1992; Isom *et al.*, 1995). β1B is a soluble, secreted splice variant of β1, comprising the β1 extracellular domain and a truncated C-terminus without a transmembrane domain, formed following intron retention (Qin *et al.*, 2003; Patino *et al.*, 2011). β1B mRNA is expressed in embryonic rat brain (enriched in DRG neurons), complimentary to the postnatal expression of β1, and adult adrenal gland and heart (Kazen-Gillespie *et al.*, 2000). β1B, like β1, is able to enhance I_{Na} magnitude and

modulate gating kinetics (Kazen-Gillespie *et al.*, 2000). In humans, β1B demonstrates some similarities to rat β1B, such as the ability to enhance I_{Na} magnitude, embryonic expression and RNA expression in the brain, but also some differences, such as little expression in the heart, postnatal expression, strong skeletal muscle expression and no effect on VGSC gating (Qin *et al.*, 2003). Unlike α-subunit orthologs which are present even in prokaryotes, β-subunits only exist in vertebrates (Winters & Isom, 2016). *Drosophila melanogaster* express a VGSC auxiliary subunit, known as *TipE*, although this double pass transmembrane protein is not considered homologous to vertebrate β-subunits, but is more similar to the vertebrate auxiliary subunits of large-conductance Ca^{2+}-activated potassium (BK_{Ca}) channels (Li *et al.*, 2011). However, rat β1 and β2 are still able to modulate the bacterial α-subunit (Molinarolo *et al.*, 2018). Vertebrate β-subunits, however, show sequence homology to other proteins with V-type Ig domains, such as myelin P0 (McCormick *et al.*, 1998). The structure of all human β-subunit ECDs have been determined (Gilchrist *et al.*, 2013; Namadurai *et al.*, 2014; Das *et al.*, 2016; Yan *et al.*, 2017). Between human β-subunits, β1 and β3 share common ancestry, and β2 and β4 share common ancestry, with β1 and β3 sharing 57 % sequence identity and β2 and β4 sharing 35 % sequence identity (Winters & Isom, 2016). β3 trimerises in the plasma membrane, dependent on the extracellular Ig loop, raising the possibility of multiple β-subunits binding multiple α-subunits and forming large multimeric signalling complexes (Namadurai *et al.*, 2014). Furthermore, homology modelling predicts β1-β3 dimers are more energetically favourable than β1-β1 dimers, suggesting the possibility of heteromeric β-subunit complexes (Liu *et al.*, 2014).

1.3.3 Post-translational modifications and interaction partners

β-subunits are subject to a variety of post-translational modifications (Figure 1.4).

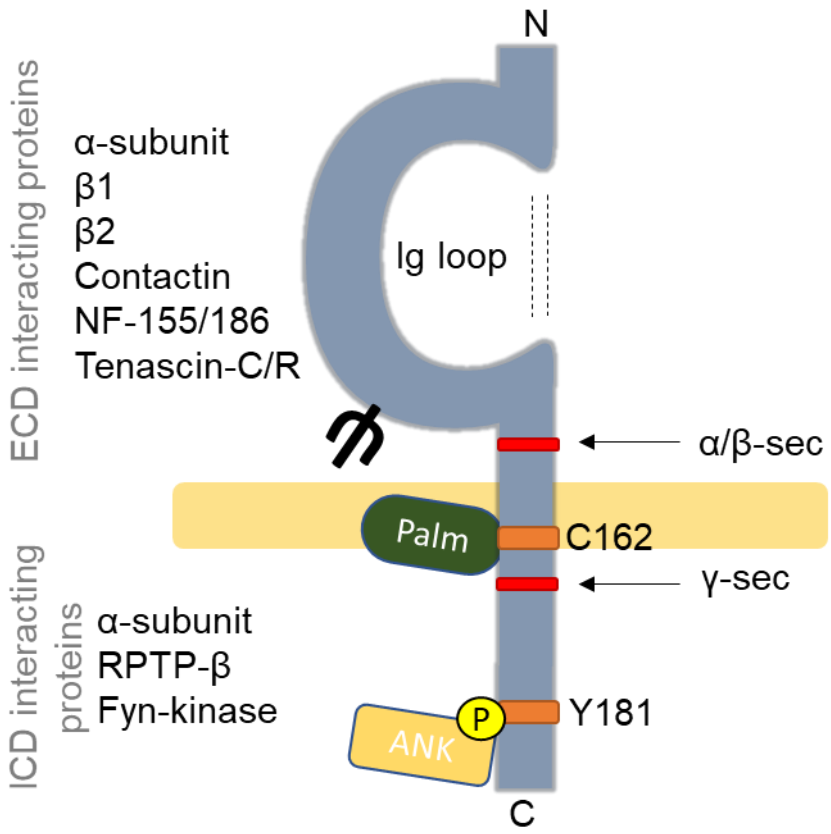

Figure 1.4 Post-translational modifications and interaction partners of β1

β1 interacts with α-subunits via the extracellular (ECD) and intracellular (ICD) domains (McCormick *et al.*, 1999; Meadows *et al.*, 2001). β1 also interacts transcellularly with itself, β2, contactin, neurofascin (NF)-155/186 and tenascin-C/R via the immunoglobulin (Ig) loop (Srinivasan *et al.*, 1998; Xiao *et al.*, 1999; Malhotra *et al.*, 2000; Kazarinova-Noyes *et al.*, 2001; Ratcliffe *et al.*, 2001; McEwen & Isom, 2004). β1 also interacts in *cis* with contactin (Brackenbury *et al.*, 2008; Brackenbury *et al.*, 2010). β1 is glycosylated within the ECD and contains a predicted palmitoylation site on the membrane-intracellular boundary (McEwen & Isom, 2004; Patino *et al.*, 2009). β1 interacts with fyn-kinase and receptor protein tyrosine phosphatase-β (RPTP-β) intracellularly (Ratcliffe *et al.*, 2000; Brackenbury *et al.*, 2008). Tyr181 is phosphorylated and binds ankyrin (Malhotra *et al.*, 2002). β1 is cleaved sequentially by secretases, starting with α- or β-secretase within the ECD, allowing for γ-secretase cleavage at the membrane-intracellular interface (Kim *et al.*, 2005; Wong *et al.*, 2005).

β-subunits are glycoproteins; reducing glycosylation abolishes β1-mediated modulation of $Na_v1.2$, $Na_v1.5$ and $Na_v1.7$, but does not affect modulation of the heavily glycosylated $Na_v1.4$, suggesting interplay between the glycosylation states of α- and β-subunit is important for VGSC function (Johnson *et al.*, 2004). Glycosylation of β2 is required for surface trafficking of $Na_v1.5$ (Cortada *et al.*, 2019). Phosphorylation of an intracellular tyrosine (Tyr181) of β1 has received much attention. Heterologous studies in Chinese hamster lung cells demonstrate phosphorylation of β1-Tyr181 mediates ankyrin-G binding and, along with contactin, is required for increasing I_{Na} carried by $Na_v1.2$ (Malhotra *et al.*, 2002; McEwen *et al.*, 2004). Tyr181 phosphorylation also regulates β1 subcellular localisation in ventricular myocytes, from transverse tubules to intercalated disks (Malhotra *et al.*, 2004). Phosphorylated β1 interacts exclusively with $Na_v1.5$, whereas non-phosphorylated β1 interacts with $Na_v1.1$, $Na_v1.3$ and $Na_v1.6$ (Maier *et al.*, 2004; Malhotra *et al.*, 2004). β1-Tyr181 is part of a tyrosine-leucine-alanine-isoleucine (YLAI) motif, found also in β3, that is a predicted clathrin-associated protein interaction site, indicating a possible mechanism for rapid VGSC sorting from the membrane (Morgan *et al.*, 2000). Receptor protein tyrosine phosphatase β (RPTPβ), which interacts with the β1-intracellular domain, β1-extracellular domain and α-subunits, modulates I_{Na} amplitude and gating kinetics (Ratcliffe *et al.*, 2000). A putative palmitoylation site on Cys162 of β1, on the transmembrane-intracellular domain boundary, may explain β1 enrichment in lipid rafts of primary mouse neurons (McEwen *et al.*, 2004; Wong *et al.*, 2005). β-subunits are also substrates of secretase enzymes, although the full impact of secretase cleavage on β-subunit function has yet to be uncovered (Kim *et al.*, 2005; Wong *et al.*, 2005). The current knowledge regarding secretase cleavage of β-subunits is reviewed later (chapter 1.5.4).

1.3.4 α-subunit interaction and modulation

β2 and β4 bind α-subunits covalently (Hartshorne *et al.*, 1982; Yu *et al.*, 2003), whereas β1 and β3 associate with α-subunits non-covalently (Hartshorne *et al.*, 1982; Morgan *et al.*, 2000). The α-β covalent interaction is mediated by Cys55 and Cys58 of β2 and β4, respectively (Chen *et al.*, 2012; Buffington & Rasband, 2013). The crystal structure of the β2-extracellular domain and bacterial Na_v channel revealed Cys910 of the $Na_v1.2$ DII P-loop as the site of β2 Ig loop binding (Das *et al.*, 2016). Both β2 and β4, but not β1 and β3, attenuate the inhibitory effect of the spider toxin, ProTx-II, on $Na_v1.2$, suggesting β2/4 interact with the same site on $Na_v1.2$ as ProTx-II (Gilchrist *et al.*, 2013; Das *et al.*, 2016). Although still uncertain, ProTx-II is thought to bind to the DI,II,IV voltage-sensor domains of $Na_v1.2$ (Bosmans *et al.*, 2008). If so, the transmembrane domains of β2 and β4 may dock at the same site. A recent cryo-EM structure of β2 in complex with $Na_v1.7$ demonstrated that Cys55 of the β2 Ig loop interacts with the extracellular side of DII of $Na_v1.7$ (Shen *et al.*, 2019). β1 interacts with α-subunits through extra- and intracellular interaction sites (Makita *et al.*, 1996; McCormick *et al.*, 1999; Meadows *et al.*, 2001; Spampanato *et al.*, 2004). A cryo-EM structure of electric eel $Na_v1.4$-β1 was recently resolved, the first structure of an α-β complex, showing the β1 transmembrane region interacted with the DIII voltage sensor and the β1 N-terminus to adjacent extracellular loops on $Na_v1.4$ (Yan *et al.*, 2017). An epilepsy-associated point mutation (D1866Y) in the C-terminus of $Na_v1.1$ weakens the $Na_v1.1$-β1 interaction (Spampanato *et al.*, 2004). Furthermore, expression of the $Na_v1.1$ K1846-R1886 peptide is sufficient to interact with β1, suggesting the β1 intracellular binding site is found in the C-terminus of $Na_v1.1$ (Spampanato *et al.*, 2004). However, α-β binding may not be that straightforward, as α-subunits are not always bound to β-subunits (Lombet & Lazdunski, 1984). Furthermore, not all β-subunits can interact with all α-subunits, for example β2 does not bind $Na_v1.7$ (Sokolov *et al.*, 2018).

The canonical function of β-subunits is to regulate α-subunits. Over thirty years ago, a pool of inactive α-subunits, consisting of ~70 % of the α-subunits in developing rat brain, were discovered to be retained intracellularly and unbound to β2 (Schmidt *et al.*, 1985). Leading on from this, α-subunits were observed to go through multiple glycosylation steps, within the endoplasmic reticulum and Golgi apparatus, increasing the molecular weight from 203 kDa to 249 kDa (Schmidt & Catterall, 1986). Only once the 249 kDa α-subunit had been formed could it bind β2 (1 h after α-subunit translation), but only ~30 % of 249 kDa α-subunit bound β2, the rest formed the intracellular pool (Schmidt & Catterall, 1986, 1987). α-β2 binding initiated a final 11 kDa modification to α-subunit, expected to be the final glycosylation step (Schmidt & Catterall, 1986). α-β2 complexes were found preferentially at the plasma membrane (4 h after α-subunit translation) and had a longer half-life than α-subunits alone, suggesting that β2 induces VGSC expression at the plasma membrane and stabilises α-subunit membrane expression (Schmidt & Catterall, 1986, 1987). From this work, Schmidt & Catterall proposed an intracellular pool of mature α-subunit exists for rapid membrane trafficking, when needed, following β2 binding. Since then, β1-3 expression has indeed been shown to induce membrane expression of α-subunits (Meadows *et al.*, 2001; Ishikawa *et al.*, 2013; Dulsat *et al.*, 2017). β3 increases $Na_v1.8$ membrane expression via masking of an ER-retention signal in the first intracellular loop of $Na_v1.8$ (Zhang *et al.*, 2008). Both β1 and β3 regulate glycosylation of surface $Na_v1.7$ (Laedermann *et al.*, 2013). Laedermann *et al.,* also proposed β1 and β3 bind $Na_v1.7$ following ER export, as they influence early glycosylation steps, unlike β2 and β4, which bind $Na_v1.7$ post-Golgi export and do not affect early glycosylation. Furthermore, all β-subunits, including β1B, can increase I_{Na}, presumably through an increase in α-subunit membrane expression (Isom *et al.*, 1992; Isom *et al.*, 1995; Fahmi *et al.*, 2001; Qin *et al.*, 2003; Bon *et al.*, 2016).

The influence of β-subunits on α-subunit function extends further than just increasing I_{Na} magnitude, however, as β-subunits also modulate the gating kinetics of α-subunits. For instance, β1 and β3 accelerate α-subunit recovery from inactivation (Merrick *et al.*, 2010; Laedermann *et al.*, 2013). β1 and β2, but not β1B, accelerate channel inactivation and current decay (Isom *et al.*, 1992; Isom *et al.*, 1995; Morgan *et al.*, 2000). However, these studies in heterologous cells fail to explore the mechanism of how β-subunits exert their effect on α-subunits and whether it is appropriate to extrapolate these observed changes elicited by one or two subunits to all β-subunits. Concerns over the compatibility of different heterologous studies is exemplified by the changes seen in the voltage threshold for half activation/inactivation. Before the identities of individual subunits were known, a β-subunit (likely β1 or β2) was shown to hyperpolarise voltage of inactivation of a neuronal α-subunit in *Xenopus* oocytes (Krafte *et al.*, 1990). In support of this, β1 and β2 both hyperpolarised the voltage of inactivation of $Na_v1.2$ in *Xenopus* oocytes (Isom *et al.*, 1992; Isom *et al.*, 1995). In contrast, coexpression of β1 or β3 with $Na_v1.5$ depolarises voltage of inactivation in *Xenopus* oocytes (Zhu *et al.*, 2017). Furthermore, coexpression of $Na_v1.7$ with each β-subunit individually in HEK293 cells shows β1 and β3 depolarise voltage of inactivation, and β2 and β4 have no effect (Laedermann *et al.*, 2013). Similarly, for voltage of activation, β3 depolarises activation of $Na_v1.3$ but hyperpolarises activation of $Na_v1.7$ in HEK293 cells (Cusdin *et al.*, 2010; Laedermann *et al.*, 2013). β4 hyperpolarises activation of $Na_v1.6$ and $Na_v1.8$ in HEK293 cells, whereas no other β-subunit has an effect (apart from β1 slightly hyperpolarising activation of $Na_v1.8$) (Zhao *et al.*, 2011). These conflicting results would suggest there is much complexity in the β-subunit mediated modulation of α-subunit gating. Complexity may arise from which α-β complex is being examined and the model system being used. Many other proteins can influence VGSC activity too, such as the large increases in I_{Na} induced by the CAMs contactin (Kazarinova-Noyes *et al.*, 2001) and NF186 (McEwen *et al.*, 2004). *in vivo* evaluation of β-subunit knockout mice models reveals another possible facet of α-subunit regulation. *Scn1b* KO mice show reduced $Na_v1.1$ and increased $Na_v1.3$

expression in hippocampal CA3 neurons and increased $Na_v1.3$ and $Na_v1.5$ expression in ventricular myocytes (Chen *et al.*, 2004; Lopez-Santiago *et al.*, 2007; Lin *et al.*, 2015). Changes in mRNA expression raise the possibilities that β-subunits influence transcription of α-subunits and/or changes in VGSC subunit expression are compensated for *in vivo*. The possibility of β-subunit affecting α-subunit transcription is supported by the observation that β2-ICD is enriched within the nucleus and induces an increase in *SCN1A* mRNA expression when expressed in SH-SY5Y cells (Kim *et al.*, 2007).

β-subunits also have several other electrophysiological effects. β4 possesses a C-terminal motif of hydrophobic residues capable of binding an open α-subunit prior to inactivation (Grieco *et al.*, 2005). This open channel block impedes inactivation, allowing for rapid reactivation of α-subunits as the membrane repolarises, known as "resurgent currents" (Grieco *et al.*, 2005). Resurgent currents bypass refractoriness and maintain the neuron in an excitable state as the membrane repolarises. These resurgent currents, carried primarily by $Na_v1.6$, are observable in cerebellar Purkinje neurons, in which fast spiking is possible (Grieco *et al.*, 2005). Resurgent currents regulate excitability of sensory neurons and contribute to peripheral neuropathies (Barbosa *et al.*, 2015; Xiao *et al.*, 2019). An intriguing feature of α-subunits is their mechanosensitivity (Tabarean *et al.*, 1999). β1 is capable of stabilising $Na_v1.7$ from mechanical stress, a potentially vital characteristic for a VGSC found in sensory neurons that experience mechanical stress with body movement (Korner *et al.*, 2018). Crosstalk between different ion channel families has emerged as a possibility, as β1 is capable of modulating K^+ channels. β1, via a tryptophan in its transmembrane domain, interacts with $K_v1.3$-VSD and depolarises voltage of activation (Kubota *et al.*, 2017). β1 further modulates activation and inactivation kinetics of $K_v1.2$ and $K_v1.6$ in *Xenopus* oocytes and regulates neuronal and

cardiac excitability via modulation of K_v channels (Deschenes & Tomaselli, 2002; Deschenes *et al.*, 2008; Marionneau *et al.*, 2012; Nguyen *et al.*, 2012).

1.3.5 Non-conducting function

β-subunits possess further non-conducting roles. β-subunits function as CAMs via the Ig loop in the extracellular domain (Srinivasan *et al.*, 1998; Malhotra *et al.*, 2000; Ratcliffe *et al.*, 2001; McEwen & Isom, 2004). β1 and β2, but not β3, can engage homophilically and recruit ankyrin to points of contact (Malhotra *et al.*, 2000; McEwen *et al.*, 2009). β1 and β2 also interact with extracellular matrix molecules tenascin-C and tenascin-R (Srinivasan *et al.*, 1998; Xiao *et al.*, 1999). Full-length tenascin-R has a cell repulsive effect when interacting with β1 or β2, however specific domains have an adhesive effect and can even increase I_{Na} in *Xenopus* oocytes co-expressing $Na_v1.2$, β1 and β2 (Xiao *et al.*, 1999). β1 interacts with a range of CAMs, including β2, neurofascin-155, neurofascin-186, nrCAM and contactin (McEwen & Isom, 2004; McEwen *et al.*, 2004). Furthermore, interaction of β1 with neurofascin-186 and contactin results in enlarged $Na_v1.2$ currents (McEwen & Isom, 2004; McEwen *et al.*, 2004). *Trans*-homophilic β1 interactions are involved in establishing correct perinexi distance between ventricular myocytes; blocking β1 adhesion results in dilated perinexi and disrupted cardiac action potential propagation between myocytes (Veeraraghavan *et al.*, 2018). β1-induced adhesion also regulates neurite outgrowth and contributes to neurodevelopment. Cerebellar granule neurons (CGNs), dissociated from wild-type mice and grown on a monolayer of β1-expressing Chinese hamster lung (CHL) cells, extend longer neurites than CGNs dissociated from *Scn1b* KO mice (Davis *et al.*, 2004). Further work using the same CGN neurite outgrowth experimental model demonstrated β1-mediated neurite outgrowth is dependent on $Na_v1.6$ activity, Fyn kinase signalling, contactin and γ-secretase cleavage (Brackenbury *et al.*, 2008; Brackenbury *et al.*, 2010; Brackenbury &

Isom, 2011). Similarly, CGN neurite extension can be stimulated by CHL cells expressing a soluble truncated form of the β1 N-terminus and can be blocked using anti-β1 antibodies, suggesting *trans*-homophilic β1 interactions can stimulate neurite outgrowth (Davis *et al.*, 2004). Interestingly, CGNs plated on a monolayer of β2-expressing CHL cells showed a shorter neurite length than CGNs grown on parental CHL cells (Davis *et al.*, 2004). Immunohistochemistry of mouse cerebellum identified β1 expression in Bergmann glia, the glial cells responsible for providing the scaffold for CGN migration during development, suggesting a possible *in vivo* role for β1 in cerebellum development (Davis *et al.*, 2004). In agreement with this, there is impaired axon pathfinding and fasciculation in the cerebellum of *Scn1b* KO mice (Brackenbury *et al.*, 2008). Although the specific involvement of adhesion was not examined, β2 enhances dendrite outgrowth and arborisation in developing rat hippocampal neurons and β4 induces neurite outgrowth in primary hippocampal neurons (Oyama *et al.*, 2006; Maschietto *et al.*, 2013).

1.4 The involvement of VGSCs in disease

1.4.1 Epilepsy

Many VGSC mutations have been identified in excitability-linked disorders, such as epilepsy (Figure 1.5, Table 1.2) (Baum *et al.*, 2014; Catterall, 2014; Bouza & Isom, 2017). Generalised epilepsy with febrile seizures plus (GEFS+) is a disorder characterised by febrile seizures in childhood followed by afebrile seizures into adulthood. *SCN1A, SCN2A* and *SCN1B* mutations have been identified in GEFS+ (Lossin *et al.*, 2002). The first identified GEFS+ mutation, C121W, was found in *SCN1B* (Wallace *et al.*, 1998). C121W abolished β1-induced fast inactivation of $Na_v1.2$ when co-expressed in *Xenopus* oocytes, and hyperpolarised inactivation and accelerated recovery from inactivation of $Na_v1.3$ in CHO cells (Wallace *et al.*, 1998; Meadows *et al.*, 2002). *In vivo,* heterozygous

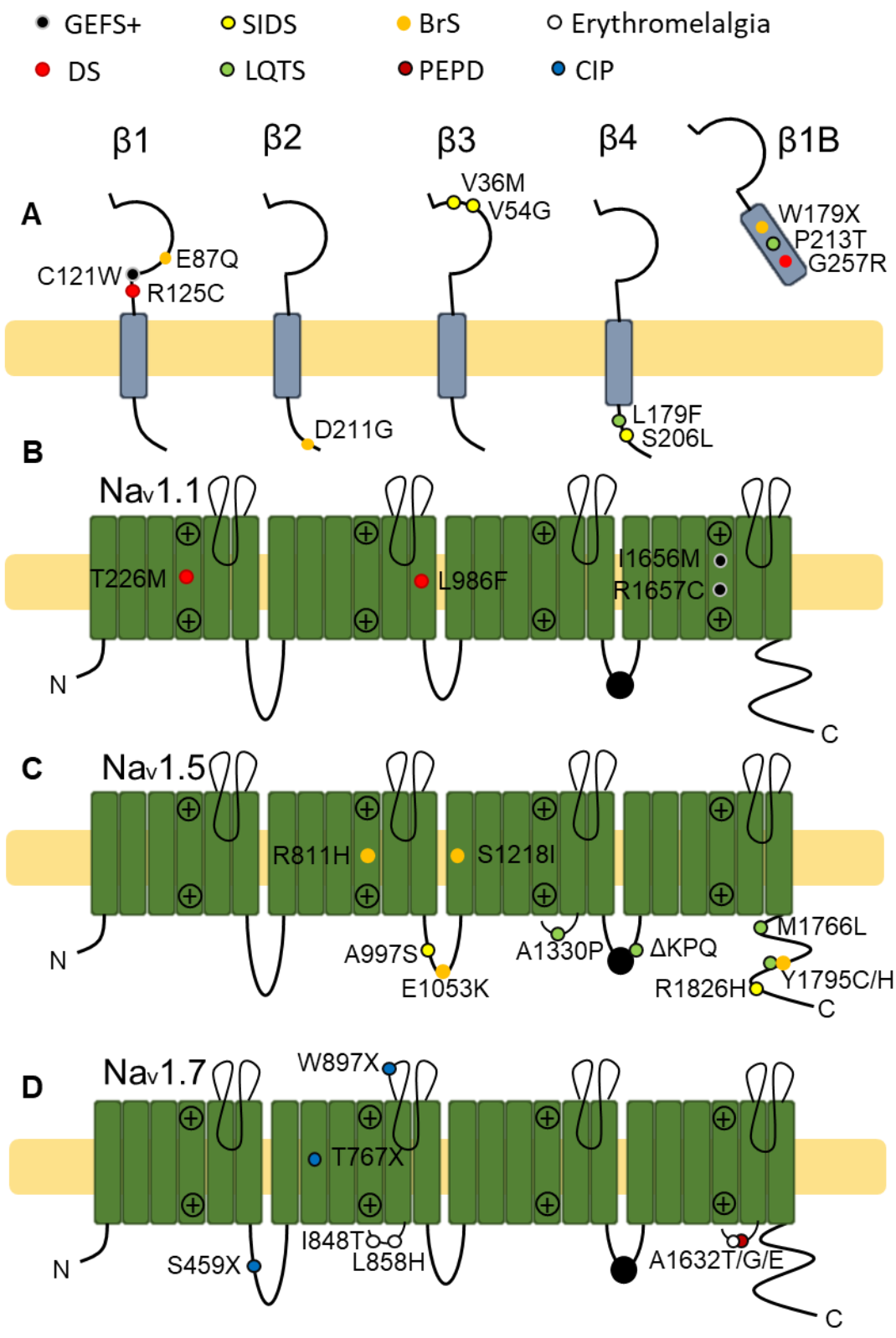

Figure 1.5 VGSC mutations implicated in excitability-linked disorders

Mutations in β-subunits (**A**), $Na_v1.1$ (**B**), $Na_v1.5$ (**C**) and $Na_v1.7$ (**D**). GEFS+: generalised epilepsy with febrile seizures plus. DS: Dravet syndrome. SIDS: suddent infantile death syndrome. LQTS: long QT syndrome. BrS: Brugada syndrome. PEPD: paroxysmal extreme pain disorder. CIP: chronic insensitivity to pain.

Table 1.2 Effects of voltage-gated Na^+ sodium channel mutations implicated in excitability-linked disorders

Disorder	Subunit	Mutation	Effect of mutation	Effect on VGSC activity
GEFS+	$Na_v1.1$	I1656M	Depolarised activation[1]	LOF
		R1657C		
	β1	C121W	No association with α[2]	
DS	$Na_v1.1$	L986F	Afunctional[1]	LOF
		T226M	Depolarisation block[3]	
	β1	R125C	Afunctional[4]	
	β1B	G257R	Afunctional[5]	
EIEE11	$Na_v1.2$	R102X	Afunctional[6]	LOF
LQTS	$Na_v1.5$	ΔKPQ	Increased $I_{Na}P$[7]	GOF
		A1330P	Depolarised inactivation/ accelerated RFI[8]	
		Y1795C	Increased I_{Na}[9]	
		M1766L	Increased I_{Na}[10]	
	β1B	P213T	Increased $I_{Na}P$[11]	
	β4	L179F	Increased I_{Na}[12]	
BrS	$Na_v1.5$	R811H	Decreased I_{Na}[13]	LOF
		S1218I	Afunctional[13]	
		E1053K	Decreased I_{Na}[14]	
	β1	E87Q	Afunctional[15]	
	β1B	W179X	Afunctional[16]	
	β2	D211G	Afunctional[17]	
SIDS	$Na_v1.5$	A997S	Increased $I_{Na}P$[18]	GOF
		R1826H		
	β3	V36M	Increased $I_{Na}P$[19]	
		V54G	Delayed inactivation[20]	
	β4	S206L	Increased $I_{Na}P$[19]	
CIP	$Na_v1.7$	S459X T767X W897X	Afunctional[21]	LOF
EM	$Na_v1.7$	I848T	Hyperpolarised activation[22]	GOF
		L858H		

		A1632T	Impaired inactivation[23]	
		A1632G	Hyperpolarised activation[24]	
PEPD	$Na_v1.7$	A1632E	Hyperpolarised activation/ depolarised inactivation[25]	GOF
PM	$Na_v1.4$	R669H	Hyperpolarised inactivation[26]	LOF
		R669C/G/W	Na^+ leak through gating pore[27]	GOF
References: 1 (Lossin *et al.*, 2003), 2 (Baroni *et al.*, 2013), 3 (Berecki *et al.*, 2019), 4 (Patino *et al.*, 2009), 5 (Patino *et al.*, 2011), 6 (Kamiya *et al.*, 2004), 7 (Bennett *et al.*, 1995), 8 (Rivolta *et al.*, 2001), 9 (Rivolta *et al.*, 2001), 10 (Matsumura *et al.*, 2017), 11 (Riuro *et al.*, 2014), 12 (Medeiros-Domingo *et al.*, 2007), 13 (Calloe *et al.*, 2013), 14 (Mohler *et al.*, 2004), 15 (Watanabe *et al.*, 2008), 16 (Watanabe *et al.*, 2009), 17 (Riuro *et al.*, 2013), 18 (Ackerman *et al.*, 2001), 19 (Tan *et al.*, 2010), 20 (Valdivia *et al.*, 2010), 21 (Cox *et al.*, 2006), 22 (Cummins *et al.*, 2004), 23 (Eberhardt *et al.*, 2014), 24 (Yang *et al.*, 2016), 25 (Estacion *et al.*, 2008), 26 (Struyk *et al.*, 2000), 27 (Sokolov *et al.*, 2008)				
Abbreviations: GEFS+: generalised epilepsy with febrile seizures plus, DS: Dravet Syndrome, EIEE11: early infantile epileptic encephalopathy 11, LQTS: Long QT syndrome, BrS: Brugada Syndrome, SIDS: sudden infantile death syndrome, CIP: chronic insensitivity to pain, EM: erythromelalgia, PEPD: paroxysmal extreme pain disorder, PM: paramyotonia, I_{Na}: Na^+ current, $I_{Na}P$: persistent Na^+ current, RFI: recovery from inactivation, VGSC: voltage-gated Na^+ channel, G/LOF: gain/loss of function				

C121W mice show aberrantly glycosylated β1, no α-subunit coupling, lack of AIS and Node of Ranvier enrichment, enhanced hippocampal pyramidal neuron excitability and present with hypothermia-induced seizures (Wimmer *et al.*, 2010; Kruger *et al.*, 2016). Interestingly, C121W impairs Ig loop formation and β1-induced adhesive properties, suggesting the impairment of β1-induced adhesion may also contribute to disease pathology (Wimmer *et al.*, 2010; Kruger *et al.*, 2016). $Na_v1.1$ mutations in GEFS+ can result in both gain-of-function and loss-of-function when examined *in vitro,* suggesting a dependence on the neuron-type (Lossin *et al.*, 2002; Lossin *et al.*, 2003). Despite the milder phenotype, sudden unexplained death in epilepsy (SUDEP) has been observed in a patient carrying an *SCN1B* GEFS+ mutation (Myers *et al.*, 2019). Dravet syndrome (formerly severe myoclonic epilepsy in infancy) is a form of epilepsy characterised by childhood febrile seizures and adulthood afebrile seizures, similar to GEFS+, except more severe, uncontrolled seizure activity results in cognitive impairment and ataxia, unlike GEFS+ (Catterall, 2014). The majority of Dravet syndrome mutations are found within *SCN1A* (Meisler & Kearney, 2005). Intriguingly, early analysis of a Dravet syndrome mutation, L986F, demonstrated complete loss of $Na_v1.1$ function (Lossin *et al.*, 2003). A mouse model heterozygous for a Dravet syndrome mutation demonstrated hypoactivity in GABAergic interneurons of hippocampal interneurons, leading to widespread excitability, ataxia and death by postnatal day 15 (Yu *et al.*, 2006; Ogiwara *et al.*, 2007). Additionally, selective hippocampal *SCN1A* deletion mimics Dravet syndrome-like symptoms, underlining the importance of hippocampal $Na_v1.1$ in Dravet syndrome (Stein *et al.*, 2019). A Dravet syndrome mutation in $Na_v1.1$, T226M, was recently investigated and demonstrated gain of function properties in CHO cells (Berecki *et al.*, 2019). However, T226M also enhanced the susceptibility of interneurons to develop depolarisation block, suggesting T226M may still impart interneuron hypoexcitability like other $Na_v1.1$ Dravet syndrome mutations (Berecki *et al.*, 2019). Similarly, the autosomal recessive R125C Dravet syndrome mutation in β1 produces an afunctional protein unable to traffic VGSCs to the cell surface (Patino *et al.*, 2009). A

similar mutation introducing a Cys residue, R89C, has been identified in a patient with Dravet syndrome-like symptoms, emphasising the importance of correct Ig loop folding (Darras *et al.*, 2019). *Scn1b*-null mice are used as a model for Dravet syndrome and demonstrate action potentials of greater magnitude, spontaneous seizures and SUDEP by postnatal day 20 (Patino *et al.*, 2009; O'Malley *et al.*, 2019). An epilepsy-related mutation unique to β1B, G257R, also produces a functional null protein that is retained intracellularly (Patino *et al.*, 2011).

Mutations in $Na_v1.2$ are seen in two childhood epilepsy syndromes; benign familial neonatal-infantile seizures 3 (BFNIS) characterised by seizures in the first 12 months of life with little neurological impairment in later life and early infantile epileptic encephalopathy 11 (EIEE11), a more severe disorder characterised by infantile, uncontrolled seizures resulting in permanent neurological impairment (Heron *et al.*, 2002; Kamiya *et al.*, 2004; Ogiwara *et al.*, 2009). $Na_v1.2$ mutations observed in BFNIS are typically missense mutations, whereas the autosomal-dominant, nonsense mutation identified in EIEE11, R102X, produces a non-functional protein truncated before the first transmembrane domain that is thought to have a dominant-negative effect on wild-type $Na_v1.2$ (Kamiya *et al.*, 2004; Shi *et al.*, 2012).

1.4.2 Cardiac arrhythmia

$Na_v1.5$ plays a key role in cardiac action potential propagation and thus aberrant function is involved in cardiac arrhythmia; however, mutations in β-subunits are also implicated (Remme & Bezzina, 2010; Bouza & Isom, 2017). $Na_v1.5$ is highly expressed in ventricle walls, His bundles and Purkinje fibres, and weakly expressed within atria, as $Na_v1.5$ is not involved in atrial action potential propagation (Remme *et al.*, 2009). Gain of function mutations in $Na_v1.5$ are associated with Long QT syndrome 3 (LQT3), characterised by

delayed repolarisation, prolonged action potentials and early after-depolarisations, potentially leading to arrhythmia and death. Identified LQT3 mutations in $Na_v1.5$ include ΔKPQ (deletion of Lys1505, Pro1506, Gln1507) that disrupts fast inactivation increasing persistent I_{Na} (Bennett *et al.*, 1995), A1330P that depolarises voltage of inactivation and enhances recovery from inactivation (Wedekind *et al.*, 2001) and Y1795C that increases I_{Na} magnitude (Rivolta *et al.*, 2001). $Na_v1.5$ loss of function mutations are associated with Brugada syndrome, characterised by slowed action potentials and cardiac conduction, potentially leading to arrhythmia and sudden death. Interestingly, Tyr1795, an amino acid implicated in LQT3 when mutated to cysteine, is also associated with Brugada syndrome when mutated to histidine, resulting in a hyperpolarised voltage of inactivation (Rivolta *et al.*, 2001). Other Brugada syndrome $Na_v1.5$ mutations include R811H that decreases I_{Na}, S1218I that shows complete loss of function, and E1053K that abolishes $Na_v1.5$ binding to Ankyrin-G, resulting in a decrease of $Na_v1.5$ surface expression (Mohler *et al.*, 2004; Calloe *et al.*, 2013). Interestingly, the frequency of a common *SCN5A* polymorphism, H558R, found in 10-20 % of the population, is reduced in arrhythmic and Brugada syndrome patients (Ackerman *et al.*, 2004; Maekawa *et al.*, 2005; Matsumura *et al.*, 2017). Co-expression of $Na_v1.5$-H558R with $Na_v1.5$-M1766L, a mutation implicated in LQT3 that enhances I_{Na}, restored normal I_{Na}, suggesting H558R impacts on trafficking (Ye *et al.*, 2003). Genetic analysis of right atrial sections obtained from patients undergoing heart surgery showed *SCN5A* expression levels were significantly higher and *SCN5A* promoter methylation significantly decreased in patients with the H558R mutation (Matsumura *et al.*, 2017). Considering H558R is found within the DI-II intracellular linker, a region of $Na_v1.5$ known to contain a nuclear-localising signal and capable of interacting with the *SCN5A* promoter when expressed alone, potentially $Na_v1.5$ is involved in nuclear signalling that is enhanced by H558R (Onwuli *et al.*, 2017).

β-subunits are also implicated in LQT syndrome and Brugada syndrome. In LQT syndrome, a proline to threonine mutation (P213T) in β1B increases persistent I_{Na} and accelerates recovery from inactivation (Riuro *et al.*, 2014). A mutation in β4, L179F, enhances $Na_v1.5$ persistent I_{Na} 3-fold compared to WT-β4 (Medeiros-Domingo *et al.*, 2007). In Brugada syndrome, multiple mutations have been identified in *SCN1B* that decrease I_{Na}, β1B is implicated, with the W179X mutation, as well as β1-E87Q (Watanabe *et al.*, 2008). The impact of the mutations on channel function was not investigated, but β1 slows decay of the persistent I_{Na} of $Na_v1.5$ and disruption of this may cause arrhythmia (Maltsev *et al.*, 2009; Mishra *et al.*, 2011). Mutations in β2 and β3 have been identified that disrupt $Na_v1.5$ trafficking to the cell surface (Ishikawa *et al.*, 2013; Dulsat *et al.*, 2017). For instance, β2-D211G reduces $Na_v1.5$ I_{Na} by almost 40 % when co-expressed in CHO cells, compared to WT-β2 (Riuro *et al.*, 2013). β4 has also been implicated in arrhythmogenesis, β4-G8S is a mutation seen 3-fold more frequently in atrial fibrillation patients than the control population (Xiong *et al.*, 2019). Gly8 is a highly conserved residue in β4 and its location within the signal peptide suggests it regulates subcellular targeting of the protein (Xiong *et al.*, 2019). G8S is also seen in ventricular tachycardia patients, along with another mutation, A145S (Yang *et al.*, 2019). Both mutations decrease surface expression of β4, without affecting any I_{Na} parameters, suggesting a possible non-conducting contribution of β4 in cardiac arrhythmia (Yang *et al.*, 2019). The involvement of β-subunits in arrhythmia may extend further than their regulation of I_{Na}, as two early repolarisation syndrome mutations in β1B have been identified that accelerate the recovery from inactivation of $K_v4.3$, the channel responsible for repolarisation of cardiomyocytes (Yao *et al.*, 2018).

1.4.3 Sudden infant death syndrome

Sudden infant death syndrome (SIDS) is the sudden unexplained death of an infant in the first year of life. Gene variants associated with cardiac channelopathies, including *SCN5A*, are observed in ~10 % of SIDS cases (Schwartz *et al.*, 1998; Ackerman *et al.*, 2001; Arnestad *et al.*, 2007). Two mutations identified in *SCN5A* (A997S and R1826H) increase persistent I_{Na} (Ackerman *et al.*, 2001). Likewise, mutations found in β3 (V36M) and β4 (S206L) increase persistent I_{Na}, further implicating persistent I_{Na} in SIDS (Tan *et al.*, 2010). A second *SCN3A* mutation (V54G) was identified in SIDS, which decreases $Na_v1.5$ I_{Na} and depolarises the voltage of inactivation when co-expressed in COS cells (Valdivia *et al.*, 2010). Interestingly, the two *SCN3B* mutations identified (V36M and V54G) decrease I_{Na}, suggesting the magnitude of depolarisation is not important but potentially the duration as V36M enhances persistent I_{Na} and V54G delays inactivation. A Brugada syndrome-associated mutation in *SCN1B,* affecting β1B (R214Q), has been observed in SIDS cases and causes decreased I_{Na} and enhanced I_K in heterologous co-expression studies (Hu *et al.*, 2012; Olesen *et al.*, 2012)

1.4.4 Pain disorders

$Na_v1.7$/*SCN9A* mutations have been reported in patients with primary erythromelalgia (Yang *et al.*, 2004). $Na_v1.7$, Nav1.8 and Nav1.9 are all expressed in DRGs and initially, $Na_v1.8$ was the focus of pain research, after it was discovered that mice lacking *Scn10a* had an increased threshold to noxious mechanical and heat stimuli (Black *et al.*, 1996; Akopian *et al.*, 1999). However, acute pain sensation has a vital physiological function, and a pertinent study a few years later demonstrated *Scn10a* null mice had no change in their chronic pain threshold compared to wildtype littermates (Laird *et al.*, 2002). Two years later, familial *SCN9A* mutations were identified in primary erythromelalgia by linkage analysis of an affected Chinese family and shortly after, selective *Scn9a* deletion

in $Na_v1.8$+ DRGs produced mice with a reduced or abolished response to various acute and inflammatory pain stimuli, implicating $Na_v1.7$ as the VGSC responsible for chronic pain sensation and unveiling $Na_v1.7$ as a major therapeutic target (Nassar *et al.*, 2004; Yang *et al.*, 2004). Familial mutations in *SCN9A* were further identified in chronic insensitivity to pain (CIP) and paroxysmal extreme pain disorder (PEPD) (Cox *et al.*, 2006; Fertleman *et al.*, 2006). CIP is a rare, autosomal recessive condition rendering patients insensitive to pain, caused by a loss of $Na_v1.7$ function (Cox *et al.*, 2006). Identified CIP mutations, S459X, I767X and W897X, produce truncated, non-conducting α-subunits (Cox *et al.*, 2006). More recently identified CIP mutations also correspond to truncated, afunctional $Na_v1.7$ subunits (Shorer *et al.*, 2014; He *et al.*, 2018; Marchi *et al.*, 2018). Erythromelalgia and PEPD, both caused by a gain of $Na_v1.7$ function, are conditions associated with episodes of extreme pain sensation of the extremities, in erythromelalgia, and of the rectal, ocular and jaw areas in PEPD (van Genderen *et al.*, 1993; Fertleman *et al.*, 2007; Fischer & Waxman, 2010). $Na_v1.7$ has an important role in neuronal excitability by amplifying small depolarising inputs and producing threshold currents close to resting V_m (Cummins *et al.*, 1998). The first study into the gating effects of erythromelalgia mutations showed that $Na_v1.7$ erythromelalgia mutations (I848T and L858H), in HEK293 cells hyperpolarised voltage of activation and slowed deactivation compared to WT-$Na_v1.7$, suggesting increased $Na_v1.7$ activity at lower V_m underpins the nociceptor hyperexcitability seen in erythromelalgia (Cummins *et al.*, 2004). PEPD mutations, on the other hand, are classically associated with a depolarised voltage of inactivation, delaying channel inactivation (Dib-Hajj *et al.*, 2008). Mutations of a single $Na_v1.7$ DIV S4-5 loop residue, Ala1632, produces a spectrum of inherited conditions. A1632E causes hyperpolarised activation and depolarised inactivation and causes a condition with dual PEPD-erythromelalgia symptoms (Estacion *et al.*, 2008). A1632T causes erythromelalgia through impaired inactivation (Eberhardt *et al.*, 2014), and A1632G causes erythromelalgia through hyperpolarised activation, depolarised inactivation and an increased sensitivity to thermal stimuli (Yang *et al.*, 2016).

VGSC subunits other than $Na_v1.7$ and Nav1.8 have been implicated in pain. Of a patient cohort diagnosed with painful peripheral neuropathy, 34/393 had a $Na_v1.7$ mutation, 15/393 had a $Na_v1.8$ mutation and 11/393 had a mutation in $Na_v1.9$ (Huang *et al.*, 2014). $Na_v1.9$ is also expressed in DRGs (Black *et al.*, 1996). Gain of function mutations in $Na_v1.9$ underpin an autosomal dominant episodic pain disorder that render DRGs hyperexcitable (Zhang *et al.*, 2013; Huang *et al.*, 2014; Kabata *et al.*, 2018). Furthermore, mutations in $Na_v1.9$ have also been identified that confer insensitivity to pain, implicating $Na_v1.9$ as a possible therapeutic target for chronic pain (Huang *et al.*, 2017). Additionally, following peripheral nerve injury, $Na_v1.6$ is the predominant α-subunit involved in DRG neuron excitation (Vysokov *et al.*, 2019).

Mutations in β-subunits are also involved in pain disorders. *Scn1b*-null mice demonstrate DRG hyperexcitability, due to a depolarising shift in the voltage of inactivation, implicating β1 in modulating nociceptor excitability (Lopez-Santiago *et al.*, 2011). Genetic analysis of diabetic patients with painful neuropathy identified a D109N mutation in β2 in the absence of *SCN9A/SCN10A/SCN11A* mutations, which depolarised the voltage of inactivation of $Na_v1.7$ in heterologous HEK293 cells and caused DRG hyperexcitability (Alsaloum *et al.*, 2019). Expression of mRNA for β1-β3 is upregulated in sensory neurons of mice following nerve injury and β2 null mice show decreased sensitisation to non-painful stimuli (allodynia) following nerve injury, suggesting β-subunits may be implicit in neuropathic pain (Blackburn-Munro & Fleetwood-Walker, 1999; Pertin *et al.*, 2005). Furthermore, knockdown of *Scn4b* in mice carrying $Na_v1.8$-T790A, the mutation found in the *Possum* mouse model of pain, reduced DRG excitability and narrowed action potentials, implicating β4-mediated open channel block in nociception (Xiao *et al.*, 2019).

1.4.5 Other excitability-linked disorders

The cerebellum is an expansive network of neurons requiring fine electrical balance and various loss-of-function mutations have been identified in $Na_v1.6$ that lead to cerebellar ataxia (Kohrman *et al.*, 1996; Smith & Goldin, 1999). An alanine to threonine mutation in the DIII S4-S5 linker of Nav1.6 in the *jolting* mouse model of ataxia causes a depolarising shift in the voltage of activation of cerebellar Purkinje neurons (Kohrman *et al.*, 1996). Mutations in *SCN8A* have also been identified in more complex neurological conditions such as sleep disorders (Papale *et al.*, 2010), depression (Wasserman *et al.*, 2005), anxiety (McKinney *et al.*, 2008) and bipolar disorder (Wang *et al.*, 2008). Mutations in the CNS VGSCs ($Na_v1.1$, 1.2, 1.3 and 1.6), as well as $Na_v1.7$, intriguingly, have been identified in autism (Weiss *et al.*, 2003; Butler *et al.*, 2017; Rubinstein *et al.*, 2018; Lena & Mantegazza, 2019; Spratt *et al.*, 2019). Mutations in CNS VGSCs have also been implicated in intellectual disabilities (Trudeau *et al.*, 2006; Shin *et al.*, 2019).

$Na_v1.4$ is the predominant skeletal muscle VGSC (Wang *et al.*, 1992). Gain of function mutations in $Na_v1.4$ underlie paramyotonia congenita, a disorder characterised by muscle rigidity due to delayed muscle relaxation (Lerche *et al.*, 1993). The first paramyotonia $Na_v1.4$ mutations identified, Gly1306 to glutamic acid, valine or alanine, resulted in delayed channel inactivation when examined by patch clamp electrophysiology (Lerche *et al.*, 1993). Other movement disorders have, too, been attributed to $Na_v1.4$. ~10 % of hypokalaemia periodic paralysis (HypoPP) cases are attributed to *SCN4A* (Sternberg *et al.*, 2001). HypoPP is an autosomal dominant disorder characterised by periods of muscle weakness and low extracellular K^+. The R669H mutation in $Na_v1.4$ occurs within DII:S4 and hyperpolarises the voltage of inactivation (Struyk *et al.*, 2000). Mutations in *SCN4A* are also seen in hyperkaliaemic periodic paralysis (HyperPP), which is a disorder characterised by episodes of muscle paralysis, similar to HypoPP, except an elevated serum K^+ is present (Cummins *et al.*, 1993).

HyperPP is caused by a gain of channel function, such as a hyperpolarisation of the activation voltage (Cummins *et al.*, 1993). A mutation in $Na_v1.4$ has also been identified in normokalaemic periodic paralysis (Sokolov *et al.*, 2008). This interesting mutation (R669Q/G/W) in DII:S4, causes a I_{Na} through the gating pore itself, following depolarisation and S4 translocation (Sokolov *et al.*, 2008).

1.4.6 Neurodegeneration

β-subunits have an emerging role in several neurodegenerative conditions (Bouza & Isom, 2017). Amyotrophic lateral sclerosis (ALS) is a disorder characterised by progressive degeneration of motor neurons. Cortical hyperexcitability is a feature of ALS and the murine model of ALS, SOD1G93A, displays an increased cortical persistent I_{Na} (Vucic *et al.*, 2008; Pieri *et al.*, 2009). Symptomatic SOD1G93A mice also show elevated β3 and decreased β1 expression within lamina IX of the spinal cord, and decreased $Na_v1.6$ expression throughout the spinal cord, compared to pre-symptomatic mice (Nutini *et al.*, 2011). This further implicated β3 and the persistent I_{Na} in ALS, as β3 promotes persistent I_{Na} of $Na_v1.2$ *in vitro,* whereas β1 has no effect (Qu *et al.*, 2001).

Alzheimer's disease also has a link with increased excitability. Patients with Alzheimer's disease represent 10 % of new onset epilepsy in patients over 65 years old and have a 6- to 10-fold greater risk of developing seizures compared with healthy age-matched individuals (Pandis & Scarmeas, 2012). There is developing evidence implicating β2 in hyperexcitability in Alzheimer's disease, although this is discussed in more detail in chapter 1.5.4 (Hu *et al.*, 2017; Hu *et al.*, 2019).

6-hydroxydopamine lesioning of mice is a common model for Parkinson's disease. In the hippocampi of lesioned rats, $Na_v1.1$ expression is increased in reactive astrocytes and

neuronal $Na_v1.3$ expression increased (Wang *et al.*, 2019). Phenytoin treatment improves learning and memory, implicating VGSCs in the cognitive decline observed in experimental models of Parkinson's disease (Wang *et al.*, 2019).

Emerging evidence suggests a link between β-subunits and Huntington's disease and multiple sclerosis (MS). Huntington's disease is associated with progressive cell death of striatal neurons caused by polyglutamine repeats in the cytoplasmic protein, Huntingtin, although the pathogenic mechanism is yet to be elucidated (Landles & Bates, 2004). Profiling of a mouse model of Huntington's disease shows a progressive decrease in striatal β4 expression, beginning at a pre-symptomatic stage (Oyama *et al.*, 2006; Bigan *et al.*, 2019). β4 was suggested to be involved in dendritic arborisation of striatal neurons (Oyama *et al.*, 2006). MS is a disorder involving demyelination and axonal degeneration (Lassmann, 2018). Treatment of experimental autoimmune encephalomyelitis (EAE) mice (an MS model) with the VGSC blocker, phenytoin, reduces axonal degeneration, implicating VGSCs in MS pathology (Lo *et al.*, 2002). Furthermore, Overexpression of a mutant $Na_v1.2$ that displays increased persistent I_{Na}, increases axonal degeneration and lethality in EAE mice (Schattling *et al.*, 2016). Deletion of *Scn2b* is also neuroprotective in EAE mice without any changes to immune function, implicating β2 upregulation of surface VGSCs in MS (O'Malley *et al.*, 2009).

1.4.7 Cancer

α- and β-subunit expression is commonly deregulated and functionally significant in cancer (Figure 1.6) (Brackenbury, 2012; Roger *et al.*, 2015; Haworth & Brackenbury, 2019). $Na_v1.2$, $Na_v1.4$, $Na_v1.5$ and $Na_v1.7$ are upregulated in highly metastatic ovarian cancer cells compared to weakly metastatic cells (Gao *et al.*, 2010). $Na_v1.6$ and Nav1.7 are upregulated in cervical cancer biopsies compared to normal cervical tissue

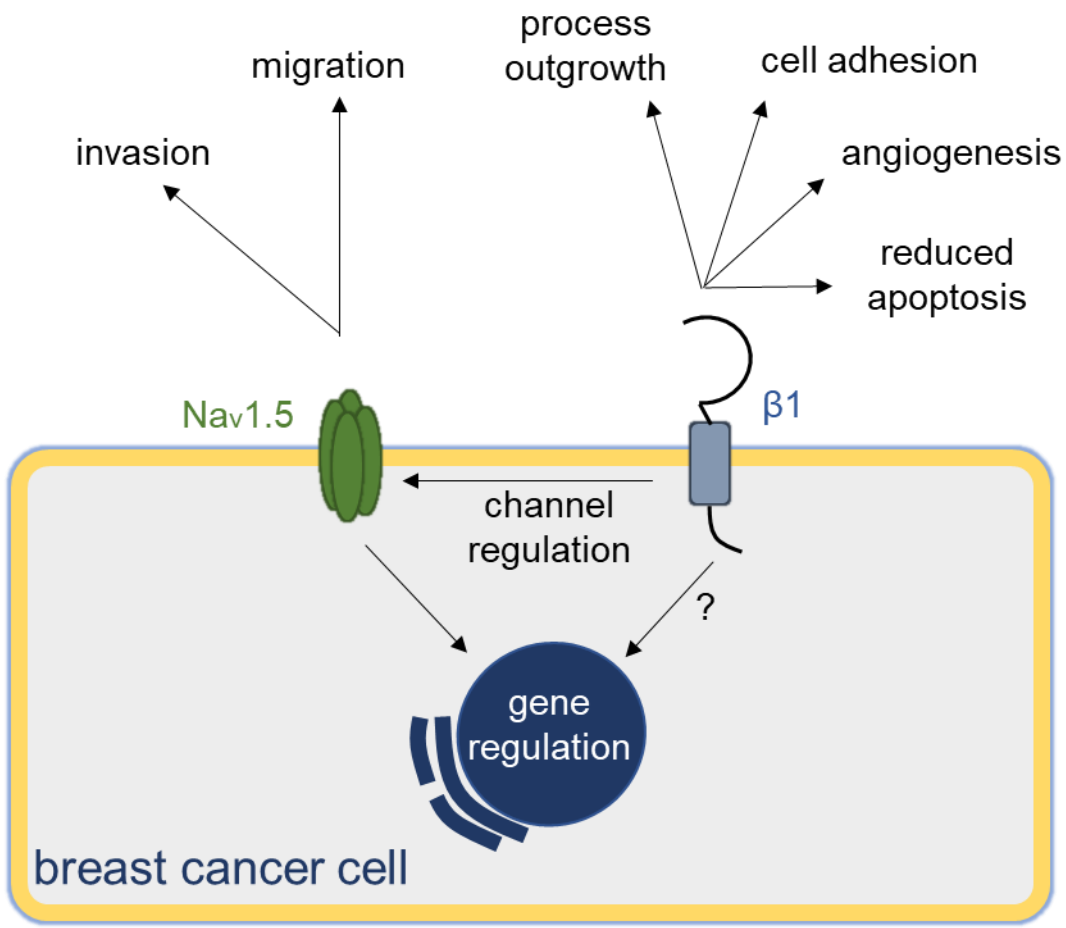

Figure 1.6 The involvement of VGSCs in breast cancer cell behaviour

$Na_v1.5$ and β1 are both upregulated in breast cancer. $Na_v1.5$ promotes migration and invasion, and β1 induces cell adhesion, promotes process outgrowth and angiogenesis, and reduces apoptosis (Malhotra *et al.*, 2000; Yang *et al.*, 2012; Nelson *et al.*, 2014). β1 also enhances I_{Na} in breast cancer cells (Chioni *et al.*, 2009). β2 has putative nuclear signalling abilities, suggesting β1 may too be involved (Kim *et al.*, 2007). $Na_v1.5$ has been shown to regulate downstream expression of a range of genes involved in colon cancer cell migration and invasion (House *et al.*, 2010).

(Hernandez-Plata *et al.*, 2012). $Na_v1.7$ is upregulated in prostate cancer cell lines (Diss *et al.*, 2001; Diss *et al.*, 2005). $Na_v1.5$ protein is upregulated in colon cancer biopsies compared to normal tissue (House *et al.*, 2010). α-subunit expression is decreased in higher grade gliomas, although the functional consequences of this loss of expression are not clear (Schrey *et al.*, 2002).,

Evidence from biopsies and cell lines suggests α-subunit may be hormonally regulated (Fraser *et al.*, 2014). In colon cancer biopsies, high $Na_v1.5$ and oestrogen receptor β immunoreactivity correlates with worse prognosis compared to high oestrogen receptor β levels alone (Peng *et al.*, 2017). In breast tumour tissue, all samples lacking $nNa_v1.5$ immunoreactivity were positive for oestrogen receptor α (Yamaci *et al.*, 2017). Furthermore, in samples negative for oestrogen receptor α expression, $nNa_v1.5$ was present at the plasma membrane, whereas in samples positive for oestrogen receptor α, $nNa_v1.5$ was present in the cytoplasm as well as the plasma membrane (Yamaci *et al.*, 2017). Overexpression of oestrogen receptor α in MDA-MB-231 breast cancer cells reduces $Na_v1.5$ mRNA expression, which is reversible upon receptor inhibition (Fraser *et al.*, 2014). Other models have further eluded to VGSC expression regulation by hormones and growth factors (Fraser *et al.*, 2014). Nuclear androgen receptor complexes associate with the promoter region of *SCN9A* and result in an increase in $Na_v1.7$ mRNA expression in ND7 neuroblastoma cells (Berwick *et al.*, 2010). In response to (5α,17β)-17-hydroxy-androstan-3-one dihydrotestosterone treatment, β1 mRNA expression is decreased in prostate cancer LNCaP cells but enhanced in prostate cancer PC3 cells (Diss *et al.*, 2008). In cultured bovine adrenal cells, insulin treatment enhanced plasma membrane β1 and $Na_v1.7$ expression (Nemoto *et al.*, 2009; Yanagita *et al.*, 2011). In respect to growth factors, epidermal growth factor enhances $Na_v1.5$ expression and VGSC inhibition with tetrodotoxin decreases the migratory capacity in breast cancer MDA-MB-231 cells (Gonzalez-Gonzalez *et al.*, 2019). In prostate cancer cells, nerve

growth factor treatment enhances $Na_v1.7$ expression and in mice bladder DRGs, vascular endothelial growth factor treatment upregulates VGSC expression and activity (Brackenbury & Djamgoz, 2007; Malykhina *et al.*, 2012).

Functionally, *in vitro* evidence has linked increased α-subunit activity in carcinoma cells with migration and invasiveness (Fraser *et al.*, 2003; Bennett *et al.*, 2004; Gao *et al.*, 2010; Hernandez-Plata *et al.*, 2012; Lopez-Charcas *et al.*, 2018). Similarly, in cervical cancer cells, $Na_v1.6$ stimulates matrix metalloprotease-2-mediated degradation of the extracellular matrix leading to invasion (Lopez-Charcas *et al.*, 2018). Microarray analysis of siRNA knockdown models showed that $Na_v1.5$ activity regulates a transcriptional network implicated in colorectal cancer invasiveness, including genes involved in cell signalling and membrane remodelling (House *et al.*, 2010). Lastly, an increase in intracellular Na^+, in cancer cells, is linked with a shift to glycolytic metabolic activity, increased proliferation and increased invasion (Leslie *et al.*, 2019). Further functions of VGSCs in breast cancer have been proposed, but they will be highlighted in chapter 1.4.7.1.

β-subunit expression is also deregulated in cancer cells. β1 is upregulated in breast cancer samples and is more highly expressed in highly metastatic compared to weakly metastatic prostate cancer cell lines, discussed in more detail in chapter 1.4.7.1 (Diss *et al.*, 2008; Nelson *et al.*, 2014). β2 also appears to be tumorigenic. β2 expression is increased in metastatic prostate tumour (Jansson *et al.*, 2014). Perineural invasion is common in prostate cancer and weakly metastatic LNCaP prostate cancer cells overexpressing β2 demonstrate an increased association with spinal cord axons and increase migration, invasion and proliferation *in vitro* (Jansson *et al.*, 2012; Jansson *et al.*, 2014). Despite the pro-metastatic behaviour of β2 *in vitro*, LNCaP-β2 cells inhibit

tumour growth, relative to LNCaP cells, when implanted into mice, suggesting β2 expression might be stage-specific during cancer progression (Jansson *et al.*, 2012). Unlike β1 and β2, β3 and β4 are considered tumour suppressive. *SCN3B* expression is strongly upregulated by p53 following DNA damage and β3 expression induces apoptosis and suppresses colony formation in osteosarcoma and glioblastoma cell lines (Adachi *et al.*, 2004). β4 expression is downregulated in thyroid and high-grade breast cancer and β4 expression is associated with favourable survival (Bon *et al.*, 2016; Gong *et al.*, 2018).

1.4.7.1 Breast cancer

The most established link between VGSCs and cancer, thus far, is in breast cancer. In women, breast cancer was the most frequently diagnosed cancer (1.7 million), constituting 30 % of female cancer diagnoses, and leading cause of female cancer-related deaths (521,900) worldwide in 2012 (Torre *et al.*, 2017; Siegel *et al.*, 2018). Breast cancer has a relatively good survival rate relative to other cancers (90 %), however this drops dramatically by breast cancer subtype and tumour stage (Siegel *et al.*, 2018).

Breast cancer is stratified by the expression profile of three receptors, oestrogen receptor, progesterone receptor and human epidermal growth factor receptor 2 (Sorlie *et al.*, 2001). Around 75 % of breast cancers are oestrogen receptor-positive (with all progesterone receptor-positive cases being oestrogen receptor-positive) and 10 % are positive for human epidermal growth factor receptor 2 expression (Cortet *et al.*, 2018). Around 10 - 15 % of breast cancers are negative for all receptors, this subtype is termed triple negative breast cancer (TNBC) (Cadoo *et al.*, 2013; Cortet *et al.*, 2018). Over 75 % of breast tumours with germline *BRCA1* mutations have a TNBC phenotype (Schmadeka

et al., 2014). TNBC has the worst prognosis, relative to other breast cancer subtypes, with the lowest overall survival and 25 - 30 % of early diagnoses progressing to metastasis (Sorlie *et al.*, 2001; Morris *et al.*, 2012; Jin *et al.*, 2018).

So far, three VGSC subunits have been implicated in breast cancer. $Na_v1.5$ protein, in particular that of the neonatal splice variant of $Na_v1.5$ (Yamaci *et al.*, 2017), is upregulated in breast tumours relative to normal breast tissue, where its expression correlates with β1 (Nelson *et al.*, 2015b). *SCN5A* mRNA is upregulated in invasive breast tumour tissue relative to normal tissue and high *SCN5A* mRNA expression correlates with decreased overall survival (Yang *et al.*, 2012). Likewise, *SCN1B* expression is upregulated in invasive breast tumours compared to normal tissue (Nelson *et al.*, 2014). β4, on the other hand, is downregulated in breast tumour tissue relative to normal tissue and *SCN4B* downregulation correlates with decreased survival (Bon *et al.*, 2016). The following paragraphs of this chapter will focus on the proposed functions of $Na_v1.5$/ β1/ β4 in breast cancer.

$Na_v1.5$, particularly the neonatal splice variant, is upregulated in metastatic breast cancer samples (Fraser *et al.*, 2005; Yang *et al.*, 2012). $Na_v1.5$ increases breast cancer cell migration and invasiveness *in vitro* (Yang *et al.*, 2012). Likewise, treatment of breast cancer cells with the *Xenopsylla cheopis* salivary protein, FS50, inhibits $Na_v1.5$ activity and reduces migration *in vitro* (Zhang *et al.*, 2018a). Additionally, EGF treatment, which stimulates epithelial-to-mesenchymal transition in breast cancer cells *in vitro*, functions through upregulation of $Na_v1.5$ (Gonzalez-Gonzalez *et al.*, 2019). The TNBC cell line, MDA-MB-231, has been used extensively in implicating VGSCs in breast cancer, raising the possibility of targeting VGSCs in TNBC. VGSC expression is enriched within the lamellipodia of MDA-MB-231 (Yang *et al.*, 2012). In a xenograft tumour model, implanted

MDA-MB-231 breast cancer cells in which $Na_v1.5$ was downregulated with shRNA developed smaller primary tumours and showed reduced metastasis (Nelson *et al.*, 2015b). Similarly, treatment of breast tumour-bearing mice with the VGSC-blocking antiepileptic phenytoin decreased tumour growth and metastasis (Nelson *et al.*, 2015a). Mechanistically, $Na_v1.5$ downregulation leads to a reduced mesenchymal morphology and decreased CD44 expression, a known oncogene in breast cancer, which stimulates distant metastasis (McFarlane *et al.*, 2015; Nelson *et al.*, 2015b). Additional mechanisms have been proposed for VGSC-induced metastasis. For example, VGSC-induced acidification of the perimembrane area, via enhanced H^+ efflux through Na^+-H^+ exchanger 1 (NHE1), stimulates cathepsin-B-mediated degradation of the extracellular matrix, permitting invasion (Gillet *et al.*, 2009; Brisson *et al.*, 2011).

β1 is upregulated in breast cancer samples and is more robustly expressed in highly metastatic compared to weakly metastatic prostate cancer cell lines (Diss *et al.*, 2008; Nelson *et al.*, 2014). Overexpressing β1-GFP in MDA-MB-231 cells promotes primary tumour growth and metastasis to multiple organs when grafted into mice, compared to implanted MDA-MB-231 cells (Nelson *et al.*, 2014). The β1-induced increase in primary and secondary tumour growth was accompanied by a decrease in apoptotic cleaved caspase-3 staining, no change in proliferative Ki67 staining and an increase in endothelial CD31 staining, suggesting increased apoptotic resistance and vascularisation underlie the tumorigenic influence of β1 (Nelson *et al.*, 2014). *In vitro*, MDA-MB-231-β1-GFP cells demonstrate increased cell-cell adhesion, I_{Na} and process outgrowth, the latter of which can be inhibited by blocking I_{Na} (Chioni *et al.*, 2009; Nelson *et al.*, 2014). Interestingly, MDA-MB-231-β1-GFP cells show decreased motility and proliferation compared to MDA-MB-231-GFP cells and knockdown of endogenous β1 in the breast cancer cell line MCF-7 increases cell migration (Chioni *et al.*, 2009). A similar phenomenon is observed in cervical cancer cells, where β1 expression decreases cell

migration (Sanchez-Sandoval & Gomora, 2019). Furthermore, treatment of mouse melanoma B16F10 cells with the proposed anti-cancer polymethoxyflavone, casticin, inhibits cell migration and invasion and causes a concomitant genomic upregulation of *SCN1B* (Shih *et al.*, 2017). β1 therefore appears to have a negative influence on migration *in vitro* and potentially induces tumour growth and metastasis through an increase in apoptotic resistance and transcellular adhesion.

Silencing of β4 in MDA-MB-231 cells increases primary tumour growth and metastasis in mice, relative to MDA-MB-231 cells overexpressing β4 (Bon *et al.*, 2016). Furthermore, loss of β4 increased α-independent, RhoA-mediated cancer cell migration and invasion (Bon *et al.*, 2016). Likewise, siRNA knockdown of β4 in cervical cancer cells increases cellular invasion (Sanchez-Sandoval & Gomora, 2019). β-subunits may contribute to cancer via increasing membrane expression of α-subunits; however the situation may be more complex. For example, the expression profile of β-subunits in cancer is not consistent, β1 and β2 are generally considered oncogenic whereas β3 and β4 are tumour suppressive (Adachi *et al.*, 2004; Jansson *et al.*, 2012; Nelson *et al.*, 2014; Bon *et al.*, 2016). Furthermore, β-subunit expression is high in weakly metastatic breast carcinoma MCF-7 cells and low in metastatic breast carcinoma MDA-MB-231 cells (Chioni *et al.*, 2009). The involvement of β-subunits in cancer is hence complex and poorly understood. β-subunit expression in cancer could depend on various factors, such as the site and stage of the tumour, the accompanying expression profile of other VGSC subunits, or other non-conducting roles of β-subunit.

MDA-MB-231 (triple-negative) and MCF-7 (oestrogen receptor positive) are two commonly used breast cancer cell lines. Both cell lines were isolated by pleural effusion, however MCF-7 cells are less metastatic and have retained epithelial-like cell

characteristics (Soule *et al.*, 1973), whereas MDA-MB-231 cells are highly metastatic and mesenchymal-like (Cailleau *et al.*, 1974). Interestingly, these two cell lines have complimentary VGSC subunit expression. MDA-MB-231 cells are characterised by high α-subunit expression (producing a visible Na^+ current) and low β-subunit expression, whereas MCF7 cells display low α-subunit expression, an absent Na^+ current, and high β-subunit expression (Fraser *et al.*, 2005; Chioni *et al.*, 2009). PCR analysis demonstrated mRNA for $Na_v1.5$ (neonatal splice variant), $Na_v1.6$ (multiple splice variants) and $Na_v1.7$ (neonatal splice variant) in both MCF-7 and MDA-MB-231 cells, with global α-subunit mRNA levels 100-fold higher in MDA-MB-231 cells than MCF-7 cells (Fraser *et al.*, 2005). However, as no Na^+ current or $Na_v1.5$ immunoreactivity was detectable in MCF-7 cells, it appears α-subunit protein is not present (Fraser *et al.*, 2005). In MDA-MB-231 cells, ~ 80 % of α-subunit mRNA is for $Na_v1.5$, which is supported by the electrophysiology data demonstrating ~ 85 % of the Na^+ current is carried by tetrodotoxin-resistant α-subunits, with $Na_v1.5$ mRNA being the only tetrodotoxin-resistant channel mRNA present in these cells (Fraser *et al.*, 2005). In regard to β-subunits, β-subunit mRNA is 30-fold greater in MCF-7 cells compared to MDA-MB-231 cells (Chioni *et al.*, 2009). Both cell lines predominantly express *SCN1B* mRNA, with trace amounts of *SCN2B* and *SCN4B* mRNA (Chioni *et al.*, 2009).

1.5 The impact of secretase cleavage on cellular homeostasis and disease

1.5.1 Introduction to secretase enzymes

Secretases are a family of enzymes that cleave over 70 single-pass transmembrane proteins (Haapasalo & Kovacs, 2011; Pardossi-Piquard & Checler, 2012). Canonical secretase cleavage occurs sequentially; an initial extracellular cleavage event by α- or

β-secretase releases a soluble extracellular domain (ECD) and leaves a C-terminal fragment (CTF) within the membrane. The CTF is then cleaved intramembranously by γ-secretase, releasing an intracellular domain (ICD) and leaving a short transmembrane peptide (Chow *et al.*, 2010). Through cleavage of a vast array of transmembrane proteins, secretases provide a vital link in conducting intracellular signalling pathways in response to extracellular cues, as well as regulating membrane protein turnover (De Strooper *et al.*, 1998; Pardossi-Piquard & Checler, 2012). Many secretase-generated ICDs translocate to the nucleus and regulate transcription, such as the ICDs from amyloid precursor protein (APP) (Kimberly *et al.*, 2001), Alcadein (Araki *et al.*, 2004), CD44 (Okamoto *et al.*, 2001) and Notch (Schroeter *et al.*, 1998). ECDs can also be involved in cell signalling, e.g. the APP-ECD (Murphy & LeVine, 2010). Secretases emerged as a major therapeutic target after the discovery that secretase processing of APP produces the β-amyloid neuritic plaques observed in Alzheimer's disease, the leading cause of dementia worldwide (Murphy & LeVine, 2010).

Secretase expression is enriched in the brain, but a widespread tissue distribution is also observed by northern blotting (Lee *et al.*, 1996; Vassar *et al.*, 1999). The widespread tissue distribution of secretases is reflected in the diverse range of roles and diseases in which they are implicated. Secretases are vital in development, including early embryonic patterning (Donoviel *et al.*, 1999), nephrogenesis (Cheng *et al.*, 2003), angiogenesis (Boulton *et al.*, 2008), cardiac morphogenesis (Nakajima *et al.*, 2004) and neurogenesis (Capell *et al.*, 1997). Mice deficient in γ-secretase are born with gross cerebral and skeletal deformities and die shortly after (Shen *et al.*, 1997). In adults, secretases maintain neuronal progenitor cell proliferation and plasticity (Gadadhar *et al.*, 2011), maintain synaptic integrity (Inoue *et al.*, 2009; Suzuki *et al.*, 2012), regulate cognition (Laird *et al.*, 2005), and regulate haematopoiesis (Grabher *et al.*, 2006), amongst other roles (Jurisch-Yaksi *et al.*, 2013). Aberrant secretase cleavage is

implicated in autoimmunity (Tournoy *et al.*, 2004), cardiomyopathy (Gianni *et al.*, 2010), Alzheimer's disease (Scheuner *et al.*, 1996) and cancer (Kondratyev *et al.*, 2012).

This section will focus on the roles of secretases in cellular homeostasis and disease and the burgeoning evidence of the role of secretase cleavage in regulating β-subunit function. α/β/γ-secretases will remain the focus, however, recent work examining APP has discovered non-canonical forms of secretase cleavage that can come before α/β-secretase; δ-secretase (Zhang *et al.*, 2015) and η-secretase (Willem *et al.*, 2015). In addition, the promiscuous enzyme responsible for γ-secretase cleaves at two other sites, known as ζ-cleavage and ε-cleavage, which occur four and seven residues downstream of the γ-secretase cleavage event in the C-terminal direction, respectively (Gu *et al.*, 2001; Zhao *et al.*, 2004).

1.5.1.1 α-secretase

α-secretase refers to a family of enzymes capable of α-cleavage of APP (Esch *et al.*, 1990). The molecular identity of α-secretase was eventually revealed to be a disintegrin and metalloprotease 10 (ADAM10), a member of the larger ADAM family, consisting of over 30 enzymes (Lammich *et al.*, 1999; Lichtenthaler, 2011). ADAMs consist of a short cytoplasmic and transmembrane domain, with extracellular metalloproteinase, EGF-like repeat, cysteine-rich and disintegrin-like domains (Giebeler & Zigrino, 2016). Initial cleavage of an inhibitory prodomain is required for Zn^{2+} binding to the metalloprotease domain, producing the catalytically active protein (Loechel *et al.*, 1999). The disintegrin-like domain facilitates cell adhesion via interactions with integrin (Eto *et al.*, 2000). ADAM10 is enriched within the Golgi apparatus and at the plasma membrane, where it is the major, constitutive proteolytic pathway for APP (Tomita *et al.*, 1998; Lammich *et al.*, 1999). ADAM10 cleavage prevents β-amyloid deposition (Esch *et al.*, 1990).

Cleavage can occur as soon as APP undergoes O-glycosylation in the Golgi apparatus (Tomita *et al.*, 1998). α-cleavage is also the major proteolytic pathway for N-cadherin, CD44, Neuregulin-1, Nectin-1 and Notch (Kohutek *et al.*, 2009; Murthy *et al.*, 2012; Hartmann *et al.*, 2015; Buchanan *et al.*, 2017). ADAM10 activity is regulated by various signalling pathways and can be stimulated artificially by the protein kinase C activator phorbol 12-myristate 13-acetate (PMA), which stimulates translocation of ADAM10 to the plasma membrane (Kohutek *et al.*, 2009; Lichtenthaler, 2011).

1.5.1.2 β-secretase

β-secretase cleavage is facilitated by β-site APP cleaving enzyme 1 and 2 (BACE1 and BACE2) and competes with α-secretase for the initial extracellular cleavage event (Chow *et al.*, 2010). Much attention has been given to BACE1 since it was revealed that sequential β- and γ-secretase cleavage produces the β-amyloid fragment of APP (Chow *et al.*, 2010). BACE1 is an aspartyl protease, consisting of a short cytoplasmic tail, single transmembrane domain and a large, glycosylated extracellular domain (Venugopal *et al.*, 2008). BACE1 is catalytically active at the cell surface, in the endolysosomal pathway and at the trans-Golgi network (Tomita *et al.*, 1998; Huse *et al.*, 2000; Chyung & Selkoe, 2003; Koh *et al.*, 2005). The subcellular location of β-cleavage remains a contentious issue, as the classical view assumes β-cleavage occurs at the plasma membrane, and plasma membrane BACE1 is even visible by optical sectioning of the membrane using total internal reflection fluorescence microscopy (Bauereiss *et al.*, 2015; Bhattacharyya *et al.*, 2016). Furthermore, β-secretase cleavage of APP is enhanced slightly following inhibition of receptor-mediated endocytosis by expressing a dominant-negative dynamin I mutant (Chyung & Selkoe, 2003). However,like other aspartyl proteases, BACE1 substrate binding is optimal at pH 4-5, the pH found within the endolysosomal pathway (Gruninger-Leitch *et al.*, 2002). Additionally, lysosomal disruption with bafilomycin A

reduces β-amyloid production in various cell types, suggesting a dependency on acidic compartments for β-cleavage (Knops *et al.*, 1995).

1.5.1.3 γ-secretase

Unlike α- and β-secretases, γ-secretase is a multimeric complex. γ-secretase is a tetramer; consisting of the enzymatic, nine-transmembrane pass presenilin (PS1), which is cleaved by autoproteolysis into two polypeptides (NTF and CTF) within the seventh transmembrane domain (TMD7) that remain in association (Capell *et al.*, 1998). Two aspartic acid residues in TMD6 and TMD7 constitute the catalytic site (Wolfe *et al.*, 1999). Presenilin associates with nicastrin, a single-pass glycoprotein, PEN-2, a double-pass transmembrane protein, and APH-1, a seven-pass transmembrane protein (Smolarkiewicz *et al.*, 2013). γ-secretase inhibitors typically bind allosterically to presenilin, due to the homology between the active sites of presenilin and signal peptidase (Sato *et al.*, 2008). For example, N-[N-(3,5-difluorophenacetyl)-L-alanyl]-S-phenylglycine t-butyl ester (DAPT) sits in a hydrophobic cavity on the cytoplasmic side of the protein, altering the conformation of TMD2 and TMD6 of presenilin, greatly reducing structure flexibility (Bai *et al.*, 2015). Presenilin expression is seen in the nuclear envelope (Kimura *et al.*, 2001), endoplasmic reticulum (Xia *et al.*, 1998), mitochondria (Area-Gomez *et al.*, 2009), Golgi apparatus (Xia *et al.*, 1998; Zhang *et al.*, 1998), endosomes (Vetrivel *et al.*, 2004), lysosomes (Pasternak *et al.*, 2003) and plasma membrane (Chyung *et al.*, 2005). Whether active γ-secretase complexes are found in all these locations is unclear, however APP cleavage by γ-secretase has been identified at the plasma membrane and in the Golgi apparatus (Xia *et al.*, 1998; Chyung *et al.*, 2005). Furthermore, γ-secretase cleavage of Notch occurs in endosomal compartments (Parks *et al.*, 2000). Intramembranous γ-secretase cleavage results in ICD release, the soluble peptide implicated in nuclear localisation and transcriptional regulation in over 30 substrates (Pardossi-Piquard & Checler, 2012).

1.5.2 Secretase-mediated regulation of protein function and localisation

The extent of secretase cleavage on VGSC β-subunit function is still unclear, however the impact of secretase cleavage on other substrates is very well documented. The role of proteolysis in regulating the function of two major substrates, APP and Notch, and its implication in disease will be discussed (Figure 1.7).

1.5.2.1 Amyloid precursor protein

APP is a single-pass transmembrane glycoprotein (~100 kDa) that is sequentially cleaved, first by α- or β-secretase, then by γ-secretase (Haapasalo & Kovacs, 2011). Three proteolytic fragments are of particular interest, APP-ICD, produced following γ-secretase cleavage, β-amyloid, the short transmembrane fragment generated by β- and γ-secretase cleavage, and APP-ECD (known as soluble APP (sAPP)), which is released following the initial α- or β-secretase cleavage event. APP-ICD translocates to the nucleus and regulates gene expression (Cao & Sudhof, 2001). sAPP is involved in paracrine signalling. and has putative neuroprotective effects through suppression of action potential firing via direct regulation of presynpatic $GABA_R$ (Reinhard *et al.*, 2013; Rice *et al.*, 2019). sAPPα, produced by α-secretase, protects neurons from excitotoxicity and induces neurite outgrowth *in vitro* (Mattson *et al.*, 1993; Gakhar-Koppole *et al.*, 2008). sAPPα also protects neurons against β-amyloid-induced neuronal damage and tau hyperphoshorylation (Tackenberg & Nitsch, 2019). sAPPβ, however, lacks the neuroprotective effects of sAPPα and is involved in synaptic pruning during development (Nikolaev *et al.*, 2009).

APP was discovered in 1987, following cloning and sequencing of the full-length protein responsible for β-amyloid, which had been identified as the aggregate involved in neuritic

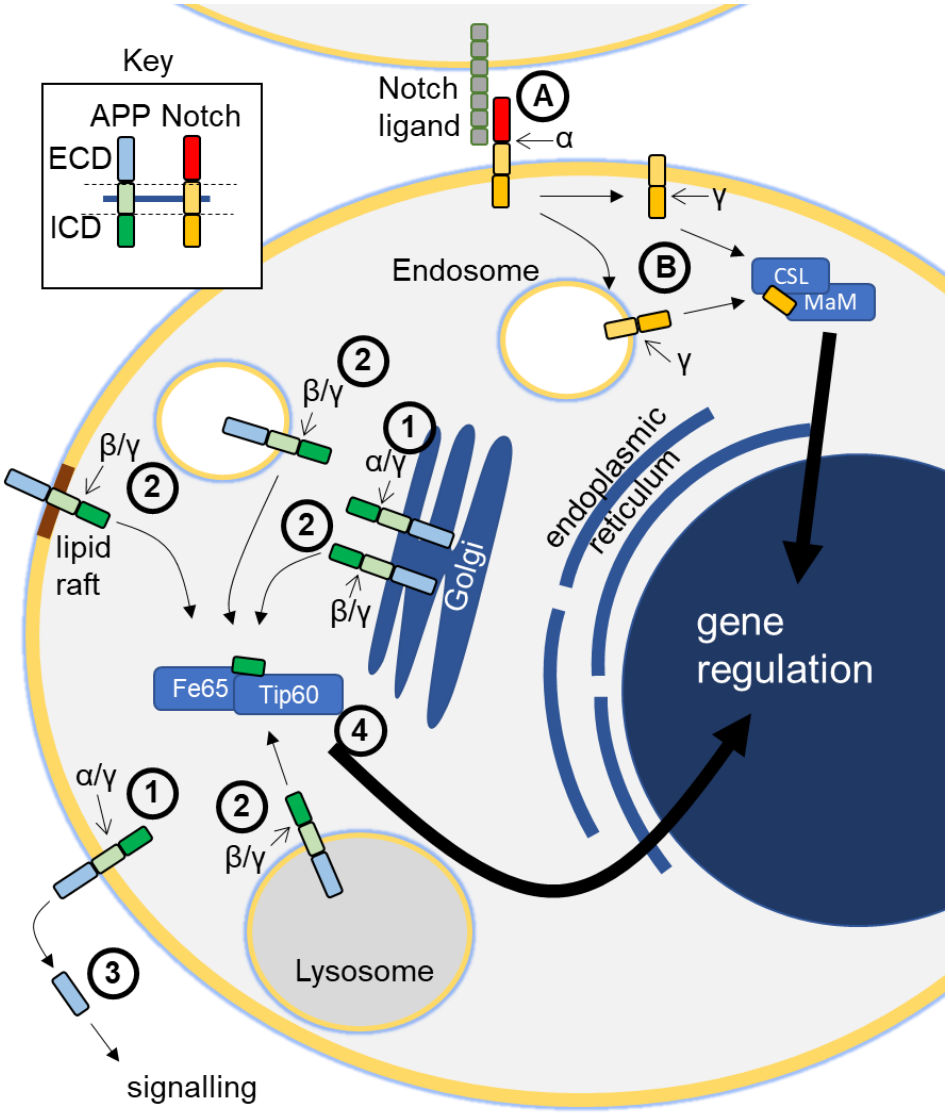

Figure 1.7 Secretase processing of amyloid precursor protein and Notch

1. APP is cleaved by α-secretase within the Golgi apparatus and at the plasma membrane (Lammich *et al.*, 1999; Tan & Gleeson, 2019). 2. β-secretase cleavage also occurs within the Golgi apparatus and at the plasma membrane, particularly within lipid rafts, as well as in the endolysosomal pathway (Tomita *et al.*, 1998; Huse *et al.*, 2000; Chyung & Selkoe, 2003; Cordy *et al.*, 2003; Tam & Pasternak, 2015). γ-secretase cleavage occurs at the plasma membrane and at internal membranes (Xia *et al.*, 1998; Chyung *et al.*, 2005; Tam & Pasternak, 2015). 3. α-secretase cleavage releases APP-extracellular domain (ECD (sAPPα)) that is involved in protecting neurons from neurotoxicity (Mattson *et al.*, 1993), decreasing intraneuronal tau hyperphosphorylation (Tackenberg & Nitsch, 2019), and promoting neurite outgrowth (Gakhar-Koppole *et al.*, 2008). sAPPβ, on the hand, has only been to developmental synaptic pruning (Nikolaev *et al.*, 2009). 4. APP-intracellular domain (ICD), produced preferentially from β-cleavage, is involved in gene regulation after complexing with Fe65 and Tip60 (Cao & Sudhof, 2001). A. Notch is cleaved by α-secretase, at the plasma membrane, following transcellular interactions with Notch ligands (Mumm *et al.*, 2000). B. Notch-ICD is produced at the plasma membrane, or intracellularly, and regulates gene expression following binding to CSL and Mastermind (MaM) (Vasquez-Del Carpio *et al.*, 2011; Baron, 2012).

plaques a few years earlier (Glenner & Wong, 1984; Kang *et al.*, 1987; Alzheimer *et al.*, 1995). The function of APP is still uncertain, although it appears to be involved in neurodevelopment and synaptogenesis, through its ECD (Roch *et al.*, 1994; Young-Pearse *et al.*, 2007). Surprisingly, APP KO mice display only minor deficits in motor control and long-term memory formation (Senechal *et al.*, 2008). However triple knockdown of APP and its homologues, APP-like proteins 1 and 2 (APLP1 and APLP2), produces cortical deformities and is lethal shortly after birth (Herms *et al.*, 2004).

APP is mainly intracellularly localised, with the majority of APP being trafficked from the trans-Golgi network (TGN) to lysosomes, potentially via early and late endosomes (Caporaso *et al.*, 1994; Tam & Pasternak, 2015; Toh *et al.*, 2017). It is processed by secretases along the way, with β-amyloid generated in the TGN and lysosomes (Choy *et al.*, 2012; Tam *et al.*, 2014). Furthermore, the low pH found in the endolysosomal pathway favours β-secretase cleavage of APP and permits membrane-embedded β-amyloid shedding into the luminal space, a prerequisite for extracellular β-amyloid deposition (Shi *et al.*, 2019). α-secretase cleavage also occurs intracellularly and is the predominant proteolytic pathway for APP, with ~ 4:1 ratio of α-secretase to β-secretase cleavage occurring in the TGN (Tan & Gleeson, 2019). However, APP, and its interaction with BACE1, is present at the plasma membrane (Bauereiss *et al.*, 2015). Dimerisation, palmitoylation and lipid raft localisation favour β-secretase cleavage, potentially requiring initial endocytosis (Cordy *et al.*, 2003; Ehehalt *et al.*, 2003; Harris *et al.*, 2009; Isbert *et al.*, 2012; Bhattacharyya *et al.*, 2016). Internalised APP can remain in recycling endosomes or be trafficked straight to the lysosome (Lorenzen *et al.*, 2010). Treatment with the plant sterol, stigmasterol, decreases β-amyloid production by preventing endocytosis (Burg *et al.*, 2013). γ-secretase cleavage is active at the plasma membrane, as well as internal membranes (Xia *et al.*, 1998; Chyung *et al.*, 2005). The majority of γ-secretase cleavage is thought to occur at the TGN (Vorobyeva *et al.*, 2014).

Transcriptionally active APP-ICD is produced preferentially after β- and γ-secretase cleavage (Belyaev *et al.*, 2010). APP-ICD binds the nuclear adaptor protein Fe65 and the histone acetylase Tip60, via a tyrosine-glutamic acid-asparagine-proline-threonine-tyrosine (YENTPY) domain (Borg *et al.*, 1996; Cao & Sudhof, 2001). APP-ICD regulates the transcription of neprilysin (β-amyloid degrading enzyme), APP, BACE1 and GSK3β, amongst others (von Rotz *et al.*, 2004; Pardossi-Piquard *et al.*, 2005; Pardossi-Piquard & Checler, 2012). Nuclear APP-ICD is difficult to detect because of its high turnover rate. Techniques used to image APP-ICD include overexpression of the APP-ICD itself, treatment with the nuclear export inhibitor Leptomycin B, and treatment with the proteasome inhibitor cycloheximide (von Rotz *et al.*, 2004; Gersbacher *et al.*, 2013). When visible, the APP-ICD, along with Fe65 and Tip60, form a speckled pattern within the nucleus (von Rotz *et al.*, 2004).

A link between APP-ICD and Down syndrome has recently emerged (Guidi *et al.*, 2017). Down syndrome is caused by triplication of chromosome 21, which contains the *APP* gene, and is associated with intellectual disability (Strydom *et al.*, 2018). Neuronal precursor cells (NPCs), in a Down syndrome mouse model, demonstrate elevated APP-ICD levels (Trazzi *et al.*, 2011). In NPCs, APP-ICD increases Ptch1 expression, inhibiting Sonic Hedgehog signalling and disrupting NPC proliferation (Trazzi *et al.*, 2011). Postnatal treatment with a γ-secretase inhibitor subsequently restored NPC proliferation in the subventricular zone and hippocampus (Giacomini *et al.*, 2015).

APP overexpression is seen in a range of cancers, including breast, pancreas, prostate and thyroid (Pandey *et al.*, 2016). APP enhances cell migration (Tang *et al.*, 2010; Jiang *et al.*, 2013) and proliferation (Venkataramani *et al.*, 2010; Lim *et al.*, 2014; Zhang *et al.*, 2018b) in various cancer cell lines *in vitro*. sAPPα is elevated in pancreatic cancer cells

and enhances cancer cell proliferation and colony formation (Woods & Padmanabhan, 2013). However, the lack of understanding of APP function limits mechanistic insight into the contribution of APP to tumour progression. APP influences migration of neuronal precursor cells during development, suggesting APP may be recapitulating developmental mechanisms to stimulate tumour cell progression (Young-Pearse *et al.*, 2007).

1.5.2.2 Notch

Notch processing and function is well understood compared to APP. Notch is a large, single-pass transmembrane protein that requires transactivation from a ligand on a different cell, stimulating α-cleavage at the plasma membrane followed by γ-cleavage, which occurs at the plasma membrane or in endocytic vesicles (Mumm *et al.*, 2000). Unlike APP-ICD, Notch-ICD contains two nuclear localisation signals, unequivocally implicating Notch-ICD in nuclear signalling (Hori *et al.*, 2013). Notch-ICD interacts with CSL and Mastermind (Mam), a dimeric transcriptional repressor, to form a transcription activating complex (Vasquez-Del Carpio *et al.*, 2011; Baron, 2012). Notch-ICD/CSL/Mam initiates a complex transcriptional network through inducing expression of basic-helix-loop-helix transcription factors (Davis & Turner, 2001). Notch signalling has a well-documented role in neural patterning during development, promoting neural differentiation in cells with active Notch signalling (Lowell *et al.*, 2006). Notch signalling also regulates proliferation of embryonic stem cells (Fox *et al.*, 2008).

Notch was first implicated in cancer following the identification of a fusion protein between T-cell receptor and Notch in T lymphoblastic leukaemia (TLL), producing a constitutively active Notch, which stimulated proliferation and inhibited cell differentiation (Ellisen *et al.*, 1991). Analysis of bone marrow of TLL patients implicated Notch signalling

in over 50 % of TLL cases (Weng *et al.*, 2004). Elevated Notch promotes tumour growth in TLL through activation of *c-Myc* transcription, a known oncogene in TLL, and downregulation of *PTEN,* a known tumour suppressor (Felsher & Bishop, 1999; Palomero *et al.*, 2006; Weng *et al.*, 2006; Palomero *et al.*, 2007). Notch has since been thoroughly implicated in a diverse range of cancers (Aster *et al.*, 2017). Notch expression level correlates with poor patient prognosis in breast and non-small cell lung cancer (Reedijk *et al.*, 2005; Donnem *et al.*, 2010). In mammary oncogenesis, Notch drives cyclin-D1 expression, directly stimulating proliferation (Kiaris *et al.*, 2004). Blocking of Notch activity with an antibody that binds Notch-ECD and inhibits α-secretase cleavage prevented tumour growth in xenograft mouse models of lung and colon cancer, implicating secretase processing of Notch as the oncogenic factor (Wu *et al.*, 2010). Furthermore, immunohistochemistry analysis of oral preneoplastic and neoplastic tissue demonstrated Notch-ICD+/c-Myc+ double positive cases showed worst overall survival, further implicating secretase processing of Notch in cancer (Gokulan & Halagowder, 2014).

1.5.3 The involvement of secretases in cancer

Emerging evidence has implicated secretase cleavage in cancer, particularly α- and γ-secretase. The effects of γ-secretase inhibition have been thoroughly investigated in cancer, discussed in detail in chapter 1.6.1, however these studies are more substrate-focused and do not report on the specific expression levels and function of γ-secretase. Therefore, this chapter will focus on what is known about the expression and the roles of the enzymes themselves. In colorectal cancer and lung cancer patients, increased α-secretase enzyme activity is observed in serum and tumour cells, respectively (Walkiewicz *et al.*, 2017; Yoneyama *et al.*, 2018). In prostate tumour sections, no difference in ADAM10 expression levels are observed compared to normal tissue, how a pronounced shift to nuclear expression from membrane expression is observed in high

grade tumours (McCulloch *et al.*, 2004). ADAM10 is overexpressed in malignant mesothelioma relative to control tissue, at the mRNA and protein level, and ADAM10 downregulation decrease tumour volume in a xenograft mouse model (Sepult *et al.*, 2019). (Walkiewicz *et al.*, 2017; Yoneyama *et al.*, 2018). Furthermore, ADAM10 inhibition in a xenograft mouse model of colorectal cancer inhibits tumour growth (Atapattu *et al.*, 2016), whereas ADAM10 overexpression induces metastasis in a similar model (Gavert *et al.*, 2007). ADAM10 cleavage stimulates migration in a range of cancer cells, however the implicated substrate can vary, such as Notch in colorectal cancer (Atapattu *et al.*, 2016), APP in breast cancer (Tsang *et al.*, 2018), and L1-CAM in colon cancer (Gavert *et al.*, 2007). Likewise, presenilin-1 is overexpressed in gastric cancer and the presenilin-1 binding protein, APH1A, is overexpressed in pancreatic cancer (Li *et al.*, 2016a; Jeon *et al.*, 2019). Knockdown of presenilin-1 expression in gastric cancer cells reduces metastasis in a xenograft mouse model, presumably through reduced Notch signalling (Chen *et al.*, 2019). A separate group demonstrated overexpression of presenilin-1 in gastric cancer cells enhances metastasis in a xenograft mouse model, however they implicated E-cadherin as the underlying substrate (Li *et al.*, 2016a). The involvement of β-secretase in cancer has been less well explored, however it has been demonstrated that BACE1 is downregulated in gastric cancer and invasive ductal breast carcinoma (Esfandi *et al.*, 2019; Yaghoobi *et al.*, 2019). Additionally, anisomycin, an antibiotic with antiproliferative and anti-invasive effects on ovarian cancer cells *in vitro* and *in vivo*, functions through downregulation of BACE1 (Chen *et al.*, 2016), suggesting that β-secretase cleavage, unlike α- and γ-, is tumour suppressive. In summary, secretases have been functionally implicated in various cancers.

1.5.4 The involvement of secretase cleavage in β-subunit function and disease

β-subunits have also been identified as secretase substrates, although it remains an underexplored area of research. β-subunits are cleaved by β-secretase and γ-secretase in primary mouse neurons and β2 was further shown to be a α-secretase substrate in Chinese hamster ovary cells (Kim *et al.*, 2005; Wong *et al.*, 2005).

Functionally, evidence suggests an involvement of secretase processing in β subunit-mediated neurodevelopment. γ-secretase cleavage of β1 stimulates β1-mediated neurite outgrowth in cerebellar granule neurons from postnatal day 14 mice (Brackenbury & Isom, 2011). γ-secretase cleavage of β2 stimulates cell adhesion and migration in CHO cells; two processes that are implicated in β1-mediated development, in the form of corticospinal tract fasciculation and CGN migration (Kim *et al.*, 2005; Brackenbury *et al.*, 2008). β-secretase cleavage of β4 facilitates neurite outgrowth and reduces filopodial protrusion in Neuro2a cells (Miyazaki *et al.*, 2007). Furthermore, BACE1 null mice present a decreased efficiency of β4-induced open channel block, causing a reduction in spontaneous action potential firing *in vitro* (Huth *et al.*, 2011).

In terms of disease, the link between BACE1, the enzyme responsible for β-secretase cleavage, β2, and excitability in Alzheimer's disease is an emerging area of research (Kovacs *et al.*, 2010). In B104 neuroblastoma cells, secretase processing of β2 resulted in an increase in $Na_v1.1$ protein expression, however this is accompanied by a decrease in I_{Na} as $Na_v1.1$ is retained intracellularly (Kim *et al.*, 2007). Likewise, expression of β2-ICD, the γ-secretase cleavage product, demonstrated nuclear localisation and an increase in $Na_v1.1$ mRNA expression in SH-SY5Y cells, suggesting secretase processing of β2 regulates $Na_v1.1$ expression (Kim *et al.*, 2007). In support of this, transgenic mice overexpressing BACE1 also demonstrated increased $Na_v1.1$ and

BACE1 null mice show decreased $Na_v1.1$ mRNA and surface protein, but an increase in membrane $Na_v1.2$ (Kim *et al.*, 2007; Kim *et al.*, 2011). The familial Alzheimer's disease mutation E280A in presenilin, the enzyme responsible for γ-secretase cleavage, also decreases β2 processing and $Na_v1.1$, mRNA and surface protein, expression (Kim *et al.*, 2014). These results suggest β2 processing by secretase enzymes increases $Na_v1.1$ expression, however, paradoxically, a decrease in I_{Na} is also observed, as $Na_v1.1$ appears to be retained intracellularly. Potentially, full-length, uncleaved β2 is required for membrane trafficking of $Na_v1.1$, suggesting secretase cleavage maintains an equilibrium between neuronal β2 and $Na_v1.1$ levels. Despite uncertainties regarding the link between β2, secretases and α-subunit expression, β2 knockdown in a mouse model of Alzheimer's disease improves cognitive decline and decreases cortical activity, recorded by EEG, suggesting a pathogenic involvement of β2 in Alzheimer's disease (Hu *et al.*, 2017; Hu *et al.*, 2019). Furthermore, reduced $Na_v1.1$ activity is seen in epilepsy due to its expression in inhibitory interneurons, suggesting increased secretase processing of β2 could be leading to seizures via a reduction of $Na_v1.1$ activity (Catterall *et al.*, 2010). However, cleavage of proteins other than β2 would also be affected by global secretase inhibition, for instance BACE1 cleavage also reduces surface expression of contactin, which increases I_{Na}, in mouse primary neurons (Kazarinova-Noyes *et al.*, 2001; Gautam *et al.*, 2014).

1.6 Therapeutic implications of secretases and VGSCs in cancer

1.6.1 Secretase inhibition in cancer

Due to the involvement of Notch in tumorigenesis, γ-secretase inhibitors (GSIs) have developed into a major therapeutic target in cancer. GSIs have demonstrated anti-tumour potency in mouse models of renal carcinoma (Bhagat *et al.*, 2017), breast cancer

in combination with docetaxel (Schott *et al.*, 2013), head and neck squamous cell carcinoma (Mao *et al.*, 2018), lung adenocarcinoma in combination with paclitaxel (Morgan *et al.*, 2017), gastric cancer in combination with fluorouracil (Lee *et al.*, 2015a), and pituitary adenomas (Feng *et al.*, 2019; Zubeldia-Brenner *et al.*, 2019). Furthermore, GSIs have a diverse range of tumour suppressive effects across different cancer types. In gastric cancer, GSI reduced AKT phosphorylation and AKT signalling (Lee *et al.*, 2015a). In head and neck squamous cell carcinoma, GSI reduced the immunosuppressive cell population via inhibition of HES1 expression (Mao *et al.*, 2018). In lung adenocarcinoma cell lines, GSI was most effective in wild-type KRAS- and BRAF-driven cell lines, compared to cell lines expressing mutant KRAS and BRAF (Morgan *et al.*, 2017). In patient-derived breast cancer tumours, a decrease in the CD44+/CD24- cancer stem cell population was observed following treatment (Schott *et al.*, 2013).

Various GSIs have even progressed onto clinical cancer trials. The GSI, PF-03084014, has shown promising results in two small scale trials of patients with Desmoid fibromatosis. An oral dose twice a day for up to 36 months reduced tumour size by >30 % in 29 % of patients (Kummar *et al.*, 2017). A second trial determined 71.4 % of patients achieved a partial response (> 20% reduction in tumour size) with a mean time to response of 11.9 months (Villalobos *et al.*, 2018). Another GSI, RO4929097, originally developed as a treatment for Alzheimer's disease, reached phase II trials but showed no clinical efficacy and was eventually discontinued (Strosberg *et al.*, 2012; De Jesus-Acosta *et al.*, 2014; Diaz-Padilla *et al.*, 2015; Lee *et al.*, 2015b). De Jesus-Acosta *et al.* showed RO4929097 was capable, however, of reducing Notch-mediated gene expression in tumour biopsies and reducing plasma SDF-1, VEGF, IL-6 and IL-8 post-treatment. Another GSI, LY900009, reached phase II trials but was ineffective (Pant *et al.*, 2016). It is not surprising these GSIs were ineffective in phase II trials, as drugs are often delivered as monotherapy to a small cohort of patients at an advanced stage. GSIs

still remain an appealing therapy in cancer treatment, with various more drugs recently passing phase I trials (Aung *et al.*, 2018; Cook *et al.*, 2018).

1.6.2 VGSC inhibition in cancer

The involvement of VGSCs in cancer is an emerging field and was thoroughly discussed in chapter 1.4.7. VGSC inhibitors have not been clinically trialled as anti-cancer drugs, however some burgeoning clinical evidence, using drugs with VGSC inhibiting ability, is available. Perioperative application of local anaesthetic reduces cancer recurrence in patients undergoing prostatectomies (Biki *et al.*, 2008). A retrospective General Practice Research Database study determined previous tricyclic antidepressant (TCA) usage reduces the chance of developing glioma and colorectal cancer (Walker *et al.*, 2011). However, more recent studies have shown current TCA users have an increased risk of developing lung cancer (Boursi *et al.*, 2015). Furthermore, TCA usage post cancer diagnosis did not reduce mortality in glioma or colorectal cancer patients or reduce the risk of breast or colorectal cancer recurrence (Walker *et al.*, 2012; Chubak *et al.*, 2016; Pocobelli *et al.*, 2019). In patients with stage III/IV melanoma, riluzole (an ALS treatment) application reduced tumour metabolic activity (Yip *et al.*, 2009).

Usage of FDA-approved drugs in mouse models of cancer have, more directly, implicated VGSCs in cancer and raise the possibility of repurposing these drugs as cancer treatments. For instance, phenytoin (anti-epileptic) treatment reduces metastasis and increases survival in mice with implanted breast tumours (Nelson *et al.*, 2015a). Furthermore, RS100642 treatment prolongs lifespan in rats with experimentally induced breast tumours (Batcioglu *et al.*, 2012). Lastly, perioperative application of lidocaine reduces pulmonary metastasis in mice with implanted breast tumours (Freeman *et al.*, 2019).

1.7 Project rationale, hypothesis and aims

This study focuses on the involvement of secretase cleavage on β1 function in a breast cancer cell model. β1 is an important protein in regulating excitability and neurodevelopment (Brackenbury & Isom, 2011). Altered β1 function occurs in epilepsy and cancer, amongst other disorders (chapter 1.4) (Bouza & Isom, 2017). Despite being identified as a secretase substrate in 2005, little is known on the functional implication of proteolysis on β1 function (Kim *et al.*, 2005; Wong *et al.*, 2005). However, the presence of secretase processing is an attractive research topic for two reasons. Firstly, secretase enzymes are of immense pharmaceutical interest due to their contribution in Alzheimer's disease and cancer, hence there is a wealth of knowledge already gathered regarding secretases and their substrates, furthermore there is a clinical demand for secretase inhibitors, some of which are currently undergoing clinical trials. Secondly, secretase cleavage theoretically releases two secreted fragments from β1, the extracellular and intracellular domains (ECD and ICD). This has a potentially profound impact on β1 function, as β1 modulates α-subunit function through these domains and induces cell-cell adhesion through the ECD (McCormick *et al.*, 1999; Malhotra *et al.*, 2000; Meadows *et al.*, 2001).

As discussed previously in 1.4.7.1, β1 is overexpressed in invasive breast tumours and increases the metastatic potential of TNBC cells when implanted into mice (Nelson *et al.*, 2014). Furthermore, β1 induces neurite-like outgrowths on breast cancer cells, a feature linked to cancer cell extravasation in breast tumour metastasis (Nelson *et al.*, 2014; Williams *et al.*, 2019). This is intriguing, because the only link thus far between secretase cleavage and β1 function is the requirement for γ-secretase cleavage in β1-induced neurite outgrowth in cerebellar granule neurons (Brackenbury & Isom, 2011). Therefore, secretase cleavage of β1 may be involved in β1-induced breast cancer cell behaviour.

The overall hypothesis of this study was that secretase cleavage regulates β1 function in MDA-MB-231 cells. MDA-MB-231 cells are a useful system to use as there is endogenous α-subunit expression and low β-subunit expression, and overexpressing β1 induces an enlarged I_{Na} and metastatic cell behaviour (Fraser *et al.*, 2005; Chioni *et al.*, 2009; Nelson *et al.*, 2014). The aim was to thoroughly assess the impact of secretase processing on β1 function, particularly β1 localisation, β1-regulated α-subunit modulation and β1-induced cell-cell adhesion, in three ways:

1. Using pharmacological inhibitors of secretase cleavage in MDA-MB-231-β1-GFP cells

2. Using MDA-MB-231 cells overexpressing β1ICD (MDA-MB-231-β1ICD-GFP)

3. Using MDA-MB-231 cells overexpressing a secretase-resistant form of β1 (MDA-MB-231-SRβ1-GFP)

Chapter 2: Methods

2.1 Cell culture

2.1.1 Cell lines

MDA-MB-231, MDA-MB-231-GFP and MDA-MB-231-β1-GFP breast cancer cells were a gift from Prof Lori Isom (University of Michigan). Transfected MDA-MB-231 cell lines were created for this study expressing β1-ICD-GFP, secretase-resistant β1-GFP and β1STOP-GFP (see chapter 2.2 for details). The molecular identity of MDA-MB-231 cells was verified by short tandem repeat analysis (Masters *et al.*, 2001).

2.1.2 Maintenance of cells

Cell culture medium consisted of Dulbecco's Modified Eagle Medium (DMEM, Life Technologies), supplemented with 5 % (v/v) foetal bovine serum (FBS, Life Technologies) and 4 mM L-glutamine (Life Technologies). All transfected cell lines used were Hygromycin B-resistant, apart from MDA-MB-231-GFP cells, which were G418-resistant. Cell culture medium was supplemented with Hygromycin B (100 µg/ml, Invitrogen) or G418 (200 µg/ml, Sigma) for transfected cell lines. Cells were grown in tissue culture-treated 10 cm diameter culture dishes (Corning) and cell culture medium was changed three times per week. Cells were maintained at 37 ^{o}C/5 % CO_2 in a Binder C150 humidified incubator. Passaging was carried out using 0.05 % (v/v) Trypsin-EDTA (Life Technologies) in phosphate buffer saline (PBS, Life Technologies) once cells had reached near-confluency. Cells were not cultured for more than ten passages following thawing from long-term liquid nitrogen storage. Approximately 50,000 cells were typically plated in a 10 cm dish and would reach near-confluency within 7 days.

2.1.3 Freezing and thawing cells

Cells were routinely stored in liquid nitrogen for long-term maintenance. For this, a confluent 10 cm dish of cells was trypsinised until cells had detached from the dish. The cell suspension was then removed, centrifuged (100 g, 5 min, room temperature) and the pellet resuspended in 1 ml of freezing medium containing 70 % (v/v) DMEM, 20 % (v/v) FBS and 10 % (v/v) cell culture grade dimethylsulfoxide (DMSO, PanReac AppliChem). Aliquots of suspension (200 µl) were transferred into cryovials (Greiner) and stored at -80 ^{o}C for a week before being transferred to liquid nitrogen for long-term storage.

Cells were thawed by warming a frozen aliquot in a 37 ^{o}C water bath for 30-60 s before pipetting the thawed cell suspension into a medium-containing 10 cm cell culture dish. Cell culture medium was replaced the following day after cells had adhered to remove DMSO.

2.1.4 *Mycoplasma* testing of cells

Cells were tested monthly for *Mycoplasma* contamination. Cells were plated onto sterile 13 mm uncoated coverslips (SLS) for 48-96 h, without antibiotic, until they had reached ~50-80 % confluency. The coverslip was then fixed with 100 % methanol (Sigma) for 30 s, stained with 4′,6-diamidino-2-phenylindole (DAPI, Sigma, 0.5 µg/ml in methanol) for 30 s, washed with methanol, washed with PBS, and finally mounted in 20 µl of glycerol (Fisher) onto a plain glass 76mm x 26mm slide (Fisher). Slides were imaged by fluorescence microscopy (see chapter 2.10). Mycoplasma-free cells presented with no cytoplasmic or extracellular DAPI signal.

2.1.5 Pharmacology

Cells were cultured with various drugs throughout this study (Table 2.1). Drugs were diluted in DMEM, applied to cells, and incubated at 37 ^{o}C/ 5 % CO_2 for the length of treatment, except for tetrodotoxin (TTX) and protoxin-II (ProTx-II), which were applied acutely in electrophysiology experiments (chapter 2.6.4).Corresponding negative control samples containing vehicle only were used, with vehicle concentration ≤ 0.1 % (v/v), for long-term incubation experiments.

2.2 Plasmid subcloning

The insert encoding *Rattus norvegicus* β1-enhancedGFP (eGFP, referred to as GFP throughout the study) was sub-cloned out of pEGFPN1-β1 (a gift from Prof Lori Isom) into pcDNA3.1 (Figure 2.1) (Invitrogen), following restriction digest of 1 µg of both plasmids with 1 U of both FastDigest NheI (Thermo) and FastDigest NotI (Thermo) for 30 min at 37 ^{o}C. Digested products were run on a 1% (w/v) agarose gel (90V, 80 min) and the required digest products were extracted and purified using a gel clean-up kit (Macherey-Nagel). Insert (30 ng) and vector (10 ng) were ligated using 6U of T4 DNA ligase (Thermo, 1h, room temperature) in a 20 µl reaction volume.

2.2.1 Transformation

Ligation product from chapter 2.2 (10 µl) was mixed with 50 µl of XL-1 Blue sub-cloning grade competent *E. coli* (Agilent) by gentle pipetting in a pre-chilled 15 ml falcon tube and the *E. coli*-DNA mix was left on ice for 20 min. The mixture was then heat pulsed (42 ^{o}C, 45 s) and left on ice for 2 min. Pre-heated (42 ^{o}C) SOC medium (0.9 ml, Thermo) was added to the *E. coli*-DNA mix and tubes incubated at 37 ^{o}C for 30 min with shaking

Table 2.1 Pharmacological agents used

Drug	Manufacturer	Concentration	Treatment length	Solvent (concentration-v/v %)
Avagacestat	Sigma	1 – 10 μM	24 h	DMSO (0.01 – 0.1)
Brefeldin-A	Biolegend	50 ng/ml	6 – 24 h	DMSO (0.0001)
Chloroquine	TCI	10 μM	24 h	Water (0.01)
DAPT	SCB	1 μM	24 h	DMSO (0.01)
L-685,458	SCB	1 – 10 μM	24 h	DMSO (0.1-0.01)
TTX	Alomone Labs	1 μM	Acute perfusion	Water (0.1)
Pro-TxII	Smartox Biotech	0.01 – 1 μM	Acute perfusion	Water (0.004 -0.4)

DAPT: N-[(3,5-Difluorophenyl)acetyl]-L-alanyl-2-phenyl]glycine-1,1-dimethylethyl ester; TTX: tetrodotoxin; Pro-TxII: Pro-Toxin II; TCI: Tokyo Chemicals Industry; SCB: Santa Cruz Biotechnology; DMSO: dimethyl sulfoxide

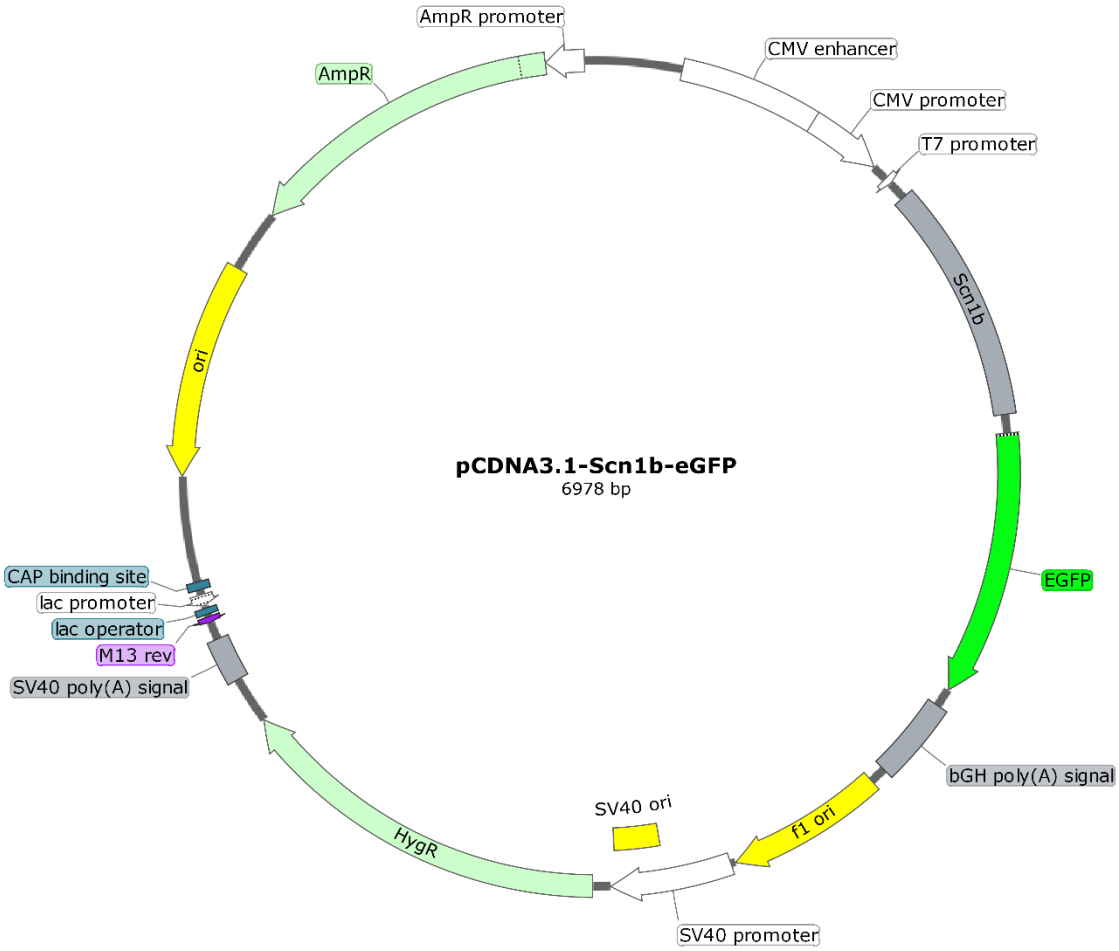

Figure 2.1 Plasmid map of pcDNA3.1-*Scn1b*

Rattus norvegicus Scn1b fused to enhanced GFP (eGFP) was subcloned into pcDNA3.1.

at 225 rpm. Transformant (150 µl) was then spread onto LB-agar containing 1 % (w/v) NaCl, 1 % (w/v) tryptone, 0.5 % (w/v) yeast extract, 2 % (w/v) agar in deionised H_2O and 100 µg/ml ampicillin in 9 cm petri dishes (Thermo) and left to incubate overnight at 37 ^oC.

2.2.2 DNA extraction

Six single colonies were picked from the overnight culture from chapter 2.2.1 and placed in separate 15 ml pre-chilled falcon tubes containing 5 ml of LB-broth (1 % (w/v) NaCl, 1 % (w/v) tryptone, 0.5 % (w/v) yeast extract in deionised H_2O with 100 µg/ml ampicillin) and incubated overnight at 37 ^oC with shaking at 225 rpm. The following day, cultures were spun at 5,000 g for 5 min at 4 ^oC and the supernatant removed. Plasmid DNA was then extracted from the pellet using a Nucleospin miniprep kit (Macherey-Nagel) into 50 µl Tris-ethylenediaiminetetraacetic acid (EDTA) elution buffer (10 mM Tris-HCl, 1mM EDTA, pH 8.0). DNA concentration and purity were measured using a Nanodrop ND-1000 (Thermo). Product was used if the concentration was >100 ng/µl and absorbance readings were 260nm/280nm >1.8 and 260nm/230nm >2.2. DNA was sequenced (Source Bioscience) to confirm correct product using T7F and/or BGH-R sequencing primers. To produce transfection-grade plasmid DNA, the process was replicated but DNA extracted using a HiSpeed plasmid midiprep kit (Qiagen). For the midiprep, DNA was extracted from 50 ml of overnight culture (a 5 ml starter culture was grown for 8 h (37^{o}C, 225 rpm) and 50 µl of starter culture was placed into 50 ml of fresh LB broth and left overnight (37^{o}C, 225 rpm)) and plasmid was eluted into 1 ml of elution buffer.

2.2.3 Site-directed mutagenesis

Various modified β1 constructs were created from pcDNA3.1-β1-GFP using PCR-based site-directed mutagenesis following the manufacturer's instructions (Phusion site-directed mutagenesis kit, Thermo). PCR reactions containing 0.02 U/µl Phusion Hot Start II DNA polymerase (Thermo), 1 ng template plasmid (pcDNA3.1-β1-GFP), 0.5 µM of both forward and reverse primers, 200 µM dNTPs (Thermo), 1x Phusion HF buffer (Thermo) made up to 25 µl in nuclease-free H_2O (Invitrogen) were prepared on ice. Primers and annealing temperatures used are outlined in Table 2.2. All primers were 5'-phosphorylated to permit blunt-end ligation of a PCR product (Integrated DNA Technologies). The PCR was run in a LifePro thermal cycler (BioER) using the following protocol: initial 98 ^{o}C – 30s; 25 cycles of 98 ^{o}C – 10s, T_A – 30s and 72 ^{o}C – 150 s; then a final 72 ^{o}C step for 10 min. PCR amplification was verified by running 5 µl of PCR reaction on a 1.5 % (w/v) agarose gel (90 V, 30-45 min). The PCR product (1-2.5 µl) was then ligated in a 10 µl reaction volume using T4 DNA Ligase (Thermo) and 1x Rapid Ligation Buffer (Thermo) for 15 min at room temperature. Ligated plasmid DNA was transformed and plasmid DNA extracted as detailed in chapters 2.2.1 and 2.2.2, except that 5 µl of ligation product was transformed into 50 µl of XL-1 Blue *E. coli*.

2.2.4 MDA-MB-231 cell transfection

Plasmid transfection into MDA-MB-231 cells was carried out in 4-well plates (Nunc). Cells were plated and left for 24-48 h until 50-80 % confluency was reached before transfection. Plasmid DNA (500 ng) was mixed with 1 µl of jetPRIME (Polyplus), made up to 50 µl in jetPRIME buffer, vortexed for 5 s, and left at room temperature for 5 min. The transfection mix was then pipetted onto the cells and cells left in the incubator at 37 ^{o}C/5 % CO_2 for 4 h, before the cell culture medium was replaced with fresh medium.

Table 2.2 Primers and annealing temperatures used for site-directed mutagenesis

Primer	Sequence	T_A (^oC)
β1-ICD-GFP F	AAGAAGATTGCTGCTGCCACG	69
β1-ICD-GFP R	CATCTTGGGTCTCCCTATAGTGAGTCGTATTA	
SRβ1-GFP F	GACAAGGCCAACAGAGATATGGC	71
SRβ1-GFP R	CTTCTTGACGACGCTGGTGTTG	
β1STOP-GFP F	CGAATTCTGCAGTCG	60
β1STOP-GFP R	CTTCTTGTAGCAGTACAC	
ICD: intracellular domain; SR: secretase-resistant; GFP: green fluorescent protein; T_A: annealing temperature		

Transfection efficiency was then assessed within 16-48 h by GFP fluorescence (chapter 2.10).

2.2.5 Stable cell line creation

To achieve a stable cell line, transiently transfected cells, which had usually grown to near-confluency 48-72 h after transfection, were passaged into a 35 mm cell culture dish (Thermo) and cultured with hygromycin B (300 µg/ml) until the non-transfected cells had died off. The hygromycin B concentration was then lowered to the normal culturing concentration of 100 µg/ml and single cells left to grow up into colonies. Colonies were selected to produce a clonal population only if they had a high proportion of GFP-positive cells, determined by fluorescence microscopy (chapter 2.10). To extract a colony from the culture dish, a cut P1000 pipette tip was placed on top of the colony, sealed with sterilised vacuum grease, and 50 µl trypsin-EDTA added on top of the colony. The colony was then lifted by pipetting the trypsin-EDTA up and down three times and transferred into a well of a 24-well plate and left in culture overnight. This was repeated for other fluorescent colonies (up to 24) present in the 35 mm dish. After further culturing for ~7 days, GFP signal was again verified by fluorescence microscopy and the clones with the highest proportion of GFP-positive cells were maintained in culture to establish stable cell lines. Typically, at least 2 clones with >25 % GFP-positive cells were retained for stable cell line creation.

2.3 Protein extraction and western blotting

Protein extraction and western blot protocols were adapted from (Nelson *et al.*, 2014).

2.3.1 Protein extraction

Cells grown in 15 cm cell culture dishes (Nunc) were isolated by scraping into PBS using a cell lifter (Fisher) and centrifugation at 5000 g for 5 min (4 ^{o}C). The cell pellet was then resuspended in 300 µl of pre-chilled Tris-EGTA-protease inhibitor (50mM Tris, 10mM EGTA, Roche protease inhibitor), lysed using 30 passes (2000 rpm) of a VWR Vos 14 homogeniser and centrifuged at 2500 g (10 min, 4 ^{o}C). The supernatant was kept and stored at -80 ^{o}C before use in subsequent western blotting. Protein concentration in the sample was measured by Bradford assay (Bradford, 1976). Briefly, 5 µl of sample was mixed with 995 µl of Bradford reagent (0.01 % (w/v) Coomassie Brilliant Blue G 250 (Serva), 5 % (v/v) methanol, 10 % (v/v) orthoscopic acid) in a polystyrene cuvette (Fisher) and absorbance at 595 nm (A_{595}) measured using a spectrophotometer (Jenway Genova), which had been pre-blanked with 100 % Bradford reagent and calibrated against a range of known concentrations of bovine serum albumin (BSA) (Figure 2.2).

2.3.2 Western blot

All western blotting steps were carried out at room temperature unless otherwise stated. Laemmli sample buffer (5 % (w/v) SDS, 0.2 % (w/v) Bromophenol Blue and 1.5 % (w/v) DTT dissolved in a solution of 50 % glycerol (v/v), 25 % β-mercaptoethanol (v/v) and 25 % Tris-HCl pH8.8 (v/v)) was added to cell lysate at a ratio of 1:4 and heated at 80 ^{o}C for 10 min prior to sodium dodecyl sulphate-polyacrylamide gel electrophoresis (SDS-PAGE). PageRuler Plus prestained protein ladder (5 µl,Thermo) and 30-100 µg of sample were loaded onto a discontinuous polyacrylamide running gel. This consisted of 7 ml of 12 % polyacrylamide separating gel containing 40 % (v/v) 30 % (w/v) acrylamide:Bis solution (National Diagnostics) and 25 % (v/v) Tris-SDS pH 8.8 solution (375 mM Tris, 3.5 mM SDS) made up to 7.5 ml in distilled H_2O, then polymerised with

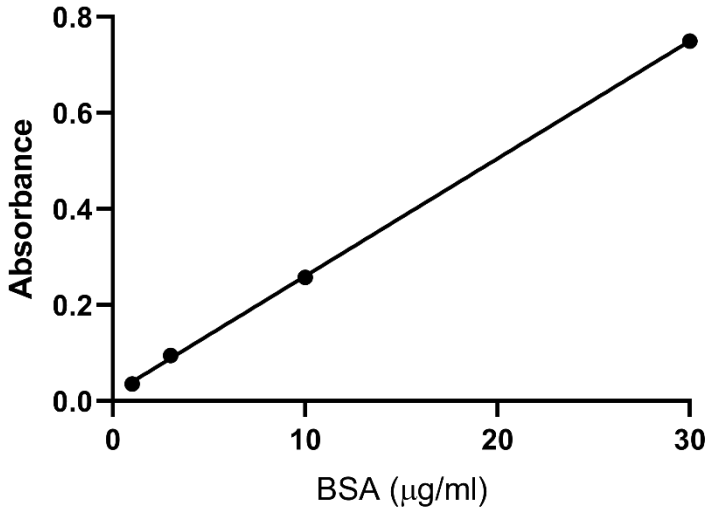

Figure 2.2 Bradford assay calibration curve

Absorbance at 595 nm at known bovine serum albumin (BSA) concentrations

50 µl of 10% (w/v) ammonium persulfate and 10 µl Tetramethylethylenediamine (TEMED, Sigma). The separating gel was overlain with ~3 ml of 4 % polyacrylamide stacking gel containing 13 % (v/v) 30 % (w/v) acrylamide:Bis solution and 25 % (v/v) Tris-SDS pH 6.8 solution (125 mM Tris, 3.5 mM SDS), made up to 5 ml in distilled H_2O, then polymerised with 12.5 µl of 10 % (w/v) ammonium persulfate and 25 µl of TEMED. SDS-PAGE was run at 120 V for 2-2.5 h in a Bio-Rad miniPROTEAN Tetra System running tank submerged in running buffer (24.8 mM Tris, 191.8 mM glycine, 3.5 mM SDS). Following SDS-PAGE, protein was transferred onto 0.45 µm pore nitrocellulose membrane, soaked in transfer buffer (249.3 mM Tris, 191.8 mM glycine, 20 % (v/v) methanol, pH 7.5), by semi-dry transfer (1.3 A, 25 V, 10 min) using a Bio-Rad TransBlot Turbo Transfer System. Protein transfer was verified by reversibly staining the membrane with Ponceau stain (0.5 % (w/v) Ponceau S (Fisher) dissolved in 5 % (v/v) glacial acetic acid) for 10 min at 125 rpm. The Ponceau stain was subsequently washed off with Tween-containing, tris-buffered saline (TBS-T; 10 mM Tris pH 7.5, 150 mM NaCl and 1 % (v/v) Tween-20) and blocked for 1 h in 5% (w/v) non-fat dried milk dissolved in TBS-T. The membrane was then incubated in primary antibody (rabbit anti-GFP (cat# ab6556, 1:2500, Abcam) or mouse anti-α-tubulin (clone DM1A, 1:10,000, Sigma)), diluted in antibody dilution buffer (3 % (w/v) BSA dissolved in TBS-T), overnight at 4 ^{o}C. The membrane was washed with TBS-T the following day and incubated with HRP-conjugated goat anti-mouse (1:1000, Thermo Scientific) or goat anti-rabbit (1:1000, Thermo Scientific) secondary antibody, diluted in antibody dilution buffer, for 2 h. The membrane was finally washed with TBS-T before protein detection by chemiluminescence. For this, the membrane was incubated with West Dura (Thermo Scientific) for 5 min before detection by either iBRIGHT western blot imaging system (Invitrogen) or X-ray film (Fujifilm). Membranes were stripped for restaining in solution containing 200 mM glycine, 3.5 mM SDS and 1 % Tween-20 (v/v) dissolved in H2O (pH 2.2) for 1 minute at 50 ^{o}C.

2.3.3 Densitometry

Protein quantity was estimated digitally from blots using the in-built ImageJ feature “Gels > Plot Lanes” to estimate the signal intensity of the β1-CTF and β1-ICD bands, from which CTF: ICD signal ratios could be calculated for each lane.

2.4 Cell-cell adhesion assay

The cell-cell (or transcellular) adhesion assay method was adapted from previous works (Wong & Filbin, 1996; Chioni *et al.*, 2009). Cells were removed from a near-confluent 10 cm dish using trypsin-EDTA, counted using a haemocytometer, and adjusted to a concentration of 2 x10^7 cells/ml in DMEM. Single cell suspension was obtained by pipetting and passing the suspension through a 24 G syringe needle. The cell suspension was then incubated at 37 ^oC with gentle agitation (25 rpm) and sampled every 30 min for 2 h, starting at T=0. To sample the suspension, 20 µl of the cell suspension was pipetted onto a plain glass 76mm x 26mm slide (Fisher), a 13 mm glass coverslip (SLS) placed on top, and the number of particles (defined as a cluster of cells of any quantity) in ten fields of view were counted, using either a Nikon Eclipse TE200 microscope with a RoleraXR CCD camera at 20x magnification or Motic AE2000 a at 20x magnification. The mean number of particles at each time point was normalised to the mean particle count at T = 0. The experiment was repeated three times.

2.5 Morphology assay

To assess cellular morphology, 10,000 cells were plated into a well of a 24 well plate and left for 72 h prior to image acquisition. Cells were then fixed using 4 % (w/v) paraformaldehyde (PFA) in PBS at room temperature for 10 min. Cells were then washed three times (5 min each) with 0.1 M phosphate buffer (PB, 81 mM Na_2HPO_4, 19 mM NaH_2PO_4, pH 7.4). Five brightfield images of each well were acquired, as well as GFP images to ensure construct expression, according to chapter 2.10. Images were exported to ImageJ for analysis. Cell morphology was assessed by manually masking the first 50 randomly selected cells and measuring circularity and Feret's diameter using the in-built analysis ImageJ plugin. Motile, mesenchymal cells display a characteristic elongated cell morphology, with a distinct leading and trailing edge, thus circularity is inversely proportional to the mesenchymal-like nature of the cell. Feret's diameter infers a complimentary parameter to circularity, as Feret's diameter measures the two furthest points on a cell (i.e. cell length), which will correspond to the leading and trailing edges of an elongated cell or two random points around the perimeter of a circular cell. The experiment was repeated three times. Circularity was defined as (Bon *et al.*, 2016):

$$circularity = 4\pi.\frac{area}{perimeter^2}$$

2.6 Electrophysiology

Membrane Na^+ currents were measured using the whole-cell patch clamp technique in voltage clamp mode, as described previously (Grimes & Djamgoz, 1998; Ding & Djamgoz, 2004; Brackenbury *et al.*, 2007).

2.6.1 Solutions

Extracellular, recording solution (physiological saline solution; PSS) contained (mM): 144 NaCl, 5.4 KCl, 1 $MgCl_2$, 2.5 $CaCl_2$, 5 HEPES, 5.6 D-glucose, adjusted to pH 7.2 with KOH. For experiments involving cells pre-treated with drug, the drug or vehicle was also included in the PSS. Intracellular patch solution (IPS) contained (mM): 5 NaCl, 145 CsCl, 2 $MgCl_2$, 1 $CaCl_2$, 10 HEPES and 11 EGTA, adjusted to pH 7.4 using CsOH. Solution osmolarity was 303 mOsm/litre.

2.6.2 Patch pipettes

Borosilicate thin wall glass capillaries (1.5 mm outside diameter x 1.17 mm inside diameter x 75 mm length; Harvard Apparatus) were initially fire-polished at both ends. After polishing, capillaries were pulled into two pipettes using a P-97 Flaming/Brown type micropipette puller (Sutter Instruments). Pipette tips were then fire polished for 3 s using a MF-830 microforge (Narishige) to give a pipette resistance of 2.5 – 4.5 MΩ when filled with IPS.

2.6.3 Recording equipment

Recordings were carried out at room temperature within a RC-26G recording chamber (Warner Instruments), attached to a P1 recording chamber (Warner Instruments), within a SA-20LZ-AL stage adapter (Warner Instruments). Gravity-fed inflow of PSS into the recording chamber was controlled by a 4-way Valvelink 8.2 valve controller (AutoMate Scientific) via a MP-series manifold (Warner Instruments). Outflow was controlled by a Dymax 5 pump (Charles Austen Pumps). The stage adapter was fitted to an Axiovert 135 fluorescent microscope (Zeiss). Recording pipettes were loaded into a 1-HL-U electrode holder (Molecular Devices) attached to a CV-203BU headstage (Molecular

Devices). Movement of the electrode was controlled digitally by a MP-225 micromanipulator (Sutter Instruments). Recordings were collected via an Axopatch 200B amplifier (Molecular Devices), to a Digidata 1550 digitizer (Molecular Devices) for analogue-digital signal conversion, connected to a computer running Clampex 10.7 software (Molecular Devices).

2.6.4 Whole cell patch clamp recording

Cells were grown on 13 mm glass coverslips (SLS), to 50 – 80 % confluency within 4 well dishes, for 1-3 days prior to recording. The coverslip was then transferred to the recording chamber filled with ~1 ml of PSS. Data were collected at a sampling rate of 50 kHz and filtered at 10 kHz. Linear leak currents were removed using P/6 subtraction (Armstrong & Bezanilla, 1977). The following voltage clamp protocols were used, compensating for series resistance by 20-40 %.

1. *VGSC Stimulation protocol:* -120 mV holding voltage (V_H) for 250 ms, -10 mV stimulation voltage (V_S) for 50 ms.
2. *Current-voltage protocol:* V_H: -120 mV for 250 ms; V_S: -80 mV for 50 ms; V_H: -120 mV for 10 ms. V_S was depolarised by +5 mV with each sweep to +30 mV.
3. *Steady-state inactivation protocol:* V_{H1}: -120 mV for 250 ms, V_S: -10 mV for 50 ms, V_{H2}: -80 mV for 10 ms. V_{H1} was depolarised by +10 mV with each sweep to 0 mV.
4. *Recovery from inactivation protocol:* V_H: -120 mV for 250 ms, V_S: 0 mV for 25 ms, V_{H2}: -120 mV for *t* ms, V_{S2}: 0 mV for 25 ms. Sweeps used the following *t* (ms): 1, 2, 3, 5, 7, 10, 15, 20, 30, 40, 50, 70, 100 ,150, 200, 250, 350, 500.

In some experiments, tetrodotoxin (1-30 μM TTX) and protoxin-II (100 nM – 1 μM ProTx-II), were directly perfused onto cells once a whole cell configuration had been achieved. Drug treatments were exchanged for PSS (and vice versa) by performing three bath changes and voltage clamp protocols run in each condition.

2.6.5 Electrophysiology data analysis

The peak current amplitude (pA) at each voltage step was divided by the whole cell capacitance (pF) to calculate the current density (pA/pF), which was plotted against the stimulation voltage to achieve an I-V curve. Activation curves were fitted by calculating conductance (G) at each voltage step from the I-V data. G-V relationships were determined using the equation (Ding & Djamgoz, 2004):

$$G = \frac{I}{V - V_{rev}}$$

Where G = conductance (nS), I = current amplitude (pA), V = holding potential (mV) and V_{rev} =reversal potential of Na^+ calculated using the Nernst equation (+86.3 mV). G was normalised to G_{max}. Normalised G-V data were fitted using the Boltzmann equation:

$$Y = \frac{1}{1 + e^{\frac{V_{\frac{1}{2}} - V}{k}}}$$

Where Y = fitted conductance value, $V_{1/2}$ = voltage that elicits half-maximal conductance, V = stimulation voltage and k = slope factor. Normalised steady-state inactivation data were also fitted to a Boltzmann function. Recovery from inactivation data, normalised to the prepulse amplitude, were plotted against the inter-stimulation duration (i.e. time for recovery) and fitted to a single exponential equation:

$$Y = 1 - e^{kt}$$

Where Y = fitted normalised current value, k = slope factor and t = inter-stimulation duration.

2.7 Immunocytochemistry

Protocol adapted from (Brackenbury *et al.*, 2010; Rofe *et al.*, 2017). Cells were grown for 24-72 h on 13 mm uncoated coverslips (SLS) until 50-80 % confluency was reached.

All following steps were carried out at room temperature. Cells were then fixed with 4 % (w/v) paraformaldehyde (dissolved in PBS) for 5 min or 100 % methanol for 10 min on ice. For digitonin-treated conditions, cells were incubated in 50 µg/ml digitonin (Santa Cruz Biotechnology) for 15 min and Triton X-100 was subsequently omitted in the following steps (Mojica *et al.*, 2015). Cells were washed three times in 0.1 M PB and blocked in PBTGS (0.3 % (v/v) Triton X-100 and 10 % (v/v) normal goat serum dissolved in 0.1 M PB) or BPS (0.5 % (w/v) BSA and 0.05 % (w/v) saponin dissolved in 0.1 M PB) for 1 h. Primary antibody (diluted in blocking solution) was applied for 1 h (antibodies diluted in BPS) or overnight (antibodies diluted in PBTGS) (Table 2.3). Cells were washed three times with blocking solution then incubated in goat anti-mouse Alexa Fluor 568, or goat anti-rabbit Alexa Fluor 568 or 647 (1:500 in blocking solution, Thermo) for 1 h (antibodies diluted in BPS) or 2 h (antibodies diluted in PBTGS). After three washes with 0.1 M PB, cells were incubated in 500 ng/ml 4',6-diamidino-2-phenylindole (DAPI, diluted in 0.1 M PB, Sigma) and mounted onto 76 mm x 26 mm glass slides (Fisher) using Prolong Gold (Invitrogen).

2.8 Confocal microscopy

Slides prepared from chapter 2.7 were imaged using a Zeiss LSM 880 laser-scanning confocal microscope with Airyscan technology, controlled by ZEN2 software. Using a Plan-Apochromat 63x oil immersion objective lens (NA = 1.4) and 1.8-7.5x zoom factor, square images were acquired with a side length of 17.8 – 73.2 µm, with optimal frame size for Airyscan acquisition (~0.034 µm/pixel). The pinhole was set to 1.25 airy unit (AU) for Airyscan imaging. For Z-stacks, a 0.16 µm step was used between planes. Images of ten cells or nuclei were acquired per experiment and the experiment repeated three

Table 2.3 Antibodies used for immunocytochemistry in this study

Antibody target	Species	Clone	Manufacturer	Dilution	Blocking solution
GFP	Mouse	N86/38	Neuromab	1:1000	PBTGS
Lamin B2	Mouse	E-3	Invitrogen	1:500	PBTGS
EEA1	Mouse	14/EEA1	BD Bioscience	1:500	BPS
LAMP-1	Mouse	H4A3	Biolegend	1:1000	BPS
Calnexin	Mouse	37/CNX	BD Bioscience	1:50	BPS
TGN-46*	Rabbit	-	Proteintech	1:1000	BPS

GFP: green fluorescent protein; EEA1: early endosome 1; LAMP-1: lysosomal associated membrane protein-1; TGN-46: *trans*-Golgi network-46; CNX: Calnexin; PBTGS: phosphate buffer (0.1 M), Triton X-100 (0.3 %), goat serum (10 %); BPS: bovine serum albumin (0.5 % w/v), phosphate buffer (0.1 M), saponin (0.05%, w/v). *TGN-46- polyclonal antibody (cat # 13573-1-AP)

times. An automatic Airyscan processing strength of 6.0 was applied to the image post-acquisition.

2.9 Fluorescence recovery after photobleaching (FRAP) and Förster resonance energy transfer (FRET)

10,000 cells were plated per well into an 8-well Lab-Tek II chambered coverglass slide (Nunc) 48 h prior to imaging. In some experiments, FM4-64 (Thermo, 120 nM) or Hoechst 33342 (Thermo, 1 µg/ml) were applied immediately prior to imaging. FRAP acquisition was carried out using a Zeiss LSM 880 confocal microscope controlled by ZEN2 software at 37 ^{o}C/5 % CO_2. GFP was imaged using a 488 nm laser (1-5 % laser power), using bidirectional scanning at maximum scan speed and a 1 airy unit pinhole.

To monitor FRAP in the cytoplasm, at 10x zoom factor and a 256 x 256-pixel frame size, a 1 µm wide bleach spot was selected in an individual cell and photobleached with 40 iterations of the 488 nm laser (100 % laser power). Images were acquired every 250 ms for 37.5 s, with photobleaching occurring after 2.5 s (i.e. 10 time points). For a higher temporal resolution, a 64 x 64-pixel frame was used, and images acquired every 12.8 ms. 1000 images were acquired, with bleaching occurring after 10 images in a 5-pixel wide region of interest. In some experiments, a bleach spot was manually drawn around half a cell and photobleached with 50 iterations of the 488 nm laser (100 % laser power) at 2.5x zoom factor and a 256 x 256-pixel frame size. Images were acquired every 100 ms for 25 s, with photobleaching occurring after 20 images. Ten time series were acquired per cell and the experiment repeated three times.

To monitor FRAP in the nucleus, GFP fluorescence within whole nuclei was photobleached as described previously (Sunn *et al.*, 2005; Bizzarri *et al.*, 2012). At 2.0x

zoom factor and a 512 x 512-pixel frame size, a bleach spot was manually drawn around the nucleus (stained by Hoechst 33342) and the whole nucleus was bleached with 40 iterations of the 488 nm laser (100 % laser power). Images were taken every 5 s until ten successive images without an increase in nuclear fluorescence were acquired (typically 5 – 10 min). 3-4 time series were taken, and the experiment repeated three times.

For FRET, cells were imaged at 2.0 – 4.0x zoom factor using a 512 x 512-pixel frame size. FM4-64 was bleached using 100 iterations of the 561 nm laser (100 % laser power) at the plasma membrane or within internal vesicles. Images were acquired every 0.6 s for 25 s, with bleaching occurring after 3 s.

2.10 Fluorescence microscopy

For fluorescence microscopy, Cells were imaged using a Nikon Eclipse TE200 epi-fluorescent microscope with a RoleraXR charge-coupled device (CCD) camera (QImaging) using SimplePCI 6 software (Hamamatsu) at 20x magnification.

2.11 Image analysis

2.11.1 Nuclear: cytoplasmic signal density ratio

Nuclear localisation was measured by calculation of the nuclear: cytoplasmic signal density ratio, from Airyscan images taken in chapter 2.8, using a previously established analytical method (Ebner *et al.*, 2007; Noursadeghi *et al.*, 2008). Fluorescence measurements were taken in ImageJ on multi-channel images, consisting of DAPI and

β1-GFP staining. Nuclear fluorescence was calculated by masking the DAPI signal and measuring the fluorescence (signal density- “mean gray value” and total fluorescence- “max gray value”) in the β1-GFP channel. To calculate cytoplasmic signal density, total fluorescence was measured across the whole cell within the field-of-view and the total nuclear fluorescence was subtracted from this. The resulting fluorescence value was divided by the difference in area of the whole cell and the nuclear mask to determine the cytoplasmic signal density:

$$cytoplasmic\ signal\ density = \frac{Ftotal_{cell} - Ftotal_{nucleus}}{Area_{cell} - Area_{nucleus}}$$

Where F_{total} = total fluorescence. The nuclear: cytoplasmic signal density ratio was calculated using the recorded nuclear and cytoplasmic signal density values.

2.11.2 FRAP analysis

A double normalisation method of data analysis was used (Phair *et al.*, 2004). Images acquired from chapter 2.9 were exported to ImageJ for data acquisition using the FRAP Norm plugin. To define the region of interest (ROI) for spot bleaches, the diameter of the ROI for the photobleached region (R_p) was estimated by taking a line profile across the bleached region and defining the diameter of the ROI as the distance between half maximal fluorescence values. For nuclear or half-cell bleaching, the ROI was manually drawn around the bleach region using the polygon function in ImageJ. A control region (R_c) was placed elsewhere in the cell and a background region (R_b) placed outside of the cell, both of the same diameter as the photobleached region (Figure 2.3). Fluorescence was measured within the three regions for every time point. R_b was subtracted from R_p and R_c initially. The photobleaching ratio (r) at each time point x was calculated by

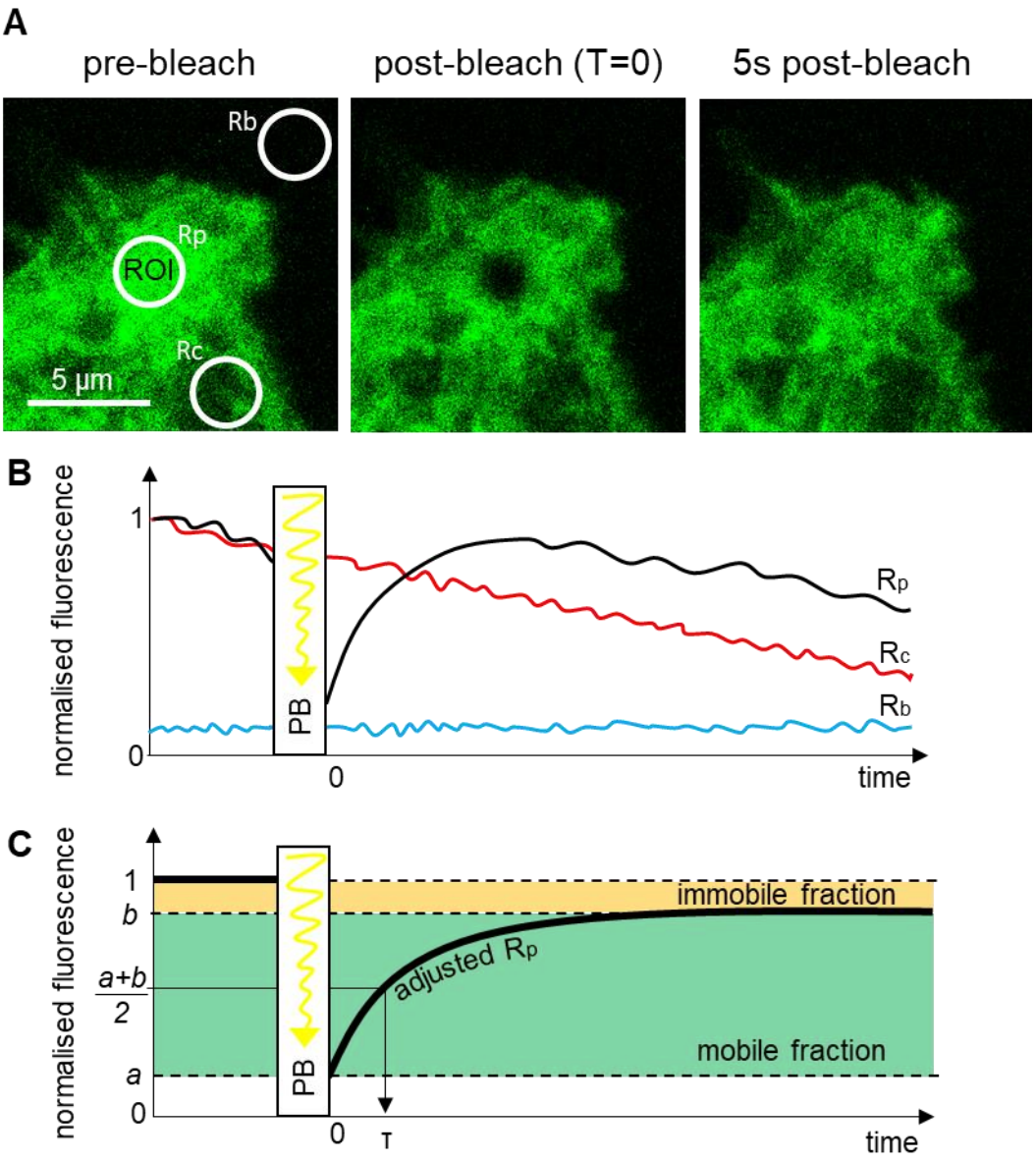

Figure 2.3 Fluorescence recovery after photobleaching in a circular region of interest

(**A**) Representative images of fluorescence recovery of GFP following photobleaching. ROI: region of interest; Rp: photobleached region; Rb: background region; Rc: control region. The first post-photobleach image marks T = 0. (**B**) Fluorescence recovery of Rp (black line), Rc (red line) and Rb (blue line). Rc and Rb are both unaffected by the photobleaching (PB) event. (**C**) Adjusted fluorescence recovery of Rp. Rp has been normalised against the rate of photobleaching, calculated from the rate decrease in Rc. τ = time constant i.e. time taken to reach half maximal fluorescence. The mobile fraction refers to the proportion of mobile GFP elements within the ROI, whereas the immobile fraction refers to the proportion of immobilised GFP elements. The presence of an immobile fraction prevents fluorescence recovery to 1.0.

dividing R_c at each given time point *x* by the initial R_c value at time point *0*, to determine the decrease in fluorescence:

$$r_x = \frac{R_{cx}}{R_{c0}}$$

where r_x represents the photobleaching ratio at time point *x,* R_{cx} = the fluorescence reading within the control region at time point *x*, and R_{c0} = fluorescence reading within the control region at time point 0. R_p at each time point *x* was then adjusted to the photobleaching ratio at each time point:

$$\text{adjusted } R_{px} = \frac{R_{px}}{r_x}$$

where R_{px} = the fluorescence reading within the photobleached region at time point *x,* and r_x = the photobleaching ratio at time point *x.* The resulting value was then normalised against the mean of the initial pre-bleach R_p readings, which were taken prior to the photobleaching event as a baseline, giving a value between 0-1. Recovery curves were then plotted and three parameters calculated: the mobile fraction, time constant (seconds) and diffusion coefficient ($\mu m^2 s^{-1}$, for spot bleaches only). The mobile fraction, which defines the proportion of fluorescent elements that are mobile relative to the whole population of fluorescent elements initially in the ROI, was calculated using:

$$\text{mobile fraction} = \frac{R_{nf} - R_{npost}}{1 - R_{npost}}$$

where R_{nf} = the final normalised fluorescence reading taken and R_{npost} = the first normalised fluorescence reading post-photobleaching. The time constant describes the time taken for 50 % of final fluorescence recovery and was fitted to a single exponential to the post-bleach recordings. The diffusion coefficient was calculated, for spot bleaches, using the equation:

$$D_{2D} = \frac{\omega^2 \gamma}{4\tau}$$

where ω = the radius of the photobleaching region (μm), τ = time constant, γ = beam circularity (γ = 0.88).

2.11.3 FRET analysis

To analyse FRET, GFP and FM4-64 fluorescence intensity was monitored within the ROI for the duration of the time series and normalised against T = 0. FM4-64 signal was monitored to ensure photobleaching occurred. GFP fluorescence intensity before and after photobleaching was then statistically compared.

2.11.4 Co-localisation analysis

To quantify the co-localisation between GFP and subcellular marker (Calnexin, GM130, TGN46, EEA1 or LAMP1), Pearson's correlation coefficient was calculated using the in-built "Coloc 2" plugin in ImageJ. First, images were split into GFP and marker channels and a ROI drawn around the cell using the GFP channel. Coloc2 was initiated using bisection threshold regression, a PSF of 3.0 pixels and a Costes randomisation value of 10 to calculate the value.

To analyse GFP overlap with the membrane markers, FM4-64 and lamin-B2, line profiles were used. 10-pixel wide, 5 μm-long line profiles were placed, with the membrane marker centred at 2.5 μm. For FM4-64, two - four line profiles were taken per cell and averaged. For lamin-B2, one line profile was taken per cell. Fluorescence intensity was normalised to the maximum value for each cell. Ten cells were measured.

2.12 Statistical analysis

GraphPad Prism 8.0 was used for all curve fitting and statistical analyses. Data were initially tested for normality using the D'Agostino & Pearson test. When normally distributed data was being compared, an F-test was used to determine differences in variance. In text, Normalised data are presented as mean ± SEM, non-normalised data as median (interquartile range - IQR). Data displayed as mean ± SEM by default, when non-normalised data is presented, "*median (IQR)*" is explicitly stated. For normalised data, comparisons between two samples were made using unpaired Student's t-test and Welch's t-test if variance between samples was comparable or different, respectively. Mann-Whitney U-test was used for non-normalised data. For multiple comparisons, one-way ANOVA with Tukey's post hoc test and Kruskal-Wallis with Dunn's multiple comparison post hoc test were used for normalised and non-normalised data, respectively. Repeated measured one-way ANOVA with Tukey's post hoc test was used to compare data collected from the same cell. Results were considered significant if $P < 0.05$. Levels of significance used: * < 0.05, ** < 0.01, *** < 0.001. The number of samples tested is referred to as n and the number of independent experiments as N.

Chapter 3: The effect of pharmacological inhibition of γ-secretase on β1 function

3.1 Introduction

γ-secretase is a multimeric complex, consisting of the enzymatic presenilin (PS) subunit and three auxiliary subunits (Smolarkiewicz *et al.*, 2013). PS is cleaved into a N-terminal fragment (NTF) and C-terminal fragment (CTF), which interact via two aspartate residues to form the intramembranous active site (Wolfe *et al.*, 1999). PS is a "sloppy" enzyme, cleaving at multiple nearby sites within a protein (Dehury *et al.*, 2019). γ-secretase inhibitors (GSIs) are divided into four subclasses: transition-state analogues (TSAs), which inhibit the PS active site, docking site inhibitors and naphthyl ketone inhibitors, which both inhibit initial docking of the substrate to PS, and nonsteroidal anti-inflammatory drugs, (NSAIDs) which target the substrate through an unknown mechanism (Sato *et al.*, 2008). A second class of γ-secretase targeting drugs, known as γ-secretase modulators (GSMs), of which NSAIDs are often classed, do not inhibit global γ-secretase cleavage but specifically modulate proteolysis of APP, preferentially producing non-amyloidogenic APP fragments (Golde *et al.*, 2013). The three GSIs used in this study are: DAPT, L-685,458 and Avagacestat. DAPT is a non-TSA that binds to PS-CTF and Avagacestat is a non-TSA that binds to PS-NTF (Morohashi *et al.*, 2006; Gertsik *et al.*, 2017). L-685,458, on the other hand, is thought to be a TSA (Eto *et al.*, 2000).

A potentially vital aspect of β1 regulation emerged when β-subunits were revealed to be substrates of secretase enzymes (Kim *et al.*, 2005; Wong *et al.*, 2005). Sequential proteolysis of β-subunits by α/β-secretase then γ-secretase releases a soluble ECD and ICD, respectively. Knowledge regarding the functional impact of γ-secretase processing on β1 is currently lacking. So far, the only evidence is that DAPT treatment inhibits β1-

mediated neurite outgrowth (Brackenbury & Isom, 2011). The underlying mechanism was not explored, however the authors speculated β1-ICD signalling could be involved. Regarding other β-subunits, β2-ICD expression in SH-SY5Y cells demonstrates nuclear localisation and a concomitant upregulation in $Na_v1.1$ mRNA and protein expression (Kim *et al.*, 2007), suggesting β2-ICD could be involved in nuclear signalling; an exciting and novel potential function of β-subunits. Additionally, DAPT treatment inhibited β2-mediated cell adhesion and migration in CHO cells, possibly through accumulation of β2-CTFs at the plasma membrane, which lack the Ig loop responsible for cell adhesion (Kim *et al.*, 2005). Mechanistically, the aforementioned evidence suggests a potential role of γ-secretase cleavage in influencing β-subunit function through production of an ICD, with distinct functional properties, and regulating β-subunit surface expression. γ-secretase cleavage may therefore impact β1-induced cell adhesion, through regulating β1 cell surface expression, and production of β1-ICD may have a range of unknown functional implications. One role β1-ICD may be involved in is β1-induced α-subunit modulation. β1 interacts with α-subunits via intracellular, as well as extracellular, sites (McCormick *et al.*, 1999; Meadows *et al.*, 2001). Cleavage of β1-ICD from the membrane may therefore disrupt the α-β association, abolishing β1-mediated modulation. Alternatively, if β1-ICD is involved in upregulating α-subunit expression, akin to the putative role of β2-ICD, then inhibiting γ-secretase cleavage may reduce α-subunit expression. In summary, the functional impact of γ-secretase cleavage on β-subunits is an enticing area of research, as little is known yet the impact could be substantial.

The subcellular localisation of β1 has yet to be comprehensively reported. Functional evidence (i.e. α-subunit modulation and transcellular adhesion) suggests β1 is present at the plasma membrane. However, in a study examining β2-$Na_v1.5$ membrane trafficking, a single experiment compared β1 to β2 distribution and stated β1 was predominantly retained within intracellular compartments (Dulsat *et al.*, 2017). How β1 is

degraded, whether by trafficking to lysosomes or to the proteasome following ubiquitination, is also unknown. As secretases are found at the plasma membrane and at internal membranes (discussed in chapter 1.5.1), β1 may be cleaved at either of these locations.

This study set out to establish the impact of secretase processing on β-subunit function. The hypothesis of this chapter is that γ-secretase cleavage regulates β1 function. The specific aims of this chapter were to:

- Investigate the involvement of γ-secretase cleavage on β1-induced α-subunit modulation
- Investigate the involvement of γ-secretase cleavage on β1-induced cell adhesion
- Determine the subcellular localisation of β1 and its secretase cleavage products

The triple-negative MDA-MB-231 breast cancer cell line was used throughout this study. MDA-MB-231 cells are a metastatic breast cancer cell line that have been the subject of secretase research previously. For instance, Notch2 processing induces cell migration and prevents apoptosis (Sehrawat *et al.*, 2014). Additionally, hypoxia-induced migration is induced through Notch processing (Villa *et al.*, 2014). Furthermore, α-secretase cleavage of APP regulates migration and proliferation of MDA-MB-231 cells (Tsang *et al.*, 2018).

3.2 Results

3.2.1 β1 expression enhances Na^+ current magnitude and accelerates recovery from channel inactivation

MDA-MB-231 cells are highly metastatic breast cancer cells with a low native β-subunit expression (Chioni *et al.*, 2009). Previous work has demonstrated overexpression of β1 in MDA-MB-231 cells increases the magnitude of I_{Na} and reduces the time to I_{Na} peak, without affecting other gating parameters, such as the voltage sensitivity of activation/inactivation and recovery from inactivation (Chioni *et al.*, 2009). As this cell model forms the basis of the overall study, firstly, the experiments from Chioni *et al.* were repeated. MDA-MB-231 cells overexpressing β1 fused to eGFP at the C-terminus (MDA-MB-231-β1GFP) were compared to MDA-MB-231-GFP cells by whole cell patch clamp recording. Peak current density generated by MDA-MB-231-β1GFP cells was 3-fold greater than cells expressing GFP alone, -16.80 ± 2.90 pA/pF and -5.16 ± 0.71 pA/pF respectively ($n = 8$, $P < 0.01$, unpaired t test) (Figure 3.1A,B, Table 3.1). The voltage dependency of channel activation (Figure 3.1C) and inactivation (Figure 3.1D), and the time course of channel recovery from inactivation (Figure 3.1E) were also measured. Significant differences detected in the gating parameters, following β1-GFP expression, were a hyperpolarised voltage at I_{Na} peak, -6.25 ± 2.46 mV compared to 0.63 ± 1.48 mV in GFP-expressing cells ($n = 8$, $P < 0.05$, unpaired t test) and an acceleration in channel recovery from inactivation, with β1-GFP expression halving the time taken for half-maximal recovery relative to GFP alone, 5.05 ± 0.52 ms and 10.17 ± 1.29 ms respectively ($n = 8$, $P < 0.01$, unpaired t test) (Table 3.1). β1-GFP expression did not alter the voltage required for channel activation, voltage required for half-maximal activation or inactivation, time to I_{Na} peak or size of the cell (measured by total membrane capacitance) compared to GFP expression (Table 3.1). A change in recovery kinetics and voltage at I_{Na} peak were not detected in Chioni *et al.,* however β1-induced acceleration of recovery from inactivation has been reported in other cellular

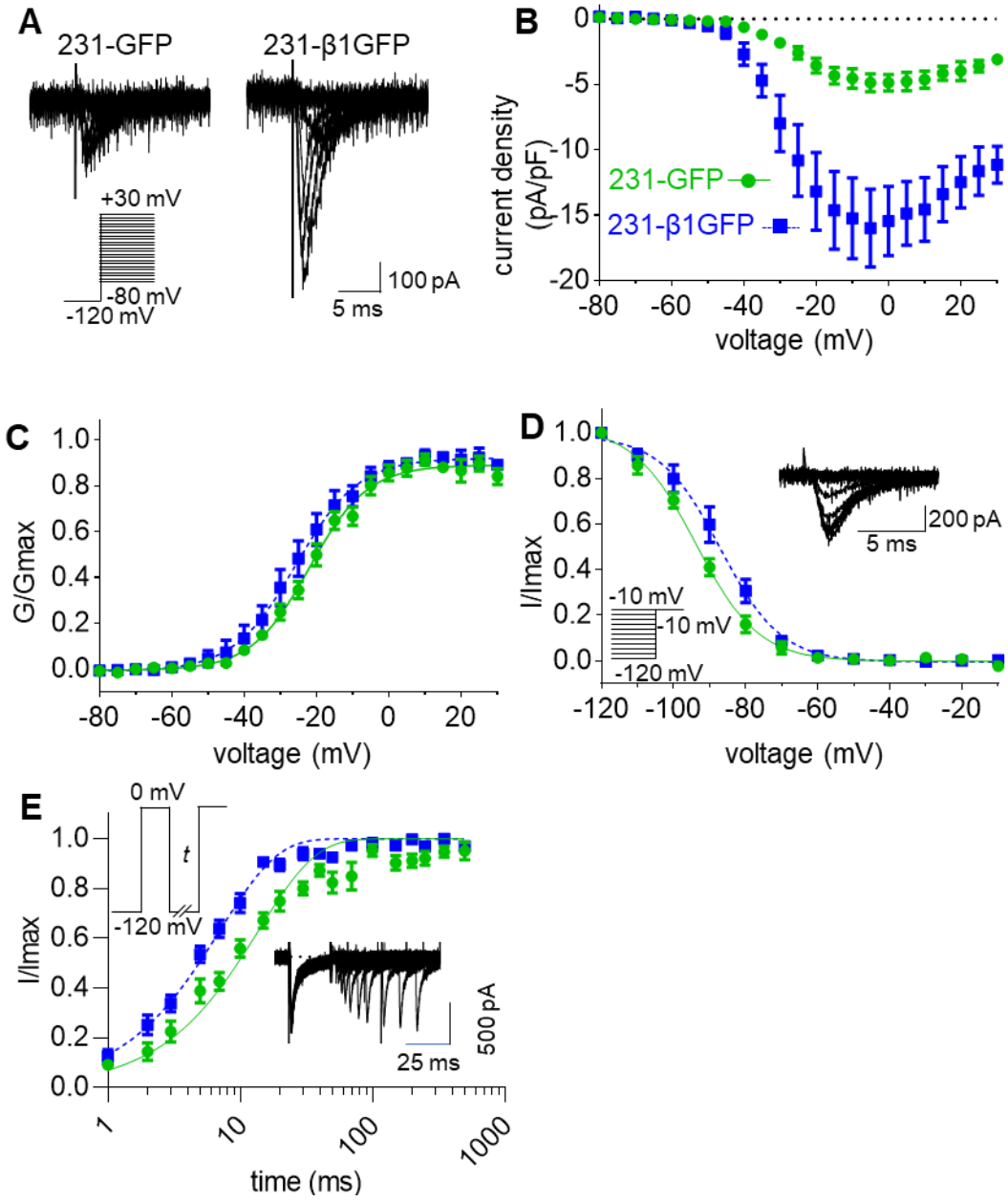

Figure 3.1 Electrophysiological properties of β1 expression in MDA-MB-231 cells

(**A**) Representative whole-cell Na^+ currents generated in MDA-MB-231-GFP and MDA-MB-231-β1GFP cells, following stimulation between -80 mV and +30 mV for 250 ms from -120 mV. (**B**) Current (I)-voltage (V) relationship between -80 mV and +30 mV. (**C**) Conductance (G)-voltage (V) relationship, from which activation $V_{1/2}$ was derived, between -80 mV and +30 mV. Fitted Boltzmann sigmoidal curve overlaid. (**D**) Steady-state inactivation. Cells were stimulated at -10 mV following a 250 ms holding voltage of between -80 mV and +30 mV. Normalised current produced following -10 mV stimulation plotted. Fitted Boltzmann sigmoidal curve overlaid. (**E**) Recovery from inactivation. Cells were stimulated at 0 mV, then held at -120 mV for *t* s before re-stimulation at 0 mV. *t* ranged from 1-500 ms. Fitted mono-exponential curve overlaid (constraints: Y0 = 0, plateau = 1). Mean ± SEM plotted for graphs in **B**-**E**. MDA-MB-231-GFP cells (n = 8, N = 3, green circles) and MDA-MB-231-β1GFP cells (n=8, N =3, blue squares).

Table 3.1 Na^+ current parameter analysis of β1 overexpression in MDA-MB-231 cells

Parameter	GFP	β1GFP
C_m (pF)	32.13 ± 5.55	25.64 ± 1.83
PCD (pA/pF) **	-5.16 ± 0.71	-16.80 ± 2.90
V_a (mV)	-45.63 ± 1.48	-45.00 ± 2.11
V_p (mV) *	0.63 ± 1.48	-6.25 ± 2.46
Activation $V_{1/2}$ (mV)	-21.34 ± 1.47	-25.38 ± 3.49
Activation *k* (mV)	7.93 ± 0.96	7.50 ± 0.54
Inactivation $V_{1/2}$ (mV)	-53.14 ± 1.56	-47.37 ± 2.96
Inactivation *k* (mV)	-8.24 ± 0.74	-7.04 ± 0.19
T_p (ms)	1.48 ± 0.19	1.44 ± 0.12
RFI $t_{1/2}$ (ms) **	10.17 ± 1.29	5.06 ± 0.52
Data displayed as mean ± SEM (n = 8, N = 3). Unpaired t test used to compare conditions * = P<0.05, ** = P<0.01. Abbreviations: C_m: membrane capacitance, PCD: peak current density, V_a: activation voltage, V_p: voltage at peak current, $V_{1/2}$: voltage for half maximal activation/inactivation, *k:* rate of activation/inactivation, T_p: time to peak, RFI $T_{1/2}$: time for half-maximal recovery from inactivation.		

models, such as HEK293 cells (Laedermann *et al.*, 2013). In summary, β1 expression in MDA-MB-231 cells increased I_{Na} magnitude and accelerated recovery from inactivation compared to GFP expression, as well as hyperpolarising shift in the voltage required for I_{Na} peak.

3.2.2 γ-secretase cleavage does not regulate the β1-induced Na^+ current

α-subunit regulation is a major role of the β1 subunit. The involvement of γ-secretase cleavage on β1-mediated α-subunit regulation has yet to be investigated. The involvement could potentially be profound, considering an α-subunit interaction site is present within the β1-ICD sequence (Meadows *et al.*, 2001). Furthermore, enhanced secretase processing of β2, through BACE1/β2 overexpression in B104 neuroblastoma cells, reduces peak current density relative to β2 overexpression alone (Kim *et al.*, 2007). Therefore, the role of γ-secretase cleavage in regulating the β1-induced I_{Na} was explored using whole cell patch clamp electrophysiology. Firstly, the occurrence of secretase processing of β1-GFP in MDA-MB-231 cells was verified. The predicted molecular weight of full-length (FL) β1-GFP is 65 kDa (Figure 3.2A). The β-secretase cleavage site has previously been identified between Leu144 and Glu145 (Wong *et al.*, 2005). Due to extensive glycosylation of the β1 Ig loop (~10 kDa), the resultant transmembrane fragment following β-secretase cleavage, β1 C-terminal fragment (CTF), is predicted to be only 37 kDa. After γ-secretase cleavage at the membrane-cytoplasm interface, a 33 kDa β1-intracellular domain is produced and released into the cell. To support these predictions, 10 µg, 25 µg and 50 µg of MDA-MB-231-β1GFP lysate was probed on a western blot using an anti-GFP antibody (Figure 3.2B). Three bands resembling FLβ1GFP, β1CTF-GFP and β1ICD-GFP were visible. Two other bands were also observed, one at ~ 55 kDa and another at ~ 27 kDa. The band at 27 kDa likely corresponds to free GFP that has been cleaved off, either within living MDA-MB-231 cells or during the protein extraction procedure. The band at 55 kDa could correspond to

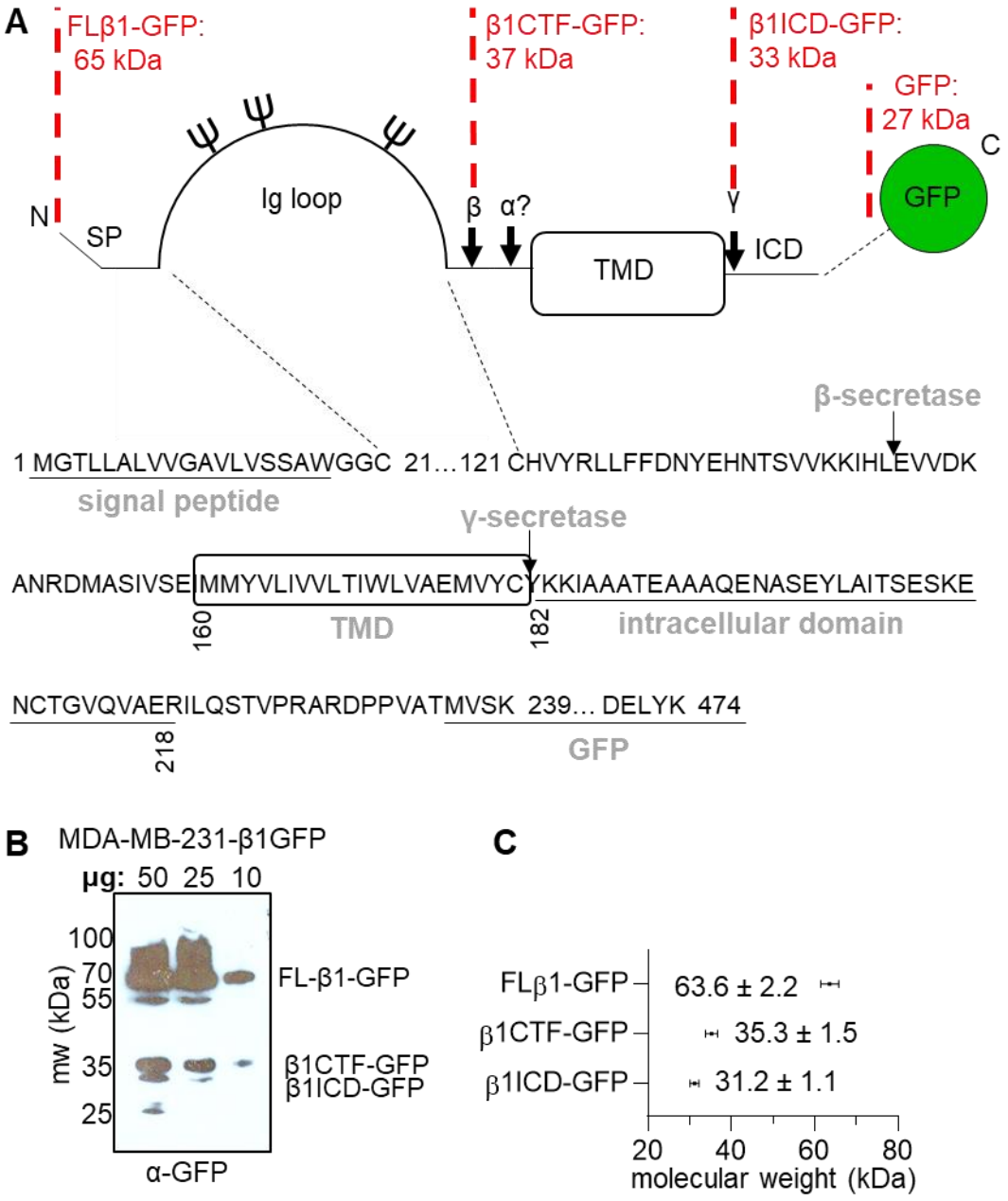

Figure 3.2 γ-secretase cleavage of β1-GFP in MDA-MB-231 cells

(**A**) Schematic of β1-GFP depicting the estimated molecular weights of secretase products. The locations of secretase cleavage noted. Glycosylation of the Ig loop denoted by ψ. The location of β-secretase cleavage has been identified between Leu144 and Glu145 (Wong *et al.*, 2005). The occurrence of α-secretase cleavage is unknown and γ-secretase cleavage is presumed to occur at the membrane-cytoplasm interface. (**B**) Western blot analysis of MDA-MB-231-β1GFP lysate using an anti-GFP antibody. (**C**) Estimation of the molecular weights of secretase products after western blotting, interpolated from the protein ladder. Data displayed as Mean ± SEM (n = 3, N = 3). Abbreviations- FL: full-length, CTF: C-terminal fragment, ICD: intracellular domain, SP: signal peptide, Ig: immunoglobulin, TMD: transmembrane domain.

the fraction of β1-GFP yet to be glycosylated, as glycosylation accounts for ~10 kDa of FLβ1 molecular weight. Interpolating from the logarithmic distances between molecular weight markers, the molecular weights of FLβ1-GFP, β1CTF-GFP and β1ICD-GFP were estimated to be 63.6 ± 2.2, 35.3 ± 1.5 and 31.2 ± 1.1 kDa respectively (n = 3) (Figure 3.2C). These estimates are very similar to initial predictions, suggesting these bands are β1-GFP and its secretase products.

The occurrence of γ-secretase cleavage was further validated using an array of inhibitors: DAPT, L-685,458, and Avagacestat (Figure 3.3A). Lysate of MDA-MB-231-β1GFP cells pre-treated with vehicle or γ-secretase inhibitor was probed via western blotting with an anti-GFP antibody. If γ-secretase cleavage is occurring, the band assumed to be β1ICD-GFP should be absent following drug treatment. Treatment of MDA-MB-231-β1GFP cells with DAPT results in an absence of the β1ICD-GFP band (Figure 3.3B). Densitometry analysis revealed a significant increase in the CTF:ICD ratio from 1.51 ± 0.50 to 22.54 ± 4.92 in vehicle vs. DAPT-treated MDA-MB-231-β1GFP cells (n = 4-5, $P < 0.01$, unpaired t-test) (Figure 3.3C). Likewise, treatment with L-685,458 or Avagacestat reduced β1-ICD generation and increased CTF:ICD ratio to 17.14 and 21.10 respectively, compared to 0.95 in vehicle-treated cells (means based on two repeats) (Figure 3.3D,E). In summary, these data confirm the presence of β1-ICD and demonstrate its formation can be inhibited using these drug treatment regimes.

Following validation of pharmacological inhibition of γ-secretase, MDA-MB-231-β1GFP cells were treated with vehicle or γ-secretase inhibitor and I_{Na} analysed using whole-cell path clamp electrophysiology. Initially, DAPT was used. Cells were assessed for their current-voltage relationship (Figure 3.4A,B), activation-voltage relationship (Figure 3.4C),

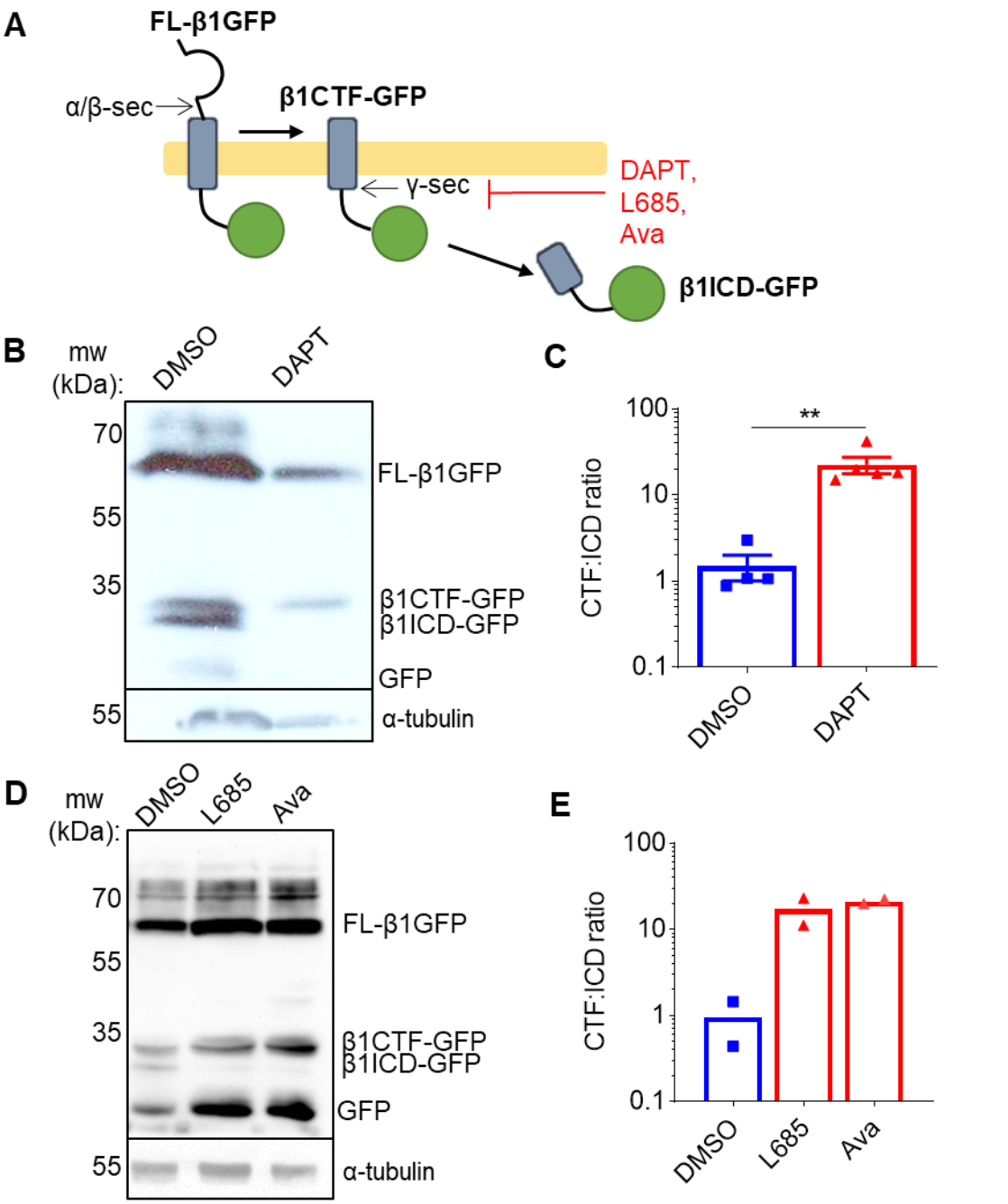

Figure 3.3 Pharmacological inhibition of γ-secretase cleavage in MDA-MB-231-β1GFP cells

(A) Schematic depicting sequential secretase processing of β1. FL: full length, CTF: C-terminal fragment, ICD: intracellular domain. γ-secretase is inhibited by DAPT, L-685,458 and Avagacestat. (**B**) Western blot of lysates (30 µg) derived from MDA-MB-231-β1GFP cells treated with DMSO (0.01 %, 24 h) or DAPT (1 µM, 24 h). Membranes probed for GFP or α-tubulin. Molecular weight (mw) noted on the left side of the blot in kilodaltons. (**C**) Quantification of CTF/ICD band intensity from B. Data displayed as mean ± SEM. Unpaired t-test used to test significance, ** = P<0.01 (n = 4-5, N = 3). (**D**) Western blot of lysates (30 µg) derived from MDA-MB-231-β1GFP cells treated with DMSO (0.1 %, 24 h), L685,458 (10 µM, 24 h) or Avagacestat (10 µM, 24 h). Membranes probed for GFP or α-tubulin. Molecular weight (mw) noted on the left side of the blot in kilodaltons. (**E**) Quantification of CTF/ICD band intensity from D (n = 2, N = 2).

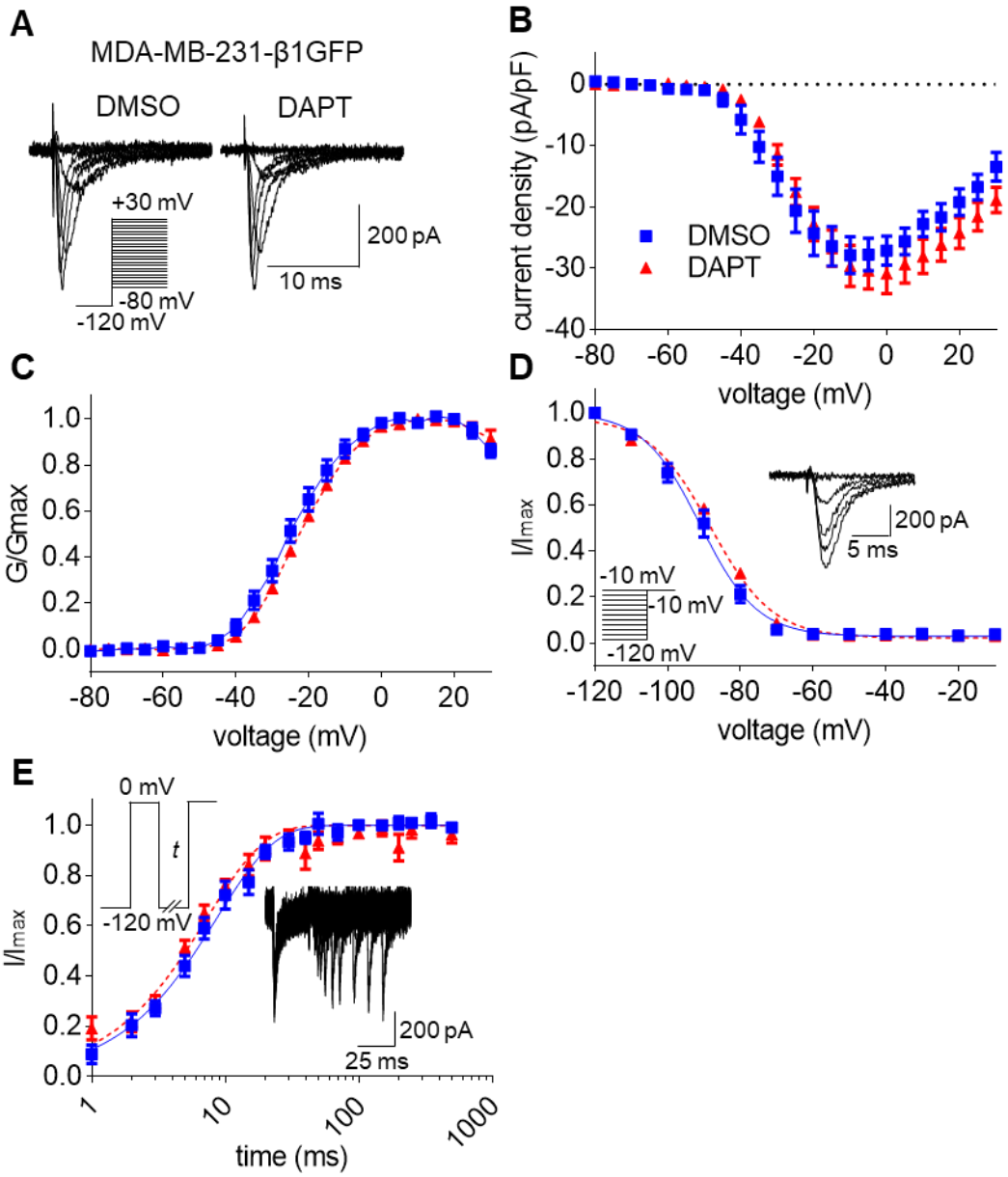

Figure 3.4 The effect of DAPT treatment on the β1-induced Na^+ current in MDA-MB-231-β1GFP cells

(**A**) Representative whole-cell Na^+ currents generated in MDA-MB-231-β1GFP cells pre-treated with DMSO (0.01 %, 24 h) or DAPT (1 μM, 24 h), following stimulation between -80 mV and +30 mV for 250 ms from -120 mV. (**B**) Current -voltage relationship between -80 mV and +30 mV. (**C**) Conductance-voltage relationship, from which activation $V_{1/2}$ was derived, between -80 mV and +30 mV. Fitted Boltzmann sigmoidal curve overlaid. (**D**) Steady-state inactivation. Cells were stimulated at -10 mV following a 250 ms holding voltage of between -80 mV and +30 mV. Normalised current produced plotted. Fitted Boltzmann sigmoidal curve overlaid. Representative trace shown. (**E**) Recovery from inactivation. Cells were stimulated at 0 mV, then held at -120 mV for *t* s before re-stimulation at 0 mV. *t* ranged from 1-500 ms. Fitted mono-exponential curve overlaid (constraints: Y0 = 0, plateau = 1). Representative trace shown. Mean ± SEM plotted for graphs in B-E. n = 8, N = 3 for both conditions.

inactivation-voltage relationship (Figure 3.4D) and recovery from inactivation (Figure 3.4E).Activation and inactivation parameters were derived and compared between vehicle and DAPT-treated cells (Table 3.2). Importantly, no differences were detected in the peak current density (n = 10 - 12, P = 0.29, unpaired t test) and recovery from inactivation (n = 8, P = 0.25, unpaired t test) following DAPT treatment, the two parameters characteristic of the β1-induced I_{Na}. Therefore, it appears DAPT treatment does not regulate the β1-induced I_{Na}. No changes in activation or inactivation kinetics were measured, apart from an increased rate of inactivation in DAPT-treated cells compared to vehicle, -8.41 ± 0.32 and -6.86 ± 0.17 respectively (n = 8, P < 0.001, unpaired t test). As β1-GFP did not affect inactivation in 3.2.1, relative to GFP, it is unlikely DAPT is regulating inactivation via β1. Therefore, this result may be an off-target effect of DAPT or an experimental anomaly. If it is a genuine effect of γ-secretase inhibition, then it will be replicated when using the other γ-secretase inhibitors.

Next, the effect of L-685,458 treatment on the β1-induced I_{Na} was tested. Initially, MDA-MB-231-β1GFP cells were pre-treated with vehicle or L-685,458 (1 μM and 10 μM; 10 μM used in Figure 3.3D) and assessed for their current-voltage relationship (Figure 3.5A,B). Calculating peak current density, 1 μM had no effect compared to vehicle, 19.3 ± 1.5 pA/pF (n = 12) and 21.9 ± 2.5 (n = 18) respectively (P = 0.69, one-way ANOVA) (Figure 3.5C). 10 μM (9.45 ± 2.5 pA/pF, n = 8), however, reduced peak current density compared to vehicle (P < 0.01, one-way ANOVA). This result suggests γ-secretase cleavage may regulate β1-induced I_{Na} and 1 μM is not sufficient to inhibit γ-secretase cleavage. However, as DAPT did not affect peak current density in MDA-MB-231-β1GFP cells, L-685,458 may be functioning independently of β1. To determine whether L-685,458 was functioning via specifically inhibiting secretase processing of β1, MDA-MB-231-GFP cells were treated with L-685,458 and peak current density measured (Figure 3.5D,E).

Table 3.2 Na^+ current parameter analysis of MDA-MB-231-β1GFP cells pre-treated with DAPT

Parameter	DMSO	DAPT
C_m (pF)	19.94 ± 1.25	21.39 ± 0.99
PCD (pA/pF) (n = 10-12)	-26.89 ± 1.86	-30.74 ± 3.21
V_a (mV)	-45.00 ± 1.89	-41.88 ± 0.91
V_p (mV)	-6.25 ± 2.63	-3.75 ± 1.57
Activation $V_{1/2}$ (mV)	-25.16 ± 1.85	-22.58 ± 0.89
Activation *k* (mV)	6.86 ± 0.36	7.08 ± 0.27
Inactivation $V_{1/2}$ (mV)	-90.65 ± 1.91	-88.18 ± 0.91
Inactivation *k* (mV)***	-6.86 ± 0.17	-8.41 ± 0.32
T_p (ms)	0.85 ± 0.05	0.80 ± 0.04
RFI $t_{1/2}$ (ms)	6.25 ± 0.73	5.25 ± 0.41
DMSO: 0.01 %, 24 h, DAPT: 1 μM, 24 h. Data displayed as mean ± SEM (n = 8-unless stated, N = 3). Unpaired t test used to compare conditions. *** = P<0.001. Abbreviations: C_m: membrane capacitance, PCD: peak current density, V_a: activation voltage, V_p: voltage at peak current, $V_{1/2}$: voltage for half maximal activation/inactivation, *k*: rate of activation/inactivation T_p: time to peak, RFI $T_{1/2}$: time for half-maximal recovery from inactivation.		

Similar to the effect seen in β1-GFP expressing cells, 1 μM did not inhibit peak current density relative to vehicle, -8.5 ± 1.3 pA/pF (n = 12) and -12.9 ± 1.9 pA/pF (n = 18), respectively (P = 0.16, one-way ANOVA) (Figure 3.5F). Furthermore, 10 μM (-4.2 ± 0.63 pA/pF, n = 8) significantly inhibited peak current density compared to vehicle (P < 0.01, one-way ANOVA). These data suggest L-685,458 is having an off-target effect in MDA-MB-231 cells to elicit an inhibition of peak current density. As a transition-state analogue, L-685,458 also inhibits signal peptidase, which has an active site structurally similar to presenilin (Ran *et al.*, 2015). Therefore, at higher concentrations, L-685,458 treatment may be interfering with endogenous signal peptidase in MDA-MB-231 and hindering proper protein transport. As 1 μM did not inhibit peak current density in either cell lines, it was used to assess the effect of γ-secretase inhibition on channel activation (Figure 3.5G), inactivation (Figure 3.5H) and recovery from inactivation (Figure 3.5I). Parameters were derived and compared between vehicle and drug treated cells (Table 3.3). However, no differences were detected following L-685,458 treatment for any activation/inactivation parameter, supporting the result using DAPT that γ-secretase inhibition does not affect the β1-induced I_{Na}. However, the ability of 1 μM L-685,458 to inhibit β1ICD-GFP formation was not verified, so it is possible γ-secretase may not be fully inhibited. Although, 1 μM L-685,458 has been used previously (Kim *et al.*, 2005; Brackenbury & Isom, 2011).

The final γ-secretase inhibitor to be tested was Avagacestat. Following the concentration issues with L-685,458, two concentrations were tested: 1 μM and 10 μM (the concentration used in Figure 3.3D). MDA-MB-231-β1GFP cells, treated with vehicle or drug, were examined for their current-voltage relationship (Figure 3.6A,B), activation-voltage relationship (Figure 3.6C), inactivation-voltage relationship (Figure 3.6D) and recovery from inactivation kinetics (Figure 3.6E). Parameters were derived from these experiments and compared between conditions (Table 3.4).

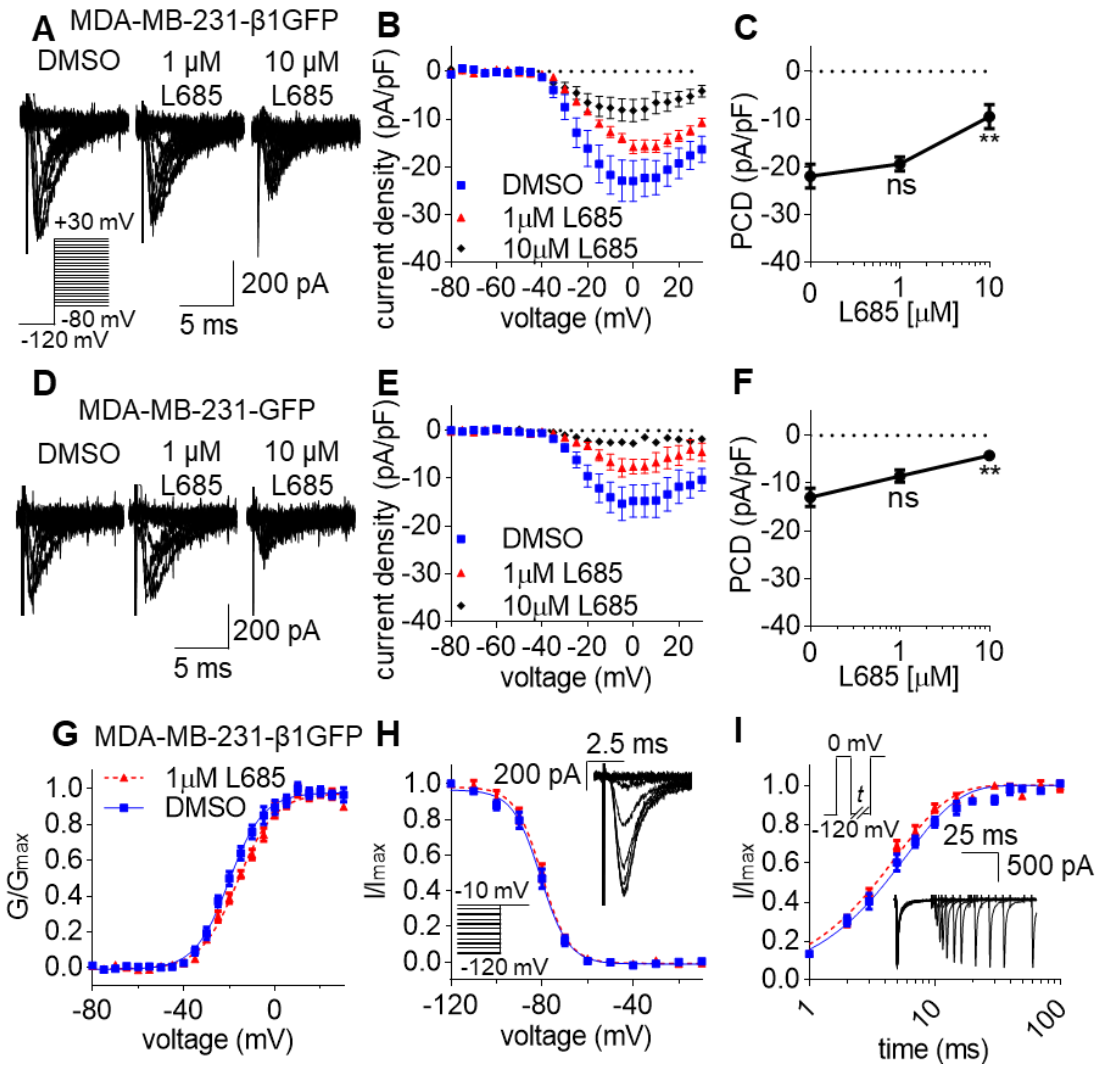

Figure 3.5 The effect of L-685,458 treatment on the β1-induced Na^+ current in MDA-MB-231-β1GFP cells

(**A**) Representative whole-cell Na^+ currents generated in MDA-MB-231-β1GFP cells pre-treated with DMSO (0.1 %, 24 h) or L-685,458 (1 μM/ 10 μM, 24 h) following stimulation between -80 mV and +30 mV for 250 ms from -120 mV. (**B**) Current -voltage relationship between -80 mV and +30 mV following pre-treatment with DMSO (n = 8, N = 3, blue squares, 0.1 %, 24 h) or L-685,458 (n = 8, N = 3, 1 μM, red triangles/ 10 μM, n = 8, N = 3, black diamonds 24 h). (**C**) Change in peak current density (PCD) generated in MDA-MB-231-β1GFP cells following DMSO treatment (n = 18, N = 3), 1 μM L-685,458 pre-treatment (n = 12, N = 3) and 10 μM L-685,458 pre-treatment (n = 7, N = 3). One-way ANOVA used to test statistical difference of L-685,458 treatments to DMSO treatment. ns = not significant, ** = P < 0.01. (**D**-**F**) Replicate A-C but using MDA-MB-231-GFP cells. Same sample sizes used. (**G**) Conductance (G) – voltage relationship (n = 8, N = 3) and (**H**) inactivation – voltage relationship (n = 8, N = 3) of MDA-MB-231-β1GFP cells pre-treated with DMSO (blue squares, 0.01 %, 24 h) or L-685,458 (red triangles, 1 μM, 24h). Fitted Boltzmann equation overlaid. (**I**) MDA-MB-231-β1GFP cells pre-treated with DMSO (blue squares, 0.01 %, 24 h, n = 8, N = 3) or L-685,458 (red triangles, 1 μM, 24h, n = 8) and recovery from inactivation measured. Fitted mono-exponential curve overlaid (constraints: Y0 = 0, plateau = 1). Representative traces shown. Mean ± SEM plotted for all graphs.

Table 3.3 Na^+ current parameter analysis of MDA-MB-231-β1GFP cells pre-treated with L-685,458

Parameter	DMSO	L-685,458
C_m (pF)	19.44 ± 0.62	21.10 ± 1.85
PCD (pA/pF) (n = 12-18)	-21.94 ± 2.47	-19.34 ± 1.50
V_a (mV)	-38.75 ± 1.83	-35.00 ± 0.94
V_p (mV)	1.88 ± 2.30	5.00 ± 2.11
Activation $V_{1/2}$ (mV)	-19.56 ± 1.38	-16.11 ± 0.92
Activation *k* (mV)	7.87 ± 0.77	8.22 ± 0.31
Inactivation $V_{1/2}$ (mV)	-80.99 ± 1.69	-80.26 ± 1.00
Inactivation *k* (mV)	-5.67 ± 0.51	-6.00 ± 0.43
T_p (ms)	0.83 ± 0.07	0.80 ± 0.04
RFI $t_{1/2}$ (ms)	4.19 ± 0.41	3.43 ± 0.17
DMSO: 0.1 %, 24 h. L-685,458: 1 μM, 24 h. Data displayed as mean ± SEM (n = 8- unless stated, N = 3)**.** Unpaired t test used to compare conditions, however no significant difference detected for any condition. Abbreviations: C_m: membrane capacitance, PCD: peak current density, V_a: activation voltage, V_p: voltage at peak current, $V_{1/2}$: voltage for half maximal activation/inactivation, *k*: rate of activation/inactivation T_p: time to peak, RFI $T_{1/2}$: time for half-maximal recovery from inactivation.		

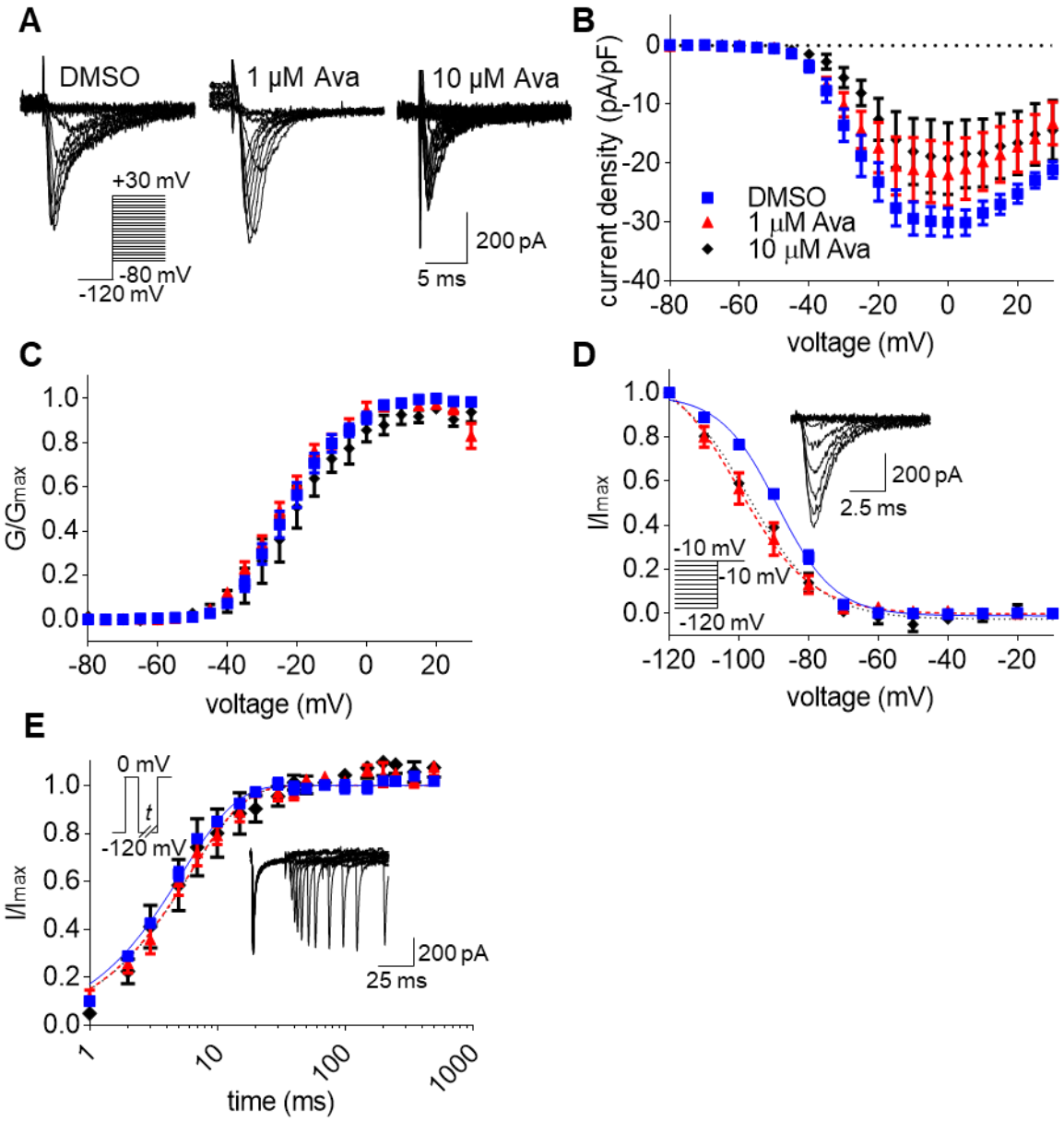

Figure 3.6 The effect of Avagacestat treatment on the β1-induced Na^+ current in MDA-MB-231-β1GFP cells

(**A**) Representative whole-cell Na^+ currents generated in MDA-MB-231-β1GFP cells pre-treated with DMSO (0.1 %, 24 h) or Avagacestat (1 μM/ 10 μM, 24 h), following stimulation between -80 mV and +30 mV for 250 ms from -120 mV. (**B**) Current -voltage relationship between -80 mV and +30 mV. (n = 8, N = 3). (**C**) Conductance-voltage relationship, from which activation $V_{1/2}$ was derived, between -80 mV and +30 mV. Fitted Boltzmann sigmoidal curve overlaid. (n = 8, N = 3). (**D**) Steady-state inactivation. Cells were stimulated at -10 mV following a 250 ms holding voltage of between -80 mV and +30 mV. Normalised current produced plotted. Fitted Boltzmann sigmoidal curve overlaid. Representative trace shown. (n ≥ 3, N = 3) (**E**) Recovery from inactivation. Cells were stimulated at 0 mV, then held at -120 mV for *t* s before re-stimulation at 0 mV. *t* ranged from 1-500 ms. Fitted mono-exponential curve overlaid (constraints: Y0 = 0, plateau = 1). Representative trace shown. (n ≥ 5, N = 3). Mean ± SEM plotted for graphs in B-E. DMSO: blue squares, 1 μM Avagacestat: red triangles, 10 μM Avagacestat: black diamonds.

Table 3.4 Na^+ current parameter analysis of MDA-MB-231-β1GFP cells pre-treated with Avagacestat

Parameter	DMSO	Ava (1 µM)	Ava (10 µM)
C_m (pF)	21.56 ± 1.07	22.18 ± 0.73	23.76 ± 2.87
PCD (pA/pF)	-31.06 ± 2.45	-23.73 ± 3.96	-20.41 ± 6.00
V_a (mV)	-45.00 ± 1.64	-44.38 ± 1.48	-42.14 ± 2.64
V_p (mV)	-1.88 ± 2.66	-3.13 ± 2.66	2.14 ± 4.74
Activation $V_{1/2}$ (mV)	-22.17 ± 1.97	-25.45 ± 1.26	-22.00 ± 3.66
Activation *k* (mV)	7.78 ± 0.31	7.69 ± 0.25	8.52 ± 2.14
Inactivation $V_{1/2}$ (mV)	-89.03 ± 1.02	*-98.90 ± 3.64	-97.43 ± 0.64
Inactivation *k* (mV)	-8.09 ± 0.34	-8.30 ± 0.40	*-10.42 ± 1.01
T_p (ms)	0.86 ± 0.05	0.75 ± 0.04	*1.05 ± 0.10
RFI $t_{1/2}$ (ms)	3.69 ± 0.15	4.58 ± 0.66	3.33 ± 0.33
DMSO: 0.1 %, 24h. Avagacestat: 1/10 µM, 24h. Data displayed as mean ± SEM (n ≥ 7, except Ava (10 µM) for inactivation experiments, which was n = 3) (N = 3)**.** One-way ANOVA used to compare conditions. * = P < 0.05. Abbreviations: Ava: Avagacestat, C_m: membrane capacitance, PCD: peak current density, V_a: activation voltage, V_p: voltage at peak current, $V_{1/2}$: voltage for half maximal activation/inactivation, *k*: rate of activation/inactivation T_p: time to peak, RFI $T_{1/2}$: time for half-maximal recovery from inactivation.			

No difference was detected in peak current density nor recovery from inactivation between conditions. A hyperpolarised shift in voltage threshold for half channel inactivation was observed in 1 μM Avagacestat-treated cells compared to control, -98.9 ± 3.6 mV and -89.0 ± 1.0 mV respectively (n = 8, P < 0.05, one-way ANOVA). An enhanced rate of inactivation was also observed in 10 μM treated cells compared to control, -10.42 ± 1.0 (n = 3) and -8.09 ± 0.3 (n = 8) respectively (P < 0.05, one-way ANOVA). Lastly, an increased time to I_{Na} peak was observed in 10 μM treated cells relative to control, 1.05 ± 0.1 ms (n = 7) and 0.86 ± 0.05 ms (n = 8) respectively (P < 0.05, one-way ANOVA). These changes in gating kinetics are likely a technical issue, as holding membrane voltage at the required value is highly dependent on the strength of the seal between membrane and pipette, or a statistical issue, as the sample size is only eight and ten parameters are being measured with a significance threshold of P = 0.05. Regarding the parameter changes elicited by β1, i.e. peak current density and recovery from inactivation, none of the γ-secretase inhibitors had an effect, suggesting γ-secretase does not regulate the β1-induced I_{Na}.

3.2.3 γ-secretase inhibition increases β1-induced cell adhesion

Transcellular adhesion is an important non-conducting function of β1 (Malhotra *et al.*, 2000). Adhesion, homophilically and heterophilically to various CAMs, is mediated through an extracellular Ig domain (Malhotra *et al.*, 2000; McEwen & Isom, 2004). As the ECD is cleaved off following secretase processing, inhibiting secretase cleavage should cause an accumulation of full-length β1 and an increase in transcellular adhesion. However, if only γ-secretase is inhibited, CTFs may instead accumulate at the plasma membrane, resulting in decreased transcellular adhesion, a phenomenon seen following DAPT-treatment of CHO-β2 cells (Kim *et al.*, 2005). Transcellular adhesion was measured using a cell-cell adhesion assay (Wong & Filbin, 1996; Chioni *et al.*, 2009), involving pre-treatment of cells in vehicle or DAPT for 24 h, then attaining a single cell

suspension using trypsin and mechanical agitation. The rate of cell-cell adhesion is measured by counting the number of particles (cell aggregates of any quantity) every 30 min for 2 h and normalising the particle count to T = 0. DAPT treatment of MDA-MB-231-β1GFP cells caused an increase in transcellular adhesion, exemplified by a decreased particle count after 90 min, 0.22 ± 0.02 (n = 30), compared to vehicle-treated cells, 0.52 ± 0.06 (n = 30, $P < 0.05$, two-way ANOVA) (Figure 3.7A,B). Treatment of MDA-MB-231 cells with DAPT, however, caused no change in transcellular adhesion (two-way ANOVA) (Figure 3.7C). These data suggest that β1 is necessary for the DAPT-induced increase in transcellular adhesion.

3.2.4 β1 is not enriched at the plasma membrane

Functional evidence from chapters 3.2.2 and 3.2.3 suggests β1 is localised at the plasma membrane. To better understand the membrane dynamics of β1, live MDA-MB-231-β1GFP cells were imaged by confocal microscopy. Endogenous GFP, as well as the membrane dye FM4-64 were visualised (Figure 3.8A). Comparing β1-GFP signal overlap with FM4-64, β1-GFP did not appear to be enriched at the plasma membrane compared to the cytosol (Figure 3.8B). To quantify membrane β1 expression, β1-GFP and FM4-64 signals were measured by line profiles spanning the plasma membrane. 3 – 4 line profiles (5 μm long) were taken equidistantly around the perimeter of the cell, avoiding intracellular vesicles with bright GFP fluorescence, averaged out, then normalised to the peak fluorescence of each respective fluorophore. The line profiles demonstrated peak β1-GFP expression was offset from the FM4-64 fluorescence peak by ~500 nm (n = 10) (Figure 3.8C). Whereas FM4-64 showed clear enrichment at the plasma membrane, β1-GFP signal was more diffuse and peaked over a large range of points along the line profile for each cell.

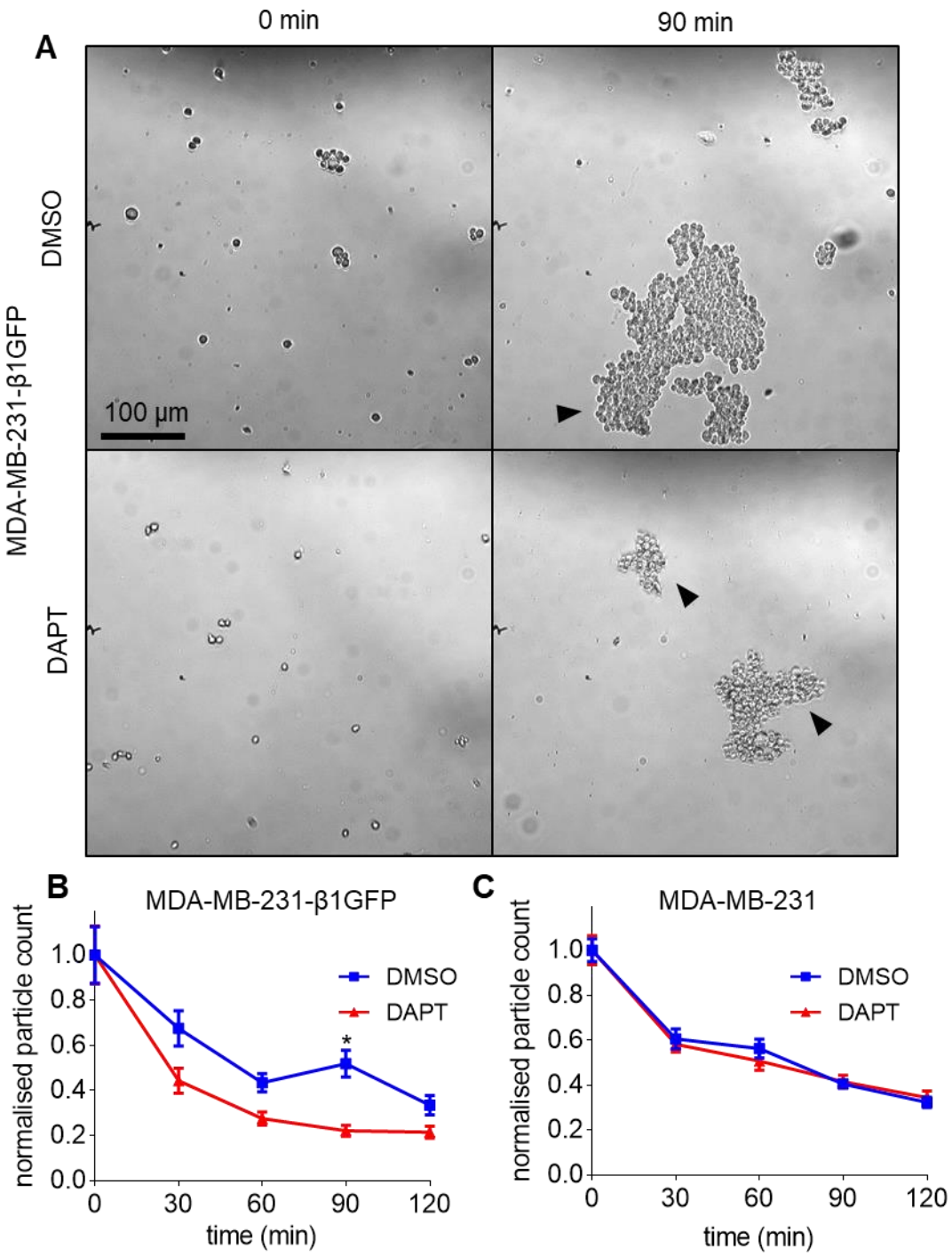

Figure 3.7 Effect of γ-secretase inhibition on β1-induced transcellular adhesion in MDA-MB-231 cells

(**A**) Single cell suspensions, pre-treated with DMSO (0.01 %, 24 h) or DAPT (1 μM, 24 h), were left to aggregate for 2 h. Treatments also included during experiment. The number of particles in a sample was counted every 30 min. Black arrows demonstrate cell aggregates after 90 min. (**B**) Quantification of the rate of transcellular adhesion of MDA-MB-231-β1GFP cells pre-treated with DMSO or DAPT (n > 25, N = 3). (**C**) Quantification of the rate of transcellular adhesion of MDA-MB-231 cells pre-treated with DMSO or DAPT (n > 25, N = 3). Two-way ANOVA used to test significance between treatments at each time point. * = P<0.05.

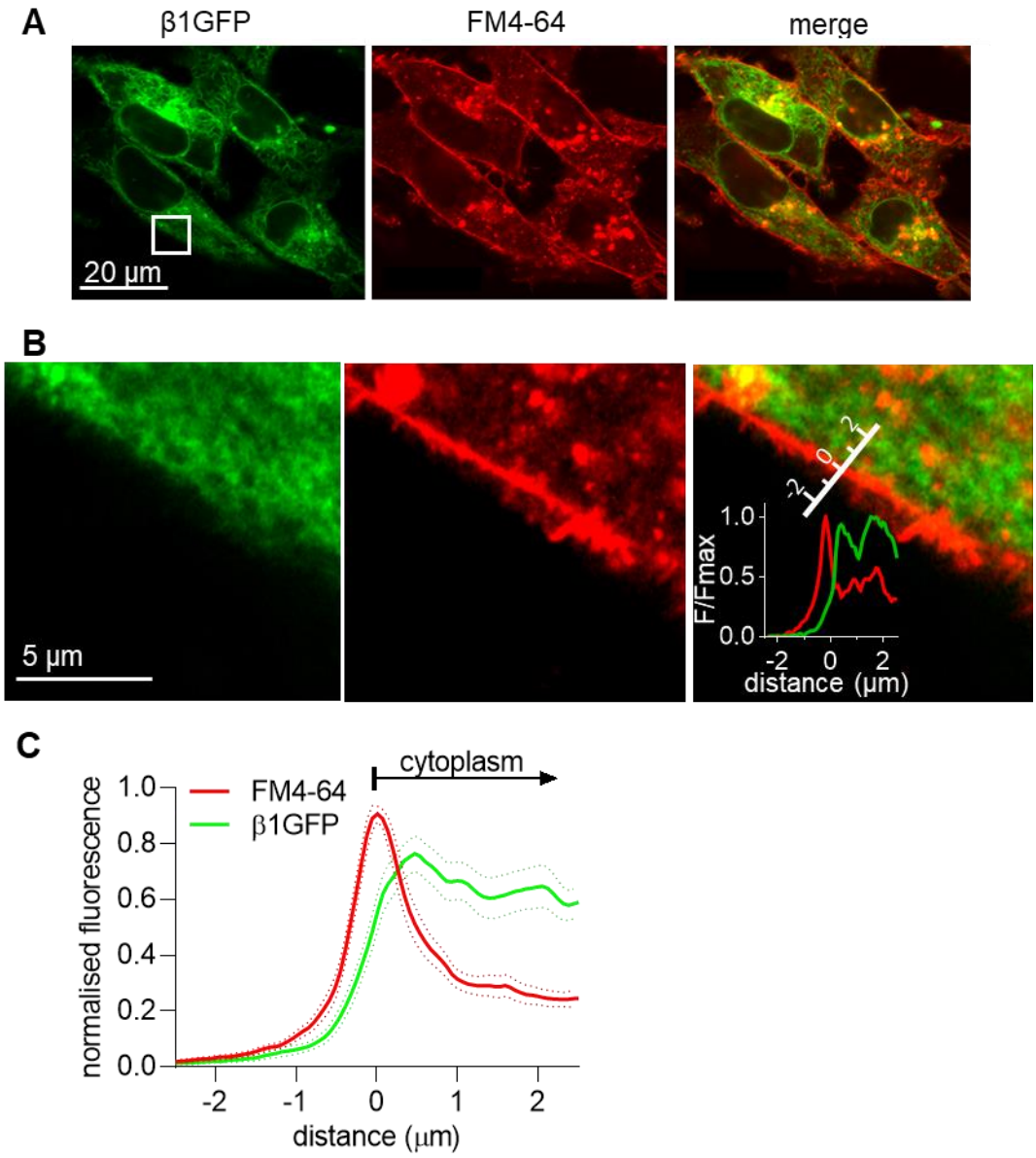

Figure 3.8 Membrane localisation of β1-GFP in MDA-MB-231-β1GFP cells

(**A**) Confocal image of live MDA-MB-231-β1GFP cells stained just prior to imaging with FM4-64 (120 nM). (**B**) Magnified image of A, focusing on the plasma membrane. Example line profile shown on merge panel demonstrating GFP/FM4-64 fluorescence (**C**) A 5 µm line profile across the plasma membrane of live MDA-MB-231-β1GFP cells. Data displayed as mean (solid line) ± SEM (dotted line). A 10-pixel wide line profile was taken at four regions around the same cell and averaged to produce a cellular average (n = 10 cells, N = 1).

As the GFP emission peak of ~509 nm is near the excitation peak of FM4-64 (~515 nm), the possibility of the GFP signal being quenched by FM4-64 at the plasma membrane was investigated. Firstly, robust colocalization of β1-GFP with FM4-64 is visible in internal vesicles, suggesting FM4-64 is not capable of completely quenching GFP signal (Figure 3.9A). To support this by quantitative means, Förster resonance energy transfer (FRET) was used to investigate fluorescence transfer between GFP and FM4-64. FRET is a microscopy technique used to assess the extent of quenching of one fluorophore by another fluorophore. Multiple methods of assessing FRET are possible, in this work, FM4-64 was photobleached and the subsequent change in GFP signal monitored. If GFP is being quenched by FM4-64, an increase in signal would be expected following photobleaching of FM4-64. FRET within internal vesicles was also examined as a control, as both fluorophores demonstrate robust signal and clear overlap, so if FRET is possible between GFP and FM4-64, it should be detectable foremost within internal vesicles. Indeed, photobleaching of FM4-64 signal within internal vesicles resulted in a 8.9 ± 0.03 % increase in GFP signal between the pre-bleach and post-bleach frames ($n = 4$, $P < 0.05$, unpaired t-test), implying FM4-64 can quench GFP signal (Figure 3.9B,C). However, the complete lack of fluorescence peak at the plasma membrane for β1-GFP is not explainable by the 8.2 % decrease in the GFP signal that would be expected if β1-GFP and FM4-64 were co-localised at the plasma membrane. When FRET at the plasma membrane was investigated, no increase in GFP signal was detected following FM4-64 photobleaching (Figure 3.9D,E). The lack of GFP fluorescence increase at the plasma membrane following FM4-64 photobleaching is likely due to lack of sufficient concentration of GFP at the plasma membrane to elicit a detectable level of FRET. FRET occurs when fluorescent molecules are within nanometre range, whereas the β1-GFP-FM4-64 peak offset observed was ~500 nm (Figure 3.8C). In summary, these data suggest that β1-GFP is most likely not enriched at the plasma membrane, compared to the robust signal β1-GFP displays within intracellular vesicles.

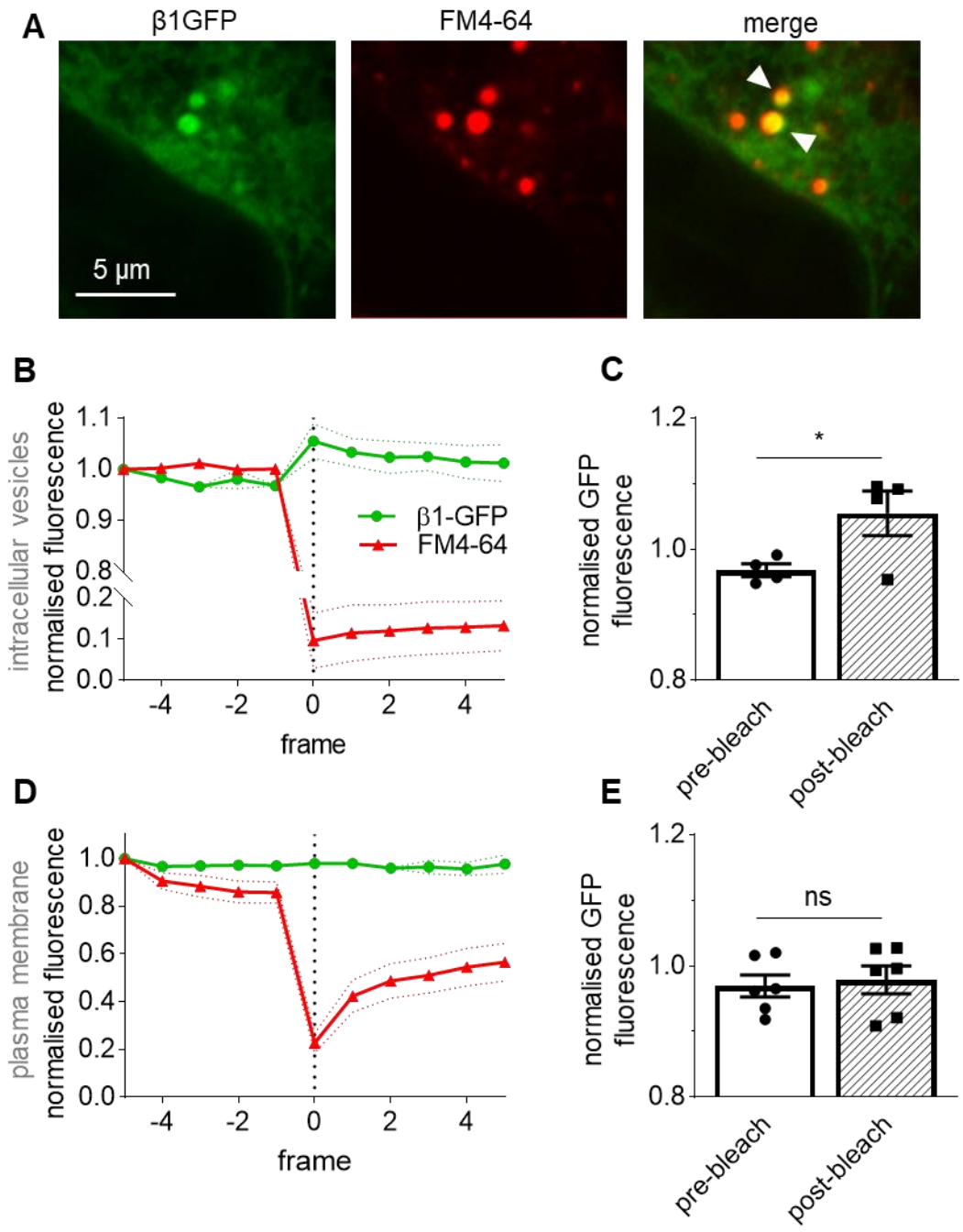

Figure 3.9 Förster resonance energy transfer (FRET) of β1-GFP and FM4-64 in MDA-MB-231-β1GFP cells

(**A**) Co-localisation of FM4-64 and β1-GFP within intracellular vesicles, adjacent to the nucleus of a live MDA-MB-231-β1GFP cell. (**B**,**D**) FRET between GFP and FM4-64 within intracellular vesicles (**B**) and at the plasma membrane (**D**). Regions of interest were photobleached using 100 iterations of a 561 nm laser (100 % laser power) to achieve 80-90 % bleaching of FM4-64. Data displayed as mean (solid line) ± SEM (dotted line). Green circles = β1-GFP. Red triangles = FM4-64 (**C**,**E**) Quantification of FRET between GFP and FM4-64 within intracellular vesicles (**C**) and at the plasma membrane (**E**) using data from B and D respectively. GFP fluorescence (normalised to fluorescence of the first frame) between the pre-bleach and post-bleach recording, within the region of interest, was compared using an unpaired t-test. n = 4 – 6, N = 1. Data displayed as mean ± SEM. ns = not significant. * = P<0.05.

3.2.5 β1 intracellular domain formation is undetectable using fluorescence recovery after photobleaching

Following the observation of low plasma membrane β1 expression in chapter 3.2.4**,** the internal localisation of β1 was investigated. The generation of β1ICD was examined using fluorescence recovery after photobleaching (FRAP) to determine if the low plasma membrane abundance is due to the overwhelming intracellular GFP signal originating from cleaved β1ICD-GFP and not full-length β1-GFP, as the GFP tag is fused to the C-terminus of β1. Live MDA-MB-231-β1GFP cells, treated with vehicle (0.01 % DMSO, 24 h) or DAPT (1 μM, 24 h), were imaged on a confocal microscope via detection of endogenous GFP. A 2 μm region of interest within the cytosol was photobleached and GFP fluorescence recovery monitored at the leading and trailing edges of MDA-MB-231-β1GFP cells (Figure 3.10). The leading and trailing edges were both examined as MDA-MB-231 cells are polarised, and secretase cleavage may be different between the two functionally distinct compartments. The FRAP procedure measures fluorescence recovery at a mid-cellular level at the leading and trailing edges of MDA-MB-231-β1GFP cells. Due to the thinness of MDA-MB-231 cells at the extremities, the photobleaching event also encapsulates plasma membrane β1 at the apical and basal membranes, as well as intracellularly retained β1. The hypothesis was vehicle-treated cells should contain a mixed population of membrane-bound β1-GFP and soluble β1ICD-GFP, whereas DAPT-treated cells should contain membrane-bound β1-GFP only. Therefore, fluorescence recovery in vehicle-treated cells should be accelerated and the mobile fraction enhanced, due to the influence of soluble β1ICD-GFP within the GFP-positive cellular elements. However, parameter analysis demonstrated no differences in mobility between vehicle and DAPT-treated cells at either the leading or trailing edges (Table 3.5). The mobile fraction is a measure of the proportion of fluorophores that are mobile during the time course, a value less than 1.0 implies a sub-population of the fluorophore is immobilised within the region of interest and not able to diffuse out.

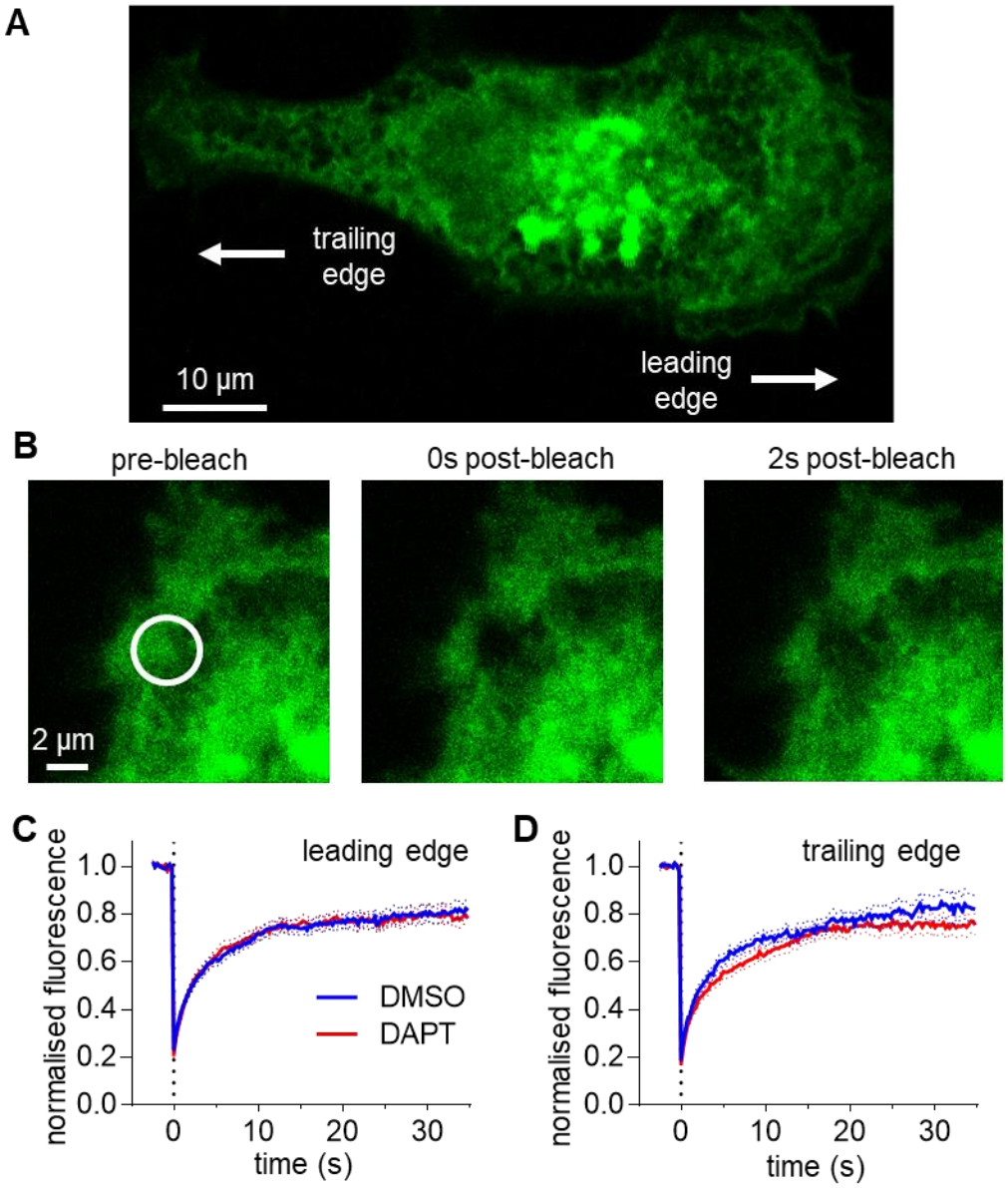

Figure 3.10 Assessing β1-ICD formation in MDA-MB-231-β1GFP cells using fluorescence recovery after photobleaching (FRAP)

(**A**) Typical polarised MDA-MB-231-β1GFP cell with the leading and trailing edges denoted. The leading edge was defined as the pole with lamellipodia present. (**B**) Representative photobleaching and recovery of GFP fluorescence at the leading edge of a live MDA-MB-231-β1GFP cell following photobleaching with a 488 nm laser (40 iterations, 100 % laser power). (**C**,**D**) Quantification of the recovery of GFP fluorescence in MDA-MB-231-β1GFP cells, after DMSO (0.01 %, 24 h, red line) or DAPT (1 µM, 24 h, blue line) pre-treatment, at the leading (**C**) and trailing (**D**) edges. Recordings were taken every 250 ms. Photobleaching event displayed as black dotted line at time = 0. Data displayed as mean (solid line) ± SEM (dotted line). n > 25, N = 3.

Table 3.5 Mobility parameters of β1-GFP at the leading and trailing edges of a MDA-MB-231-β1GFP cell following DAPT treatment

	Leading edge		Trailing edge	
	DMSO (n=28)	DAPT (n=27)	DMSO (n=25)	DAPT (n=26)
Mobile fraction	0.68 (0.60-0.88)	0.72 (0.62-0.79)	0.74 (0.63-0.95)	0.69 (0.49-0.92)
	P = 0.55		P = 0.19	
time constant (s)	2.49 (1.82-2.97)	2.33 (1.89-2.76)	2.70 (1.97-3.21)	2.52 (2.13-3.21)
	P = 0.60		P = 0.82	
D_{2D} ($\mu m^2 s^{-1}$)	0.11 (0.09-0.18)	0.11 (0.08-0.14)	0.11 (0.07-0.16)	0.10 (0.07-0.14)
	P = 0.72		P = 0.73	

Comparisons between DMSO-DAPT treatment for each parameter at each location made using a Mann-Whitney test, P-value displayed underneath each comparison. Data displayed as median (IQR). n > 25, exact n number displayed next to each condition. N = 3. Abbreviations: D_{2D}: diffusion coefficient.

Soluble β1ICD-GFP was expected to be freely mobile, while membrane bound β1-GFP may be immobilised. No different in the mobile fraction was detected at the leading edge (DMSO-treated cells: 0.68 (median, n = 28, IQR: 0.60 – 0.88), DAPT-treated cells: 0.72 (median, n = 27, IQR: 0.62 – 0.79), P = 0.55, Mann-Whitney U test) or trailing edge (DMSO-treated cells: 0.74 (median, n = 25, IQR: 0.63 – 0.95), DAPT-treated cells: 0.69 (median, n = 26, IQR: 0.49 – 0.92), P = 0.19, Mann-Whitney U test), suggesting β1ICD-GFP is undetectable, or it is similarly as immobilised as β1-GFP. Regardless, the GFP signal does not appear to be freely mobile. The time constant is used to calculate the diffusion coefficient, which is a measure of the rate of diffusion and the metric that is most likely to distinguish a soluble from transmembrane protein. A typical diffusion coefficient for a transmembrane protein can range from 0.001 – 0.1 $\mu m^2 s^{-1}$, whereas 1 – 20 $\mu m^2 s^{-1}$ is typical for soluble GFP (Kusumi *et al.*, 1993; Swaminathan *et al.*, 1997; Calvert *et al.*, 2010; Gura Sadovsky *et al.*, 2017). The time constant is the time taken for half-maximal fluorescence recovery in the region of interest and thus is dependent on the size and geometry of the region of interest. Whereas the diffusion coefficient predicts the rate of Brownian diffusion, taking into account the time constant and the size of the region of interest.

An increased time constant and decreased diffusion coefficient was expected in DAPT-treated MDA-MB-231-β1-GFP cells, as there is no β1ICD-GFP present. However, no difference was calculated between the time constants of DMSO- and DAPT-treated cells at the leading edge (DMSO-treated cells: 2.49 s (median, n = 28, IQR: 1.82 – 2.97), DAPT treated cells: 2.33 s (median, n = 27, IQR: 1.89 – 2.76), P = 0.60, Mann-Whitney U test) or trailing edge (DMSO-treated cells: 2.70 s (median, n = 25, IQR: 1.97 – 3.21), DAPT-treated cells: 2.52 s (median, n = 26, IQR: 2.13 – 3.21), P = 0.82, Mann-Whitney U test). Furthermore, no difference between the diffusion coefficients between conditions at the leading edge (DMSO-treated cells: 0.11 $\mu m^2 s^{-1}$ (median, n = 27, IQR: 0.09 – 0.18),

DAPT-treated cells: 0.11 $\mu m^2 s^{-1}$ (median, n = 27, IQR: 0.08 – 0.14), P = 0.72, Mann-Whitney U test) or trailing edge (DMSO-treated cells: 0.11 $\mu m^2 s^{-1}$ (median, n = 25, IQR: 0.07 – 0.16), DAPT-treated cells: 0.10 $\mu m^2 s^{-1}$ (median, n = 26, IQR: 0.07 – 0.14), P = 0.73, Mann-Whitney U test) was observed. Thus, the data here suggest that the predominantly intracellular GFP signal observed in MDA-MB-231-β1GFP is still characteristic of transmembrane proteins and little/no detectable β1ICD is present within the region of interests tested. Possible reasons for this are: β1ICD-GFP is being generated in a restricted spatial location within the cell, the proportion of β1ICD-GFP present within the region of interest is overwhelmed by the amount of β1-GFP and is undetectable, or β1ICD-GFP remains associated with the membrane after γ-secretase cleavage.

3.2.6 β1 is expressed in the endolysosomal pathway

A noticeable feature of β1-GFP expression is the bright puncta localised in the perinuclear region, assumed to be of vesicular origin. APP and Notch are both found within the endolysosomal pathway and are both processed by γ-secretase within this pathway (Vaccari *et al.*, 2008; Tam & Pasternak, 2015). To test the hypothesis that these β1-GFP puncta are endosomal in origin, fixed MDA-MB-231-β1GFP cells were co-stained for early endosome antigen 1 (EEA1), an early endosomal marker, and co-localisation determined using super resolution confocal with Airyscan microscopy. To investigate whether γ-secretase cleavage may be occurring within endosomes MDA-MB-231-β1GFP cells were treated with DAPT (1 μM, 24 h) and co-localisation measured. The hypothesis was that inhibition of β1-GFP proteolysis within endosomes would cause an accumulation of endosomal GFP signal, as β1ICD-GFP is not cleaved and released into the cell but retained at the membrane as part of β1-GFP or β1CTF-GFP. In DMSO-treated cells, β1-GFP puncta demonstrated partial EEA1 co-localisation, suggesting β1-

GFP is being endocytosed from the plasma membrane, however, not all β1-GFP puncta co-localise with EEA1, so β1-GFP must also be found within other vesicles (Figure 3.11A). In DAPT-treated cells, a comparable, partial β1-GFP puncta co-localisation with EEA1 was also observed (Figure 3.11B). Co-localisation was quantified and compared between conditions in an attempt to discriminate any potential differences in EEA1+ β1-GFP expression following DAPT treatment. Co-localisation between GFP and EEA1 signal was measured using Pearson's correlation coefficient (PCC). If γ-secretase inhibition causes an accumulation of endosomal β1-GFP, a higher PCC would be expected in DAPT-treated cells. However, following co-localisation analysis, a decrease in PCC was observed in DAPT-treated compared to DMSO-treated MDA-MB-231-β1GFP cells, 0.47 (median, IQR: 0.41 – 0.52, n = 25) and 0.53 (median, IQR: 0.48 – 0.55, n = 26) respectively (P = 0.02, Mann-Whitney U test) (Figure 3.11C). This result suggests that endosomes are not a site of γ-secretase processing of β1, but perhaps γ-secretase inhibition sequesters β1-GFP at the plasma membrane, thus reducing endosomal enrichment.

As β1 demonstrates only partial endosomal co-localisation, fixed MDA-MB-231-β1GFP cells were co-stained for lysosomal associated membrane protein 1 (LAMP1), to determine if a population of β1-GFP puncta are lysosomal in origin. lysosomes are a common site of secretase processing of APP (Tam & Pasternak, 2015). Co-localisation was again quantified, using PCC, with and without DAPT treatment. LAMP1/β1-GFP co-localisation was present in vehicle and DAPT-treated cells (Figure 3.12A,B). however no difference was seen in the degree of co-localisation between DMSO and DAPT treated cells (P = 0.44, Mann-Whitney u test), 0.52 (median, n = 27, IQR: 0.45 – 0.60) and 0.52 (median, n = 23, IQR: 0.43 – 0.56) respectively (Figure 3.12C), suggesting lysosomes are not a site of γ-secretase processing of β1-GFP.

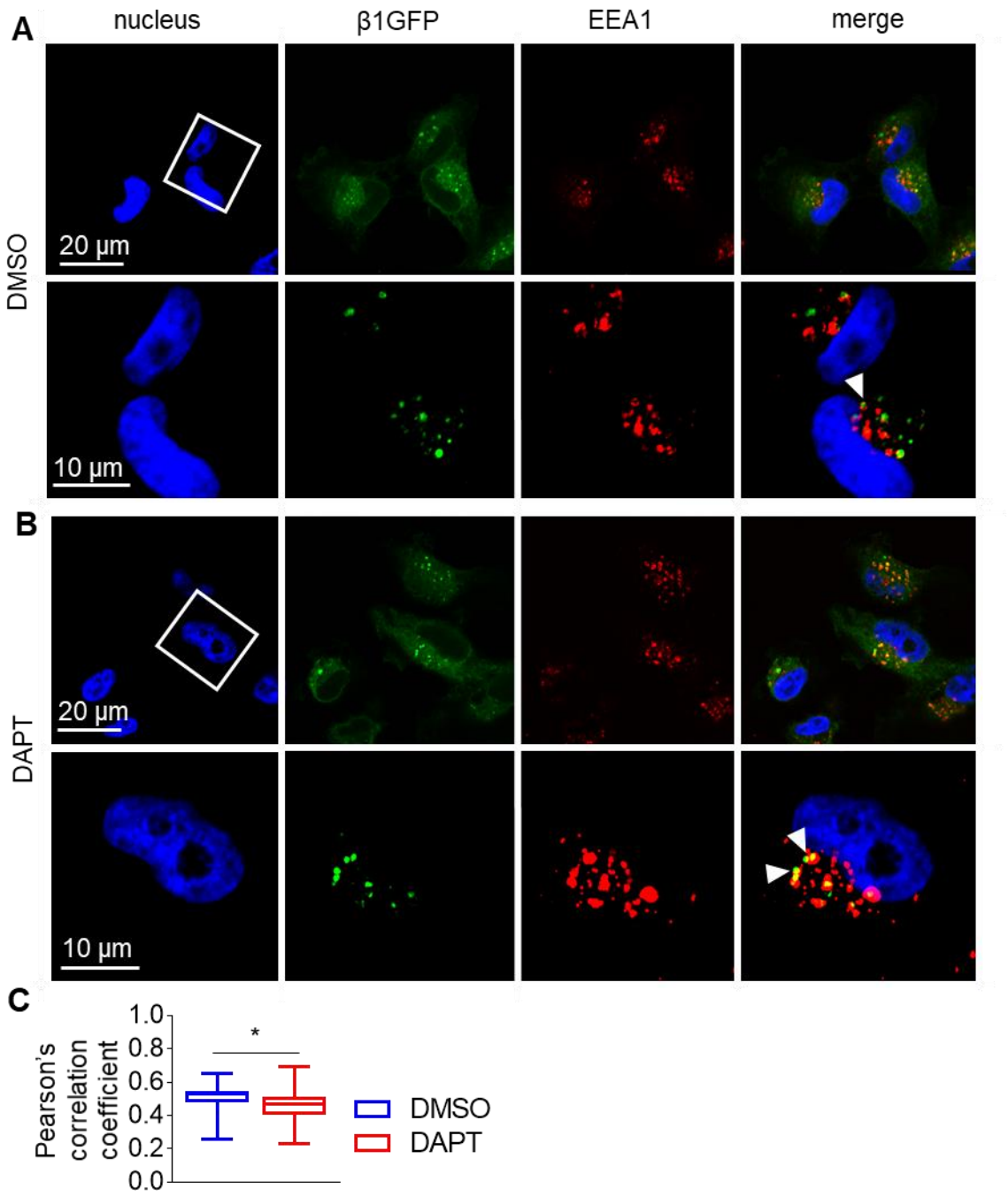

Figure 3.11 Assessing changes in β1 localisation in early endosomes of MDA-MB-231-β1GFP cells following γ-secretase inhibition

(**A**,**B**) MDA-MB-231-β1GFP cells, pre-treated with DMSO (**A**, 0.01 %, 24 h) or DAPT (**B**, 1 μM, 24 h), were stained for EEA1, DNA (using DAPI) and endogenous GFP detected using a confocal microscope. For each condition, a magnified image with a raised lower pixel threshold limit is given below the unmagnified image. The raised lower pixel threshold allows for best visualise of the punctate expression profile of β1-GFP. White arrows indicate regions of co-localisation of β1-GFP and EEA1. (**C**) Quantification of the co-localisation of GFP and EEA1 was calculated using Pearson's correlation coefficient. Data displayed as min-max box plots. n > 25, N = 3. Mann Whitney test used to test for significance. * = $P < 0.05$.

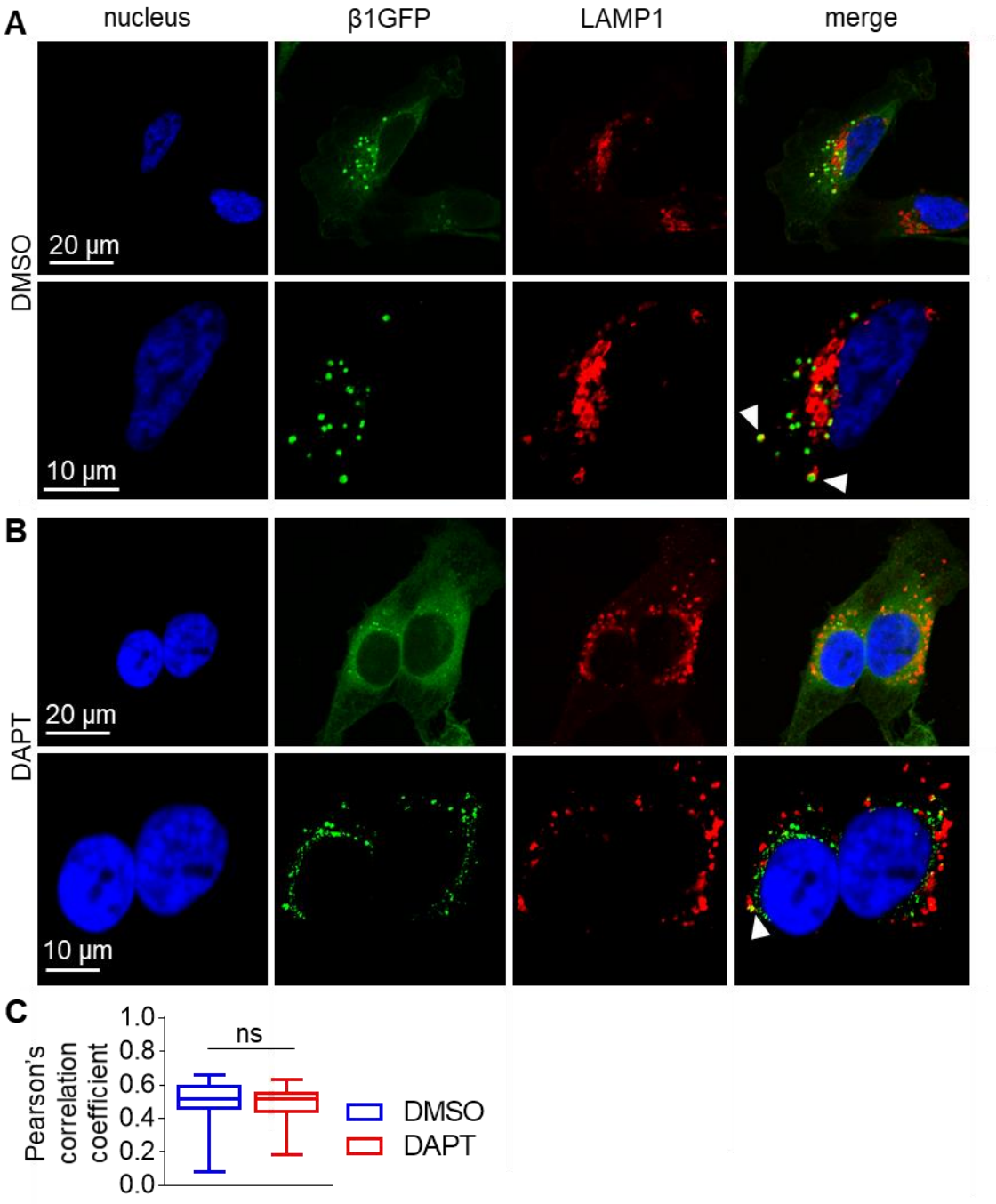

Figure 3.12 Assessing changes in β1 localisation in lysosomes of MDA-MB-231-β1GFP cells following γ-secretase inhibition

(**A**,**B**) MDA-MB-231-β1GFP cells, pre-treated with DMSO (**A**, 0.01 %, 24 h) or DAPT (**B**, 1 μM, 24 h), were stained for LAMP1 (lysosome marker), DNA (using DAPI) and endogenous GFP detected using a confocal microscope. For each condition, a magnified image with a raised lower pixel threshold limit is given below the unmagnified image. The raised lower pixel threshold allows for best visualise of the punctate expression profile of β1-GFP. White arrows indicate regions of co-localisation. (**C**) Co-localisation was quantified using Pearson's correlation coefficient. Data displayed as min-max box plots. n ≥ 23, N = 3. Mann Whitney test used to test for significance. ns = not significant.

Lysosomes appeared to not be a site of γ-secretase processing of β1, however, β1-GFP/LAMP1 co-localisation was detected, suggesting lysosomes may be the site of β1-GFP degradation. To test whether β1-GFP was indeed being degraded in lysosomes, MDA-MB-231-β1GFP cells were treated with chloroquine. Chloroquine inhibits lysosomal degradation and causes a characteristic swelling of lysosomes (Mauthe *et al.*, 2018). MDA-MB-231-β1GFP cells pre-treated with chloroquine display enlarged intracellular vesicles, lined with β1-GFP signal, which are not seen in negative control cell, supporting the hypothesis that β1 is degraded in lysosomes (Figure 3.13).

3.2.7 β1 displays partial nuclear localisation

The fate of many γ-secretase-generated ICDs is translocation to the nucleus in order to regulate gene expression (Haapasalo & Kovacs, 2011). To examine whether any β1-GFP signal was present in the nucleus, fixed MDA-MB-231-β1GFP cells were permeabilised with Triton X-100 or digitonin. Triton X-100 is a detergent capable of permeabilising all cellular membranes, whereas digitonin is incapable of permeabilising the nuclear membrane, thus not permitting antibody access to nuclear antigens (Mojica *et al.*, 2015). This was confirmed by staining for the inner nuclear membrane protein, Lamin B2. Cells permeabilised with Triton X-100, unlike digitonin, showed Lamin B2 signal, confirming that digitonin treatment, unlike Triton X-100, was incapable of permeabilising the nuclear membrane (Figure 3.14A). To determine β1-GFP nuclear localisation, the nuclear: cytoplasmic signal density ratio was determined following Triton X-100 and digitonin incubation (Figure 3.14B). The nuclear: cytoplasmic signal density ratio was significantly reduced in digitonin-permeabilised cells compared to Triton X-100 permeabilised cells, 0.45 ± 0.02 (n = 28) and 0.55 ± 0.01 (n = 26) respectively, suggesting a small fraction of β1-GFP signal may be present within the nucleus ($P < 0.001$, unpaired t test) (Figure 3.14C).

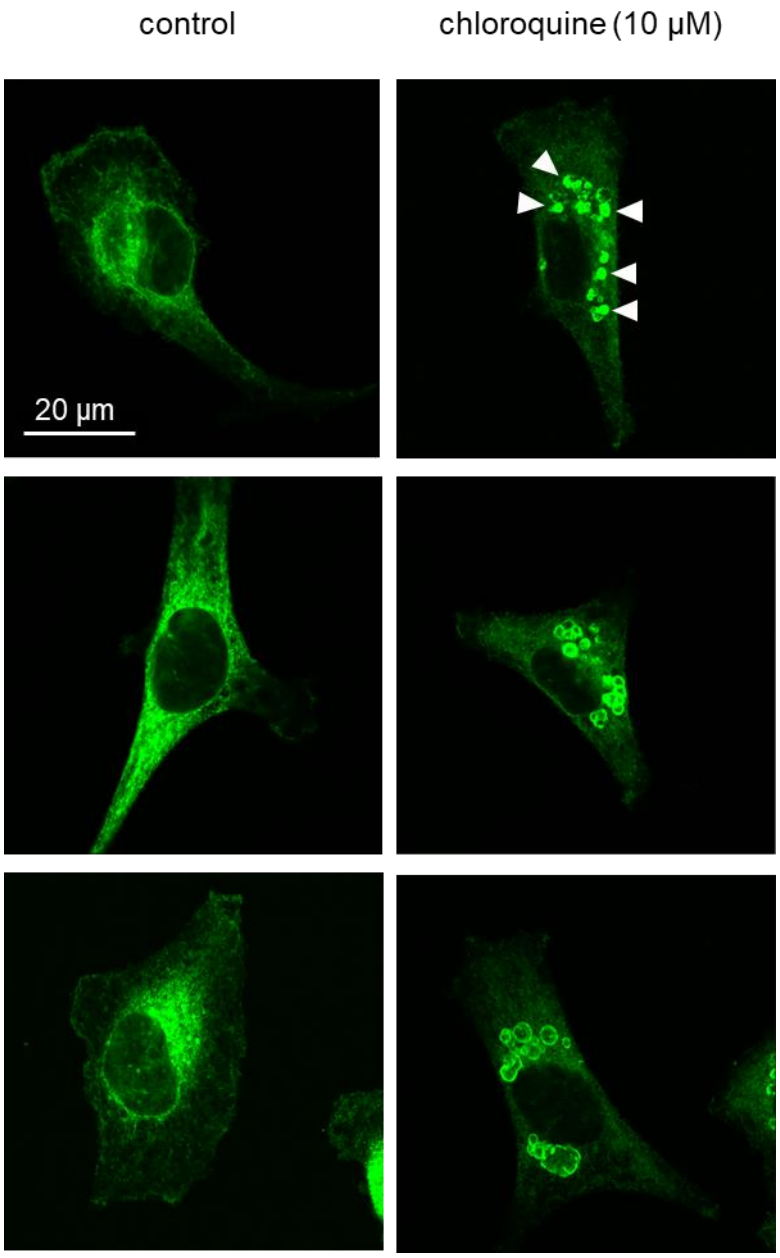

Figure 3.13 Lysosomal degradation of β1-GFP in MDA-MB-231-β1GFP cells

MDA-MB-231-β1GFP cells were pre-treated without (control) or with chloroquine (10 μM, 24h). Cells were then fixed and endogenous GFP detected using a confocal microscope with Airyscan technology. White arrows indicating enlarged lysosomes.

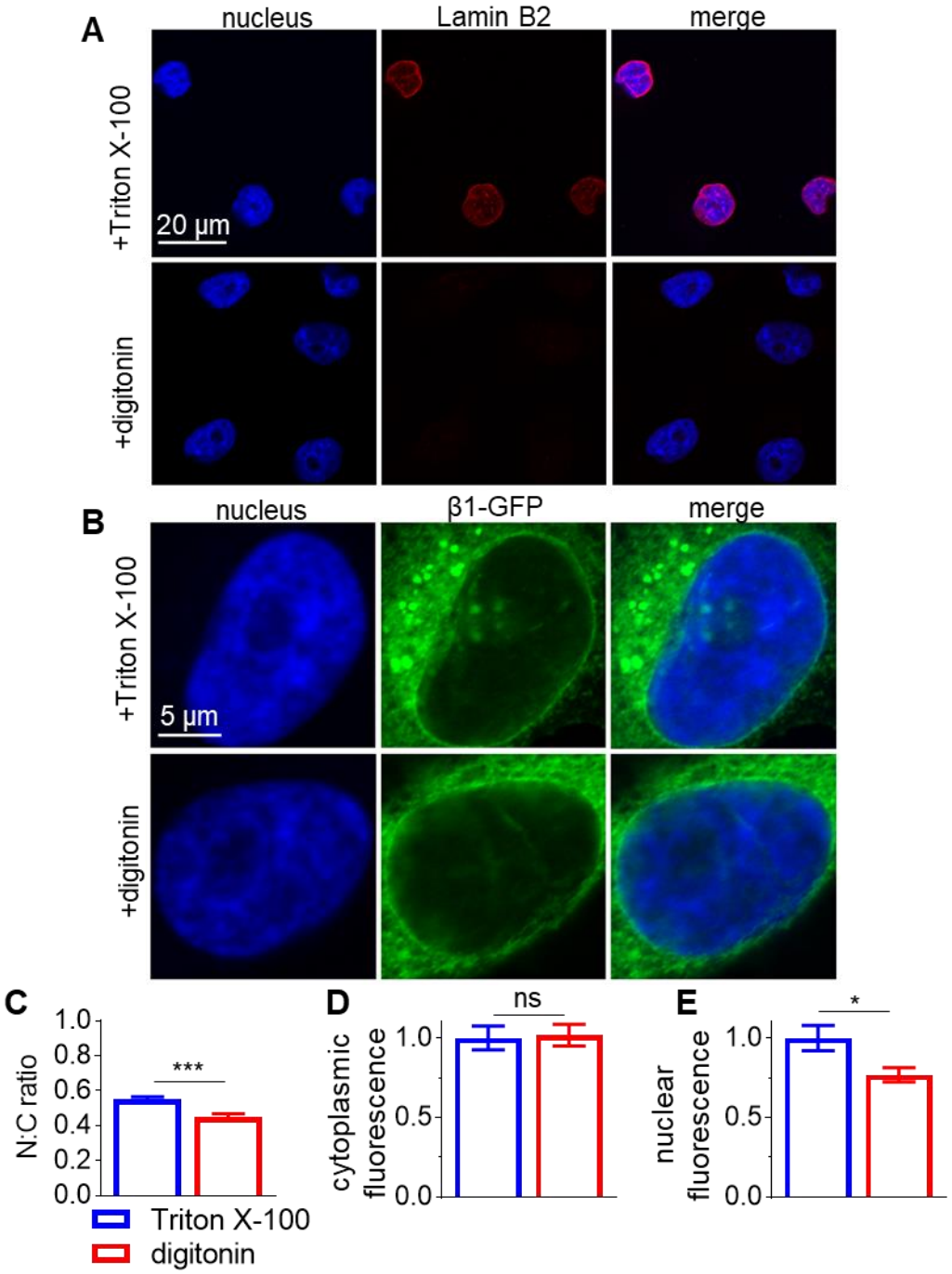

Figure 3.14 Nuclear localisation of β1-GFP in MDA-MB-231-β1GFP cells

(**A**,**B**) MDA-MB-231-β1GFP cells were fixed and permeabilised with Triton X-100 (0.3 %) or digitonin (50 µg/ml). Cells were labelled for Lamin B2 (**A**) or GFP (**B**) and imaged on a confocal microscope. (**C**) Quantification of the nuclear: cytoplasmic (N:C) signal density ratio between Triton X-100 (blue, left hand column) and digitonin (red, right hand column) permeabilised cells. Data displayed as mean ± SEM. Unpaired t-test used to test significance. *** = P<0.001. n = 27 – 28, N = 3. (**D**,**E**) Comparison of the (**D**) cytoplasmic fluorescence intensity and (**E**) nuclear fluorescence intensity between MDA-MB-231-β1GFP cells permeabilised with Triton X-100 (blue left bar) or digitonin (red right bar). Data normalised to Triton X-100 permeabilised cells for D,E, Data displayed as Mean ± SEM. n = 27 – 28, N = 3. Unpaired t test used to test significance. ns = not significant. * = P < 0.05.

Both Triton X-100 and digitonin permeabilised cells demonstrated a comparable cytoplasmic fluorescence intensity (Figure 3.14D, $n = 27$, $P = 0.86$, unpaired t test), suggesting a change in cytoplasmic fluorescence intensity was not responsible for the difference in nuclear : cytoplasmic signal density ratio. The nuclear fluorescence intensity of digitonin-permeabilised cells was, however, reduced by 23 % compared to Triton X-100 permeabilised cells (Figure 3.14E, $n = 27$, $P < 0.05$, unpaired t test), verifying the reduced nuclear: cytoplasmic signal density ratio seen in digitonin-permeabilised is due to reduced nuclear signal.

A noteworthy observation from the previous experiment was a clear enrichment of β1-GFP encircling the nucleus. In a separate experiment, MDA-MB-231-β1GFP cells were co-stained for DAPI, β1-GFP and Lamin B2, and co-localisation assessed using line profiles across the nuclear membrane (Figure 3.15A,B). Lamin B2 and DAPI were offset by ~500 nm, consistent with Lamin B2 being a nuclear membrane protein (n = 10 cells) (Figure 3.15C). β1-GFP and Lamin B2, however, showed a clear co-localisation, although the β1-GFP peak was offset in the cytoplasmic direction by ~40 nm. Furthermore, intranuclear Lamin B2 signal, arising from nuclear membrane invaginations, also displayed β1-GFP co-localisation. In summary, β1-GFP localised close to Lamin B2, with an offset of ~ 40 nm. This offset is below the resolution limit of confocal with Airyscan microscopy and so, is difficult to interpret, however the perinuclear space is 30 – 50 nm wide, suggesting the β1-GFP signal may be originating from the outer nuclear membrane or the endoplasmic reticulum, which is continuous with the outer nuclear membrane (Lusk *et al.*, 2007; Linde & Stick, 2010), rather than the inner nuclear membrane itself.

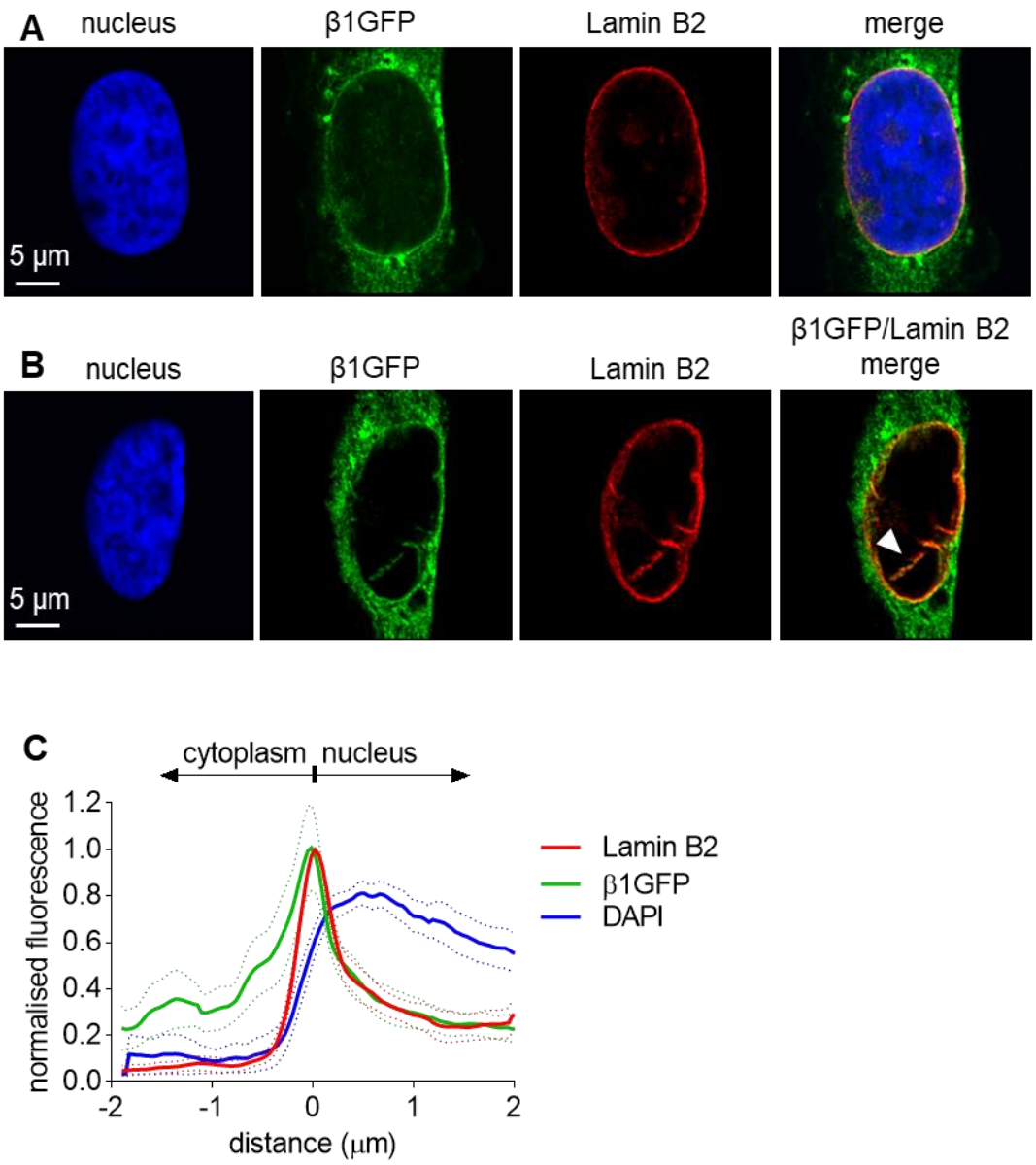

Figure 3.15 Co-localisation of β1-GFP with the inner nuclear membrane marker Lamin B2 in MDA-MB-231-β1GFP cells

(**A**,**B**) MDA-MB-231-β1GFP cells, fixed, labelled for DNA (using DAPI), GFP and Lamin B2, and imaged using a confocal microscope with Airyscan technology. Examples of a nucleus free of invaginations (**A**) and with invaginations (**B**, marked with white arrow) are given. DAPI left out of merge in B to increase clarity on the β1-GFP-Lamin B2 overlap. (**C**) Quantification of the β1-GFP-Lamin B2 overlap. A 4 µm long, 10-pixel wide line profile was taken across the nuclear membrane of MDA-MB-231-β1GFP cells. Data displayed as mean (solid line) ± SEM (dotted line) (n = 10, N = 1).

3.3 Discussion

This chapter aimed to advance understanding of the role of γ-secretase cleavage in regulating β1 function in MDA-MB-231 cells. β1 expression in MDA-MB-231 cells increased current density and accelerated channel recovery from inactivation. Using three different γ-secretase inhibitors (DAPT, L-685,458, Avagacestat) demonstrated no involvement of γ-secretase cleavage in regulating the β1-induced I_{Na}. DAPT treatment did, however, accelerate β1-induced cell adhesion, raising the possibility of an increase in cell surface β1 following γ-secretase inhibition. Surprisingly, when MDA-MB-231-β1GFP cells were imaged, plasma membrane β1 expression was undetectable. Instead, β1-GFP was enriched within intracellular compartments, including endosomes and lysosomes, as well as an unidentified perinuclear compartment. Considering the fact β1-GFP co-localised with the inner nuclear membrane marker, Lamin B2, the perinuclear compartment is likely the nuclear membrane or the closely associated endoplasmic reticulum. A small fraction of nuclear β1-GFP was detected, although further work is required to determine the localisation and role of β1-ICD.

β1 expression in MDA-MB-231 cells increased peak current density, presumably through an increase in VGSC membrane expression, as has been demonstrated previously (Meadows *et al.*, 2001; Chioni *et al.*, 2009). β1 also accelerated recovery from inactivation, a previously reported phenomenon, although the mechanistic basis is still unclear (Laedermann *et al.*, 2013). Charge neutralisation mutations of DIV:VSD delay recovery from inactivation, suggesting DIV:VSD relaxation is required for recovery from inactivation (Capes *et al.*, 2013). Furthermore, recent crystallisation of the electric eel $Na_v1.4$-β1 complex determined β1 interacts with DIV:VSD, implicating direct modulation of VSD movement as a possible mechanism for β1-induced RFI acceleration (Yan *et al.*, 2017).

γ-secretase inhibition was ineffective in modulating β1-induced I_{Na}. This was unexpected, owing to the involvement of β1-ICD in binding α-subunit and the putative role of β2-ICD in regulating α-subunit expression (Meadows *et al.*, 2001; Kim *et al.*, 2005). It would therefore appear that β1-ICD is not involved in binding α-subunits or regulating α-subunit expression. β1 can also interact with α-subunits through an extracellular binding site (McCormick *et al.*, 1998), which may be the dominant interaction site in this cell model. γ-secretase inhibition did, however, increase β1-induced transcellular adhesion, suggesting a possible increase in plasma membrane β1 expression. This may occur through accumulation of full-length β1 at the cell surface, due to inhibition of the cleavage pathway. Interestingly, γ-secretase inhibition decreases β2-mediated cell adhesion in Chinese hamster ovary cells (Kim *et al.*, 2005), supporting the idea that secretase cleavage can regulate β-mediated cell adhesion but suggesting this process may be cell type-dependent or β-subunit dependent.

Assuming β1-induced cell adhesion depends on the plasma membrane expression of β1, it would appear that peak current density is not proportional to membrane expression of β1, as γ-secretase inhibition simultaneously increased adhesion, yet did not increase peak current density. However, membrane β1 accumulation may not necessarily be accompanied by α-subunit membrane accumulation. The endocytic fates of the two subunits is distinct, as α-subunits are eventually degraded via the proteasome (Rougier *et al.*, 2005), whereas novel evidence presented here suggests that chloroquine treatment and LAMP1 co-localisation within this study demonstrated β1 is degraded within lysosomes, suggesting β1 may accumulate at the plasma membrane following DAPT treatment but α-subunits are internalised as usual.

Despite functional evidence of plasma membrane β1 expression and confocal imaging revealing co-localisation of β1 with two endocytic markers- EEA1 and internalised FM4-64, direct imaging of membrane β1 was inconclusive. The lack of cell surface enrichment may be an intrinsic property of β1, as overwhelming intracellular β1 expression has been reported previously in Madin-Darby canine kidney cells, unlike β2, which showed membrane enrichment (Dulsat *et al.*, 2017). More sensitive method of plasma membrane β1 detection would be beneficial for dissecting the membrane dynamics of β1 at resting state and following γ-secretase inhibition. For instance, APP also demonstrates low plasma membrane enrichment yet various methods have been used to detect its cell-surface expression, including cell surface biotinylation (Haass *et al.*, 1992), induced exocytosis using Ca^{2+}-ionophores (Allinquant *et al.*, 1994), and imaging phluorin-tagged APP (Bauereiss *et al.*, 2015).

This study attempted to locate the subcellular site of secretase cleavage of β1 using the γ-secretase inhibitor, DAPT, and various imaging techniques. Firstly, using FRAP, DAPT treatment was expected to reduce the mobility of GFP elements within MDA-MB-231-β1GFP cells as production of soluble, rapidly diffusing β1ICD-GFP was prevented. The diffusion coefficient for soluble GFP in mammalian cells is typically 15 – 20 $\mu m^2 s^{-1}$ (Gura Sadovsky *et al.*, 2017), whereas transmembrane proteins diffuse at 0.1 – 1 $\mu m^2 s^{-1}$, although much difference is observed depending on cell model, and acquisition and analysis methodology used (Kusumi *et al.*, 1993). However, no β1ICD fraction was detectable at the leading or trailing edge of the cell. This could be due to multiple reasons. For instance, such a small fraction of β1ICD-GFP may be produced that it is undetectable amongst the overwhelming full-length β1-GFP fraction. β1ICD-GFP mobility may be too fast to detect, as the acquisition process was not optimised to detected movement of soluble elements. β1ICD-GFP may be immobilised at the membrane and not freely mobile. Or β1ICD production is localised to a cellular compartment and not occurring at

the leading or trailing edge. Due to the lack of success using FRAP, the only conclusion that can be deduced is that β1ICD-GFP production is not abundant and easily detectable. The multitude of possible reasons for this will be addressed in subsequent chapters. The second technique used to investigate β1ICD-GFP production was co-localisation analysis. Early endosomes and lysosomes were investigated, as lysosomes are a known location of secretase processing (Lorenzen *et al.*, 2010). It was hypothesised that DAPT treatment would cause a lysosomal and endosomal accumulation of β1-GFP if secretase cleavage within lysosomes was prevented, which would be detected as an increase in the proportion of cellular β1-GFP within endosomes/lysosomes following co-localisation analysis. However, co-localisation analysis suggested γ-secretase processing is not occurring within the endolysosomal pathway, as no increase in correlation between β1-GFP and endosomal or lysosomal markers was detected. However, a decrease in correlation was detected between β1-GFP and EEA1 following DAPT-treatment, suggesting relative β1 enrichment elsewhere. If secretase cleavage is occurring at the plasma membrane, γ-secretase inhibition may induce β1 accumulation at the plasma membrane and reduce endocytosis, resulting in reduced correlation with EEA1. Decreased β1GFP/EEA1 correlation following DAPT treatment therefore supports the theory that γ-secretase inhibition increases surface β1 expression, proposed following the finding that DAPT treatment enhances β1-mediated transcellular adhesion. The discovery that β1 is enriched within the endolysosomal pathway was, in itself, a novel discovery, however it would be appear that γ-secretase is not clearly occurring within the pathway using this co-localisation analysis. Methods used previously to monitor secretase processing of APP, include dual-labelling APP with N-terminal and C-terminal fluorescent tags and monitoring terminus dissociation by subcellular fractionation (Coughlan *et al.*, 2013; Parenti *et al.*, 2017; Tan & Gleeson, 2019).

Nuclear localisation of secretase generated ICDs and subsequent gene regulation is a common phenomenom (Haapasalo & Kovacs, 2011). Imaging MDA-MB-231-β1GFP cells using the detergent digitonin, which prevents antibody access into the nucleus, revealed a small fraction of nuclear β1-GFP signal. However, whether this nuclear fraction is secretase-dependent was not tested and would be informative. Furthermore, nuclear signal was still detectable in digitonin-permeabilised samples, suggesting digitonin did not fully restrict nuclear antibody access or cytoplasmic GFP signal above/below the nucleus is being detected within the nucleus. Furthermore, MDA-MB-231 nuclei contain abundant invaginations, demonstrated by Lamin-B2 staining, which co-localise with β1-GFP signal and would be detectable within the perimeter of nuclei using this analysis technique. Visualisation of nuclear APP-ICD has required proteasome inhibition, nuclear export inhibition and ICD overexpression to determine nuclear expression, owing to the low abundance/high turnover of APP-ICD (von Rotz *et al.*, 2004; Gersbacher *et al.*, 2013). Nuclear fractionation and Gal4/LexA-fusion proteins have also been used to determine nuclear expression and transcriptional function of APP (Cao & Sudhof, 2001; Kimberly *et al.*, 2001).

An intriguing co-localisation of β1-GFP and the inner nuclear membrane marker Lamin B2 was detected in this study. Membrane-spanning proteins such as APP and NCAM are detectable in nuclear fractions and cell adhesion molecules are known to insert into the nuclear membrane, so potentially β1 has a presently unknown function within the nuclear membrane (Kleene *et al.*, 2010; Okamoto, 2012). However, as the ER is continuous with the nuclear membrane, and ER markers also co-localise with Lamin B2, it is possible ER-bound β1 is overlapping with Lamin B2 (Linde & Stick, 2010).

3.4 Conclusion

The hypothesis of this results chapter was that γ-secretase cleavage regulates β1 function, with focus on the electrophysiological properties of β1, the cell adhesive properties of β1 and the subcellular fate of β1-ICD. Although, it is apparent β1 is being cleaved by γ-secretase in MDA-MB-231 cells, it is still not clear what the functional impact of proteolysis on β1 is, or where γ-secretase cleavage is occurring. Using multiple γ-secretase inhibitors, secretase processing was credibly revealed to not affect the electrophysiological properties of β1. γ-secretase inhibition did increase β1-induced cell adhesion and decrease early endosome co-localisation, suggesting γ-secretase cleavage may regulate plasma membrane β1 expression, although quantifying cell-surface β1 expression after γ-secretase inhibition would be required to support these findings. Lastly, β1-ICD production was not detectable at the leading or trailing edges of the cell, or within the endolysosomal pathway. A small fraction of β1-GFP was detectable within the nucleus, supporting the possibility that β1-ICD localises to the nucleus. However, the fate of β1-ICD is still largely uncertain and will be explored in the following chapter to try and ascertain a possible role of γ-secretase cleavage in regulating β1 function.

Chapter 4: Expression and functional analysis of β1-intracellular domain

4.1 Introduction

γ-secretase cleavage, following an α- or β-secretase cleavage event, regulates the function of many type I transmembrane proteins (Haapasalo & Kovacs, 2011). γ-secretase cleavage can occur at the plasma membrane, as well as within internal membranes, such as lysosomes and the trans-Golgi network (Chyung *et al.*, 2005; Tam *et al.*, 2014; Tan & Gleeson, 2019). The subsequent generation of an ICD allows for efficient intracellular cell signalling, often leading to nuclear trafficking and gene regulation. Some examples of functionally characterised ICDs include: LRP8-ICD, which regulates synaptic plasticity, $P75^{NTR}$-ICD, which inhibits cell cycle progression and induces apoptosis, and Notch-ICD, which regulates cell fate determination during neurodevelopment (Lowell *et al.*, 2006; Parkhurst *et al.*, 2010; Telese *et al.*, 2015). Notch-ICD is a well-documented oncogene, due to its integral involvement in proliferation and differentiation (Ellisen *et al.*, 1991). In triple-negative breast cancer cells, Notch signalling upregulates *Myc* expression (Stoeck *et al.*, 2014). Additionally, immunohistochemistry analysis of patient oral tumour biopsies shows Notch-ICD expression correlates with tumour progression and Notch-ICD+/c-Myc+ double positive cases have reduced overall survival compared to other oral cancer cases (Gokulan & Halagowder, 2014)

The functional consequences of β1-ICD generation have yet to be reported. Inhibition of γ-secretase cleavage prevents β1-induced neurite outgrowth in cultured cerebellar granule neurons (Brackenbury & Isom, 2011). However, whether neurite outgrowth is directly due to β1-ICD generation or some other aspect of β1 behaviour, such as protein turnover, was not investigated. Unlike β1-ICD, β2-ICD has been the subject of research. β2-ICD localises to the nucleus, as well as throughout the cytoplasm, when

overexpressed in neuronal SH-SY5Y cells, which is accompanied by an increase in $Na_v1.1$ mRNA and protein expression (Kim *et al.*, 2007). Furthermore, in neuroblastoma B104 cells overexpressing BACE1 and β2, secretase processing is enhanced, $Na_v1.1$ expression also increased, yet I_{Na} reduced (Kim *et al.*, 2007). This led the authors to conclude that β2-ICD is directly involved in upregulating *SCN1A* gene expression but is not sufficient in trafficking $Na_v1.1$ to the cell surface.

The involvement of β-subunit ICDs in metastatic cell behaviour has yet to be investigated. However, inhibiting γ-secretase cleavage decreases β2-induced transcellular adhesion and migration in CHO-β2 cells, suggesting that secretase processing may regulate surface expression of β2 or β2-ICD induces a cell adhesion/migration signalling pathway (Kim *et al.*, 2005). However, β2-ICD expression in CHO-β2 cells did not have an effect on cell migration, suggesting β2-ICD is not responsible for β2-induced cell migration (Kim *et al.*, 2005). Whereas expression of β2-CTF in CHO-β2 cells did have an inhibitory effect on β2-induced cell migration, suggesting β2-CTF accumulation caused the negative effect on β2 function induced by γ-secretase inhibition (Kim *et al.*, 2007). Furthermore, a transmembrane β4 construct lacking the Ig loop, similar to β4-CTF, is capable of recapitulating β4-induced inhibition of MDA-MB-231 migration and invasion (Bon *et al.*, 2016). These results hint at a tumour-suppressive role of β4, which is independent from the extracellular Ig loop and implicates a possible involvement of secretase processing of β-subunits in regulating metastatic cell behaviour. In summary, the mechanism by which β-subunits contribute to cancer cell behaviour is unclear, although links between the CTFs/ICDs of β2 and β4 and regulation of cell migration and adhesion have emerged, suggesting a possible contribution of secretase processing in regulating β-subunit function in cancer cells. However, the functional activity of the β1ICD in metastatic breast cancer cells is still unknown.

4.1.1 Hypothesis and aims

The rationale of this chapter was to focus on β1-ICD, as it is the final secretase-generated product of β1 and if secretase processing is involved in regulating β1 function, overexpression of β1-ICD should recapitulate these functions.

Results from chapter 3 offered some insight into the possible function of β1-ICD in breast cancer cells. γ-secretase inhibition did not reduce the β1-induced I_{Na}, implying β1-ICD is not involved in the process. Additionally, γ-secretase inhibition slightly increased β1-induced cell adhesion, suggesting β1-ICD may have a negative impact on cell adhesion, or alternatively, that γ-secretase inhibition increases plasma membrane expression of β1. β1-GFP demonstrated a small fraction of nuclear fluorescence, supporting the possibility that β1-ICD is transported to the nucleus. These results from the previous chapter formed the basis of the rationale of this chapter. The hypothesis of this chapter was, therefore, that the β1-ICD, when overexpressed in MDA-MB-231 cells, would locate to the nucleus to partially recapitulate the functional effects of full-length β1.

The specific aims of the chapter were:

- To investigate the nuclear localisation of β1-ICD
- To determine if β1-ICD is capable of inducing an enlarged I_{Na}, similar to β1
- To assess whether β1-ICD is sufficient to recapitulate β1-induced metastatic cell behaviours, namely β1-induced cell adhesion and morphology changes.

4.2 Results

4.2.1 Generation of the β1-intracellular domain construct

To isolate the functional effects of β1-ICD, a β1ICD-GFP construct was generated using site-directed mutagenesis of a plasmid encoding β1 with a C-terminal eGFP tag (Figure 4.1A). The forward primer was placed at the start of the β1-ICD sequence, corresponding to Tyr182, and the reverse primer placed before the start of the β1 sequence, in order to delete the entire β1-ECD and TMD regions. The plasmid was then transfected into MDA-MB-231 cells to produce MDA-MB-231-β1ICDGFP cells (Figure 4.1B).

4.2.2 β1-intracellular domain localises to the nucleus

β2-ICD overexpression in neuronal SH-SY5Y cells displays uniform β2-ICD expression throughout the cell and a concomitant increase in $Na_v1.1$ mRNA and protein expression, suggesting a possible function in transcription regulation (Kim *et al.*, 2007). To establish whether β1-ICD displays a similar expression profile, β1ICD-GFP was overexpressed in MDA-MB-231 cells and spatial expression assessed using confocal with Airyscan super-resolution microscopy. β1ICD-GFP expression was compared against soluble GFP and full-length β1-GFP, to establish whether β1-ICD resembled a soluble protein or retained any β1-like subcellular distribution characteristics (Figure 4.2A). β1ICD-GFP shows a similar ubiquitous expression throughout the cell to GFP, whereas β1-GFP expression is restricted from the nucleus and clearly enriched within the perinuclear region (Figure 4.2B). To ascertain whether nuclear enrichment of β1ICD-GFP was different to GFP, the nuclear: cytoplasmic GFP signal density ratio was calculated for MDA-MB-231-GFP, MDA-MB-231-β1GFP, and MDA-MB-231-β1ICDGFP (Figure 4.3A). β1-GFP displayed a significantly lower nuclear: cytoplasmic ratio compared to GFP (0.82 ± 0.06 and 1.75 ±

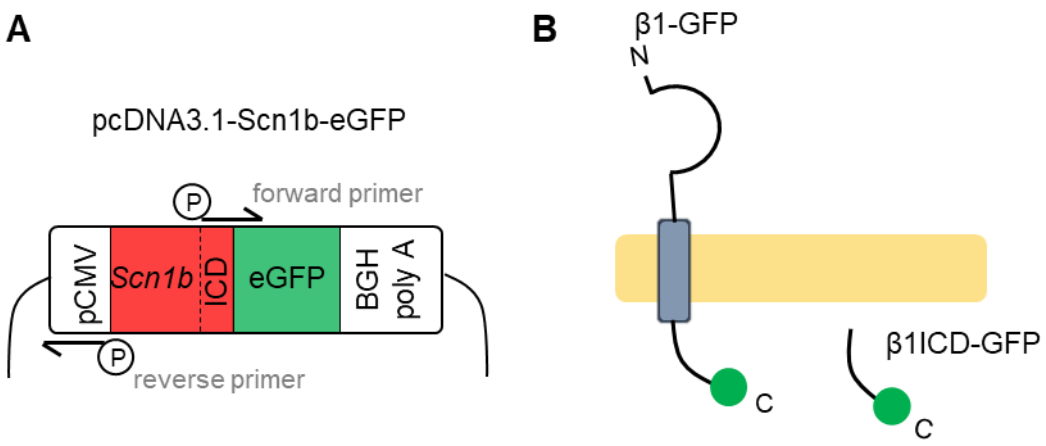

Figure 4.1 Generation of a β1-intracellular domain construct using site-directed mutagenesis

(**A**) Site-directed mutagenesis of pcDNA3.1 encoding β1-eGFP. The forward primer was placed at the start of the ICD sequence (Tyr182) and the reverse primer placed before the start of β1 causing a 546 base pair deletion, corresponding to the β1-ECD and TMD. Both primers were 5' phosphorylated (P) for efficient post-PCR ligation. CMV promoter and BGH polyadenylation site also shown. (**B**) Diagram of full-length β1-GFP alongside β1-ICDGFP.

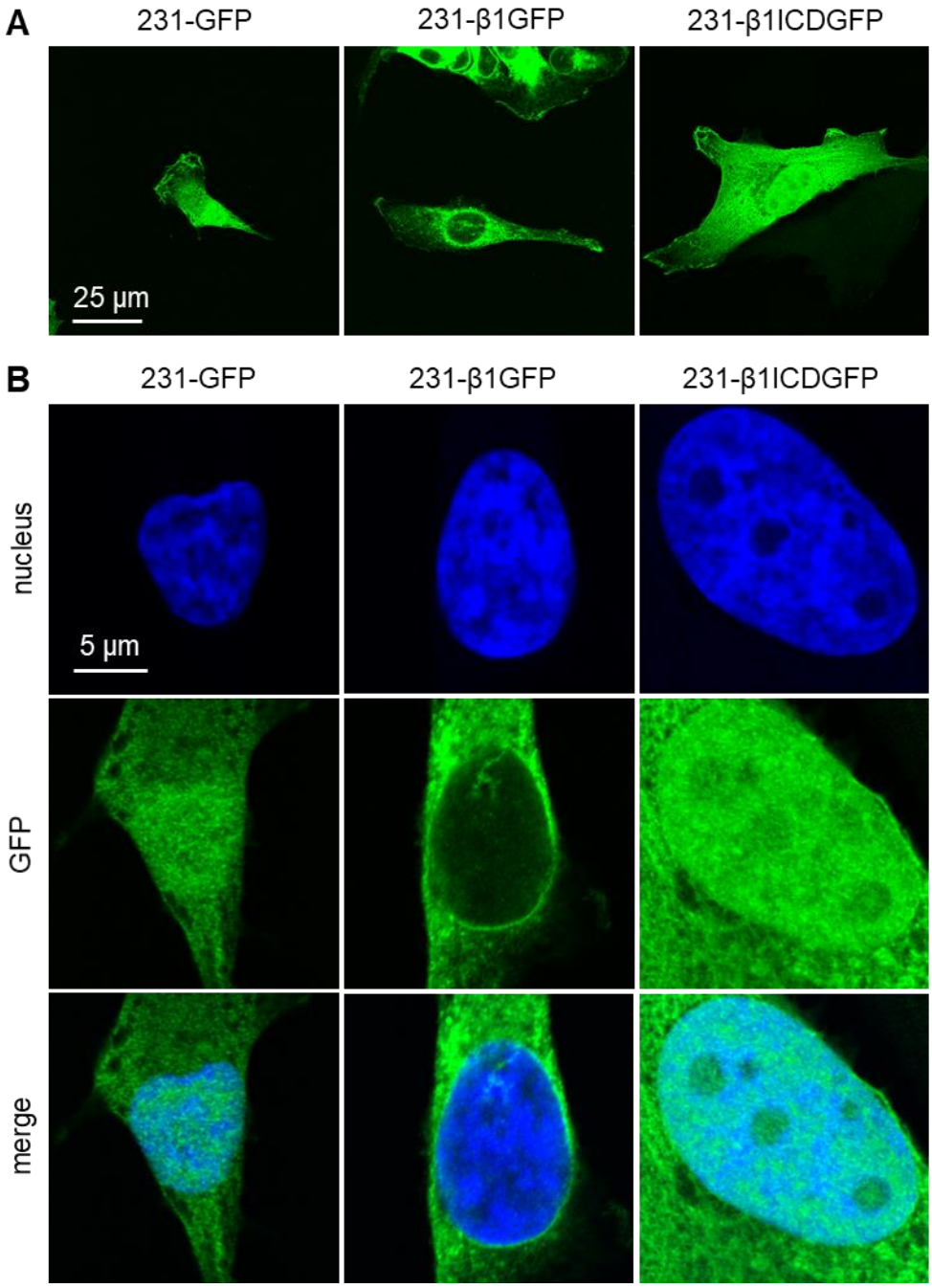

Figure 4.2 Nuclear enrichment of β1-ICD in MDA-MB-231-β1ICDGFP cells

(**A**) whole-cell images of the GFP signal within fixed MDA-MB-231 cells expressing GFP, β1-GFP or β1ICD-GFP, acquired using confocal microscopy with Airyscan technology. (**B**) Magnified images, of the same example cells from **A**, focused on the cell nuclei at the mid-nuclear plane. Images split into DAPI signal (blue), GFP signal (green) and a merged image of both channels.

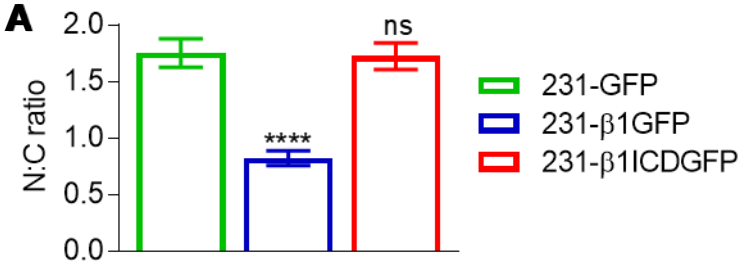

Figure 4.3 Quantification of the nuclear enrichment of β1-ICD in MDA-MB-231-β1ICDGFP cells

(A) Nuclear : cytoplasmic signal density ratio (N:C ratio) of MDA-MB-231 cells expressing GFP (green bar, n = 14), β1-GFP (blue bar, n = 14) or β1ICD-GFP (red bar, n = 17) (N = 3). Data displayed as mean ± SEM. Ordinary one-way ANOVA used to test significance. ns = not significant, **** = P < 0.0001.

0.13 respectively, n = 14, P<0.0001). β1ICD-GFP, however, demonstrated a similar nuclear: cytoplasmic ratio to GFP (1.73 ± 0.12, n = 17, P = 0.98, one-way ANOVA), suggesting soluble β1ICD-GFP potentially diffuses freely throughout the cell, similar to GFP.

4.2.3 Nuclear import kinetics of β1-intracellular domain

Given that the β1ICD was present in the nucleus, the next step was to establish how it localised there. Nuclear import of NLS-tagged cargo requires cytoplasmic factors and ATP (Adam *et al.*, 1990). Nuclear import of APP-ICD and Notch-ICD, for example, occurs via trafficking of multimeric complexes (Kimberly *et al.*, 2001; Vasquez-Del Carpio *et al.*, 2011). GFP, on the other hand, is small enough for passive diffusion through nuclear pores, taking ~80 s to reach half-maximal nuclear recovery in CHO cells (Cardarelli *et al.*, 2007). For soluble proteins, a theoretical molecular weight limit of up to 100 kDa restricts nucleocytoplasmic diffusion, as determined by nuclear enrichment of different sized GFP oligomers (Wang & Brattain, 2007). However, research in yeast cells measuring the dynamic process of nuclear import, estimated a cubic relationship between molecular weights above 27 kDa and time taken for nuclear import (Timney *et al.*, 2016). Accepting this cubic relationship, if β1ICD-GFP (32 kDa) is freely diffusing into the nucleus, nuclear import would be expected to take ~70 % longer than GFP (27 kDa). However, if β1-ICD is translocating into the nucleus as part of a large multimeric complex, like other secretase generated ICDs, it should be imported more slowly, over a longer time scale. The nuclear import rates of β-subunit ICDs has yet to be investigated, however, for comparison, the glucocorticoid receptor-HSP90-FKBP52 complex (> 200 kDa) takes ~ 5 min to reach half maximal nuclear enrichment (Gallo *et al.*, 2007).

To investigate nuclear import, FRAP was performed using MDA-MB-231-GFP and MBA-MB-231-β1ICDGFP cells. Nuclei were masked using Hoechst 33342 stain and the nuclear GFP signal was bleached using a 488 nm laser (Figure 4.4A). Images were subsequently acquired every 250 ms to measure fluorescence recovery (Figure 4.4B). Accordingly, two parameters were derived. Firstly, the mobile fraction denotes the proportion of GFP elements within the ROI that are freely mobile. A freely diffusing protein will demonstrate fluorescence recovery back to 1. Secondly, the time constant denotes the time taken for half-maximal fluorescence recovery and is proportional to the rate of fluorescence recovery. The mobile fraction in the nucleus was comparable between proteins (GFP: 1.00 ± 0.03 and β1ICD-GFP: 0.86 ± 0.07, n = 10, P = 0.08, unpaired t-test), suggesting both proteins are mobile within the nucleus (Figure 4.4C). However, the time constant was 2.5-fold longer for β1ICD-GFP than GFP, 124.5 (median, IQR: 89.7 – 150.6) s and 53.1 (median, IQR: 37.6 – 62.3) s respectively (n = 10, P < 0.001, Mann-Whitney U-test), supporting the hypothesis that β1ICD-GFP nuclear import is significantly slower than GFP due to complex import (Figure 4.4D).

4.2.4 β1-intracellular domain displays GFP-like, cytoplasmic mobility kinetics

β1ICD-GFP demonstrates different nuclear import kinetics to GFP, however the mechanism underlying this phenomenon is unclear. To test whether β1ICD-GFP moves universally slower throughout the cell, for instance due to aggregation, FRAP was next used to assess cytoplasmic mobility. Unrestricted GFP diffusion within solution is ~ 85 – 100 $\mu m^2 s^{-1}$, but within the cytoplasmic milieu of a cell, this is reduced to ~ 1 – 20 $\mu m^2 s^{-1}$ (Swaminathan *et al.*, 1997; Calvert *et al.*, 2010; Gura Sadovsky *et al.*, 2017). If β1ICD-GFP mobility was reduced compared to GFP, this would be represented by a faster time

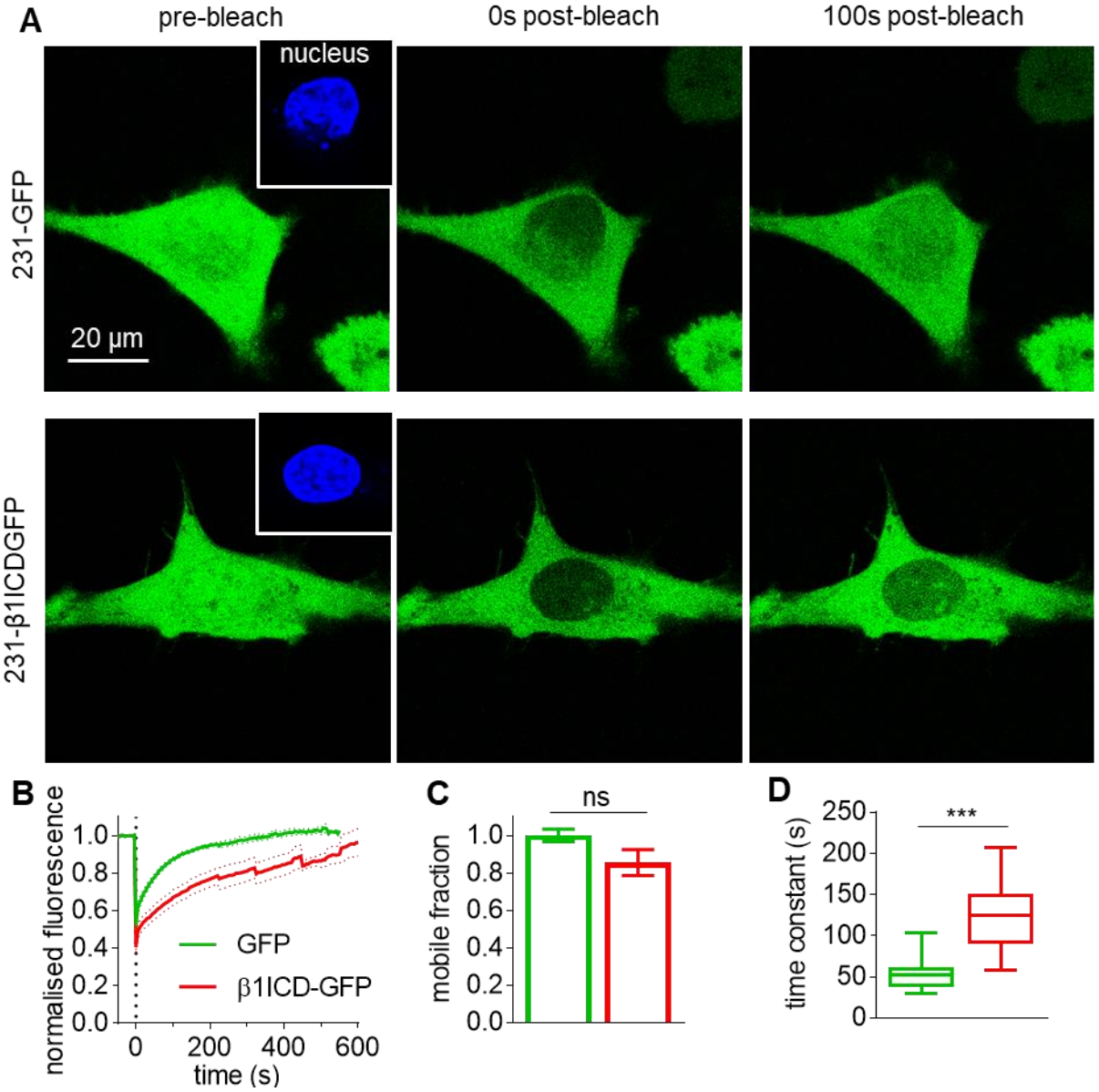

Figure 4.4 Kinetics of β1ICD-GFP nuclear import in MDA-MB-231-β1ICDGFP cells quantified using FRAP

(**A**) Live-cell confocal imaging of MDA-MB-231-GFP (top row) and MDA-MB-231-β1ICDGFP (bottom row) cells. Cells were imaged every 250 ms and photobleached with a 488 nm laser (100 % laser power, 40 iterations). Time series were acquired until five successive images without an increase in nuclear fluorescence were acquired. Images displayed are immediately prior to photobleaching (first column), immediately following photobleaching (second column) and 100 s after photobleaching (third column). Nuclei were photobleached following masking of the Hoechst 33342 signal (shown in subpanels in the first column, blue). (**B**) Nuclear fluorescence recovery in MDA-MB-231 cells expressing GFP (green) or β1ICD-GFP (red). Lines shown as mean (solid line) ± SEM (dotted line). n = 10. (**C**) Mobile fraction of GFP (green) and β1ICD-GFP (red) in MDA-MB-231-GFP and MDA-MB-231-β1ICGFP cells, respectively. Data displayed as mean ± SEM. n = 10, N = 3. Unpaired t-test used to test for significance. ns = not significant. (**D**) Time taken for half-maximal nuclear fluorescence recovery (time constant, s) in MDA-MB-231 cells expressing GFP (green) or β1ICD-GFP (red). Data displayed as min-max box plots due to non-normalised distribution of data. n= 10, N = 3. Mann-Whitney U-test used to test for significance. *** = $P < 0.001$.

constant/ reduced diffusion coefficient. Furthermore, if β1ICD-GFP mobility is being impeded or immobilised by another protein, a reduced mobile fraction may be detected.

Two FRAP approaches were used, initially a circular region of interest (diameter ~ 1.5-2 μm) was photobleached in live MDA-MB-231 cells expressing GFP or β1ICD-GFP and fluorescence recovery monitored over 1 s, with images acquired every 14 ms (Figure 4.5A,B). The mobile fractions of GFP and β1ICD-GFP were similar, 0.91 (median, IQR: 0.77 – 1.00) and 1.00 (median, IQR: 0.94 – 1.06), respectively (n = 15, P = 0.07, Mann-Whitney U test) (Figure 4.5C). Similar non-significant differences were detected in the time constant (GFP – 0.11 ± 0.01 s and β1ICD-GFP – 0.13 ± 0.02 s, n = 15, P = 0.13, Welch's t-test) (Figure 4.5D) and diffusion coefficient (GFP – 6.9 ± 1.0 $\mu m^2 s^{-1}$ and β1ICD-GFP – 5.1 ± 0.6 $\mu m^2 s^{-1}$, n = 15, P = 0.15, unpaired t-test) (Figure 4.5E). These data suggest β1ICD-GFP exists in a freely mobile state within the cytosol, similar to GFP.

Measuring diffusion of GFP and β1ICD-GFP via spot bleach requires high temporal resolution and only a 30 – 40 % reduction of GFP signal was detected post-bleach (Figure 4.5B), due to the rapid flux of soluble protein in/out of the region of interest during the photobleaching step. Therefore, a second FRAP technique was employed to measure cytoplasmic diffusion, to see if the same result was achieved. Accordingly, half of the cell was photobleached and fluorescence recovery monitored every 25 ms over 20 s (Figure 4.6A,B).

Using this technique, a marginally enhanced 40 – 50 % decrease in GFP signal was recorded post bleach. However, diffusion coefficients could not be calculated as the calculation assumes a circular ROI. Using this second technique, again no difference in the mobile fraction was detected between GFP and β1ICD-GFP, 0.966 ± 0.02 and 0.971

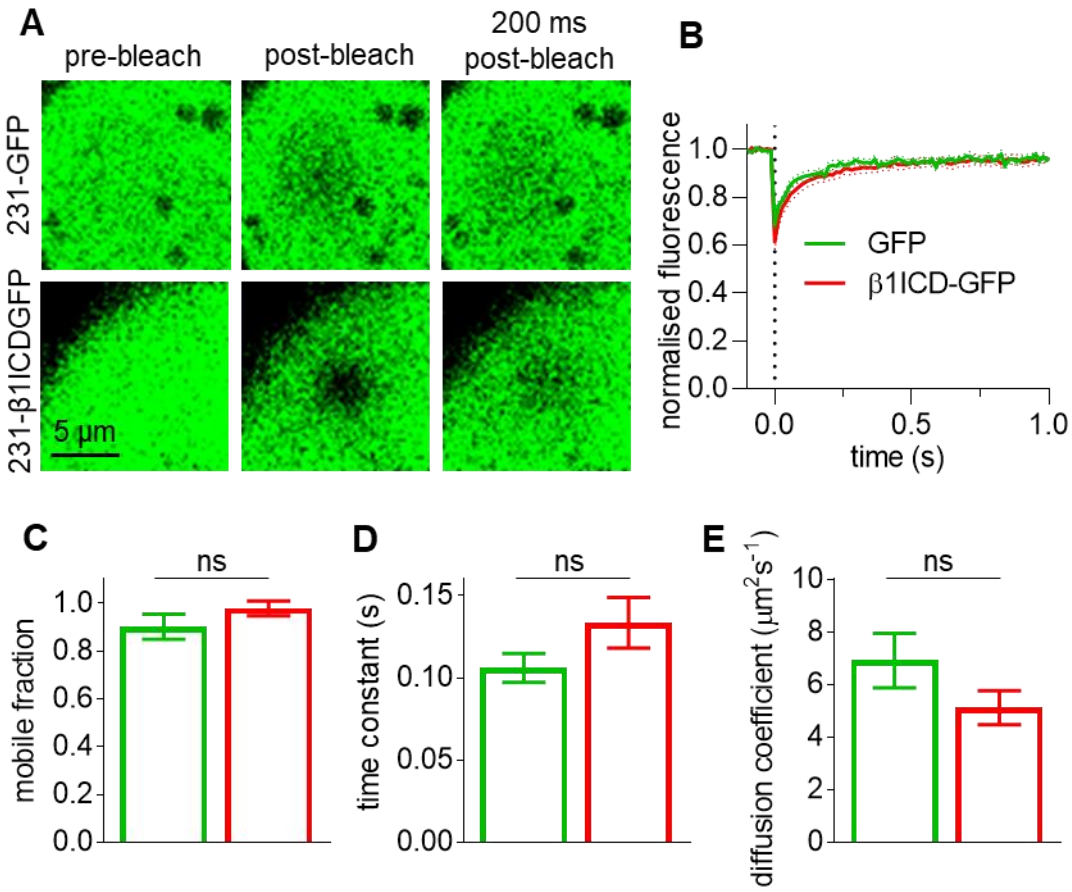

Figure 4.5 Cytoplasmic mobility of β1ICD-GFP in MDA-MB-231-β1ICDGFP cells determined using FRAP within a circular region of interest

(**A**) Live-cell confocal imaging of MDA-MB-231-GFP (top row) and MDA-MB-231-β1ICDGFP (bottom row) cells. Cells were imaged every 14 ms for 2 s and a 1.5 - 2 µm wide region-of-interest photobleached with a 488 nm laser (100 % laser power, 40 iterations). Images displayed are immediately prior to photobleaching (first column), immediately following photobleaching (second column) and 200 ms after photobleaching (third column). (**B**) Fluorescence recovery within the circular region of interest of MDA-MB-231 cells expressing GFP (green) or β1ICD-GFP (red). Data displayed as mean (solid line) ± SEM (dotted line). n = 15, N = 3. (**C-E**) Quantification of the mobile fraction (**C**), time taken for half-maximal fluorescence recovery (time constant, s) (**D**) and diffusion coefficient (**E**) in MDA-MB-231 cells expressing GFP (green) or β1ICD-GFP (red) (n = 15, N = 3). Data displayed as mean ± SEM. Unpaired t-test used to test significant. ns = not significant.

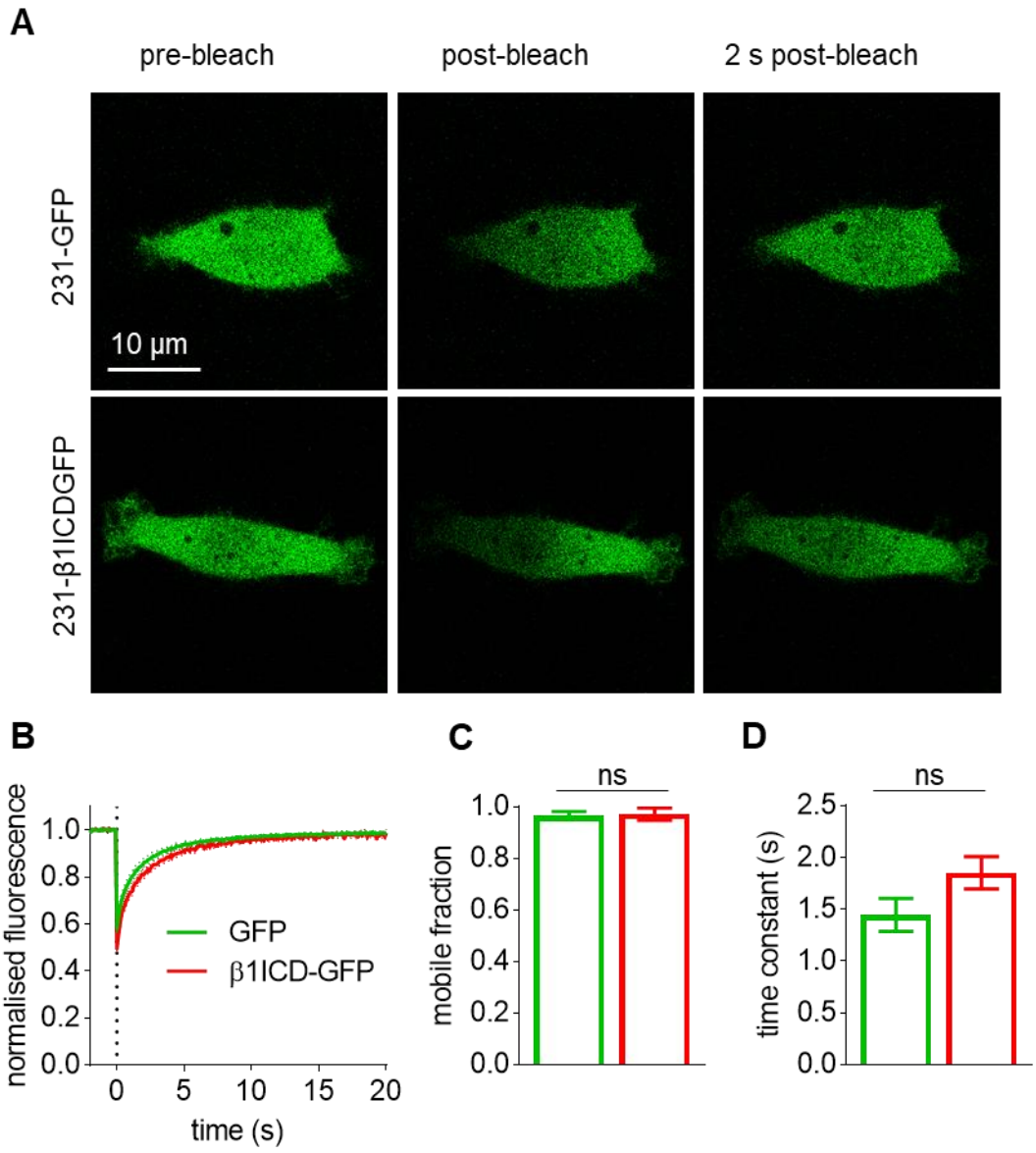

Figure 4.6 Cytoplasmic mobility of β1ICD-GFP in MDA-MB-231-β1ICDGFP cells determined using half-cell FRAP

(**A**) Live-cell confocal imaging of MDA-MB-231-GFP (top row) and MDA-MB-231-β1ICDGFP (bottom row) cells. Cells were imaged every 100 ms for 25 s and half of the cell photobleached with a 488 nm laser (100 % laser power, 50 iterations). Images displayed are immediately prior to photobleaching (first column), immediately following photobleaching (second column) and 2 s after photobleaching (third column). (**B**) Fluorescence recovery within the photobleached half of the MDA-MB-231 cell expressing GFP (green) or β1ICD-GFP (red). Data displayed as mean (solid line) ± SEM (dotted line). n = 15, N = 3. (**C**, **D**) Quantification of the mobile fraction (**C**) and time taken for half-maximal fluorescence recovery (time constant, s) (**D**) of GFP (green bar, n = 27) or β1ICD-GFP (red bar, n = 32) in MDA-MB-231 cells (N = 3). Data displayed as mean ± SEM. Unpaired t-test used to test significant. ns = not significant.

± 0.02 respectively (n ≥ 27, P = 0.85, Welch's t-test) (Figure 4.6C). Similarly, no significant difference was detected in the time constants between GFP and β1ICD-GFP, 1.35 (median, IQR: 0.95 – 2.00) s and 1.78 (median, IQR: 1.15 – 2.50) s respectively (n ≥ 27, P = 0.07, Mann-Whitney U test) (Figure 4.6D), supporting the notion that β1ICD-GFP is a soluble protein.

4.2.5 β1-intracellular domain enhances Na^+ current and accelerates channel recovery from inactivation

The first approach to functionally characterise β1-ICD was to test its electrophysiological properties. β1 induces an enlarged I_{Na} when over-expressed in MDA-MB-231 cells (Chioni *et al.*, 2009). This increased I_{Na} is insensitive to γ-secretase inhibition with DAPT, suggesting release of the β1-ICD is not involved in the β1-induced increase in I_{Na}. Secretase processing of β2 in B104 neuroblastoma cells causes an increase in $Na_v1.1$ expression, however $Na_v1.1$ is retained intracellularly and a decrease in I_{Na} is seen following enhanced secretase processing of β2 (Kim *et al.*, 2007). Therefore, it was expected that I_{Na} in cells overexpressing β1-ICD would resemble the I_{Na} in MDA-MB-231-GFP cells; i.e. no increase in peak current density or accelerated recovery from inactivation, characteristics of β1 over-expression in MDA-MB-231 cells. To investigate this, whole cell patch clamp recording was performed on MDA-MB-231-GFP, MDA-MB-231-β1GFP and MDA-MB-231-β1ICDGFP cells, and IV relationship measured (Figure 4.7A,B). As before, β1-GFP induced a peak current density almost 3-fold greater than in control GFP-expressing cells, -11.7 ± 0.9 pA/pF and -4.36 ± 0.66 pA/pF respectively (n = 15, P<0.0001, one-way ANOVA). Interestingly, β1ICD-GFP also induced an enlarged I_{Na} (-9.33 ± 1.03 pA/pF) compared to GFP (n = 15, P < 0.01, one-way ANOVA) (Figure 4.7C). Gating effects were also measured; channel activation (Figure 4.8A),

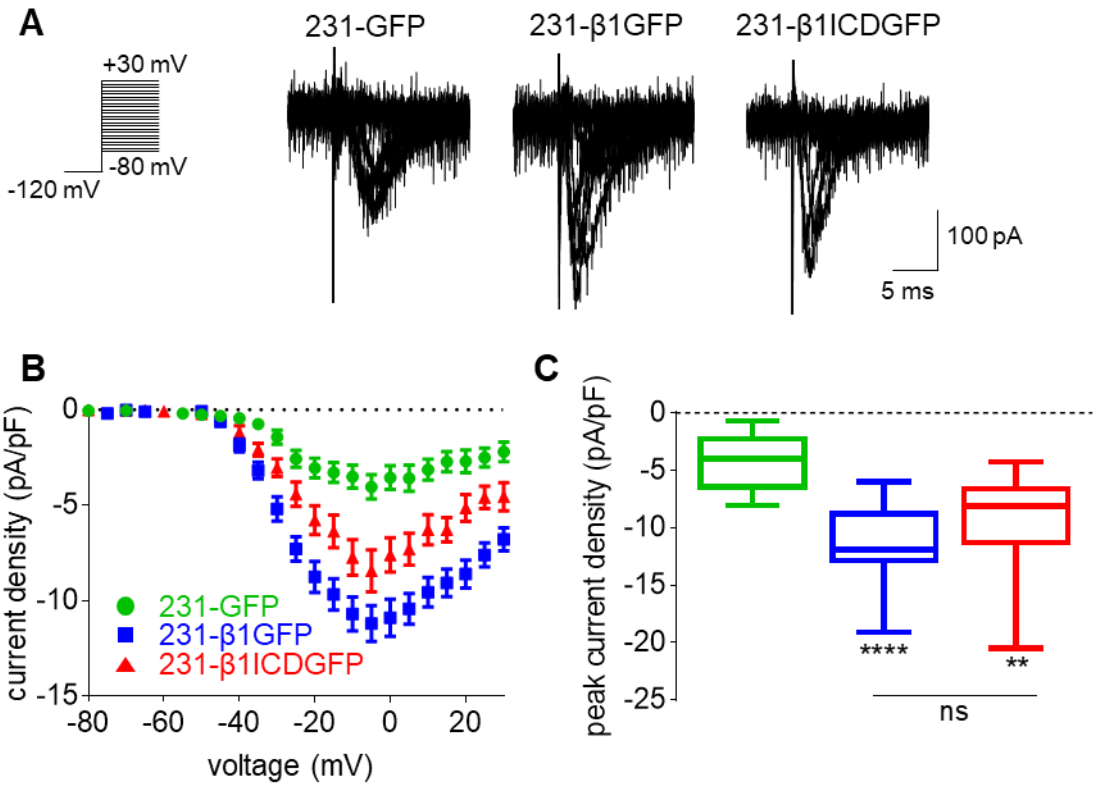

Figure 4.7 Electrophysiological properties of β1-ICD expression in MDA-MB-231 cells determined using whole cell patch clamp recording

(**A**) Representative whole-cell Na^+ currents generated in MDA-MB-231-GFP, MDA-MB-231-β1GFP and MDA-MB-231-β1ICDGFP cells, following stimulation between -80 mV and +30 mV, for 250 ms, from -120 mV. Every third sweep shown. (**B**) Current (I)-voltage (V) relationship between -80 mV and +30 mV of MDA-MB-231-GFP (n = 14, green circles), MDA-MB-231-β1GFP (n = 15, blue squares) and MDA-MB-231-β1ICDGFP (n = 16, red triangles) cells (N = 3). (**C**) Peak current densities generated from cells in **B**. Kruskal-Wallis test used to test significance. ns = not significant. ** = P < 0.01. **** = P < 0.0001. All data displayed as Mean ± SEM.

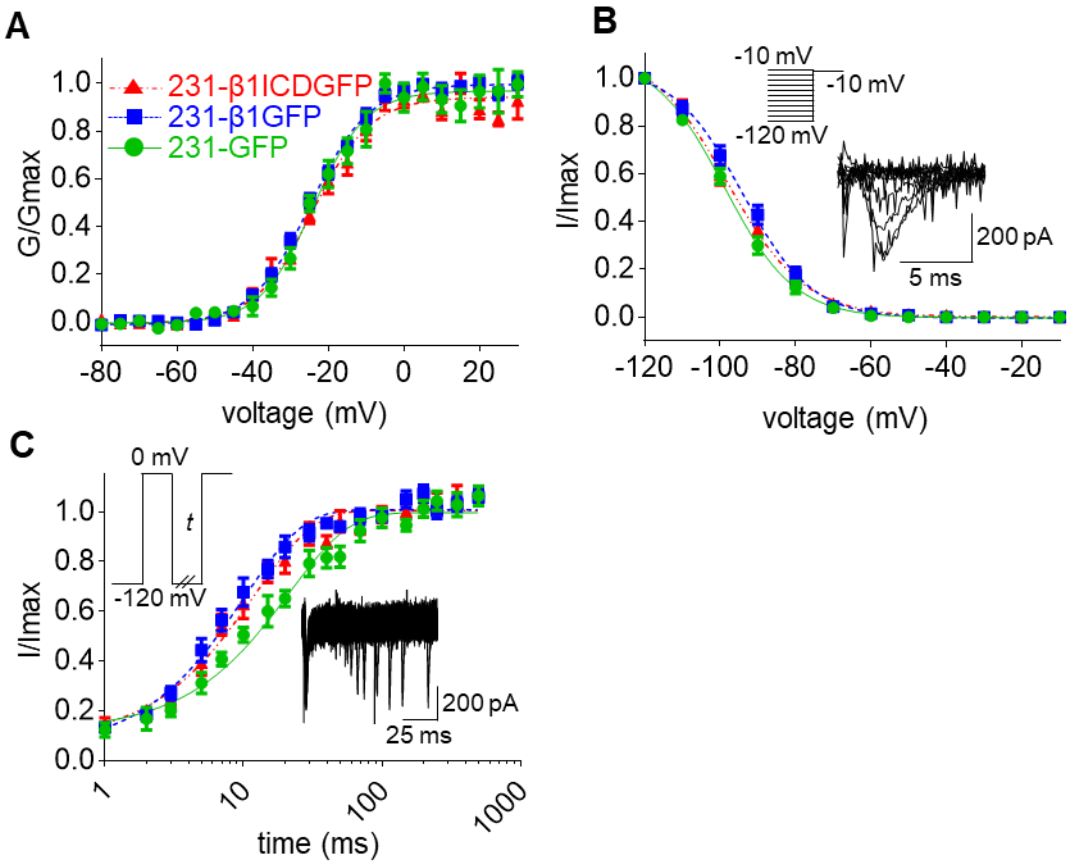

Figure 4.8 VGSC gating kinetics of MDA-MB-231-β1ICDGFP cells

(**A**) Conductance (G)-voltage (V) relationship, from which activation $V_{1/2}$ was derived, between -80 mV and +30 mV. (**B**) Steady-state inactivation. Cells were stimulated at -10 mV following a 250 ms holding voltage of between -120 mV and -10 mV. Normalised current produced following -10 mV stimulation plotted. (**C**) Recovery from inactivation. Cells were stimulated at 0 mV, then held at -120 mV for t s before re-stimulation at 0 mV. t ranged from 1-500 ms. **A**-**C** Data plotted as Mean ± SEM. **A,B** MDA-MB-231-GFP cells (n =14, green circles, green solid lines) MDA-MB-231-β1GFP cells (n = 15, blue squares, blue dashed lines) and MDA-MB-231-β1ICDGFP (n = 16 red triangles, red dashed lines) (N = 3). **C** all conditions n = 8, N = 3.

steady-state inactivation (Figure 4.8B), and recovery from inactivation measured (Figure 4.8C). Statistical analysis is presented in Table 4.1. β1ICD-GFP accelerated recovery from inactivation compared to GFP, 7.98 ± 1.3 ms and 12.49 ± 1.25 s respectively (n = 10, P < 0.05), similar to β1-GFP (6.15 ± 0.6 ms, n = 10, P < 0.01, one-way ANOVA), suggesting β1-ICD is sufficient to induce a β1-like I_{Na}. Activation and steady-state inactivation kinetic parameters were calculated, although no significant differences were observed, except a marginally depolarised voltage for half-maximal inactivation in β1-GFP expressing cells compared to GFP expressing cells, -94.1 ± 0.9 pA/pF and -98.9 ± 0.9 pA/pF respectively (n=15, P<0.05, one-way ANOVA). MDA-MB-231-β1ICDGFP cells were also smaller than MDA-MB-231-β1GFP cells, demonstrated by a reduced membrane capacitance (a measure of plasma membrane surface area), 19.8 ± 1.3 pF and 30.6 ± 4.1 pF respectively (n = 15, P<0.05, one-way ANOVA). In summary, β1-ICD recapitulated a β1-like increase in peak current density and recovery from inactivation when expressed in MDA-MB-231 cells. Differences were also detected in the membrane capacitance between β1-GFP and β1ICD-GFP expressing cells, as well as the voltage threshold for half-maximal inactivation between β1-GFP and GFP expressing cells. As MDA-MB-231-β1GFP and MDA-MB-231-β1ICDGFP cells showed comparable membrane capacitances to MDA-MB-231-GFP cells, it is unlikely that β1 enlarges cells or β1-ICD contracts cells, so the difference is likely due to slightly larger β1-GFP expressing cells and slightly smaller β1ICD-GFP expressing cells being recorded from in this experiment inadvertently. As only β1-GFP depolarised inactivation, it is possible that N-terminal interactions with the α-subunit are responsible, which β1ICD-GFP does not possess. However, as β1-induced depolarisation of channel inactivation has not been consistently reported in this study, it may just be an effect seen in this experiment.

Table 4.1 Na^+ current parameters in MDA-MB-231 cells expressing GFP, β1-GFP or β1ICD-GFP

Parameter	GFP	β1-GFP	β1ICD-GFP
C_m (pF)	26.35 ± 3.96	30.59 ± 4.09	^19.84 ± 1.33
PCD (pA/pF)	-4.36 ± 0.66	****-11.7 ± 0.92	**-9.33 ± 1.03
V_a (mV)	-46.43 ± 2.31	-52.00 ± 1.94	-46.56 ± 2.22
V_p (mV)	-2.86 ± 2.21	-2.67 ± 1.45	-3.75 ± 1.25
Activation $V_{1/2}$ (mV)	-24.01 ± 0.81	-24.72 ± 0.43	-24.05 ± 0.89
Activation *k* (mV)	6.97 ± 0.72	7.76 ± 0.38	7.67 ± 0.62
Inactivation $V_{1/2}$ (mV)	-98.90 ± 0.92	*-94.09 ± 0.94	-98.00 ± 1.50
Inactivation *k* (mV)	-9.31 ± 0.65	-9.16 ± 0.73	-10.24 ± 1.03
T_p (ms)	1.21 ± 0.11	1.21 ± 0.08	0.96 ± 0.08
RFI $t_{1/2}$ (ms) (n = 8)	12.49 ± 1.25	**6.15 ± 0.59	*7.98 ± 1.32
Data displayed as mean ± SEM (n =14 – 16 unless stated, N = 3). Significance tested using one-way ANOVA. * = P < 0.05, ** = P < 0.01, **** = P < 0.0001 relative to MDA-MB-231-GFP cells. ^ = P < 0.05 relative to MDA-MB-231-β1GFP cells. Abbreviations: C_m: membrane capacitance, PCD: peak current density, V_a: activation voltage, V_p: voltage at peak current, $V_{1/2}$: voltage for half maximal activation/inactivation, T_p: time to peak, RFI $T_{1/2}$: time for half-maximal recovery from inactivation.			

4.2.6 Pharmacological characterisation of the Na^+ current generated by β1-intracellular domain

The I_{Na} composition can be further analysed using VGSC-inhibiting toxins. Tetrodotoxin (TTX) reversibly inhibits a class of α-subunits ($Na_v1.1$-1.4, 1.6, 1.7) at a lower concentration ("TTX-sensitive" channels) than other α-subunits ($Na_v1.5$, 1.8, 1.9; "TTX-resistant" channels). In MDA-MB-231 cells, the TTX-resistant $Na_v1.5$ channel is the predominantly expressed α-subunit, although $Na_v1.6$ and $Na_v1.7$ mRNA is detectable (Fraser *et al.*, 2005). Additionally, ~10 – 15 % of I_{Na} is blocked by 1 μM TTX in MDA-MB-231 cells (Fraser *et al.*, 2005). Unpublished work from our lab has demonstrated that β1 expression in MDA-MB-231 cells increases TTX-sensitivity at 1 μM, most likely through trafficking of TTX-sensitive channels to the plasma membrane. To test whether β1-ICD is also capable of increasing TTX-sensitivity in MDA-MB-231 cells, MDA-MB-231-GFP, MDA-MB-231-β1GFP and MDA-MB-231-β1ICDGFP cells were reversibly perfused with 1 μM TTX during recording and current density measured before perfusion, after perfusion and after washout (Figure 4.9A). Current densities for each cell were normalised to the initial, pre-perfusion recording and the normalised peak current density following TTX treatment compared to the initial and washout recordings (Figure 4.9B). Following 1 μM TTX application, the I_{Na} in MDA-MB-231-GFP cells decreased to 0.89 ± 0.1, although this was not statistically significant compared to the pre-perfusion I_{Na} ($n = 9$, $P = 0.17$) and post-washout I_{Na} ($n = 9$, $P = 0.59$, RM one-way ANOVA). 1 μM TTX perfusion significantly reduced the I_{Na} in MDA-MB-231-β1GFP cells, however, to 0.67 ± 0.02 ($n = 9$, $P<0.0001$, RM one-way ANOVA). Likewise, 1 μM TTX perfusion significantly reduced I_{Na} in MDA-MB-231-β1ICDGFP cells to 0.65 ± 0.03 ($n = 9$, $P<0.0001$, RM one-way ANOVA). These data suggest β1-ICD induces trafficking of TTX-sensitive α-subunits to the plasma membrane, similar to β1.

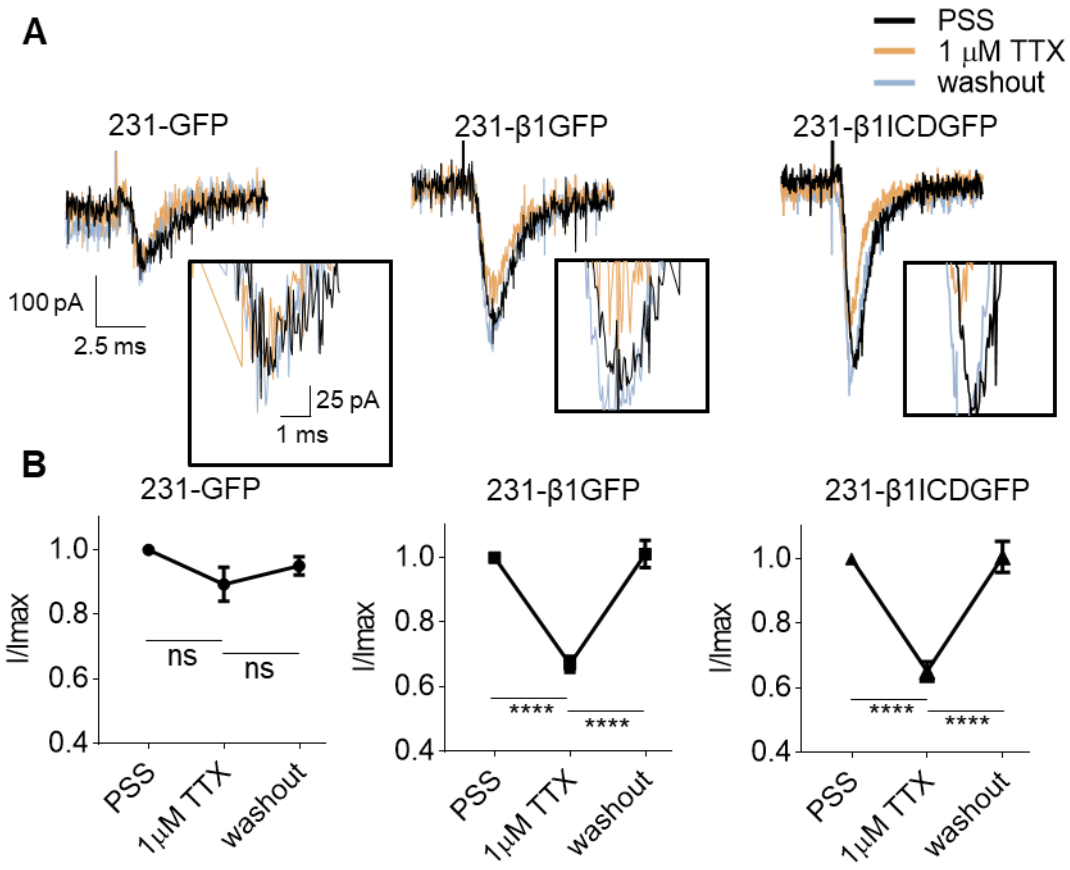

Figure 4.9 Analysis of the composition of the Na^+ current induced by β1-ICD using tetrodotoxin and ProToxin-II

(**A**) Representative traces of the I_{Na} generated in MDA-MB-231 cells expressing GFP, β1-GFP or β1ICD-GFP in standard recording solution (PSS, black line), following 1 μM TTX perfusion (orange line) and following PSS washout (grey line), determined using whole-cell patch clamp electrophysiology. (**B**) Quantification of the reduction in current density following 1 μM TTX perfusion and recovery following PSS washout in MDA-MB-231 cells expressing GFP, β1-GFP or β1ICD-GFP. Current density normalised to initial recording in PSS bath solution. Data displayed as mean ± SEM. n = 9, N = 3. Significance determined using repeat-measure one-way ANOVA. ns = not significant. **** = P < 0.0001.

An attempt to further characterise the nature of the TTX-sensitive I_{Na} in MDA-MB-231-β1GFP cells was performed using ProToxin-II (ProTx-II). ProTx-II is a $Na_v1.7$ specific blocker, which has demonstrated complete $Na_v1.7$ inhibition at 100 nM and complete VGSC inhibition at 1 μM in heterologous HEK293 cells (Schmalhofer *et al.*, 2008). The exact nature of ProTx-II binding is still uncertain however, as two binding sites for ProTx-II in $Na_v1.7$ were independently identified, one in the voltage-sensor domain of domain II and the other in the S3-S4 extracellular loop of domain IV (Shen *et al.*, 2019; Xu *et al.*, 2019)(Figure 4.1A). Although, when tested on MDA-MB-231-β1GFP cells, no I_{Na} inhibition was seen at 100 nM or 1 μM (n= 3 – 4) (Figure 4.10B,C). A possible explanation for this result is that the toxin does not inhibit neonatal splice variants of α-subunits, which are predominant in MDA-MB-231 cells (Fraser *et al.*, 2005). This is supported by the fact the $Na_v1.5$/$Na_v1.7$ neonatal splice variants have altered amino acid sequences within the S3-S4 loop of domain I and multiple mutations within the S3-S4 loops of $Na_v1.7$ that interfere with ProTx-II binding have been identified (Cestele *et al.*, 1998; Fraser *et al.*, 2005; Xiao *et al.*, 2010). Alternatively, the effect of ProTx-II may be inhibited by β-subunit shielding. β2 and β4 are both able to attenuate the inhibitory effect of ProTx-II through shielding the ProTx-II binding site on the α-subunit, although I_{Na} inhibition was still noticeable at 100 nM in these cases and β1 docks at the voltage-sensor domain of domain III, away from the ProTx-II binding sites (Fraser *et al.*, 2005; Gilchrist *et al.*, 2013; Das *et al.*, 2016).

In summary, the pharmacology data demonstrate that β1-ICD is able to increase the proportion of TTX-sensitive I_{Na}, possibly through surface trafficking of α-subunits to the plasma membrane.

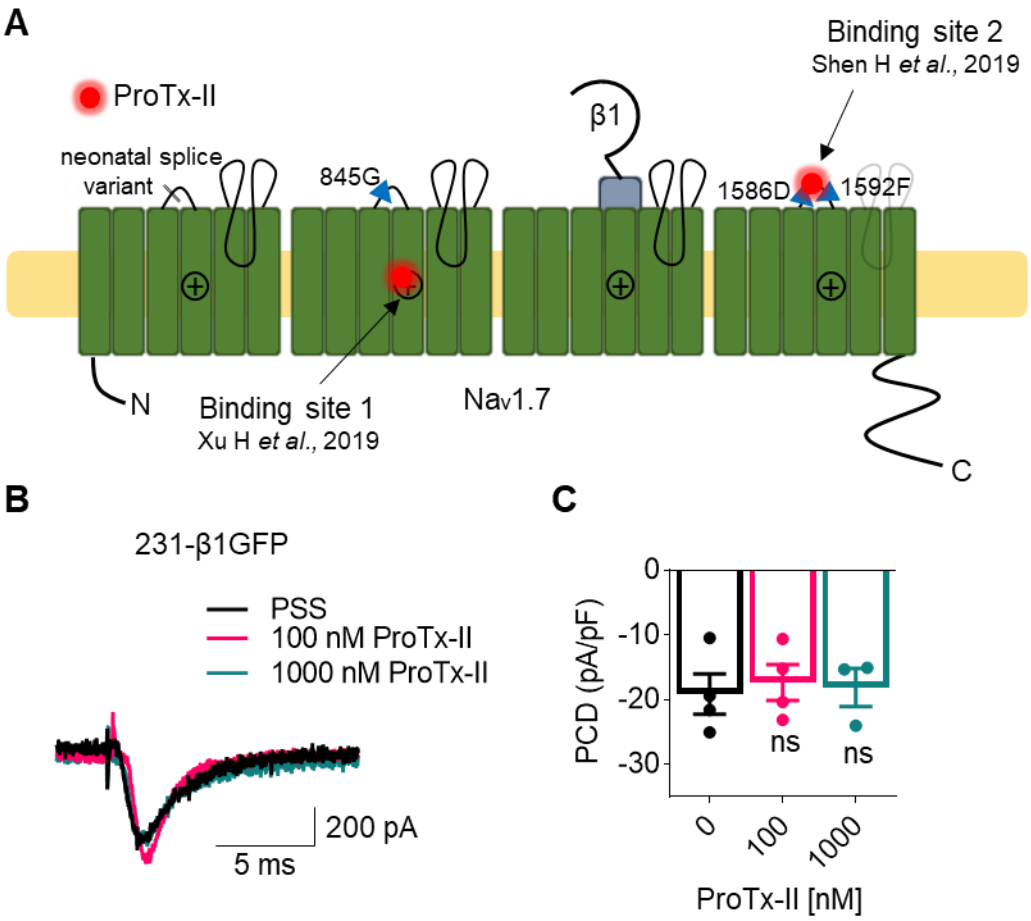

Figure 4.10 The effect of ProTx-II on the Na^+ current generated in MDA-MB-231-β1GFP cells

(**A**) Schematic of $Na_v1.7$ depicting the binding sites of ProTx-II. ProTx-II depicted as red circles. Crystallography of $Na_v1.7$, in complex with ProTx-II, has demonstrated binding sites within the voltage-sensor domain of D2 (neurotoxin binding site 2) as well as a binding site within the extracellular S3-S4 loop of domain IV (neurotoxin binding site 3) (Shen *et al.*, 2019; Xu *et al.*, 2019). Multiple mutations in $Na_v1.7$ (blue triangles) have been identified that interfere with ProTx-II binding, including G845N in the DII:S3-S4 extracellular loop and mutations of 1586Asp and 1592Phe in the DIV:S3-S4 extracellular loop (Cestele *et al.*, 1998; Xiao *et al.*, 2010). Approximate location of the neonatal splice variants of $Na_v1.7$(D206N) and $Na_v1.5$ within the D1:S3-S4 extracellular loop shown (Belcher *et al.*, 1995; Fraser *et al.*, 2005). The docking site of β1, at DIII:S4 shown (Yan *et al.*, 2017). (**B**) Current density generated in MDA-MB-231-β1GFP cells in PSS solution (black), 100 nM ProTx-II (magenta) and 1 μM ProTx-II (cyan). (**C**) Quantification of **B**. Data displayed as mean ± SEM. n = 3-4, N = 2. Significance determined using one-way ANOVA. ns = not significant.

4.2.7 β1-intracellular domain does not recapitulate the effect of β1 on cell adhesion or morphology

To further investigate whether β1-ICD can fully functionally recapitulate β1, the capacity of β1-ICD to induce metastatic cellular behaviours (cell adhesion and morphology), typically associated with the β1 extracellular Ig loop, was examined. Cell adhesion was quantified by acquiring a single cell suspension and measuring the rate at which cells reaggregate. β1, as a CAM, enhances the rate of cell adhesion relative to non-expressing cells (Chioni *et al.*, 2009). In chapter 3.2.3, β1 demonstrated its ability to enhance the rate of cell adhesion when expressed in MDA-MB-231 cells. Accordingly, the aggregation rate of MDA-MB-231-β1ICDGFP cells was compared to MDA-MB-231-GFP cells (Figure 4.11A). Both cell lines aggregated at a comparable rate, determined by comparison of normalised particle number at each time point between MDA-MB-231-GFP and MDA-MB-231-β1ICDGFP cells (Figure 4.11B) (n = 40, two-way ANOVA). These data suggest β1-ICD does not induce cell-cell adhesion, unlike full-length β1.

Next, the ability of β1-ICD to induce cell morphological changes in cultured cells was assessed. β1 is capable of inducing increased process length and reduced process width when expressed in MDA-MB-231 cells *in vitro* (Chioni *et al.*, 2009). The mechanism was not explored, although it was hypothesised that β1-induced process elongation was due to adhesion via the extracellular Ig loop. However, if the mechanism is instead regulated by intracellular signalling or the β1-induced I_{Na}, then β1-ICD should also be able to induce β1-like morphology changes.

Brightfield images of fixed cells were acquired and parameters used to quantify cell morphology, circularity index and cell length, were analysed (Figure 4.12A).

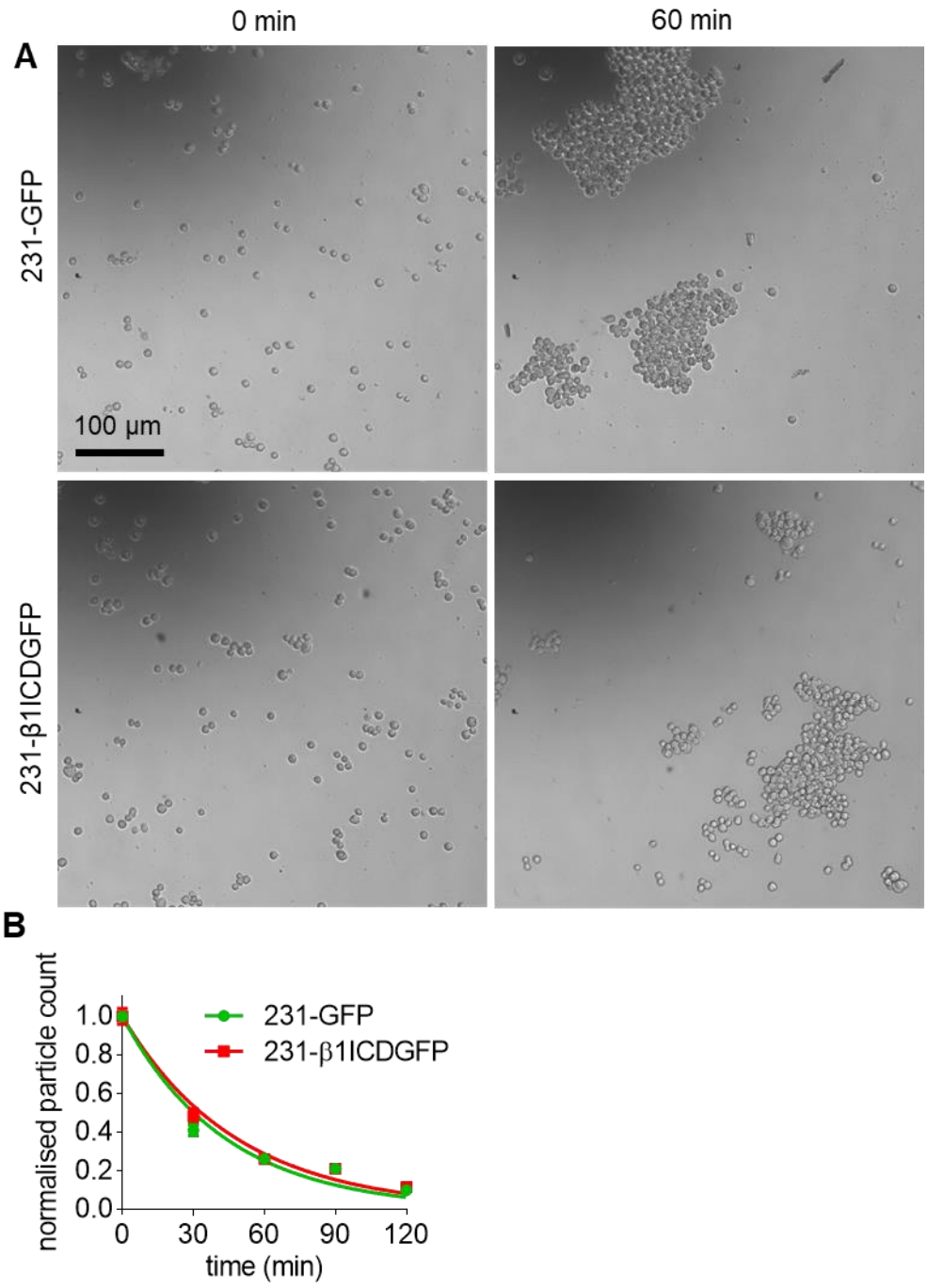

Figure 4.11 The cell adhesive capacity of β1-ICD in MDA-MB-231-β1ICDGFP cells

(**A**) Single cell suspensions of MDA-MB-231-GFP (top row) and MDA-MB-231-β1ICDGFP (bottom row) cells were left to aggregate for 2 h. The number of particles in a sample were counted every 30 min (**B**) Quantification of the rate of transcellular adhesion of MDA-MB-231-GFP (green) and MDA-MB-231-β1ICDGFP (red) cells (n = 40, N = 4). Particle count at each time point (30, 60, 90 and 120 min) normalised to T = 0. Data displayed as Mean ± SEM. Two-way ANOVA used to test significance between treatments at each time point, but no significant difference detected.

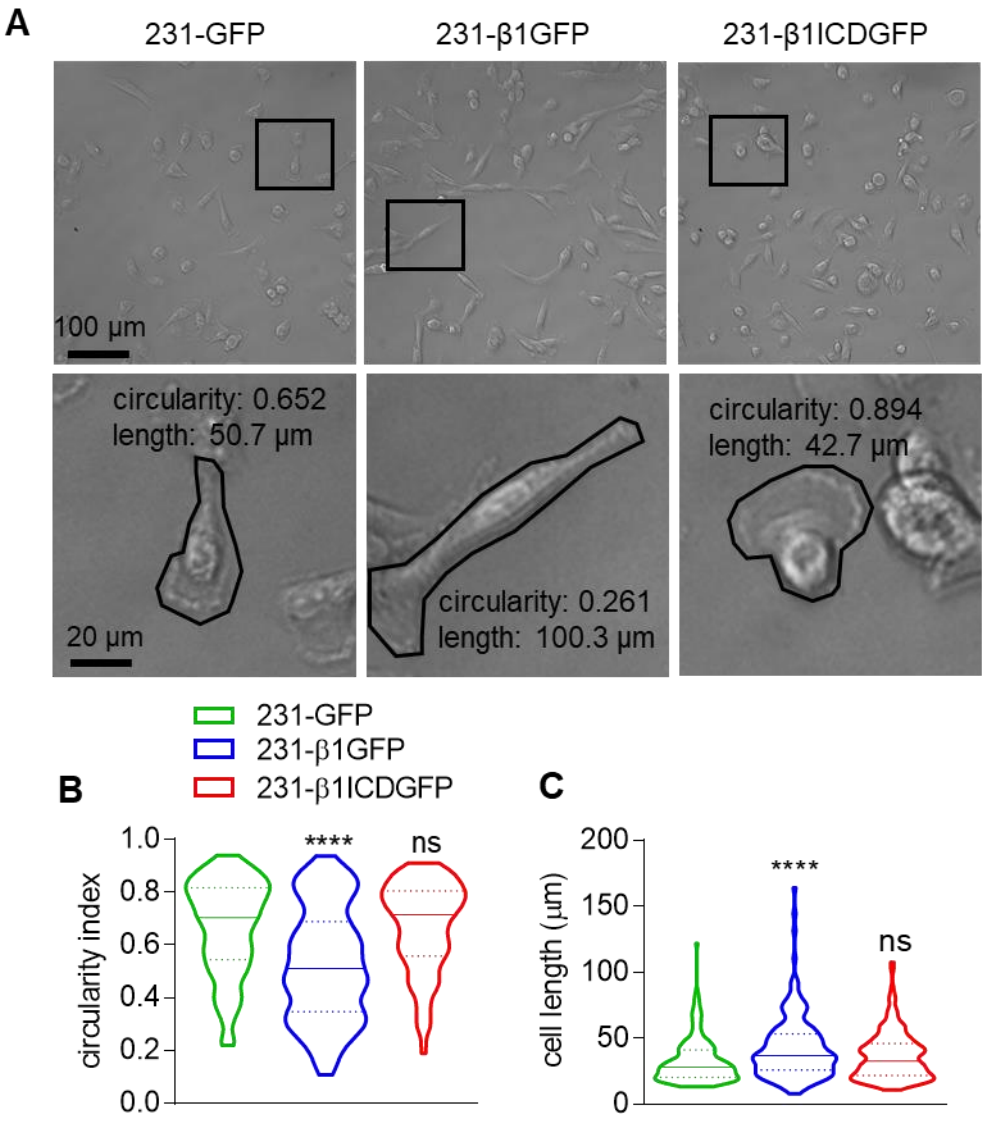

Figure 4.12 Cell morphology analysis of MDA-MB-231-β1ICDGFP cells

(**A**) Brightfield images of MDA-MB-231-GFP, MDA-MB-231-β1GFP and MDA-MB-231-β1ICDGFP at 20x magnification (L-R). Bottom row displays the same images as top row with masks over example cells depicting circularity index and Feret's diameter, a measure of cell length (µm). (**B**) Quantification of circularity index (left) and cell length (right) of MDA-MB-231-GFP (green), MDA-MB-231-β1GFP (blue) and MDA-MB-231-β1ICDGFP (red) cells. n = 150, N = 3. Data displayed as violin plots, solid horizontal line represents median, dashed horizontal lines represent lower/upper quartiles. Significance tested using a Kruskal-Wallis test. ns = not significant. **** = $P < 0.0001$.

Circularity is a measure of cell roundness and takes into account cell area relative to perimeter. Cell length is calculated from the 'Feret's diameter' of a cell, which is the distance between the two furthest points of a cell. MDA-MB-231 cells are polarised, so the Feret's diameter will usually measure the distance between the leading and trailing edges of a cell. As β1 induces process outgrowth in MDA-MB-231 cells, β1-GFP expression should result in reduced circularity and increased cell length, relative to GFP-expressing cells (Chioni *et al.*, 2009). Indeed, MDA-MB-231-β1GFP cells had a reduced circularity compared to MDA-MB-231-GFP cells, 0.51 (median, IQR: 0.35 – 0.69) and 0.70 (median, IQR: 0.54 – 0.82) respectively (n = 150, P <0.0001, Kruskal-Wallis test) (Figure 4.12B). MDA-MB-231-β1ICDGFP cells, however, demonstrated a similar circularity index (0.71, IQR: 0.55 – 0.82) to MDA-MB-231-GFP cells (n = 150, P >0.999, Kruskal-Wallis test). Furthermore, measuring cell length demonstrated the same result. MDA-MB-231-β1GFP cells (37.0 μm (median), IQR: 26.0 – 53.4) were significantly (P<0.0001) longer than MDA-MB-231-GFP cells (28.3 μm (median), IQR: 20.5 – 41.3), whereas MDA-MB-231-β1ICDGFP cells (32.8 μm (median), IQR: 22.0 – 46.1) were indistinguishable from GFP-expressing cells (n = 150, P = 0.14, Kruskal-Wallis test) (Figure 4.12C). In summary, comparing cell morphology has demonstrated a requirement for β1-ECD to induce cellular elongation, supporting the theory that the Ig loop is responsible for β1-induced cell morphology changes and verifying there is no involvement of β1-ICD.

4.3 Discussion

The data in this chapter show that β1-ICD is present in the nucleus when overexpressed in MDA-MB-231 cells. However, GFP shares a similar spatial expression profile to β1-ICD, presumably owing to their small molecular weight (~ 30 kDa), allowing for diffusion

throughout the cell. Furthermore, β1-ICD displayed comparable cytoplasmic mobility kinetics to GFP. When the nuclear import kinetics of GFP and β1-ICD were compared using FRAP however, β1-ICD displayed a surprising 2.5-fold slower import rate than GFP, suggesting a potential distinction between the import mechanism of GFP and β1-ICD. Functionally, β1-ICD did not recapitulate β1-like cell adhesion and morphology changes. However, β1-ICD was sufficient in inducing a β1-like I_{Na}, namely an increase in peak current density, an acceleration of channel recovery from inactivation and an increase in the proportion of TTX-sensitive α-subunits at the plasma membrane.

The ability of β1-ICD to induce a β1-like I_{Na} was a surprising result, as γ-secretase inhibition did not reduce the β1-induced I_{Na}. Together, these results suggest that β1-ICD contains the required domains to induce an enlarged I_{Na} and its release to soluble form following secretase processing is not a requirement for an enlarged I_{Na}. Such an explanation raises concerns over using β1-ICD overexpressing cells as a model for secretase-processed β1, as it does not take into consideration the β1-ICD sequence found on membrane-bound full-length β1 and β1-CTF that may still be functionally active prior to γ-secretase cleavage. Regardless, this result leads to the intriguing question of how β1-ICD is mechanistically enhancing I_{Na}? Deletion of the β1-ICD sequence from β1 leads to reduced $Na_v1.2$ surface expression relative to wild-type β1 and a GEFS+ mutation within the intracellular portion of $Na_v1.1$ attenuates β1 binding, suggesting α-subunit interaction sites within β1-ICD (Meadows *et al.*, 2001; Spampanato *et al.*, 2004). Additionally, isolated APP-ICD is capable of modulating $Na_v1.6$, dependent on phosphorylation of a single residue by cyclin-dependent kinase 5 and c-Jun N-terminal kinase 3, Thr668 (Li *et al.*, 2016b). Biotinylation of cell surface proteins demonstrated that $Na_v1.6$ membrane expression is reduced in HEK-$Na_v1.6$ cells transfected with APP siRNA, whereas total $Na_v1.6$ expression is not affected (Li *et al.*, 2016b). Therefore, it appears APP-ICD is sufficient in trafficking $Na_v1.6$ to the plasma membrane. Considering

APP-ICD is a soluble protein of similar size to β1ICD, there is an α-subunit interaction site within β1-ICD, and full-length β1/β1-ICD enhance the TTX-sensitive proportion of I_{Na}, it raises the possibility of β1-ICD mediated trafficking of α-subunits to the plasma membrane as the mechanism underlying the enlarged I_{Na}. The theory of a direct α-β1ICD interaction is supported by the finding β1-ICD is capable of accelerating channel recovery from inactivation, as β-subunit induced changes in gating kinetics are typically mediated by direct interaction between subunits. Additionally, β2-ICD is associated with the membrane fraction when overexpressed in CHO cells, suggesting a sub-population of β-subunits ICDs may be immobilised at the plasma membrane (Kim *et al.*, 2005). In summary, the electrophysiology data strongly suggests β1-ICD is involved in α-subunit trafficking to the cell surface. Confirming an increase in plasma membrane α-subunit expression, for instance by biotinylation of surface proteins, would be required to validate the model.

Direct trafficking and modulation of α-subunits by β1-ICD would explain the increase in I_{Na} magnitude and the acceleration of recovery from inactivation observed when β1-ICD is overexpressed in MDA-MB-231 cells. However, not even a fraction of immobilised β1-ICD was observed in the cytoplasm by FRAP. Furthermore, co-expression experiments in *Xenopus* oocytes have demonstrated β1-ECD is sufficient for modulating $Na_v1.2$ (McCormick *et al.*, 1999). However, no change in peak current density was reported in McCormick *et al.* and the only gating kinetic investigated was an acceleration of inactivation, suggesting there are major discrepancies between using *Xenopus* oocytes and MDA-MB-231 cells as model systems.

The ability to observe and quantify β1/β1-ICD and α-subunits at the plasma membrane would provide a very useful tool for verifying cell surface trafficking of α-subunits and β1-

ICD localisation at the plasma membrane. Additionally, continued work with specific α-subunit inhibitors would identify the channel isoforms contributing to the TTX-sensitive I_{Na} observed in MDA-MB-231-β1GFP/β1ICDGFP cells. Endogenous $Na_v1.6$ and $Na_v1.7$ mRNA expression is present in MDA-MB-231 cells, suggesting these channels may form inactive pools within MDA-MB-231 cells and contribute to the TTX-sensitive I_{Na} following β1/β1-ICD-mediated trafficking (Fraser *et al.*, 2005).

If β1-ICD is not involved in cell surface trafficking of α-subunits, it may be enhancing I_{Na} through nuclear signalling. As β1-ICD expression induces a TTX-sensitive Na^+ current, that would implicate $Na_v1.1$ – 4, $Na_v1.6$ or $Na_v1.7$ as the upregulated α-subunit. β2-ICD induces mRNA and protein expression of $Na_v1.1$ (Kim *et al.*, 2007). β1 knockdown in breast cancer MCF7 cells increases expression of neonatal $Na_v1.5$ mRNA expression (Chioni *et al.*, 2009). Furthermore, *Scn1b* KO mice show reduced $Na_v1.1$ and increased $Na_v1.3$ expression in hippocampal CA3 neurons and increased $Na_v1.3$ and $Na_v1.5$ expression in ventricular myocytes, suggesting possible β1-mediated regulation of α-subunit expression (Chen *et al.*, 2004; Lopez-Santiago *et al.*, 2007; Lin *et al.*, 2015). ProTx-II, a selective $Na_v1.7$ inhibitor, was used to determine if $Na_v1.7$ membrane expression was increased in β1GFP- and β1ICDGFP-expressing cells. However, the Na^+ current was not inhibited, even at concentrations that should have inhibited global Na^+ current, suggesting ProTx-II is an unsuitable inhibitor to use. β1ICD-GFP did demonstrate nuclear expression, however it resembled GFP spatial expression. This was not unexpected, as APP-ICD also shows uniform expression when overexpressed in HEK293 cells and only demonstrates nuclear enrichment when co-expressed with the proteins that constitute its nuclear shuttling complex (Fe65 and Tip60) or nuclear export is inhibited (von Rotz *et al.*, 2004). Similar methods may be required to reveal nuclear enrichment of β1-ICD.

The hypothesis regarding β1-ICD nuclear signalling was that β1-ICD is actively trafficked into the nucleus, similar to other secretase-generated ICDs. For example, Notch-ICD forms a multimeric signalling complex with Mastermind and CSL, and is trafficked into the nucleus via importin-α3 (Vasquez-Del Carpio *et al.*, 2011; Sachan *et al.*, 2013). Whereas imaging of fixed cells demonstrated comparable spatial localisation between β1ICD-GFP and GFP, analysis of nuclear import demonstrated significantly slower import for β1ICD-GFP compared to GFP, consistent with the notion that β1ICD is trafficked into the nucleus as part of a complex and does not diffuse into the nucleus like GFP. A marginally increased time course for import would however be expected for β1ICD-GFP compared to GFP if it were diffusing through nuclear pores. According to the experimentally verified cubic relationship between molecular weight and time taken for nuclear import, the five additional kilodaltons of β1ICD-GFP should increase nuclear import time by ~ 70 % compared to GFP (Timney *et al.*, 2016). However, nuclear import was increased by 150 %. Whether this discrepancy is due to differences in model systems and β1-ICD is in fact diffusing into the nucleus or due to active β1-ICD complex trafficking is still unclear at this point. Methods such as ATP depletion, temperature reduction and nuclear import inhibition can be used to verify active nuclear import (Adam *et al.*, 1990; Soderholm *et al.*, 2011). If β1-ICD is, in fact, involved in nuclear signalling, it may be involved in regulating α-subunit expression, similar to β2. However, the fact γ-secretase inhibition did not affect the magnitude of I_{Na} suggests β1-ICD cleavage is not required in the β1-induced I_{Na}.

β1-ICD was not sufficient for inducing β1-like *in vitro* metastatic cell behaviour, namely enhanced transcellular adhesion and cell elongation. This result allowed for multiple interpretations. Firstly, it negates the possibility β1-ICD inducing a β1-like I_{Na} through increased expression of β1, as an accompanying increase in the rate of cell adhesion and enhanced cell elongation is not observed in MDA-MB-231-β1ICDGFP. Secondly, it

verifies the importance of the β1 Ig loop in β1-mediated transcellular interactions. Transcellular interactions through the extracellular Ig loop are a vital aspect of β1-regulated neurodevelopment, permitting fasciculation and neurite outgrowth (Brackenbury *et al.*, 2008). In addition, β1-induced neurite outgrowth is γ-secretase dependent (Brackenbury & Isom, 2011). A similar ability of β1 to induce neurite-like outgrowths in MDA-MB-231 cells has been reported, raising the possibility γ-secretase cleavage may regulate β1-induced process outgrowth in breast cancer cells (Nelson *et al.*, 2014). However, the fact β1-ICD expression alone did not enhance cell length or reduce cell circularity suggests β1-ICD generation may not underlie β1-induced neurite outgrowth, but perhaps γ-secretase cleavage is regulating β1 turnover or membrane expression. This could be determined by inhibiting γ-secretase and quantifying the resulting change in membrane β1 expression by western blot. Lastly, as MDA-MB-231-β1ICDGFP cells induce a β1-like I_{Na} but are not able to mimic the cell adhesive capacity of MDA-MB-231-β1GFP cells, they provide a potentially very informative tool in understanding β1-induced metastasis, as they allow for study of the consequences of the enlarged I_{Na} in isolation from the function of the β1 Ig loop. As mice implanted with MDA-MB-231-β1GFP cell-derived tumours experience increased metastasis compared to control cells (Nelson *et al.*, 2014), replicating the experiment using β1ICD-GFP cells would determine if the β1-induced I_{Na} is required for β1-induced metastasis.

4.4 Conclusion

This chapter set out to investigate the function of β1-ICD, when overexpressed in MDA-MB-231 cells, with emphasis on assessing the nuclear signalling and electrophysiological function of β1-ICD. β1-ICD demonstrated nuclear expression, however whether this is functionally relevant or a consequence of the small size of β1-

ICD requires further work to fully understand. Interestingly, β1-ICD induced a β1-like I_{Na}, suggesting the domains of β1 necessary for enhancing I_{Na} in MDA-MB-231 cells are found within the ICD sequence. Lastly, β1-ICD did not recapitulate β1-induced cell adhesion and morphology changes, supporting the idea that the β1 Ig loop is responsible for these functions and not the ICD. To fully dissect the secretase-dependency of β1 function, the following chapter focuses on the functional characterisation of full-length β1 in the absence of secretase cleavage.

Chapter 5: Expression and functional analysis of secretase-resistant β1

5.1 Introduction

VGSC β-subunits were originally recognised as β-secretase substrates using heterologous studies in HEK cells, neuroglioma HTB-148/H4 cells and mouse embryonic fibroblasts (Wong *et al.*, 2005). The exact β-secretase cleavage sites within β-subunits were discovered using matrix-assisted laser desorption/ionisation-time of flight (MALDI-TOF) mass spectrometry, with β1 being cleaved between Leu144 and Glu145 (Wong *et al.*, 2005). β2 was further confirmed to be a substrate of α-secretase, raising the possibility VGSC β-subunits are also substrates of α-secretase (Kim *et al.*, 2005). The functional impact of α-/β-secretase cleavage on β-subunits has scarcely been explored, however. Co-expression of β2-CTF, but not β2-ICD, with full-length β2 in CHO cells inhibits β2-induced cell migration, leading the authors to conclude β2-CTF can inhibit β2 function (Kim *et al.*, 2005). Overexpression of β4-CTF, or co-expression of β4 with BACE1, in Neuro2a cells accelerates neurite extension, implicating β-secretase as a regulator of β4-mediated neurite outgrowth although the contribution of γ-secretase cleavage was not investigated (Miyazaki *et al.*, 2007). Additionally, a β4-CTF-like protein (β4 lacking its Ig loop) is capable of inhibiting MDA-MB-231 cell migration, similar to full-length β4 (Bon *et al.*, 2016).

α-/β-secretase cleavage has a potential dual effect on β-subunit function, as it not only produces a transmembrane CTF, but also releases a soluble ECD. As discussed in chapter 1.3.4, many mutations in β1 that affect α-subunit gating are located in the ECD and an α-subunit interaction site is located within the β1-ECD (McCormick *et al.*, 1999). Furthermore, the soluble β1 splice variant, β1B, is capable of α-subunit modulation (Kazen-Gillespie *et al.*, 2000), suggesting β1-ECD may retain the ability to modulate α-subunits after shedding or conversely, β1-mediated α-subunit gating may be lost

following β1-ECD secretion. Similarly, β1-induced transcellular adhesion is mediated by the extracellular Ig loop, suggesting α-/β-secretase cleavage may have a negative impact on cell adhesion (Isom & Catterall, 1996). Additionally, following extracellular secretase cleavage, both APP-ECD and Notch-ECD are involved in paracrine and juxtracrine cell signalling respectively, raising the possibility β-ECDs may also be involved in cell signalling. APP-ECD has demonstrated the ability to directly potentiate pre-synaptic GABA receptors suppressing neuronal activity *in vivo* (Rice *et al.*, 2019). Notch binds to its transcellular ligands via ECD interactions, which induces secretase processing (Mumm *et al.*, 2000).

α-secretase activity has been implicated in cancer, with increased breast tumour ADAM10 mRNA expression correlating with decreased patient disease-free survival and increased ADAM10 protein expression seen in high-grade compared to low-grade breast tumours (Mullooly *et al.*, 2015). Knockdown of ADAM10 in MDA-MB-231 cells decreases cell migration and overexpression of ADAM17 in MDA-MB-231 cells enhances cell proliferation, invasion and VEGF secretion (Zheng *et al.*, 2009; Mullooly *et al.*, 2015). α-secretase is a desirable target in cancer, due to its regulation of Notch function. The contribution of β-secretase in cancer, on the other hand, has yet to be explored and its expression in MDA-MB-231 cells is unreported.

Data in Chapter 3 demonstrated γ-secretase inhibition does not affect the β1-induced I_{Na}. Conversely, β1ICD-GFP is sufficient to induce a β1-like I_{Na}, suggesting the presence of β1-ICD is the requirement for the β1-induced I_{Na}. Therefore, α-/β-secretase cleavage should not affect the ability of β1 to induce an enlarged I_{Na}. On the other hand, β1ICD-GFP was incapable of inducing β1-like cell adhesion and morphology changes, whereas γ-secretase inhibition increased the rate of β1-induced cell adhesion, potentially through

increased full-length β1 at the plasma membrane. Therefore, α-/β-secretase cleavage inhibition should not affect β1-induced cell adhesion and morphology changes and may, in fact, increase the rate of cell adhesion and decrease cell circularity/ increase cell length, as more full-length β1 should be present.

Chapter 3 did not reveal any effect of γ-secretase cleavage on β1 localisation. Using FRAP, no difference in β1 mobility was detected following γ-secretase inhibition. Likewise, co-localisation studies revealed early endosomal and lysosomal localisation of β1, but the degree of co-localisation was not affected by γ-secretase inhibition, suggesting secretase processing may not occur within the endolysosomal system. On the other hand, if α-/β-secretase cleavage of β1 at the plasma membrane is a pre-requisite for endocytosis, then α-/β-secretase inhibition should decrease β1 enrichment within endosomes.

5.1.1 Hypothesis and aims

The hypothesis of this chapter was that extracellular secretase cleavage regulates β1 function and localisation. I aimed to test this hypothesis by:

- Creating a mutated β1 construct that is resistant to α-/β-secretase cleavage – secretase-resistant β1 (SRβ1)
- Assessing whether SRβ1 is sufficient to recapitulate β1-induced metastatic cell behaviours, namely β1-induced cell adhesion and morphology changes
- Comparing the subcellular localisation of SRβ1 to β1
- Comparing the electrophysiological properties of SRβ1 to β1

5.2 Results

5.2.1 Generation of a secretase-resistant form of β1

To assess the impact of secretase processing of β1 in MDA-MB-231 cells, while avoiding using pharmacological inhibitors that would inhibit proteolysis of other endogenous secretase substrates, a secretase-resistant β1 (SRβ1) construct was generated through amino acid deletion and transfected into MDA-MB-231 cells. β-secretase cleavage of β1 has been identified and the cleavage site located (between Leu144 and Glu145) (Wong *et al.*, 2005). β2 is the only β-subunit that has been demonstrated to be cleaved by α-secretase (Kim *et al.*, 2005). However, the location of the cleavage site was not determined. In this study, β-secretase was focused upon, as the cleavage site is known. Six amino acids (Ile142-147Val) (Figure 5.1A), three each side of the cleavage site, were deleted from pcDNA3.1 encoding β1-GFP by site-directed mutagenesis to produce SRβ1-GFP (Figure 5.1B,C). Following site-directed mutagenesis, pcDNA3.1-SRβ1-GFP was transfected into MDA-MB-231 cells and a stable cell line generated through prolonged antibiotic treatment and single cell colony expansion. Lysate of MDA-MB-231-SRβ1-GFP cells was probed with an anti-GFP antibody by western blot and compared against MDA-MB-231-β1GFP lysate. Any inhibition of extracellular secretase cleavage would be expected to reduce the abundance of β1CTF-GFP/β1ICD-GFP. Excitingly, SRβ1-GFP showed complete inhibition of secretase processing, demonstrated by the absence of a β1CTF-GFP band (Figure 5.1D). The complete inhibition of secretase processing suggests either α-secretase does not cleave β1 in MDA-MB-231 cells or α-secretase cleavage is also inhibited by the deletion mutation. Furthermore, both FLβ1-GFP and SRβ1GFP ran at the same weight. This is an important result as it suggests SRβ1GFP is being glycosylated similar to FLβ1-GFP.

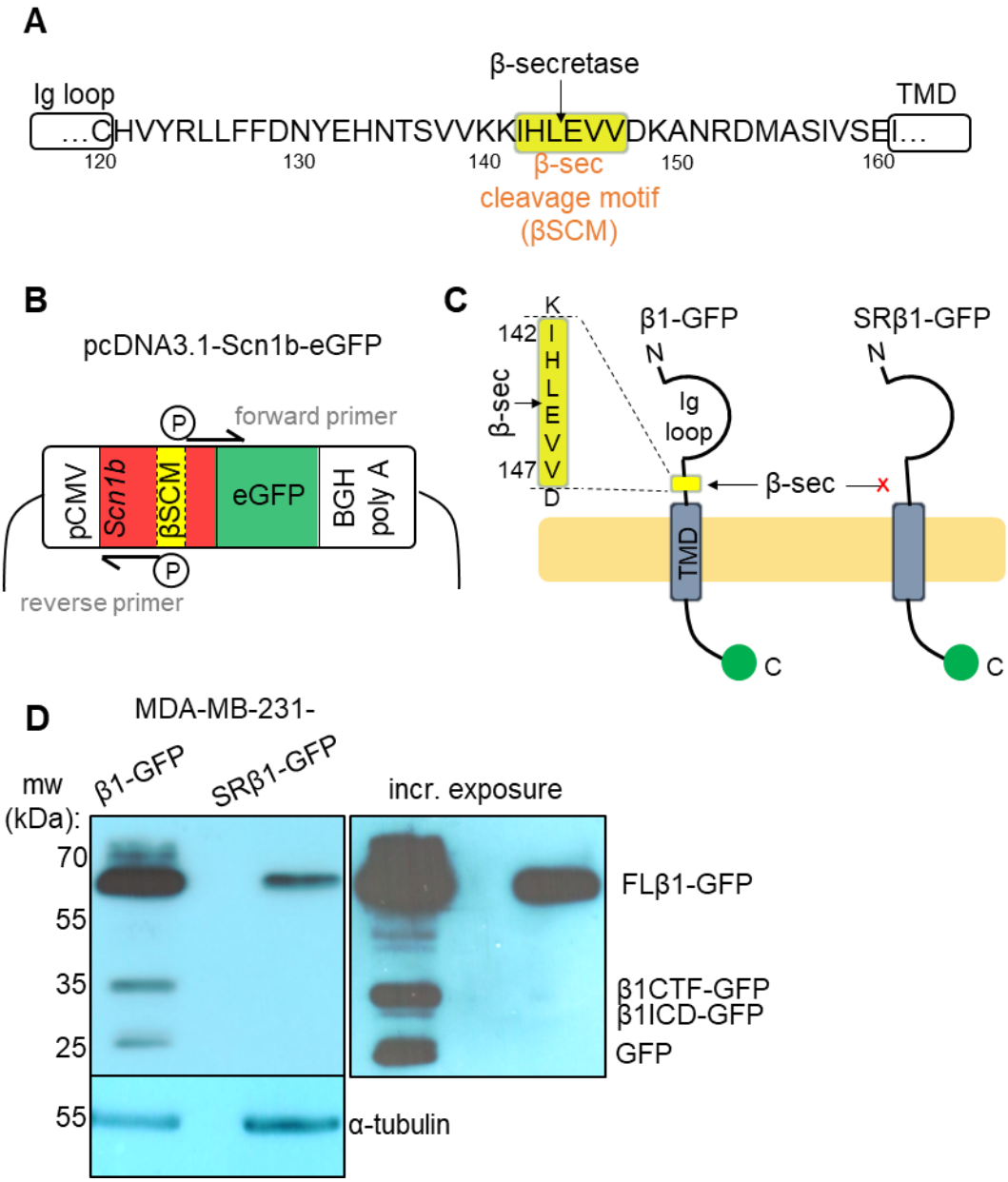

Figure 5.1 Generation of a secretase-resistant β1 construct

(**A**) Location of the β-secretase cleavage site between Leu144 and Glu145 of β1 (Wong *et al.*, 2005). The occurrence of α-secretase cleavage of β1 has not been reported. The 142Ile-147Val motif flanking the β-secretase cleavage site was deleted by site-directed mutagenesis (**B**). 5' phosphorylated (P) primers were designed to flank the DNA sequence that encodes 142Ile-147Val to produce a β1 construct resistant to β-secretase cleavage, known as secretase-resistant (SR) β1 (**C**). Ig: immunoglobulin, TMD: transmembrane domain, βSCM: β-secretase cleavage motif. (**D**) Western blot analysis of lysate from MDA-MB-231 cells expressing β1-GFP or SRβ1-GFP probed for anti-GFP. α-tubulin used as a loading control. The molecular weight in kilodaltons is provided on the left side of the blot. Two different exposures of the same membrane provided to exemplify the absence of secretase cleavage in SRβ1-expressing cells. FL: full-length, CTF: C-terminal fragment, ICD: intracellular domain.

5.2.2 Secretase-resistant β1 induces β1-like cell adhesion and morphology changes

As the six amino acid deletion to generate SRβ1-GFP may impair β1 structure and functionality independently of secretase inhibition, SRβ1-GFP was tested by transcellular adhesion and morphology assays, to ensure SRβ1-GFP is correctly folded, present at the plasma membrane, functionally active and practical to use in further assays. The β1 Ig loop is assumed to underpin β1-induced transcellular adhesion and process outgrowth (Isom & Catterall, 1996), supported by evidence from Chapter 4 demonstrating β1ICD-GFP expression did not induce either change. Accordingly, if SRβ1-GFP is being correctly folded and exported to the plasma membrane, it should induce β1-like adhesion and morphology changes. The ability to accelerate the rate of transcellular adhesion was first examined. β1-GFP is known to increase the rate of adhesion, when expressed in MDA-MB-231 cells, compared to GFP alone (Chioni *et al.*, 2009). Therefore, the rate of transcellular adhesion was compared between MDA-MB-231-GFP and MDA-MB-231-SRβ1GFP cells, to verify SRβ1 also accelerates the rate of cell adhesion. Transcellular adhesion was measured by obtaining a single cell suspension and counting the number of particles in ten fields of view at 30 min intervals and normalising the count to T = 0 (Figure 5.2A). If SRβ1-GFP is functionally active it should increase the rate of aggregation compared to parental cells. Indeed, SRβ1-GFP did enhance the rate of cell adhesion. Particle counts at 30 min ($P < 0.01$) and 60 min ($P < 0.01$) were reduced in MDA-MB-231-SRβ1GFP cells compared to MDA-MB-231-GFP cells (n = 40, two-way ANOVA) (Figure 5.2B), suggesting SRβ1-GFP is functionally active at the plasma membrane and able to induce transcellular adhesion, similar to β1-GFP.

Similar to transcellular adhesion, cellular elongation occurs in β1-GFP-expressing cells (Chioni *et al.*, 2009) and not in β1ICD-GFP -expressing cells (Chapter 4), suggesting it is another function induced by the Ig loop that is independent of secretase cleavage.

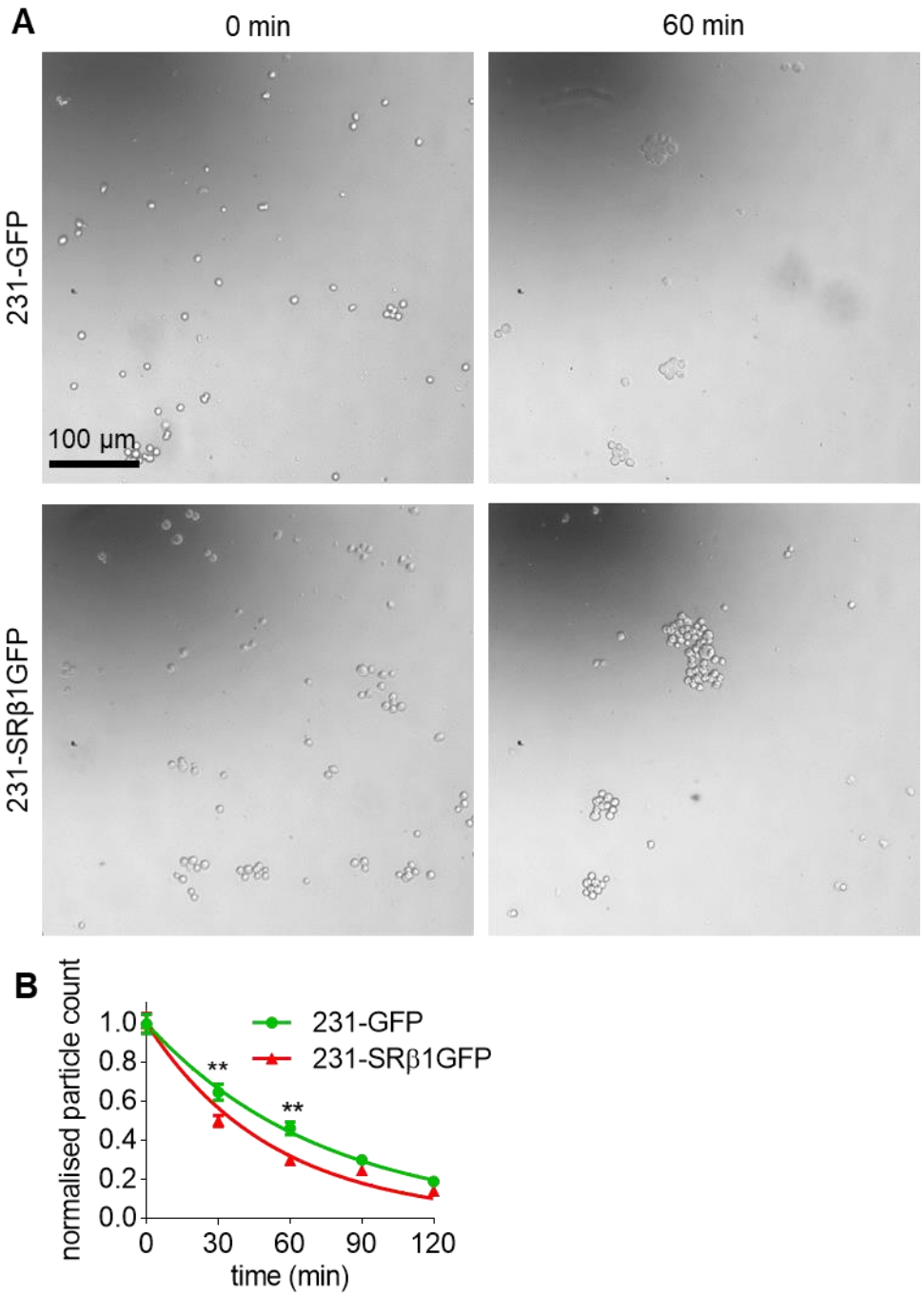

Figure 5.2 Transcellular adhesion assay of MDA-MB-231-SRβ1GFP cells

(**A**) Single cell suspensions of MDA-MB-231-GFP cells (top row) and MDA-MB-231-SRβGFP cells (bottom row) were left to aggregate for 2 h at 37 ^{o}C with gentle agitation at 25 rpm. The number of particles (cell aggregates of any quantity) in a sample were counted every 30 min. Example images at 0 and 60 min given. (**B**) Quantification of the rate of transcellular adhesion of MDA-MB-231-GFP (green circles) and MDA-MB-231-SRβ1GFP (red triangles) cells (n = 40, N = 3). Particle count at each time point normalised to t = 0. Data displayed as Mean ± SEM. Two-way ANOVA used to test significance between treatments at each time point. ** = $P < 0.01$.

Cellular morphology was measured by acquiring images of fixed cells, exporting the images to ImageJ, and manually masking fifty cells and measuring cell circularity and cell length using in-built features in ImageJ. Morphology was quantified and compared between MDA-MB-231 cells expressing GFP, β1-GFP and SRβ1-GFP, to examine whether SRβ1 can induce similar morphology changes to β1-GFP (decreased circularity and increased cell length; Figure 5.3A). Both MDA-MB-231-β1GFP (median – 0.54 (IQR: 0.37 – 0.68), n = 150, $P < 0.0001$) and MDA-MB-231-SRβ1GFP cells (median – 0.52 (IQR: 0.38 – 0.71), n = 150, $P < 0.0001$) demonstrated decreased circularity compared to MDA-MB-231-GFP cells (median – 0.71 (IQR: 0.58 – 0.82), n = 150, Kruskal-Wallis test; Figure 5.3B), supporting the result from the adhesion assay that SRβ1-GFP is functionally active. Furthermore, the circularity index was comparable between MDA-MB-231-β1GFP and MDA-MB-231-SRβ1GFP cells ($P > 0.9999$). Both β1-GFP (median – 37.8 μm (IQR: 25.8 – 50.3), n = 150, $P < 0.05$) and SRβ1-GFP (median – 53.2 μm (IQR: 36.8 – 79.2), n = 150, $P < 0.0001$) induced cell elongation relative to GFP expression (median – 30.1 μm (IQR: 20.7 – 44.9), n = 150) (Figure 5.3C), further suggesting SRβ1-GFP is a functional protein. However, MDA-MB-231-SRβ1GFP cells were also 40 % longer than MDA-MB-231-β1GFP cells ($P < 0.0001$). This could be due to differences in expression levels between cell lines resulting in more SRβ1 at the plasma membrane or secretase processing negatively regulating the abundance of β1 at the plasma membrane. Further work is required to resolve these possibilities.

5.2.3 Secretase-resistant β1 shows similar endolysosomal distribution to wild-type β1

Following functional validation of SRβ1, the subcellular distribution of SRβ1 was compared to β1-GFP to further understand the similarities between β1 and SRβ1.

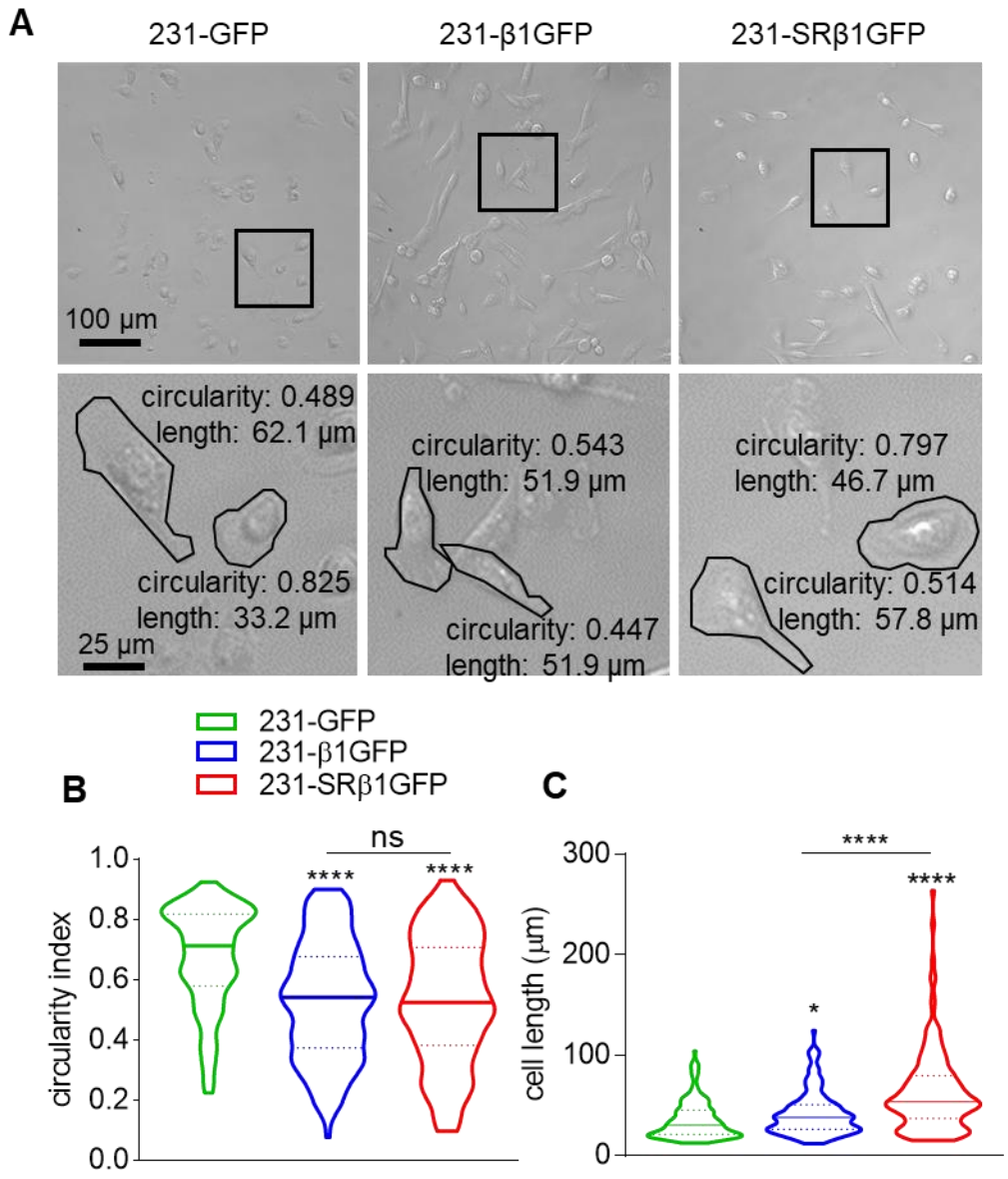

Figure 5.3 Cell morphology analysis of MDA-MB-231-SRβ1GFP cells

(**A**) Brightfield images of MDA-MB-231-GFP, MDA-MB-231-β1GFP and MDA-MB-231-SRβ1GFP cells taken at 20x magnification (top row). Black boxes signify the region of the image that is enlarged in the bottom row. Example cells shown with circularity index and Feret's diameter (analogous to cell length) measurements. (**B**,**C**) Quantification of circularity index (**B**) and cell length (**C**) of MDA-MB-231-GFP (green, left), MDA-MB-231-β1GFP (blue, middle) and MDA-MB-231-SRβ1GFP cells (red, right). Data displayed as min-max violin plots with median denoted as thick horizontal line and quartiles denoted as dashed horizontal lines. n = 150, N = 3. Kruskal-Wallis test used to test for significance. ns = not significant. * = $P < 0.05$. **** = $P < 0.0001$.

γ-secretase cleavage can occur within the endolysosomal pathway (Lorenzen *et al.*, 2010; Tam *et al.*, 2014). In Chapter 3, β1-GFP expression was observed in early endosomes and lysosomes and γ-secretase inhibition decreased β1GFP/EEA1 co-localisation, suggesting secretase processing of β1 is not occurring within the endolysosomal pathway but may be occurring at the plasma membrane. To further this result, the co-localisation of SRβ1-GFP and β1-GFP with EEA1 (early endosome marker) and LAMP1 (lysosome marker) in fixed MDA-MB-231 cells was quantified and compared. If both proteins show a similar enrichment in early endosomes and lysosomes, it would suggest β1 progresses through the endolysosomal pathway without γ-secretase cleavage occurring, as γ-secretase cleavage would result in release of soluble β1ICD-GFP from the endolysosomal membrane causing a decrease in GFP signal at the vesicle membrane. Furthermore, if both proteins show a similar enrichment in early endosomes and lysosomes, it would support the result obtained using the γ-secretase inhibitor, DAPT, which showed γ-secretase inhibition did not increase β1 localisation in endosomes or lysosomes (Chapter 3.2.6). Imaging using confocal microscopy with Airyscan technology demonstrated both β1-GFP and SRβ1-GFP co-localise with EEA1 in the perinuclear region of MDA-MB-231-β1GFP and MDA-MB-231-SRβ1GFP cells, respectively (Figure 5.4A,B). Quantification of GFP/EEA1 co-localisation, using Pearson's correlation coefficient, showed an enhanced enrichment of β1-GFP (0.47 ± 0.02, n = 29), compared to SRβ1-GFP (0.39 ± 0.02 , n = 28), with EEA1 (P = 0.003, unpaired t test) (Figure 5.4C), supporting the idea that γ-secretase regulates β1 plasma membrane dynamics but does not cleave β1 within endosomes.

Next, the enrichment of β1-GFP and SRβ1-GFP within lysosomes, using the marker LAMP1, was quantified and compared in MDA-MB-231-β1GFP and MDA-MB-231-SRβ1GFP cells. If lysosomal localisation of β1 is secretase-independent, then a similar co-localisation of β1-GFP and SRβ1-GFP with LAMP1 is to be expected.

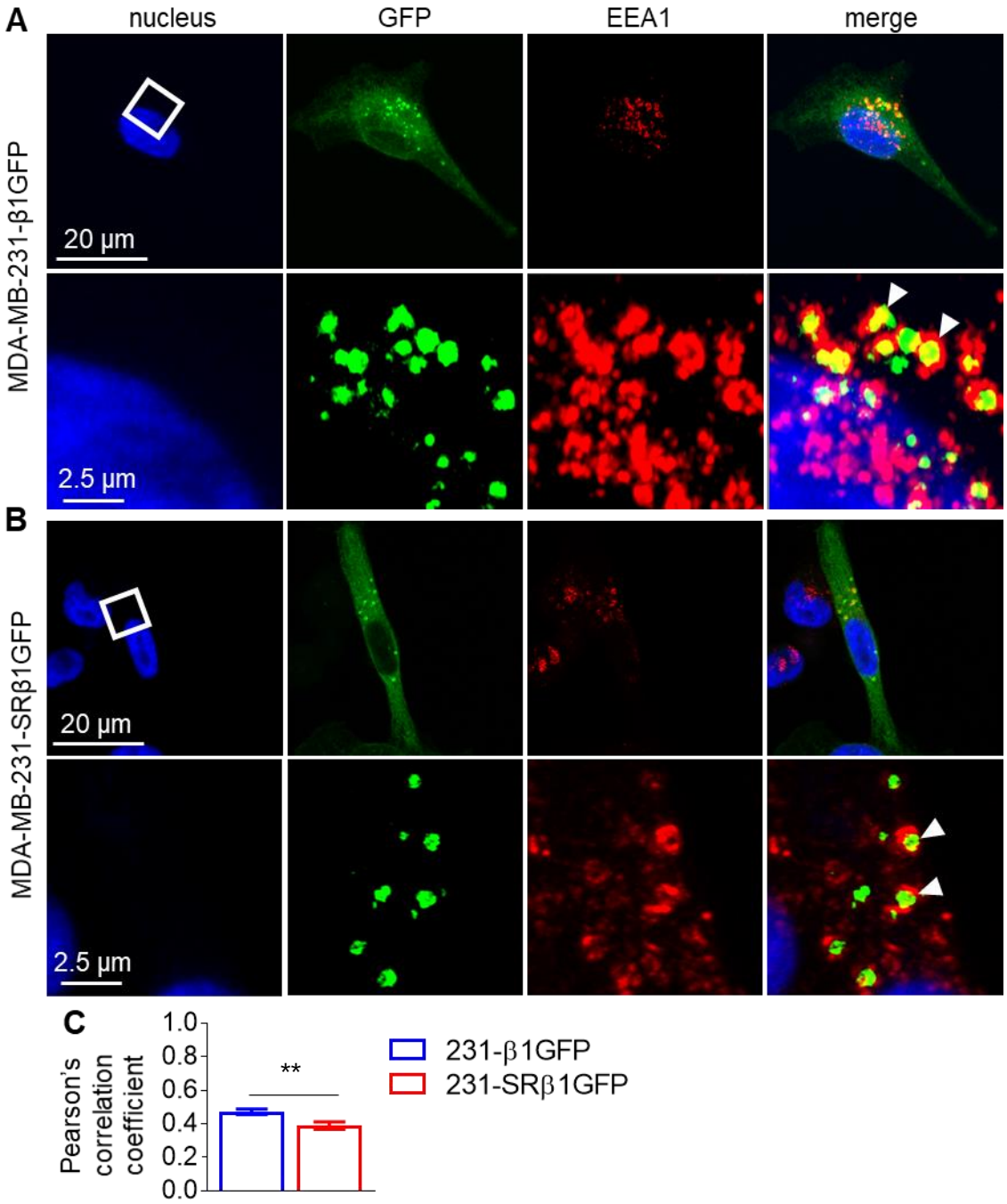

Figure 5.4 Comparison of the early endosomal distribution of β1-GFP and SRβ1-GFP in MDA-MB-231 cells

(**A**,**B**) Images acquired using confocal microscopy with Airyscan technology of MDA-MB-231-β1GFP (**A**) and MDA-MB-231-SRβ1GFP (**B**) cells labelled for anti-EEA1. Nuclei stained for using DAPI DNA stain. Top row- example cells at 63x magnification with 2.5x zoom factor. White boxes signify region of image that is enlarged in the bottom row. Display settings of GFP in the bottom row altered so puncta are visible without surrounding cellular GFP signal. White arrows denote areas of GFP/EEA1 co-localisation. (**C**) Pearson's correlation coefficient was used to estimate co-localisation between β1GFP or (n = 29, blue, left bar) SRβ1GFP (n = 28, red, right bar) (N = 3) and EEA1. Data shown as mean ± SEM. Unpaired t-test used for statistical comparison. ** = $P < 0.01$.

Fixed MDA-MB-231-β1GFP and MDA-MB-231-SRβ1GFP cells were imaged using confocal microscopy with Airyscan technology and immunolabelled for LAMP1 (Figure 5.5A,B). Both cell lines demonstrate GFP/LAMP1 co-localisation, suggest both β1-GFP and SRβ1-GFP are trafficked to lysosomes. Quantification of LAMP1 co-localisation with GFP, by comparing PCCs, revealed a similar co-localisation of β1-GFP and SRβ1-GFP with LAMP1, 0.54 ± 0.02 (n = 29) and 0.51 ± 0.02 (n = 28) respectively (P = 0.23, unpaired t test) (Figure 5.5C). The comparable expression profiles of β1 and SRβ1 suggest that β1 is not cleaved by secretases within lysosomes.

Lastly, to confirm SRβ1-GFP degradation in lysosomes, MDA-MB-231-SRβ1GFP cells were treated with chloroquine and subcellular distribution of SRβ1-GFP compared against negative control cells. Chloroquine treatment prevents complete lysosome vesicle formation and causes a characteristic swelling of lysosomes (Mauthe *et al.*, 2018). MDA-MB-231-SRβ1GFP cells treated with chloroquine demonstrated enlarged perinuclear vesicles enriched with SRβ1-GFP (Figure 5.6A), suggesting SRβ1-GFP is degraded in lysosomes, similar to β1-GFP. To determine whether β1ICD is also degraded in lysosomes, MDA-MB-231-β1ICDGFP cells were treated with chloroquine (Figure 5.6B). Enlarged perinuclear vesicles, presumably lysosomes, devoid of GFP signal were present, suggesting chloroquine treatment worked, but β1ICD-GFP is not present within lysosomes, raising the possibility that β1-ICD is degraded by the proteasome instead. This would be an interesting result, as APP is degraded in lysosomes, yet APP-ICD is degraded by the proteasome (von Rotz *et al.*, 2004; Tam *et al.*, 2014). Proteasomal degradation of APP-ICD dictates its turnover in the nucleus (Gersbacher *et al.*, 2013), suggesting proteasomal activity may also regulate the half-life and function of β1-ICD.

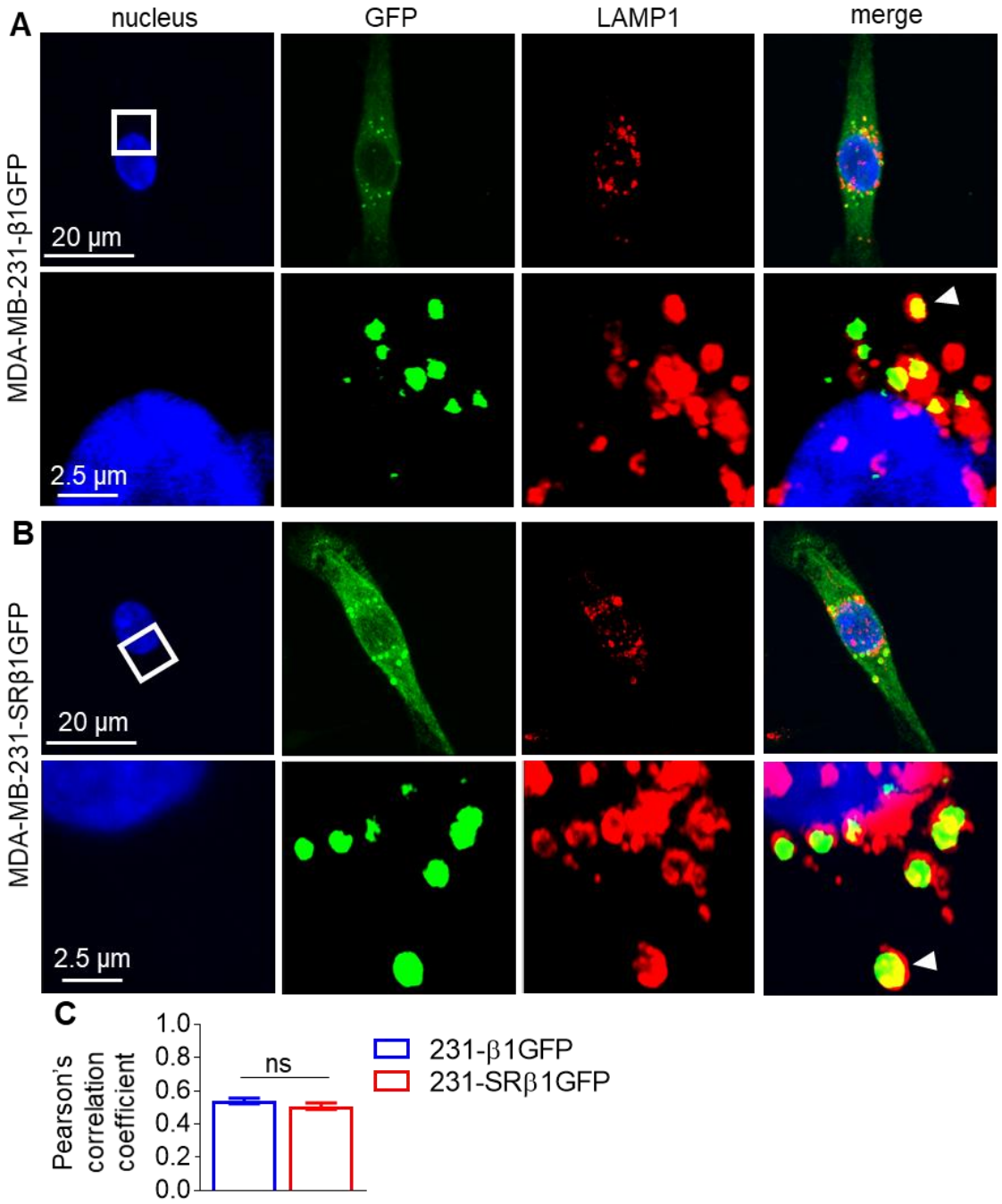

Figure 5.5 Comparison of the lysosomal distribution of β1-GFP and SRβ1-GFP in MDA-MB-231 cells

(**A**,**B**) Images acquired using confocal microscopy with Airyscan technology of MDA-MB-231-β1GFP (**A**) and MDA-MB-231-SRβ1GFP (**B**) cells labelled for anti-LAMP1. Nuclei stained for using DAPI DNA stain. Top row- example cells at 63x magnification with 2.0x zoom factor. White boxes signify region of image that is enlarged in the bottom row. Display settings of GFP in the bottom row altered so puncta are visible without surrounding cellular GFP signal. White arrows denote areas of GFP/LAMP1 co-localisation. (**C**) Pearson's correlation coefficient of GFP/LAMP1 signals in MDA-MB-231-β1GFP cells (n = 29, blue, left bar) and MDA-MB-231-SRβ1GFP cells (n = 30, red, right bar) (N = 3). Data shown as mean ± SEM. Unpaired t-test used for statistical comparison. ns = not significant.

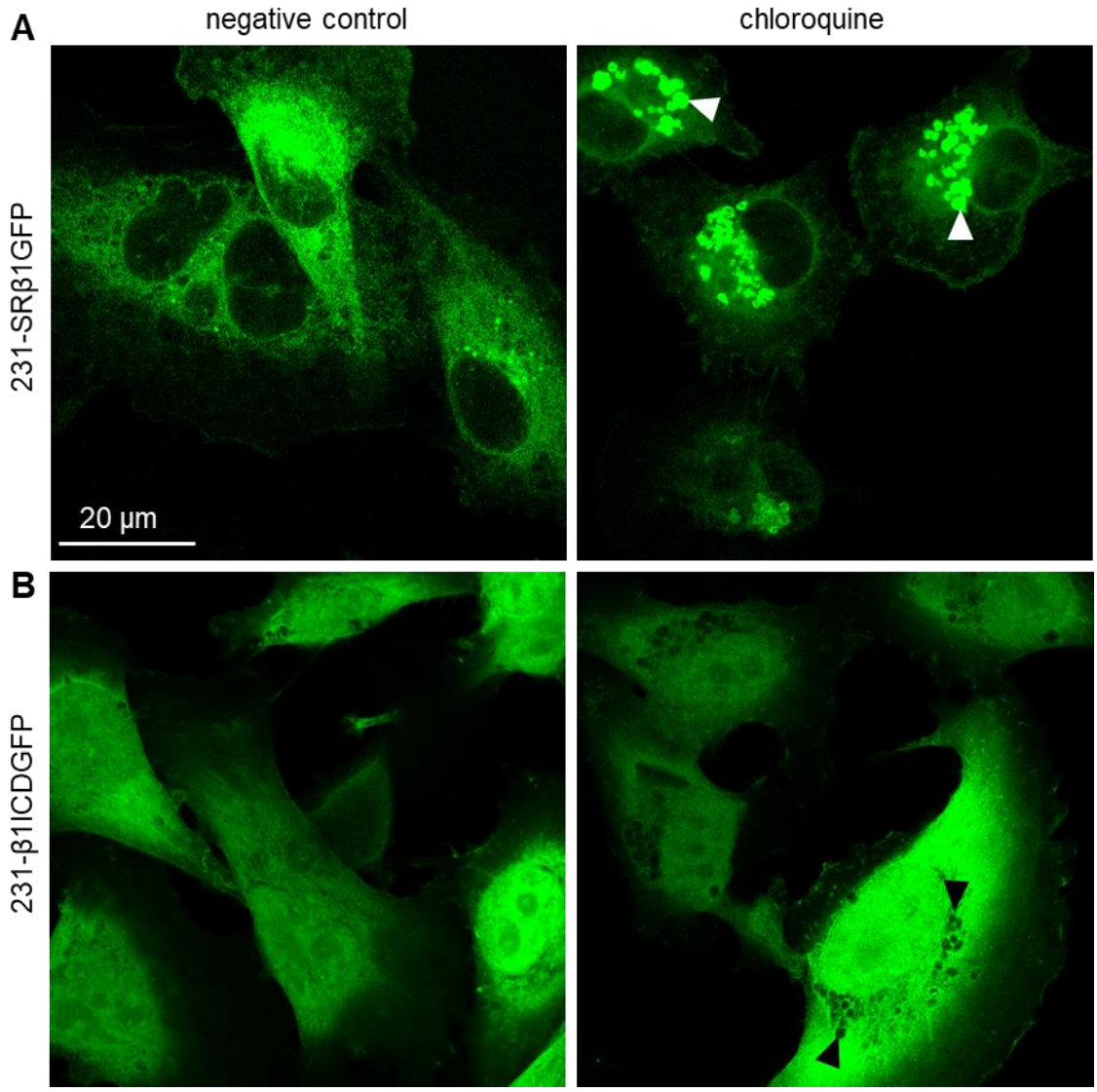

Figure 5.6 Lysosomal degradation of SRβ1-GFP but not β1ICD-GFP in MDA-MB-231 cells

MDA-MB-231-SRβ1-GFP cells (**A**) and MDA-MB-231-β1ICD-GFP cells (**B**) were pre-treated with chloroquine (10 μM, 24h) prior to fixation. Cells were imaged using a confocal microscope with Airyscan technology and endogenous GFP detected. White arrows indicate enlarged lysosomes lined with SRβ1-GFP. Black arrows indicate enlarged lysosomes devoid of β1ICD-GFP.

5.2.4 Secretase-resistant β1 shows similar subcellular distribution to wild-type β1

Other subcellular sites of secretase cleavage were examined to determine if there is any difference between β1 and SRβ1 spatial expression that may be explainable by secretase processing of β1. The organelles examined were the endoplasmic reticulum (ER) and Golgi apparatus, both sites of secretase processing (Chyung *et al.*, 1997; Area-Gomez *et al.*, 2009; Tan & Gleeson, 2019). Furthermore, as the subcellular distribution of β-subunits has yet to be characterised, any results could be novel findings.

Firstly, the distribution of β1 and SRβ1 within the Golgi apparatus was investigated. Fixed MDA-MB-231-β1GFP and MDA-MB-231-SRβ1GFP cells were immunolabelled for the *cis*-Golgi marker, GM130, and the *trans*-Golgi marker, TGN46. Confocal microscopy with Airyscan technology was used to image labelled cells. The *cis*-Golgi occupied a small region adjacent to the nucleus (Figure 5.7A,B). While GM130 signal overlapped with β1-GFP/SRβ1-GFP expression, no clear enrichment of β1-GFP/SRβ1-GFP within the *cis*-Golgi structure, relative to the surrounding GFP fluorescence, was observable. Both β1-GFP and SRβ1-GFP showed a comparable PCC with GM130 ($P = 0.22$, unpaired t test), 0.32 ± 0.02 ($n = 29$) and 0.29 ± 0.01 ($n = 30$) respectively (Figure 5.7C). Both β1-GFP and SRβ1-GFP overlapped with TGN46 signal. However, similar to the co-localisation of β1-GFP/SRβ1-GFP with GM130, no distinct *trans*-Golgi GFP enrichment was noticeable against the surrounding GFP fluorescence (Figure 5.8A,B). A comparable PCC was measured between GFP and TGN46 signals in MDA-MB-231-β1GFP and MDA-MB-231-SRβ1GFP cells, 0.55 (median, IQR: 0.42 – 0.65, $n = 25$) and 0.55 (median, IQR: 0.49 – 0.61, $n = 29$) respectively ($P = 0.96$, Mann-Whitney U test) (Figure 5.8C). The *trans*-Golgi network is a site of both endocytosis and exocytosis for APP, as well as APP proteolysis (Choy *et al.*, 2012; Tam *et al.*, 2014), however despite its importance in APP regulation, no difference was detected in the Golgi enrichment of β1-GFP compared to SRβ1-GFP.

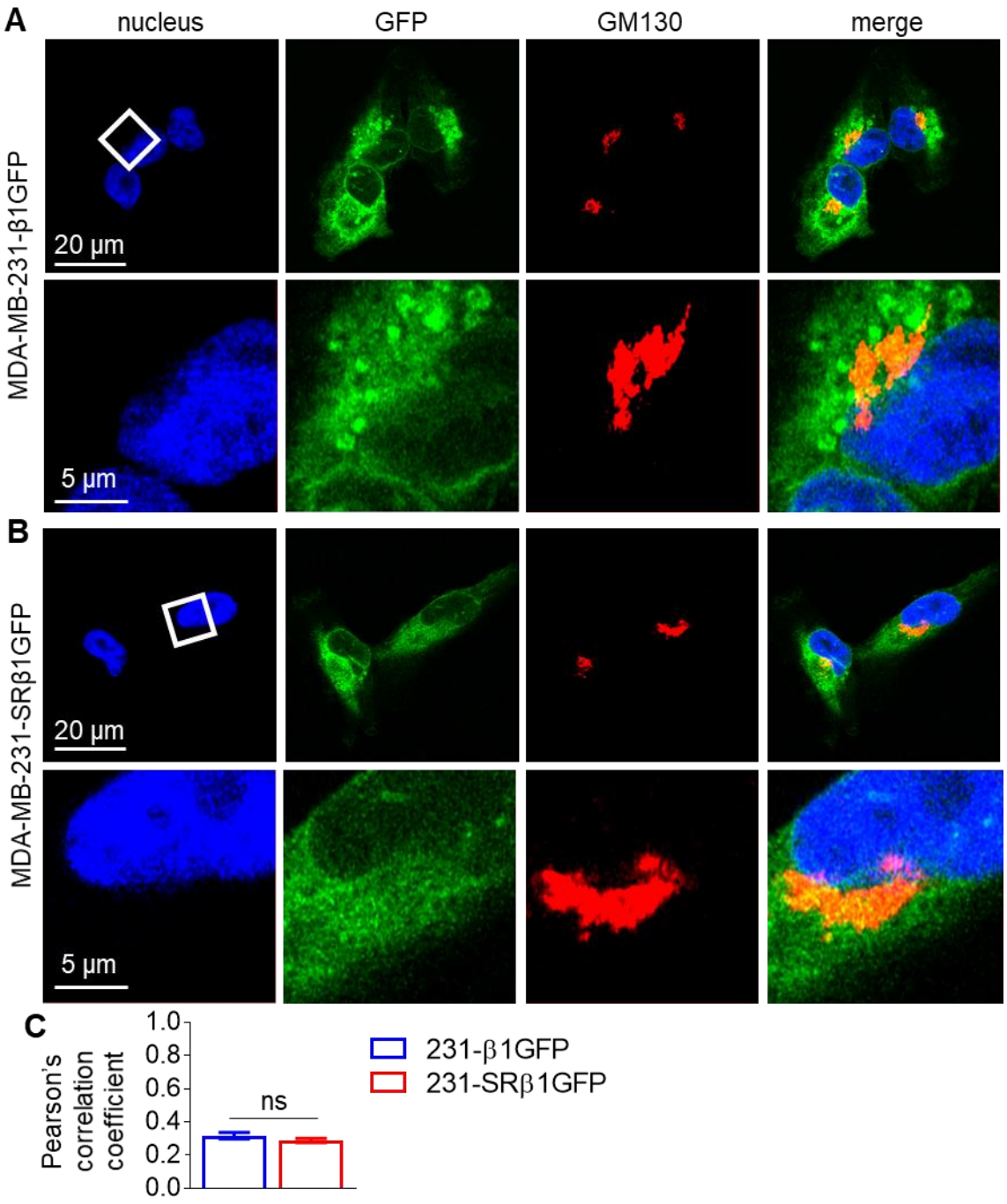

Figure 5.7 Expression of β1-GFP and SRβ1-GFP in the *cis*-Golgi of MDA-MB-231 cells

(**A**,**B**) Images acquired using confocal microscopy with Airyscan technology of MDA-MB-231-β1GFP cells (**A**) and MDA-MB-231-SRβ1GFP cells (**B**) labelled for anti-GM130, a marker for the *cis*-Golgi. Top row depicts cells imaged with a 63x objective lens and 2.0x zoom factor. White boxes denote areas of images that were enlarged to produce the images in the bottom row. (**C**) Pearson's correlation coefficient between GM130 and GFP of MDA-MB-231-β1GFP cells (n = 29, blue, left box plot) and MDA-MB-231-SRβ1GFP cells (n = 28, red, right box plot) (N = 3). Data shown as mean ± SEM. unpaired t test used to test for statistical significance. ns = not significant.

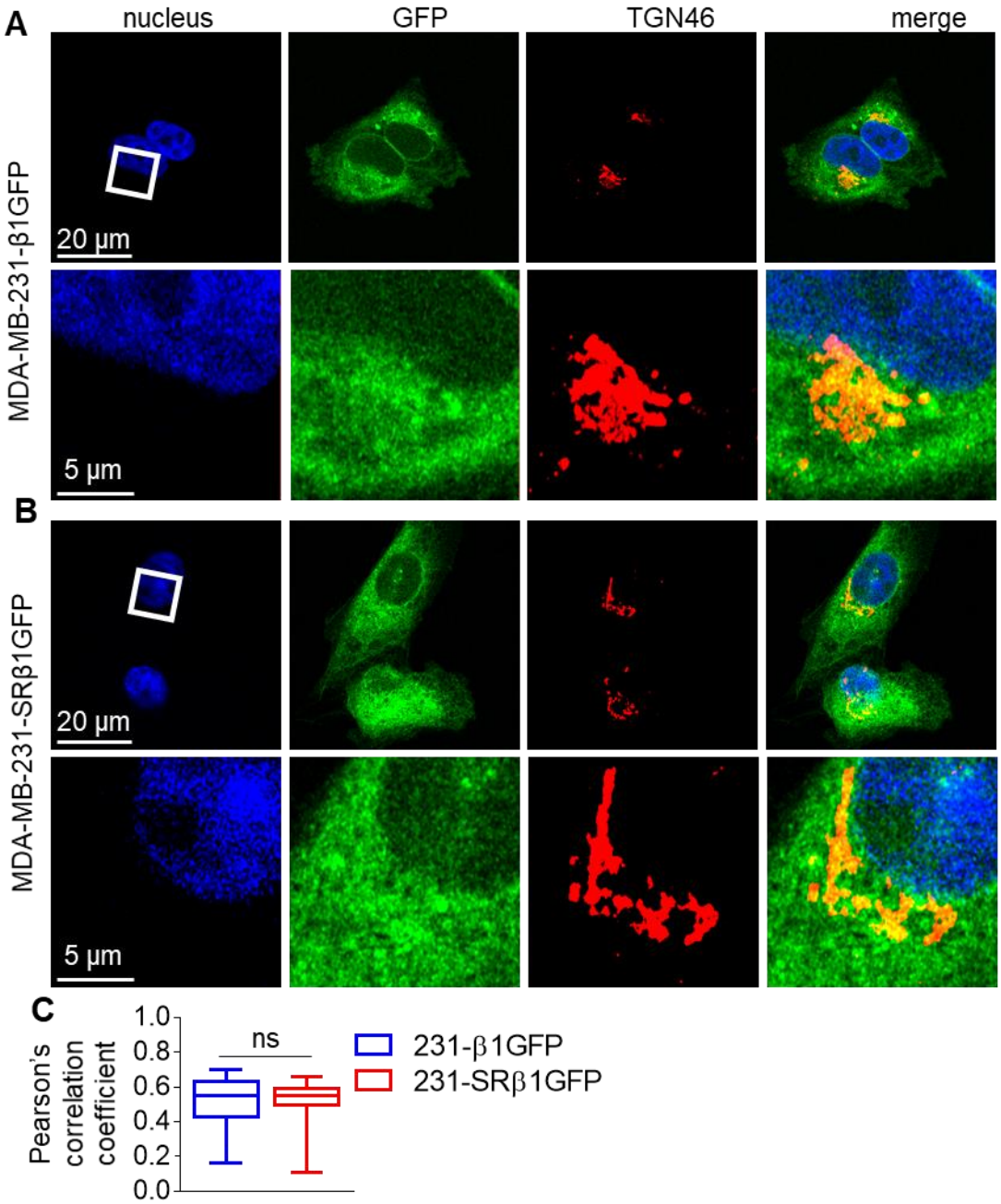

Figure 5.8 Expression of β1-GFP and SRβ1-GFP in the *trans*-Golgi of MDA-MB-231 cells

(**A**,**B**) Images acquired using confocal microscopy with Airyscan technology of MDA-MB-231-β1GFP cells (**A**) and MDA-MB-231-SRβ1GFP cells (**B**) labelled for anti-TGN36, a marker for the *trans*-Golgi. Top row depicts cells imaged with a 63x objective lens and 2.0x zoom factor. White boxes denote areas of images that were enlarged to produce the images in the bottom row. (**C**), estimation of TGN46 co-localisation with GFP, using Pearson's correlation coefficients, in MDA-MB-231-β1GFP cells (n = 25, blue, left box plot) and MDA-MB-231-SRβ1GFP cells (n = 29, red, right box plot) (N = 3). Data shown as min-max box plot. Mann-Whitney U test used to test for statistical significance. ns = not significant.

Next, the ER distribution of β1 and SRβ1 was assessed. Fixed MDA-MB-231-β1GFP and MDA-MB-231-SRβ1GFP cells were immunolabelled for the ER maker calnexin. Confocal microscopy with Airyscan technology was used to detect anti-calnexin and endogenous GFP and co-localisation determined by PCC calculation. In both cell lines, a clear co-localisation of calnexin with β1-GFP or SRβ1-GFP was observed (Figure 5.9A,B). For both proteins, a robust GFP expression is apparent within the perinuclear region of the cell and this expression overlaps with calnexin signal, suggesting a significant portion of β1-GFP/SRβ1-GFP is localised within the ER. In fact, after quantification of co-localisation, significantly more SRβ1-GFP (0.56 (median, IQR: 0.50 – 0.63),, n = 28) than β1-GFP (0.79 (median, IQR: 0.73 – 0.82),, n = 28) was detected within the ER ($P < 0.0001$, Mann-Whitney U test) (Figure 5.9C),suggesting an increased enrichment of SRβ1-GFP within the ER compared to β1-GFP. This could be due to an increased expression level of SRβ1-GFP in MDA-MB-231-SRβ1GFP cells compared to β1-GFP in MDA-MB-231-β1GFP cells and the excess SRβ1-GFP is being retained within the ER, or β1-GFP being cleaved by γ-secretase at the ER membrane and β1ICD-GFP is therefore being lost from the ER membrane and released within the cytoplasm.

To determine if there is a potential difference in expression levels between the two cell lines, total cell area and total cell GFP fluorescence of the 2D images of fixed MDA-MB-231-β1GFP and MDA-MB-231-SRβ1GFP cells used in Figure 5.7 - Figure 5.9 were measured (Figure 5.10A). GFP signal density, a measure of the concentration of GFP within the cell, was also calculated by dividing total fluorescence by cell area. Total GFP fluorescence and GFP signal density, for both cell lines, were normalised to the MDA-MB-231-β1GFP average. MDA-MB-231-β1GFP and MDA-MB-231-SRβ1GFP cells had a comparable area, 584.3 μm^2 (median, IQR: 481.5 – 696.8, n = 80) and 589.9 μm^2 (median, IQR: 467.9 – 728.6, n = 88) respectively ($P = 0.54$, Mann-Whitney U test) (Figure 5.10B).

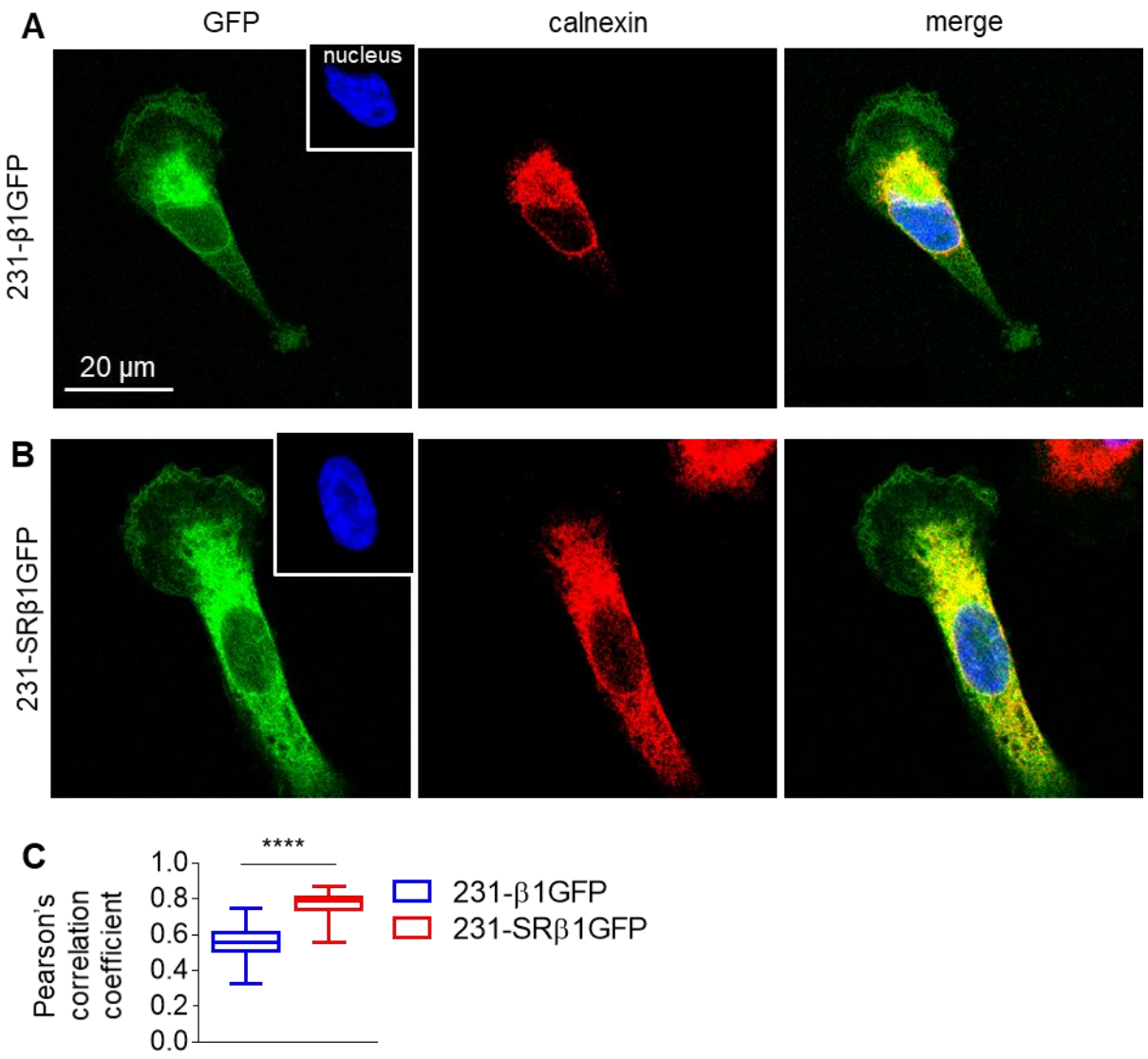

Figure 5.9 The expression of β1-GFP and SRβ1-GFP within the endoplasmic reticulum of MDA-MB-231 cells

(**A**,**B**) Images acquired using confocal microscopy with Airyscan technology of MDA-MB-231-β1GFP (**A**) and MDA-MB-231-SRβ1GFP (**B**) cells labelled for anti-calnexin. Nuclei stained for using DAPI DNA stain. (**C**) Pearson's correlation coefficient between GFP and calnexin inMDA-MB-231-β1GFP cells (n = 28, blue, left bar) and MDA-MB-231-SRβ1GFP cells (n = 28, red, right bar) (N = 3). Data shown as min-max box plots. Mann-Whitney U test used for statistical comparison. **** = P < 0.0001.

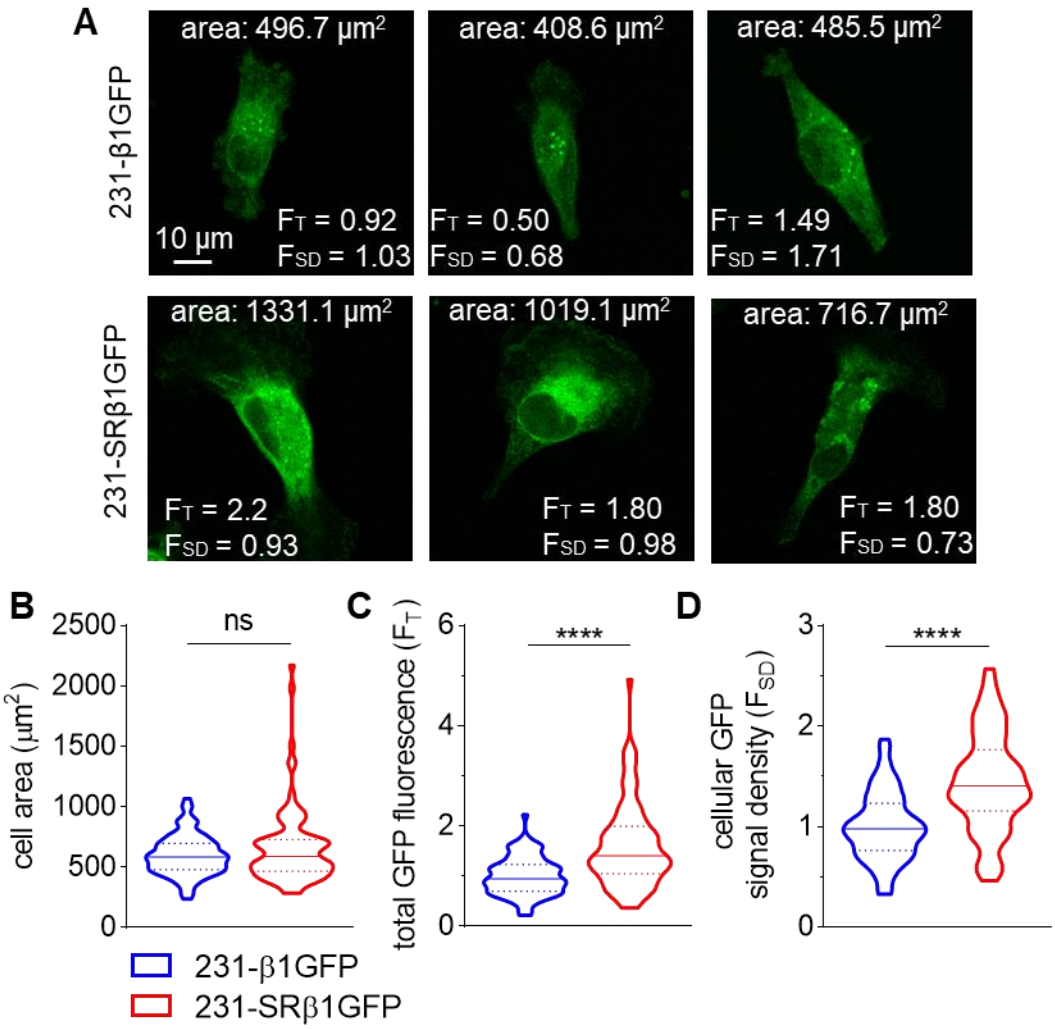

Figure 5.10 Comparison of GFP fluorescence in MDA-MB-231-β1GFP and MDA-MB-231-SRβ1GFP cells

(**A**) Examples of MDA-MB-231-β1GFP and MDA-MB-231-SRβ1GFP cells showing GFP fluorescence. Same 488 nm laser settings (5.0 % laser power, 720 master gain, 2.50 digital gain) used throughout experiment. Cells analysed on ImageJ to obtain cell area, total cellular GFP fluorescence (F_T) and cellular GFP signal density (F_{SD}) parameters. F_T and F_{SD} normalised to mean MDA-MB-231-β1GFP values. (**B**,**C**,**D**) Statistical comparison of cell area (**B**), normalised F_T (**C**) and normalised F_{SD} (**D**) between MDA-MB-231-β1GFP cells (n = 80, blue left plot) and MDA-MB-231-SRβ1GFP cells (n = 88, red right plot) (N = 9). Data displayed as min-max violin plot with median shown as thick horizontal line and quartiles as dotted horizontal lines. Mann-Whitney U test used for comparison. ns = not significant, **** = P < 0.0001.

However, total cell GFP fluorescence was almost 50 % higher in MDA-MB-231-SRβ1GFP (1.45 (median, IQR: 1.10 – 2.10), n = 88) than MDA-MB-231-β1GFP cells (1.00 (median, IQR: 0.74 – 1.29), n = 80, P < 0.0001, Mann-Whitney U test) (Figure 5.10C), suggesting more SRβ1-GFP is expressed than β1-GFP or degradation of β1-GFP is accelerated compared to SRβ1-GFP, in the respective cell lines. Likewise, GFP signal density was higher in MDA-MB-231-SRβ1GFP (1.44 ± 0.05, n = 88) than MDA-MB-231-β1GFP cells (1.00 ± 0.04, n = 80, P < 0.0001, unpaired t test) (Figure 5.10D), further suggesting SRβ1GFP is expressed at a higher level than β1GFP. Higher SRβ1-GFP expression may explain why SRβ1GFP is more enriched in the ER, as more is being produced and is overloading the ER.

Next, FRAP was used to compare the mobility of β1GFP and SRβ1GFP in live cells at the leading edge of cells and in the ER (Figure 5.11A,B). If γ-secretase cleavage is occurring, soluble β1ICD-GFP will be present within the GFP fluorescence of β1GFP-, but not SRβ1GFP-, expressing cells and should therefore decrease the time constant (time taken for half-maximal fluorescence recovery), increase the diffusion coefficient (rate of 2D diffusion due to Brownian motion), and increase the mobile fraction (proportion of mobile GFP elements) due to its rapid, unrestricted diffusion. In Chapter 3, a difference in mobility kinetics was not detected in DAPT-treated MDA-MB-231-β1GFP cells at the leading or trailing edges compared to vehicle-treated cells, suggesting β1ICD-GFP generation is not occurring or is difficult to detect at these locations. To address the potential problem that β1ICD-GFP movement may have been too fast to detect, the image acquisition procedure was optimised to maximise temporal resolution (using the procedure developed in Chapter 4 to detect soluble GFP diffusion) for this experiment, so a difference in mobility at the leading edge may be detected between β1-GFP and SRβ1-GFP.

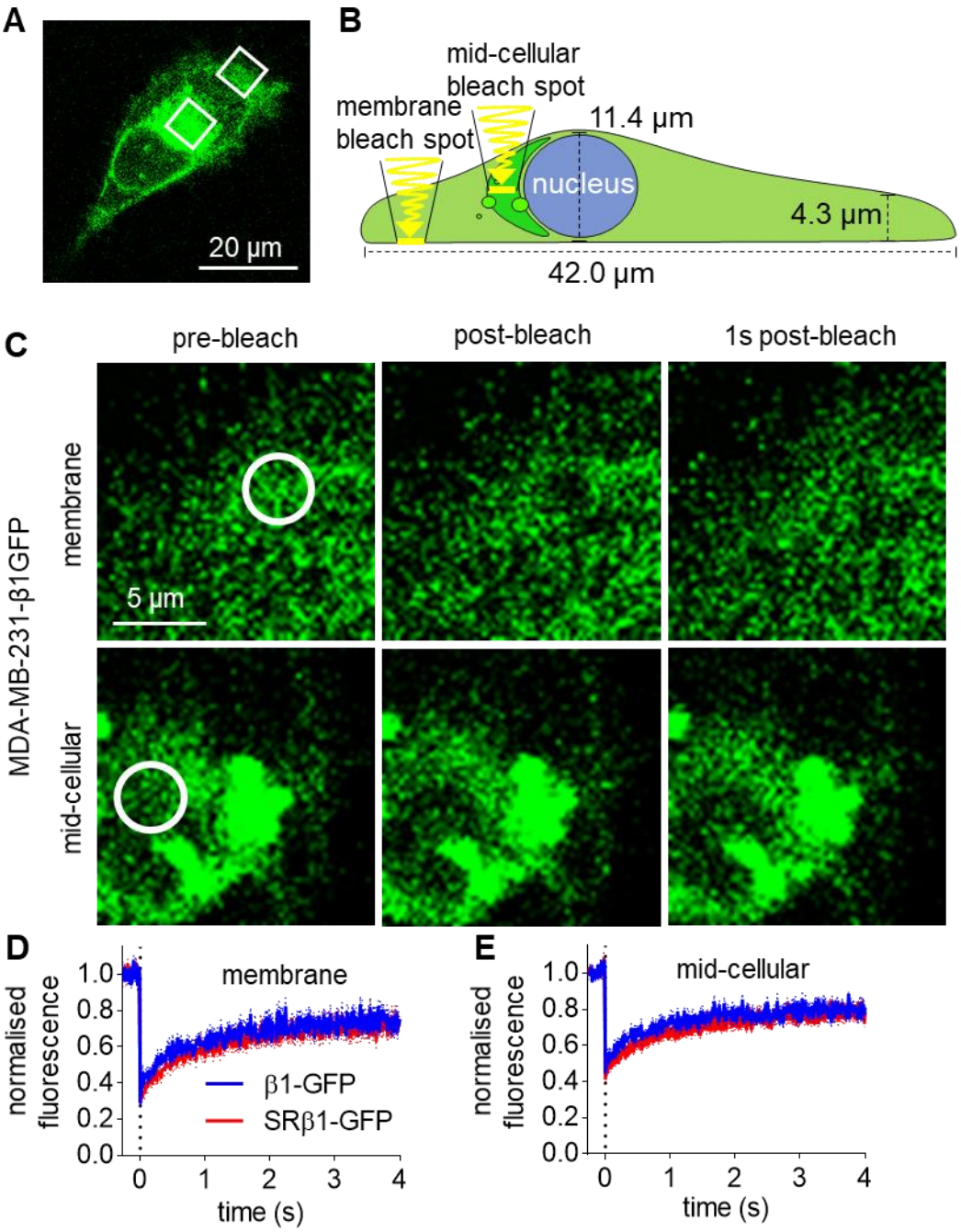

Figure 5.11 Comparison of β1-GFP and SRβ1-GFP mobility in MDA-MB-231 cells

(**A**) typical polarised MDA-MB-231-β1GFP cell imaged using confocal microscopy with Airyscan technology. White boxes marking the leading edge (characterised by lamellipodia) and the perinuclear region, consisting mainly of ER and is a site of robust GFP fluorescence. (**B**) Schematic of a side-view of an MDA-MB-231-β1GFP cell with average cellular dimensions and bleach spots marked. (**C**) Representative photobleaching and recovery of GFP fluorescence at the leading edge (top row) and perinuclear region (bottom row) of a live MDA-MB-231-β1GFP cell following photobleaching with a 488 nm laser (40 iterations, 100 % laser power). (**D**,**E**) Quantification of the recovery of GFP fluorescence in MDA-MB-231-β1GFP cells (blue) and MDA-MB-231-SRβ1GFP cells (red) at the leading edge (**D**) and perinuclear region (**E**). Recordings were taken every 25 ms. Data displayed as mean (solid line) ± SEM (dotted line). n > 25, N = 3. Dotted vertical line at T = 0 denotes photobleaching event.

Accordingly, a 2 μm region was photobleached at the leading edge of MDA-MB-231-β1GFP and MDA-MB-231-SRβ1GFP cells and images acquired every 25 ms for 6 s (Figure 5.11C,D). However, no difference between the time constants of β1-GFP (0.89 s (median, IQR: 0.44 – 1.53), n = 18) and SRβ1-GFP (0.72 s (median, IQR: 0.43 – 1.42), n = 19) was detected (P = 0.45, unpaired t test) (Table 5.1). Similarly, no difference between the diffusion coefficients of β1-GFP (0.12 $\mu m^2 s^{-1}$ (median, IQR: 0.09 – 0.20, n = 17)) and SRβ1-GFP (0.11 $\mu m^2 s^{-1}$ (median, IQR: 0.05 – 0.15, n = 18)) was detected (P = 0.50, Mann-Whitney U test). The mobile fractions of β1-GFP and SRβ1-GFP were also comparable, 0.59 (median, IQR: 0.42 – 0.70, n = 19) and 0.65 (median, IQR: 0.34 – 0.84, n = 17) respectively (P = 0.35, Welch's t test). The parity between β1-GFP and SRβ1-GFP mobility at the leading edge supports the idea that γ-secretase cleavage is not occurring at the leading edge or the proportion of β1ICD-GFP within the GFP fluorescence of MDA-MB-231-β1GFP cells is too miniscule to detect.

To investigate whether γ-secretase is occurring at the ER membrane, the 2 μm region of interest was placed at a mid-cellular plane of the cell within the strongly fluorescent perinuclear region, corresponding to the location of the ER. GFP was bleached within MDA-MB-231-β1GFP and MDA-MB-231-SRβ1GFP cells, and fluorescence recovery measured over 6 s, with image acquisition occurring every 25 ms (Figure 5.11C,E). No difference in the time constants of β1-GFP (1.13 s, IQR: 0.41 – 2.63, n = 19) and SRβ1-GFP (0.85 s, IQR: 0.53 – 1.58, n = 18) was detected (P = 0.46, Mann-Whitney U test) (Table 5.1). The diffusion coefficients were also comparable between β1-GFP (0.12 $\mu m^2 s^{-1}$, IQR: 0.05 – 0.22, n = 18) and SRβ1-GFP (0.12 $\mu m^2 s^{-1}$, IQR: 0.08 – 0.26, n = 19, P = 0.56, Mann-Whitney U test).

Table 5.1 Mobility parameters of β1-GFP and SRβ1-GFP in MDA-MB-231 cells

	Leading edge		Mid-cellular	
	β1-GFP	SRβ1-GFP	β1-GFP	SRβ1-GFP
Mobile fraction	0.59 (0.42-0.70)	0.65 (0.34-0.84)	0.66 (0.30-0.86)	0.59 (0.39-0.94)
	P = 0.35		P = 0.80	
time constant (s)	0.89 (0.44-1.53)	0.72 (0.43-1.42)	1.13 (0.41-2.64)	0.85 (0.53-1.58)
	P = 0.45		P = 0.46	
D_{2D} ($\mu m^2 s^{-1}$)	0.12 (0.09-0.20)	0.11 (0.05-0.15)	0.12 (0.05-0.22)	0.12 (0.08-0.26)
	P = 0.50		P = 0.56	
Comparisons between β1-GFP and SRβ1-GFP for each parameter at each location made using Mann-Whitney U tests or unpaired t test, P-value displayed underneath each comparison. Data displayed as median (IQR). n ≥ 17, N = 3. Abbreviations: D_{2D}: diffusion coefficient.				

Furthermore, the difference between mobile fractions of β1-GFP (0.66 (median, IQR: 0.30 – 0.86), n = 18) and SRβ1-GFP (0.59 (median, IQR: 0.39 – 0.94), n = 19) was insignificant (P = 0.80, unpaired t test). These data suggest γ-secretase cleavage is not occurring in the ER or β1ICD-GFP formation is too low to detect, e.g. if too little β1ICD-GFP is generated to detect or if its formation is spatially restricted to a certain domain of the cell.

5.2.5 Secretase-resistant β1 induces a β1-like Na^+ current

α-subunit modulation is an integral function of β1 and so far, this study has revealed that the β1-induced I_{Na} (increased I_{Na} magnitude and accelerated channel recovery from inactivation) is secretase-independent and β1-ICD is sufficient in inducing a β1-like I_{Na}. These results suggest that the β1-ICD sequence has to be present to modulate I_{Na}, regardless of whether it is freely mobile or still attached to membrane-bound β1. Therefore, SRβ1-GFP should be able to induce a β1-like I_{Na} when expressed in MDA-MB-231 cells. To test this, whole cell patch clamp recording was carried out on MDA-MB-231-GFP, MDA-MB-231-β1GFP and MDA-MB-231-SRβ1GFP cells to determine the peak current density and activation/inactivation kinetics of each cell line. Initially, cells were stimulated, from a holding potential of -120 mV, at progressive increments of 5 mV starting from -80 mV (Figure 5.12A) to determine the I_{Na}-voltage relationship (Figure 5.12B) and activation kinetics (Figure 5.12C). No difference was detected between MDA-MB-231-GFP, MDA-MB-231-β1GFP and MDA-MB-231-SRβ1GFP cells for the voltage threshold of channel activation (-47.7 ± 2.8 mV, -53.7 ± 1.9 mV and -54.3 ± 1.8 mV respectively (n = 15, one-way ANOVA)), voltage threshold for half-maximal channel activation (-24.2 ± 0.7 mV, -27.6 ± 1.7 mV and -24.1 ± 1.5 mV respectively (n = 15, one-

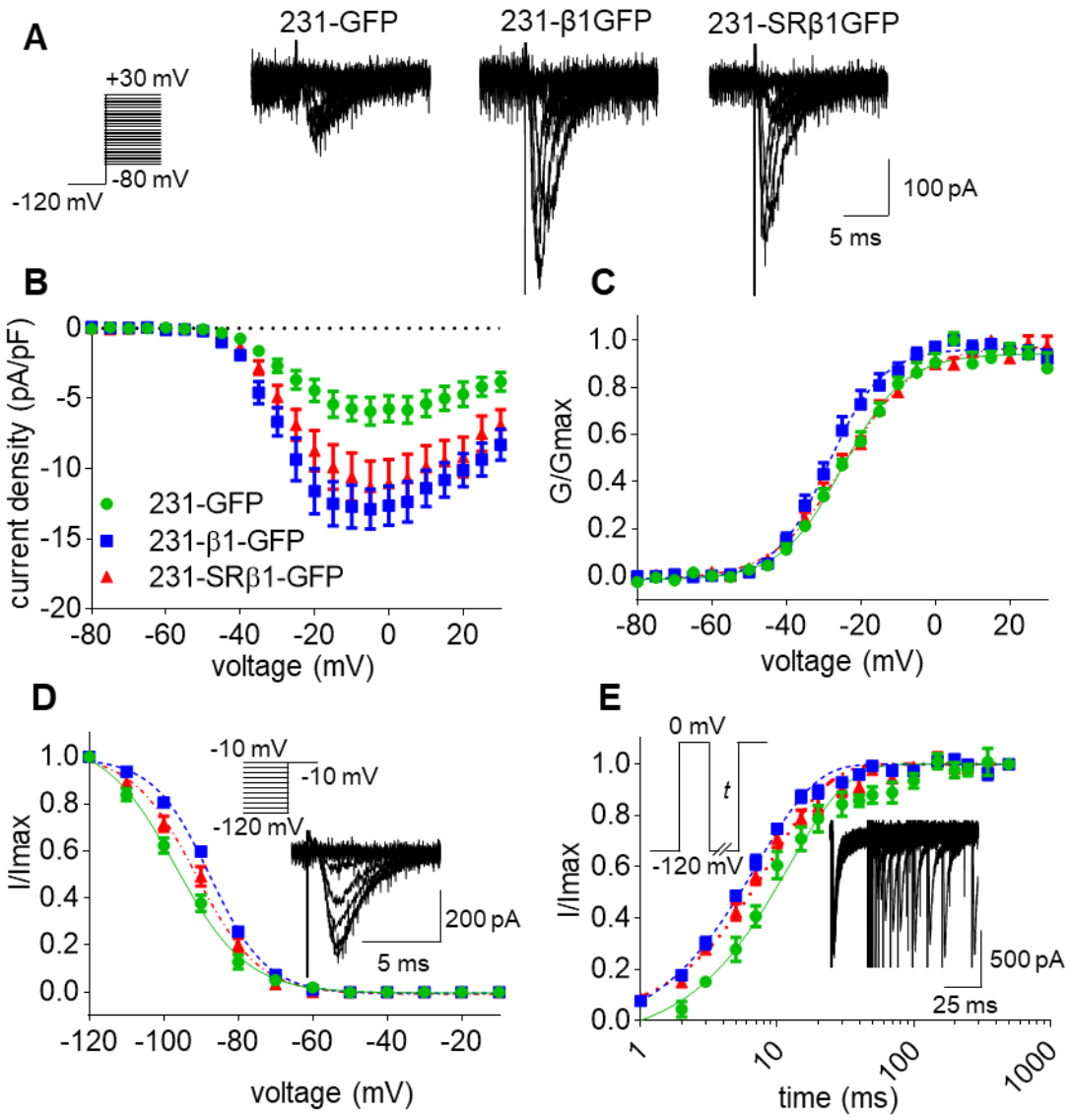

Figure 5.12 Electrophysiological properties of SRβ1-GFP expression in MDA-MB-231 cells determined using whole cell patch clamp electrophysiology

(**A**) Representative whole-cell Na^+ currents generated in MDA-MB-231-GFP, MDA-MB-231-β1GFP and MDA-MB-231-SRβ1GFP cells, following stimulation between -80 mV and +30 mV, for 250 ms, from -120 mV. Every third sweep shown. (**B**) Current (I)-voltage (V) relationship between -80 mV and +30 mV. (**C**) Conductance (G)-voltage (V) relationship, from which activation $V_{1/2}$ was derived, between -80 mV and +30 mV. Fitted Boltzmann curves overlain. (**D**) Steady-state inactivation. Cells were stimulated at -10 mV following a 250 ms holding voltage of between -120 mV and -10 mV. Normalised current produced following -10 mV stimulation plotted. Fitted Boltzmann curves overlain. (**E**) Recovery from inactivation. Cells were stimulated at 0 mV, then held at -120 mV for t s before re-stimulation at 0 mV. t ranged from 1-500 ms. Fitted monoexponential curves overlain. **B**-**E** Data plotted as Mean ± SEM. **B**-**D** MDA-MB-231-GFP cells (n =15, green circles, green solid lines) MDA-MB-231-β1GFP cells (n = 15, blue squares, blue dashed lines) and MDA-MB-231-β1ICDGFP (n = 15, red triangles, red dashed lines) (N = 3). **E** n = 8, N = 3.

way ANOVA)) or the voltage at peak current (-3.33 ± 1.9 mV, -8.67 ± 2.2 mV and -5.33 ± 2.4 mV respectively (n = 15, one-way ANOVA); Table 5.2). Similarly, no difference was detected for the time taken to I_{Na} peak between MDA-MB-231-GFP (1.1 s (median, IQR: 0.9 – 1.53)), MDA-MB-231-β1GFP (1.0 s (median, IQR: 0.8 – 1.1)) and MDA-MB-231-SRβ1GFP cells (1.1s (median, IQR: 0.8 – 1.3); n = 15, Kruskal-Wallis test). However, both β1-GFP (-13.9 ± 1.6 pA/pF, n = 15, P < 0.001, one-way ANOVA) and SRβ1-GFP (-11.6 ± 1.8 pA/pF, n = 15, P < 0.05, one-way ANOVA) induced an enlarged I_{Na} compared to GFP alone (-5.6 ± 0.7 pA/pF, n = 15). The voltage-dependence of inactivation (Figure 5.12D) and the recovery from inactivation (Figure 5.12E) were next examined. A depolarised shift in the voltage-dependence of inactivation was observed in MDA-MB-231-β1GFP (-87.4 ± 0.7 mV, n = 15, P < 0.001, one-way ANOVA) and MDA-MB-231-SRβ1GFP (-90.9 ± 1.6 mV, n = 13, P < 0.05, one-way ANOVA) cells relative to MDA-MB-231-GFP (-96.8 ± 2.1 mV, n = 13) (Table 5.2). Expression of β1-GFP (5.50 ± 0.2 s, n =8, P < 0.001, one-way ANOVA) and SRβ1-GFP (6.07 ± 0.3 s, n =8, P < 0.001, one-way ANOVA) accelerated the time taken for half-maximal recovery from inactivation compared to GFP alone (12.2 ± 1.7 s, n = 8). These data show that SRβ1 induces a β1-like I_{Na}, namely an increased peak I_{Na} density and accelerated recovery from inactivation, supporting the hypothesis that the β1-ICD sequence is integral in inducing the β1-like I_{Na}, independent of secretase cleavage.

Tetrodotoxin (TTX) is a VGSC blocker that inhibits certain α-subunits ($Na_v1.1$, $Na_v1.2$, $Na_v1.3$, $Na_v1.4$, $Na_v1.6$, $Na_v1.7$) at a lower concentration than other α-subunits ($Na_v1.5$, $Na_v1.8$, $Na_v1.9$). In Chapter 4, both β1-GFP and β1ICD-GFP expressing MDA-MB-231 cells expressed a I_{Na} that was reduced by 30 – 40 % following 1 μM TTX treatment, whereas no reduction in I_{Na} was detectable in MDA-MB-231-GFP cells. To test whether SRβ1 induces a similar TTX-sensitive I_{Na}, 1 μM TTX was perfused onto MDA-MB-231-GFP, MDA-MB-231-β1GFP and MDA-MB-231-SRβ1GFP cells (Figure 5.13A) and the

Table 5.2 Na^+ current parameter analysis of SRβ1-GFP overexpression in MDA-MB-231 cells

Parameter	231-GFP	231-β1GFP	231-SRβ1GFP
C_m (pF)	25.11 ± 2.00	29.23 ± 2.95	27.71 ± 2.84
PCD (pA/pF)	-5.64 ± 0.73	***-13.91 ± 1.64	*-11.56 ± 1.8
V_a (mV)	-47.67 ± 2.8	-53.67 ± 1.98	-54.33 ± 1.75
V_p (mV)	-3.33 ± 1.93	-8.87 ± 2.26	-5.33 ± 2.36
Activation $V_{1/2}$ (mV)	-24.19 ± 0.07	-27.08 ± 1.72	-24.05 ± 1.54
Activation *k* (mV)	10.42 ± 1.52	8.30 ± 0.78	9.43 ± 0.92
Inactivation $V_{1/2}$ (mV)	-96.8 ± 2.1	***-87.37 ± 0.72	*-90.87 ± 1.58
Inactivation *k* (mV)	-9.88 ± 0.74	-8.01 ± 0.42	-9.19 ± 0.54
T_p (ms)	1.19 ± 0.1	1.08 ± 0.09	1.11 ± 0.09
RFI $T_{1/2}$ (ms) (n = 8)	12.21 ± 1.70	***5.50 ± 0.22	***6.07 ± 0.32
Data displayed as mean ± SEM (n = 12 – 15 unless stated, N = 3). Significance tested using one-way ANOVA or Kruskal-Wallis test. * = P < 0.05, ** = P < 0.01, *** = P < 0.001 relative to MDA-MB-231-GFP cells. Abbreviations: C_m: membrane capacitance, PCD: peak current density, V_a: activation voltage, V_p: voltage at peak current, $V_{1/2}$: voltage for half maximal activation/inactivation, T_p: time to peak, RFI $T_{1/2}$: time for half-maximal recovery from inactivation.			

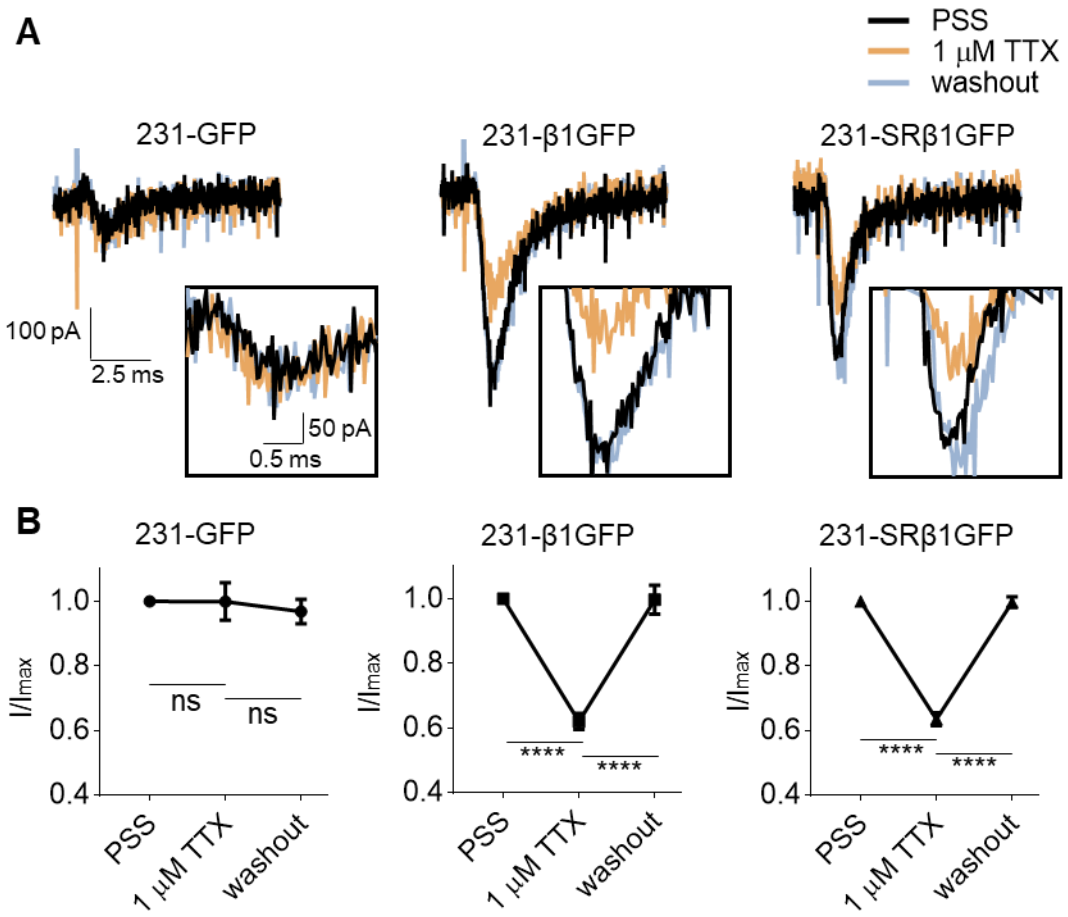

Figure 5.13 Reduction in Na^+ current magnitude induced by tetrodotoxin in MDA-MB-231-SRβ1GFP cells

(**A**) Representative traces of the I_{Na} in MDA-MB-231 cells expressing GFP, β1-GFP or SRβ1-GFP in standard recording solution (PSS, black line), following 1 μM TTX perfusion (orange line) and following PSS washout (grey line), determined using whole-cell patch clamp electrophysiology. (**B**) Quantification of the reduction in peak current density following 1 μM TTX perfusion and recovery following PSS washout in MDA-MB-231 cells expressing GFP, β1-GFP or SRβ1-GFP. I_{Na} normalised to initial recording in PSS bath solution. Data displayed as mean ± SEM. n = 6, N = 3. Significance determined using repeat-measure one-way ANOVA. ns = not significant. **** = P < 0.0001.

reduction, and subsequent recovery following washout, in I_{Na} magnitude was measured and normalised to the initial I_{Na} measurement (Figure 5.14B). Consistent with previous results, 1 µM TTX application did not significantly reduce the I_{Na} in MDA-MB-231-GFP cells (n = 6, one-way ANOVA). Furthermore, in MDA-MB-231-β1GFP cells, 1 µM TTX application reduced I_{Na} to 0.62 ± 0.02, which was significantly smaller than the starting I_{Na} (1.00, n = 6, P < 0.0001, RM one-way ANOVA) and I_{Na} following washout (1.00 ± 0.04, n = 6, P < 0.0001, RM one-way ANOVA). In MDA-MB-231-SRβ1GFP cells, 1 µM TTX application reduced I_{Na} to 0.63 ± 0.02, which was also significantly smaller than the starting I_{Na} (1.00, n = 6, P < 0.0001, RM one-way ANOVA) and I_{Na} following washout (1.00 ± 0.01, n = 6, P < 0.0001, RM one-way ANOVA). Therefore, SRβ1 induces a I_{Na} similar to β1 and increases the proportion of TTX-sensitive α-subunits at the plasma membrane.

Lastly, to attempt to distinguish between the I_{Na} generated in MDA-MB-231-β1GFP and MDA-MB-231-SRβ1GFP cells, brefeldin A (BFA) was used. BFA inhibits ER-to-Golgi transport, thereby preventing progression of VGSCs from the ER to the plasma membrane (Figure 5.14A). Therefore, a reduction in I_{Na} magnitude is observed following BFA treatment as VGSCs are cleared from the membrane (Rougier *et al.*, 2005). If β1-GFP undergoes secretase-mediated proteolysis at the plasma membrane, it may lose its association with α-subunits, whereas SRβ1 would not, resulting in a decrease in I_{Na} magnitude. BFA was applied (50 ng/ml) to MDA-MB-231-β1GFP (Figure 5.14B) and MDA-MB-231-SRβ1GFP cells (Figure 5.14C) and I_{Na} recorded at 0 h, 6 h, 12 h and 24 h. However, no differences between I_{Na} between cell lines, at any time point, were detected (n ≥ 8, two-way ANOVA) (Figure 5.14D; Table 5.3) In summary, these data suggest there is no difference in the turnover of VGSCs induced by β1-GFP or SRβ1GFP.

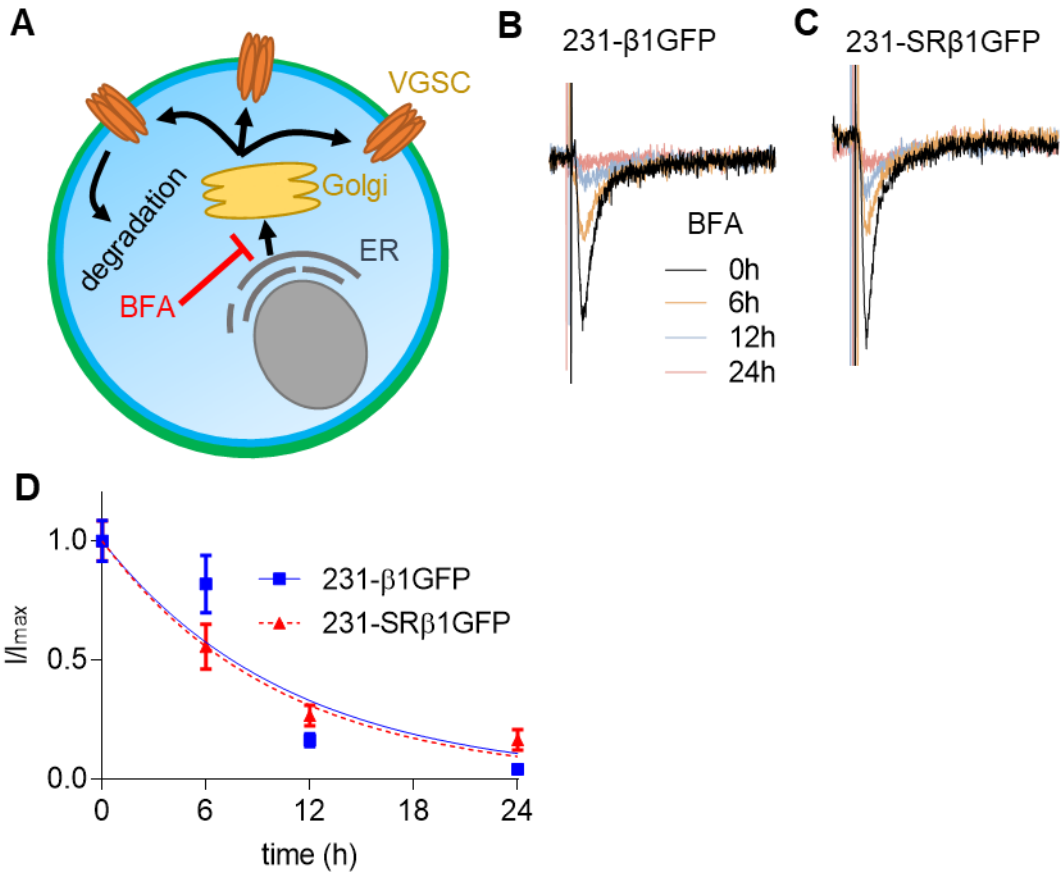

Figure 5.14 Na^+ current decay induced by brefeldin A in MDA-MB-231 cells expressing β1-GFP or SRβ1-GFP

(**A**) Mechanism of action of brefeldin A (BFA). BFA inhibits ER to Golgi transport, preventing VGSC exocytosis. VGSCs at the plasma membrane are still endocytosed and degraded. (**B**,**C**) Representative traces of the I_{Na} in MDA-MB-231 cells expressing β1-GFP (**B**) or SRβ1-GFP (**C**) after 0 h (black line), 6 h (orange line), 12 h (grey line) and 24 h (brown line) BFA treatment. BFA was maintained in the recording solution. (**D**) Quantification of I_{Na} decay induced by BFA. Data displayed as mean ± SEM. n ≥ 8, N = 3. Two-way ANOVA used to test for statistical significance at each time point, although no significance calculated.

Table 5.3 Time course of the reduction in Na^+ current magnitude in MDA-MB-231-β1GFP and MDA-MB-231-SRβ1GFP cells induced by brefeldin A

Time (BFA treatment)	231-β1GFP	231-SRβ1GFP
0 h	1.00 ± 0.09 (n = 12)	1.00 ± 0.09 (n = 12)
6 h	0.82 ± 0.12 (n = 11)	0.56 ± 0.09 (n = 14)
12 h	0.17 ± 0.03 (n = 12)	0.27 ± 0.04 (n = 10)
24 h	0.04 ± 0.02 (n = 8)	0.17 ± 0.04 (n = 10)
Data displayed as mean ± SEM. N = 3. I_{Na} normalised to mean T = 0 value for each cell line. Significance tested using two-way ANOVA, but no significance detected at any time point.		

5.2.6 Deletion of β1-ICD prevents β1 from induced an enlarged Na^+ current

This study has so far indicated that the β1-ICD sequence is responsible for inducing an enlarged I_{Na} in a secretase-independent manner. To prove this, a β1 construct lacking the β1-ICD sequence (β1STOP) was generated and expressed in MDA-MB-231 cells (Figure 5.15A). β1STOP has been used previously to demonstrate there is an α-subunit interaction site within the β1-ICD sequence (Meadows *et al.*, 2001). β1STOP was designed as previously described, by truncating β1 after Lys165 (McCormick *et al.*, 1998).

Here, I hypothesise that β1STOP does not increase I_{Na} magnitude or accelerate channel recovery from inactivation, both characteristic changes elicited by β1 and β1-ICD. Other activation and inactivation parameters were also measured. Using whole cell patch clamp recording, MDA-MB-231-GFP, MDA-MB-231-β1GFP and MDA-MB-231-β1STOP-GFP cells were examined for their current-voltage relationship (Figure 5.15B,C), activation-voltage relationship (Figure 5.15D), inactivation-voltage relationship (Figure 5.15E) and recovery from inactivation kinetics (Figure 5.15F). As per previous experiments, no differences were expected in the activation and steady-state inactivation kinetics. Parameter analysis is summarised in (Table 5.4). However, hyperpolarised shifts in the voltage threshold for channel activation ($n \geq 8$, $P < 0.05$, one-way ANOVA), voltage threshold for half-maximal channel activation ($n \geq 8$, $P < 0.01$, one-way ANOVA) and voltage at peak I_{Na} current ($n \geq 8$, $P < 0.01$, one-way ANOVA) were observed in MDA-MB-231-β1GFP cells compared to MDA-MB-231-GFP cells. A similar hyperpolarised shift was seen in the voltage at I_{Na} peak in MDA-MB-231-β1STOP-GFP cells compared to MDA-MB-231-GFP cells ($n \geq 9$, $P < 0.01$, one-way ANOVA). However, no change in the voltage thresholds for half-maximal inactivation was detected across conditions ($n = 6$, one-way ANOVA). Changes in the activation kinetics have not been

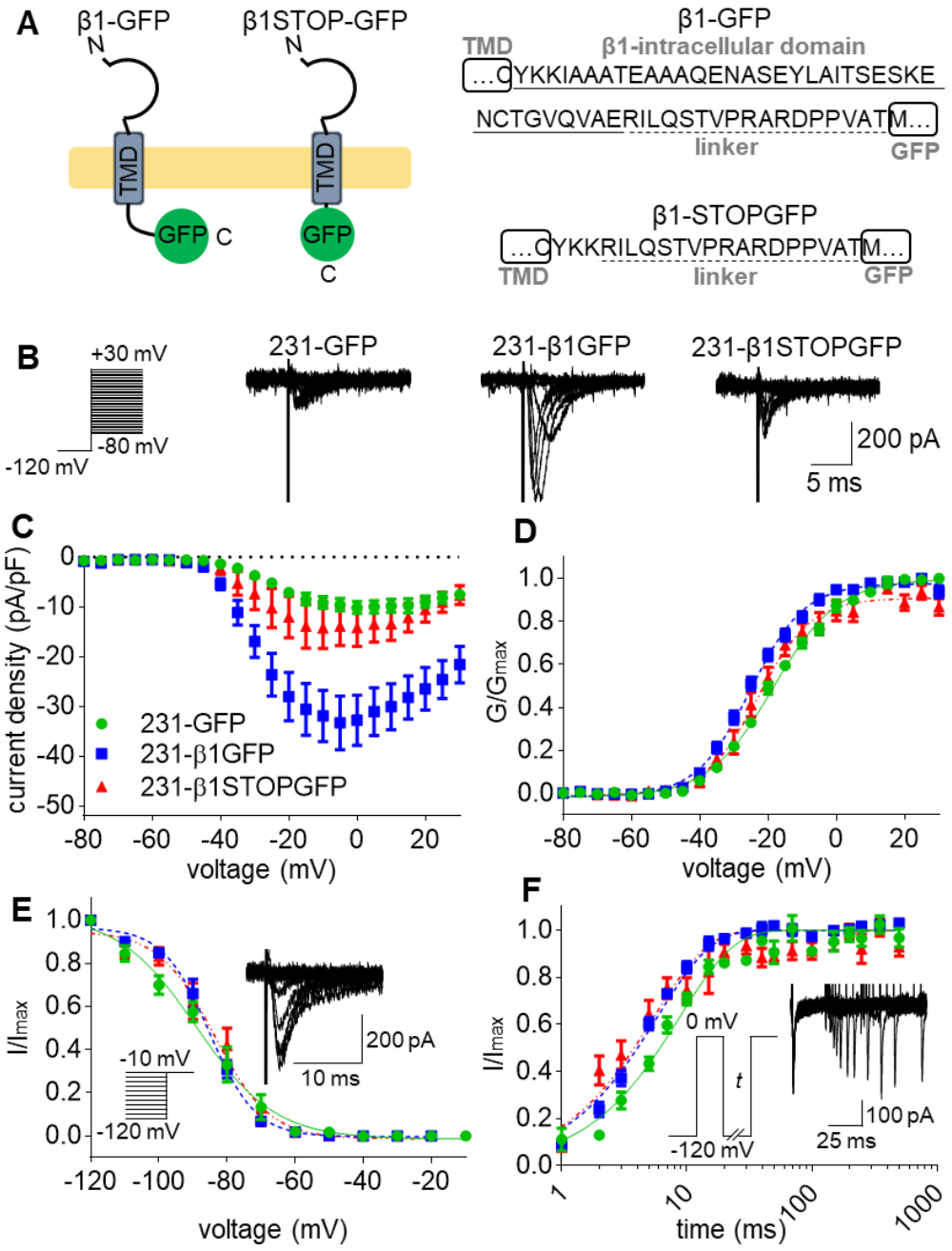

Figure 5.15 Electrophysiological properties of β1STOP-GFP expression in MDA-MB-231 cells determined using whole cell patch clamp electrophysiology

(**A**) β1STOP was generated following deletion of the β1-ICD sequence as detailed in (McCormick *et al.*, 1998) (**B**) Representative whole-cell Na^+ currents generated following stimulation between -80 mV and +30 mV, for 250 ms, from -120 mV. Every third sweep shown. (**C**) Current (I)-voltage (V) relationship between -80 mV and +30 mV. (**D**) Conductance (G)-voltage (V) relationship, between -80 mV and +30 mV. Fitted Boltzmann curves overlain. (**E**) Steady-state inactivation- reduction in I_{Na} as holding voltage increased from -120 mV to – 10 mV. Fitted Boltzmann curves overlain. (**F**) Recovery from inactivation. Cells were stimulated at 0 mV, then held at -120 mV for t s before re-stimulation at 0 mV. t ranged from 1-500 ms. Fitted monoexponential curves overlain. C-F Data plotted as Mean ± SEM. MDA-MB-231-GFP cells (n =12, green circles, green solid lines) MDA-MB-231-β1GFP cells (n = 8, blue squares, blue dashed lines) and MDA-MB-231-β1STOPGFP (n = 9, red triangles, red dashed lines) (N = 3).

Table 5.4 Na^+ current parameter analysis of β1STOP-GFP overexpression in MDA-MB-231 cells

Parameter	231-GFP	231-β1GFP	231-β1STOPGFP
C_m (pF)	22.44 ± 1.44	20.54 ± 1.27	*17.04 ± 0.98
PCD (pA/pF) (n = 15)	-9.89 ± 1.25	***-28.56 ± 3.61	^-15.27 ± 2.92
V_a (mV)	-37.08 ± 1.44	*-43.75 ± 1.57	^-36.11 ± 2.49
V_p (mV)	4.58 ± 2.17	**-6.88 ± 2.10	**-5.55 ± 2.11
Activation $V_{1/2}$ (mV)	-18.06 ± 1.11	**-25.18 ± 0.94	-21.86 ± 1.89
Activation *k* (mV)	9.54 ± 0.65	7.72 ± 0.23	**6.73 ± 0.50
Inactivation $V_{1/2}$ (mV)	-88.51 ± 3.18	-85.62 ± 1.35	-83.81 ± 2.73
Inactivation *k* (mV)	-9.61 ± 1.52	-6.44 ± 0.57	-6.56 ± 0.73
T_p (ms)	1.00 ± 0.08	0.93 ± 0.11	0.94 ± 0.10
RFI $T_{1/2}$ (ms)	6.25 ± 0.42	**4.10 ± 0.29	*4.16 ± 0.70
Data displayed as mean ± SEM (n ≥ 5 unless stated, N = 3). Significance tested using one-way ANOVA or Mann-Whitney U test. * = P < 0.05, ** = P < 0.01, *** = P < 0.001 relative to MDA-MB-231-GFP cells. ^ = P < 0.05 relative to MDA-MB-231-β1GFP cells. Abbreviations: C_m: membrane capacitance, PCD: peak current density, V_a: activation voltage, V_p: voltage at peak current, $V_{1/2}$: voltage for half maximal activation/inactivation, T_p: time to peak, RFI $T_{1/2}$: time for half-maximal recovery from inactivation.			

observed in previous chapters and could reflect the smaller sample sizes or anomalous behaviour of MDA-MB-231-GFP cells in this experiment. Regardless, consistent with the original hypothesis, β1-GFP expression (-27.2 pA/pF (median, IQR: -36.5 to -14.6), n = 15) induced an enlarged I_{Na} compared to GFP (-8.6 pA/pF (median, IQR: -13.7 – -7.3, n = 15, P < 0.001, Kruskal-Wallis test)), whereas β1STOP-GFP did not induce an enlarged I_{Na} compared to GFP (-10.3 pA/pF (median, IQR: -20.3 – -6.7), n = 15, P = 0.89, Krusal-Wallis test). However, contrary to the hypothesis, both β1-GFP (4.1 ± 0.3 s, n = 6, P < 0.01, one-way ANOVA) and β1STOP-GFP (4.2 ± 0.7 s, n = 5, P < 0.05, one-way ANOVA) accelerated half-maximal recovery from inactivation relative to GFP-expressing cells (6.3 ± 0.4 s, n = 8). Whereas the inability of β1STOP to induce an enlarged I_{Na} fits the model that β1ICD is required for α-β association in MDA-MB-231 cells, the ability of β1STOP to accelerate recovery from inactivation does not. Perhaps gating of α-subunits are facilitated by the β1 N-terminus as well as ICD, whereas the increase in I_{Na} magnitude is dependent on the β1ICD sequence.

5.3 Discussion

This chapter utilised a novel secretase-resistant β1 construct to assess the impact of secretase cleavage on β1 function in MDA-MB-231 cells. SRβ1 recapitulated β1-induced cell adhesion and morphology characteristics, suggesting it was functional at the plasma membrane. Typically, the increase in the rate of cell adhesion induced by β1 is greater than that seen when SRβ1 was expressed, however this may be due to differences in the transfection efficiency or expression levels between different cell lines. SRβ1-GFP and β1-GFP showed similar subcellular distribution within endosomes, lysosomes, ER and Golgi apparatus and similar lateral mobility at the leading edge and ER. However, SRβ1-GFP expression was more enriched within the ER compared to β1-GFP and β1-

GFP expression more enriched within the *trans*-Golgi compared to SRβ1-GFP. Consistent with the hypothesis developed from the first two results chapters that the β1-ICD sequence is required to induce a β1-like I_{Na}, SRβ1 induced a β1-like I_{Na}, whereas β1STOP failed to enhance I_{Na}, although β1STOP did accelerate channel recovery from inactivation.

SRβ1 was generated following deletion of six amino acids (142Ile – 147Val) that flank the β-secretase site. Imparting secretase-resistance in a protein through introduction of a novel mutation has yet to be documented in the literature. However, there are many characterised familial Alzheimer's disease mutations of APP that interfere with secretase cleavage. For instance, a range of mutations within the transmembrane domain of APP impair γ-secretase cleavage through prevention of substrate recognition (Xu *et al.*, 2016). Introduction of a large amino acid in place of a smaller one (e.g. G1753Y) is a common mutation within the transmembrane domain of APP that reduces γ-secretase cleavage (Xu *et al.*, 2016). An APP mutation near the β-secretase cleavage site (A673T), known as the "Icelandic mutation," reduces APP-CTF formation and is protective against Alzheimer's disease and cognitive decline (Jonsson *et al.*, 2012). These APP mutations that impair secretase processing are typically point mutations, so there were concerns that deletion of six amino acids within β1 would have more widespread effects on β1 function, such as impaired folding, glycosylation and trafficking. However, SRβ1 had a similar molecular weight to β1, suggesting glycosylation of SRβ1 was retained. Furthermore, SRβ1 was capable of inducing β1-like cell adhesion, cell elongation and α-subunit modulation, suggesting SRβ1 was being trafficked to the plasma membrane and was functionally active. It was notable that the six amino acid deletion within β1 prevented all extracellular secretase cleavage. Either α-secretase does not cleave β1 in MDA-MB-231 cells or α-secretase cleavage was also inhibited. β2 was the only β-subunit verified as an α-secretase substrate, raising the possibility that β1 is not a substrate (Kim

et al., 2005). The site of α-secretase cleavage of β2 was undetermined, so it is difficult to compare the homology of the cleavage site between β1 and β2. The enzyme responsible for α-secretase cleavage of β2, ADAM10, is indeed endogenously expressed in MDA-MB-231 cells (Mullooly *et al.*, 2015). Furthermore, western blot analysis of MDA-MB-231-β1GFP cells has only demonstrated a single band for β1-CTF, supporting the idea that α-secretase cleavage is absent or occurs very near to β-secretase cleavage. To verify α-secretase cleavage of β1 is not occurring, an α-secretase inhibitor could be used to see if β1CTF-GFP expression is reduced or ADAM10 could be overexpressed, or α-secretase activity could be stimulated using phorbol 12-myristate 13-acetate, to see if β1CTF-GFP expression is increased. Regardless, SRβ1 appears to be a functionally active protein and a useful tool in determining a role of secretase processing in regulating β1 function.

β1-GFP and SRβ1-GFP showed a similar subcellular distribution, except β1-GFP expression in the ER was lower compared to SRβ1-GFP. SRβ1-GFP was also shown to be more highly expressed than β1-GFP within their respective cell lines, although other techniques, such as flow cytometry, are best used to quantify cell fluorescence than imaging as they are more sensitive and can measure millions of cells within a sample. The higher total expression could explain the enhanced enrichment of SRβ1-GFP within the ER, if too much is being synthesised and is therefore congesting the ER. Conversely, the ER is a known site of secretase processing (Chyung *et al.*, 1997; Area-Gomez *et al.*, 2009), so β1 may be processed and β1ICD-GFP released from the ER and into the cytoplasm. However, β1ICD-GFP was not detected within the perinuclear region using FRAP, although β1ICD-GFP has not been detected in any region of the cell using this FRAP approach during this study, potentially because too little β1ICD-GFP is produced to be detected or β1ICD-GFP is retained at the membrane and not freely mobile, suggesting a limitation to this FRAP approach.

As β1-GFP correlated with EEA1 expression more robustly than SRβ1-GFP, it could suggest β1-GFP is retained within the recycling endosomal system more so than SRβ1-GFP. However, if a higher proportion of β1 is in *post*-Golgi compartments, β1-GFP would have sustained the I_{Na} for longer than SRβ1-GFP following BFA treatment, as BFA does not affect recycling of *post*-Golgi vesicles to/from the plasma membrane (Caporaso *et al.*, 1994). Conversely, if β1-GFP enrichment in endosomes is due to a decreased half-life at the plasma membrane compared to SRβ1-GFP, an accelerated I_{Na} decay following BFA treatment would be expected. The rationale for using BFA was that presence of full-length β1 at the plasma membrane would be the limiting step for VGSC clearance. However, as no difference was observed between β1-GFP and SRβ1-GFP, secretase cleavage does not appear to dictate VGSC clearance. Nonetheless, before any hypotheses are made, it would be important to know if treating MDA-MB-231-β1GFP cells with a β-secretase inhibitor causes a SRβ1-like shift towards ER enrichment and decreased endosomal expression. Furthermore, it would be informative to know if β1-GFP is being cleaved by β-secretase within the ER or at the plasma membrane, as our C-terminal GFP tagged constructs do not report on cleavage of the Ig domain. The subcellular distribution of APP cleavage has been investigated previously through subcellular fractionation or dual-labelling the N- and C-terminus with different fluorophores, to see where they dissociate (Area-Gomez *et al.*, 2009; Parenti *et al.*, 2017).

SRβ1 was capable of inducing a β1-like I_{Na}, supporting the hypothesis that secretase cleavage does not affect β1-mediated α-subunit modulation. The β1-ICD sequence was predicted to be responsible for inducing a β1-like I_{Na} (increased I_{Na} magnitude and accelerated recovery from inactivation), so a β1 construct lacking the β1-ICD sequence, β1STOP, was generated to test that hypothesis. β1STOP has been used previously to demonstrate that β1ICD is required for ankyrin recruitment at cell-cell contacts and required for α-subunit interaction and modulation (McCormick *et al.*, 1998; Malhotra *et*

al., 2000; Meadows *et al.*, 2001). When expressed in MDA-MB-231 cells, β1STOP did not enlarge I_{Na} magnitude, however β1STOP did accelerate the time taken for half-maximal recovery from inactivation. Unexpected hyperpolarised shifts in the voltage threshold of activation were observed in β1-GFP and β1STOP-GFP expressing cells relative to GFP-expressing cells as well. β1-induced hyperpolarisation of activation was not observed elsewhere in this study, so it is unclear whether it is a genuine gating effect or perhaps MDA-MB-231-GFP displayed an anomalous depolarised shift in activation for this experiment. Heterologous studies in *Xenopus* oocytes have demonstrated that β1STOP can modulate $Na_v1.2$ when expressed at high enough concentrations (Meadows *et al.*, 2001), suggesting β1STOP-induced acceleration of channel recovery from inactivation may be an artefact of overexpression. Conversely, the N-terminus of β1STOP may retain the ability to modulate α-subunits already at the plasma membrane, as β1-ECD is known to modulate $Na_v1.2$ (McCormick *et al.*, 1998; McCormick *et al.*, 1999). In summary, these results support the hypothesis that β1-ICD is required to enhance the magnitude of I_{Na}. Quantification of plasma membrane VGSC expression would be very informative in determining if the increase in β1-induced I_{Na} magnitude is due to increased VGSC trafficking to the plasma membrane. Biotinylation of cell surface proteins, antibody labelling of α-subunits, or use of fluorescently conjugated toxins could be used to detect membrane α-subunit expression. However, low VGSC abundance at the plasma membrane of MDA-MB-231 cells may be an issue. Overexpression of α-subunits or using a different cell line may be required.

5.4 Conclusion

The hypothesis of this chapter was that extracellular secretase cleavage regulates β1 function and localisation. To address this, a novel secretase-resistant β1 construct was designed that is resistant to extracellular secretase cleavage through deletion of six

amino acids that flank the β-secretase cleavage site. However, SRβ1 mostly resembled β1 in terms of subcellular distribution and function (cell adhesion, cell elongation, α-subunit modulation). These results implicate SRβ1 as a very promising tool in dissecting the impact of secretase cleavage on β1 function in the future, as the six amino acid deletion used to create SRβ1 appears to have had minimal effect on β1 glycosylation, folding and localisation.

The ability of SRβ1 to induce a β1-like I_{Na} led to the hypothesis that β1-ICD is integral in α-subunit regulation. A β1 construct lacking the β1-ICD sequence did not induce an enlarged I_{Na}, suggesting β1-ICD is required for the enlarged I_{Na} seen in MDA-MB-231 cells, potentially through promoting plasma membrane trafficking of TTX-sensitive VGSCs.

Chapter 6: Discussion

Despite β1 being identified as a secretase substrate in 2005, little is known about the functional impact following secretase cleavage (Wong *et al.*, 2005). The only insight being γ-secretase inhibition prevents β1-mediated neurite outgrowth in primary cerebellar granule neurons (Brackenbury & Isom, 2011). In recent years, a role for VGSCs in cancer has emerged (Patel & Brackenbury, 2015). Using MDA-MB-231 cells in a xenograft model of breast cancer, treatment with phenytoin and knockdown of $Na_v1.5$ both reduce metastasis, whereas overexpression of β1 increases metastasis and reduces survival (Nelson *et al.*, 2014; Nelson *et al.*, 2015a; Nelson *et al.*, 2015b). The mechanism of how β1 is contributing to breast cancer metastasis is still unclear. However, if secretase cleavage regulated β1-mediated breast cancer metastasis, this would advance our understanding of VGSCs and secretases in cancer, as well as provide a potential therapeutic target for cancers overexpressing β1. This led to the hypothesis of this study: secretase cleavage regulates β1 function in breast cancer cells. This study aimed to dissect the contribution of secretase cleavage to β1 function by using γ-secretase inhibitors on β1-expressing MDA-MB-231 cells as well as developing various β1 constructs for expression in MDA-MB-231 cells, specifically β1-ICD and SRβ1. By applying these three approaches in various functional and imaging assays, this work has provided insight into the contribution of secretase cleavage in regulating β1 function in breast cancer cells.

6.1 Subcellular distribution of β1

Current knowledge of the subcellular localisation of β1 suggests β1 and β3, but not β2 and β4, associate with α-subunits within the ER and Golgi, where they influence α-subunit glycosylation (Laedermann *et al.*, 2013). Furthermore, β1, unlike β2,

demonstrates low abundance at the plasma membrane (Dulsat *et al.*, 2017), although all β-subunits are enriched within lipid raft fractions of primary mouse cortical neurons (Wong *et al.*, 2005). In the present study, β1 demonstrated co-localisation with markers for the ER, *cis*- and *trans*-Golgi, early endosomes and lysosomes, with particular enrichment within the ER, endosomes and lysosomes (Figure 6.1). Additionally, treatment with the lysosomal inhibitor, chloroquine, induced β1 accumulation within lysosomes, suggesting this is where β1 is degraded. Such analysis of the subcellular distribution of β1 has not been reported previously. The most surprising aspect of β1 distribution was the low expression at the plasma membrane. In fact, assessing the co-localisation of β1 with the membrane marker FM4-64 revealed no detectable plasma membrane expression, with cytoplasmic β1 signal offset to FM4-64 by ~500 nm. The low β1 plasma membrane expression has been noted before, suggesting it could be an intrinsic feature of β1 across different cell types (Dulsat *et al.*, 2017). However, the major roles of β1, namely α-subunit modulation and transcellular adhesion, imply β1 must be at the plasma membrane and the co-localisation of β1 with endosomal markers, from this study, implicate β1 is at the plasma membrane before endocytosis. Although, direct Golgi to early endosome trafficking is observed for APP (Toh *et al.*, 2017). VGSC activity has previously been linked with potentiation of endocytosis in lung cancer cell lines, suggesting β1 may be being rapidly internalised due to the I_{Na} generated in MDA-MB-231 cells (Onganer & Djamgoz, 2005). Additionally, the I_{Na} decay induced by BFA treatment in the present study was significantly accelerated compared to previous work conducted in HEK cells (Rougier *et al.*, 2005), supporting the idea that the rate of VGSC turnover may be relatively high in MDA-MB-231 cells, which may contribute to the low surface β1 expression.

The β1 construct used in this study is fused to GFP at the β1 C-terminus. This design allows for monitoring of secretase processing, as β1ICD-GFP release from the

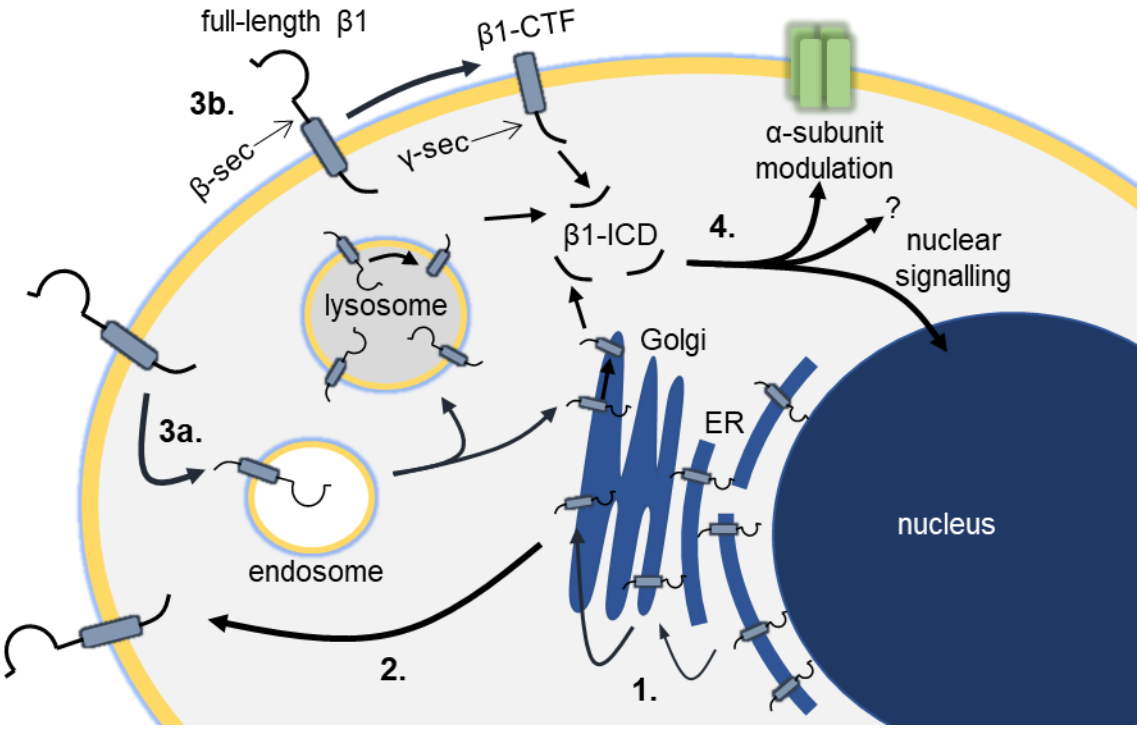

Figure 6.1 Subcellular localisation of β1

1. β1 progresses through the endoplasmic reticulum and Golgi apparatus. The majority of cellular β1 is sequestered within the ER. 2. A fraction of β1 is trafficked to the cell surface. 3. β1 is either processed by secretases at the plasma membrane (3a) or is internalised and processed by secretases on internal membranes (3b). 4. β1-ICD is produced and may be degraded or possess functional roles. β1-ICD was shown to be sufficient to induce a β1-like I_{Na}, suggesting it may remain associated to an α-subunit upon formation. Alternatively, it may translocate to the nucleus and regulate gene expression. Otherwise, β1-ICD may possess a currently unidentified role or be degraded rapidly.

membrane should result in decreased GFP fluorescence at the respective membrane. Therefore, in this study, the subcellular distribution of β1 was compared against β1 after DAPT-treatment or SRβ1. Secretase processing occurs at the plasma membrane as well as at some of the internal membranes examined, such as the ER, *trans*-Golgi and lysosomes (Area-Gomez *et al.*, 2009; Choy *et al.*, 2012; Tam *et al.*, 2014). However, neither SRβ1 nor β1 in DAPT-treated cells showed an increase in their endolysosomal enrichment compared to β1, suggesting γ-secretase cleavage is not occurring within endosomes or lysosomes. However, both SRβ1 and β1 in DAPT-treated cells showed decrease endosome co-localisation compared to β1, suggesting secretase cleavage regulates β1 membrane clearance. Quantitative differences were detected between β1 and SRβ1 distribution, with β1 demonstrating decreased ER expression compared to SRβ1. This difference could be due to secretase processing of β1-GFP, within the ER, resulting in decreased fluorescence compared to SRβ1-GFP.

To further evaluate γ-secretase processing of β1, FRAP was used at various locations within the cell to attempt to detect β1ICD-GFP in live MDA-MB-231-β1GFP cells. In a separate experiment, β1ICD was estimated to diffuse at ~5 $\mu m^2 s^{-1}$ in a freely mobile state, similar to that of GFP. SRβ1-GFP or β1-GFP in DAPT-treated cells (i.e. no β1ICD-GFP present), on the other hand, moved at ~0.1 $\mu m^2 s^{-1}$, typical of a transmembrane protein (Kusumi *et al.*, 1993), with ~30 % of protein being immobile. Therefore, it was expected that the presence of β1ICD-GFP within MDA-MB-231-β1GFP cells would enhance mobility parameters, relative to DAPT-treated MDA-MB-231-β1GFP or MDA-MB-231-SRβ1GFP cells. FRAP was performed at the cell extremities and within the perinuclear region. However, no differences in mobility kinetics were detected, suggesting β1-ICD is not present within these locations or this FRAP technique is not sensitive enough due to low β1-ICD abundance. The presence of an immobile fraction for β1 and SRβ1 is intriguing and could represent the fraction bound to α-subunits, as α-subunits are known

to be almost completely immobilised in neuronal membranes (Angelides *et al.*, 1988; Joe & Angelides, 1993). Alternatively, there is an ankyrin binding site within the β1 C-terminus, which is inhibited by Tyr181 phosphorylation (Malhotra *et al.*, 2002). Ankyrin binding of neurofascin, which is also inhibited by tyrosine phosphorylation, is known to decrease neurofascin lateral mobility (Garver *et al.*, 1997), raising the possibility that ankyrin binding of β1 may be responsible for immobilisation. If this were the case, β1STOP should demonstrate unrestricted lateral mobility. Additionally, as the ankyrin binding site lies within β1-ICD, β1ICD-GFP being generated in MDA-MB-231-β1GFP cells may remain immobilised at the membrane, explaining the lack of increased mobility kinetics when compared to MDA-MB-231-SRβ1GFP cells or MDA-MB-231-β1GFP cells treated with DAPT.

Assays for transcellular adhesion and cell morphology were used throughout this study. The functional implications of these results will be discussed later, however these assays provide an indirect readout of β1 plasma membrane expression, as the extracellular Ig loop is assumed to underpin both β1-induced transcellular adhesion and cell elongation (Isom & Catterall, 1996; Chioni *et al.*, 2009). Interestingly, DAPT treatment accelerated β1-induced cell adhesion, suggesting secretase processing may regulate the expression of full-length β1 at the plasma membrane. In support of this, SRβ1 induced cell elongation to a significantly greater degree than β1 and SRβ1 demonstrates lower endosomal enrichment compared to β1(discussed in the previous paragraph), suggesting more SRβ1 at the plasma membrane. However, increased surface SRβ1 is also explained by the fact that global SRβ1-GFP expression in MDA-MB-231-SRβ1-GFP cells was higher than β1-GFP in MDA-MB-231-β1GFP cells.

In conclusion, β1 is found within the endolysosomal pathway, ER and Golgi although it is still unclear whether secretase cleavage affects β1 localisation. β1 demonstrates overwhelming intracellular expression with an undetectable fraction at the plasma membrane, a phenomenon observed for APP, but not for β2 (Caporaso *et al.*, 1994; Dulsat *et al.*, 2017). Phosphorylation of an intracellular tyrosine dictates subcellular localisation and mobility of the L1 family of cell adhesion molecules, through limiting ankyrin binding (Garver *et al.*, 1997). Interestingly, the intracellular tyrosine (Tyr181) that facilitates ankyrin binding is found within β1 but not present in β2, raising the possibility that Tyr181 is involved in regulating β1 subcellular localisation and may be responsible for the differences seen in the spatial expression profile of β1 and β2 (Malhotra *et al.*, 2002).

β1-ICD was originally hypothesised to translocate to the nucleus where it regulates gene expression, as proposed for β2-ICD (Kim *et al.*, 2007). Interestingly, ankyrin binding to Drosophila L1-CAM negatively regulates nuclear levels of L1-CAM, suggesting ankyrin binding favours membrane targeting (Kakad *et al.*, 2018). Kakad *et al.* also note that C-terminal GFP-tagging of L1-CAM significantly interfered with nuclear translocation, an issue that may be relevant to the present study. Regardless, a small fraction of β1-GFP fluorescence appeared to originate from the nucleus, supporting the hypothesis of nuclear β1-ICD translocation. Furthermore, overexpression of β1ICD-GFP alone in MDA-MB-231 cells demonstrated nuclear localisation. However, this phenomenon could be attributed to the small size of β1ICD-GFP permitting stochastic diffusion through nuclear pores, as GFP showed similar nuclear expression. To discern a difference in nuclear localisation of GFP and β1ICD-GFP, FRAP was used to determine the nuclear import rates of both proteins, as a slower time course of import was expected for β1ICD-GFP if it is being actively transported into the nucleus as part of a protein complex. Interestingly, a slower rate of nuclear import was observed for β1ICD-GFP, compared to

GFP, supporting the hypothesis. However, this slower time course of nuclear import may still be explained by slower diffusion of β1ICD-GFP due to its slightly larger size. Further work is required to determine if β1ICD is trafficked into the nucleus and regulates gene expression. However, the ability of β1-ICD to induce a β1-like I_{Na} suggests β1-ICD may be functionally active at the membrane and may therefore remain associated with the VGSC following secretase processing of β1 in MDA-MB-231-β1GFP cells.

6.2 Electrophysiological consequences of β1 expression

β1 expression induces a range of different electrophysiological changes depending on the model system used. Enhanced I_{Na}, changes in activation/inactivation kinetics, and accelerated recovery from inactivation have all been reported (Zhao *et al.*, 2011; Laedermann *et al.*, 2013; Zhu *et al.*, 2017). β1 overexpression in MDA-MB-231 cells consistently induced an increase in I_{Na} magnitude and an accelerated channel recovery from inactivation, with some changes in activation/inactivation kinetics sporadically seen. The increase in I_{Na} magnitude is likely due to surface trafficking of α-subunits (Isom *et al.*, 1992; Meadows *et al.*, 2001). As β1 is thought to interact with the voltage-sensing domain of DIII (Yan *et al.*, 2017; Zhu *et al.*, 2017), it may accelerate recovery from inactivation through a direct interaction with the voltage-sensing domain. Alternatively, N-terminal glycosylation of β1 has been shown to regulate gating kinetics through the presence of negatively charged sialic acid (Johnson *et al.*, 2004). A TTX-sensitive I_{Na} was also observed following β1 expression, an intriguing result that suggests β1 traffics TTX-sensitive α-subunits that may be retained in intracellular pools within MDA-MB-231 cells. $Na_v1.6$ and $Na_v1.7$ mRNA expression is present within MDA-MB-231 cells, implicating one of these channels, unless another TTX-sensitive α-subunit is upregulated following β1 expression (Chioni *et al.*, 2009).

An issue with consistency arose across the patch clamp experiments presented in this study. Four separate experiments are presented here that include MDA-MB-231-GFP and MDA-MB-231-β1GFP controls. In all four, current density was increased, and time taken for half-maximal channel recovery from inactivation accelerated, in β1-GFP expressing cells compared to GFP expressing cells, resulting in these two features characterising the "β1-like I_{Na}." However, in two experiments each, the voltage threshold for half-maximal channel inactivation was depolarised and the voltage at peak I_{Na} was hyperpolarised. Similarly, in one experiment each, the voltage threshold for channel activation was hyperpolarised and the voltage threshold for half-maximal channel activation hyperpolarised. Due to the inconsistent appearance of these changes in gating kinetics, it is difficult to conclude whether they are genuinely induced by β1 or are technical issues. As the I_{Na} detected in MDA-MB-231 is relatively smaller than that seen in other cell models used in VGSC research, slight changes in gating kinetics may be difficult to detect. Alternatively, voltage clamping requires a very stable seal between cell membrane and the pipette mounted on the electrode. If one of the control cell lines used is more difficult to seal onto than the other, or if MDA-MB-231 are difficult to seal onto in general, it would make precise voltage control of the cell membrane more difficult for the amplifier and may contribute to erratic gating kinetic results. As peak current density and recovery from inactivation were the most reliable parameters, they became the focus of the project.

The impact of secretase processing on β1-induced α-subunit modulation remained an exciting, unexplored area of research prior to this study. So far, emerging evidence has linked secretases to β2 electrophysiology. Overexpression of β2-ICD in SH-SY-5Y cells demonstrates nucleus expression and causes upregulation of $Na_v1.1$ expression (Kim *et al.*, 2007). In BACE1-null mice neurons, both β2 proteolysis and $Na_v1.1$ expression is reduced (Kim *et al.*, 2011). Additionally, α-subunit interaction sites are found within β1-

ICD and β1-ECD (McCormick *et al.*, 1999; Meadows *et al.*, 2001), the two domains released following secretase processing, further supporting the possibility of a role of secretase cleavage in β1-induced α-subunit modulation. However, the effect of secretase processing on β1-induced α-subunit modulation was examined in this study thoroughly, using pharmacology and β1 constructs, yet no link was detected. Initially, MDA-MB-231-β1GFP were treated with a range of γ-secretase inhibitors (DAPT, L685,458 and Avagacestat) and no changes in I_{Na} magnitude or channel recovery from inactivation were detected, relative to untreated cells. Furthermore, SRβ1 expression also induced a β1-like I_{Na}, supporting the previous result that secretase cleavage does not regulate β1-medatied α-subunit modulation. Interestingly, β1-ICD, alone, could induce a β1-like I_{Na}. This result suggests that even following secretase processing, β1-induced α-subunit modulation may be maintained through β1-ICD. The ability of β1-ICD to increase I_{Na} magnitude and TTX-sensitivity was surprising, as it suggests soluble β1-ICD is capable of enhancing surface trafficking of α-subunits. Additionally, β1-ICD accelerated channel recovery from inactivation, suggesting that if β1-induced recovery from inactivation is a result of direct modulation, it occurs on the cytoplasmic side of the channel. Importantly, β1-ICD did not induce β1-like transcellular adhesion or cell elongation, confirming that β1-ICD was not functioning via endogenous full-length β1, for instance through upregulation of *SCN1B* expression. Soluble ion channel auxiliary subunits do exist, Ca_vβs, K_vβs and K^+-channel interacting proteins (KChIPs) are all soluble proteins that can modulate channel activation/inactivation kinetics and increase channel surface expression (in the case of Ca_vβs and KChIPs) (Pragnell *et al.*, 1994; An *et al.*, 2000; Yang *et al.*, 2001; Altier *et al.*, 2011). Furthermore, many mutations that occur on the cytoplasmic surface of Na_v α-subunits disrupt channel activation/inactivation kinetics (Chapter 1), supporting the idea that alterations to the structure of the cytoplasmic side of α-subunits induced by interaction with β1-ICD could regulate channel recovery from inactivation. Together, these data suggest secretase processing does not

regulate β1-mediated α-subunit modulation but the β1-ICD sequence itself is sufficient to induce a β1-like I_{Na} in MDA-MB-231 cells.

To validate the importance of β1-ICD, β1STOP-GFP was constructed and expressed in MDA-MB-231 cells. β1STOP has been used previously to demonstrate an α-subunit interaction site, as well as the ankyrin binding site, within β1-ICD (Meadows *et al.*, 2001; Malhotra *et al.*, 2002). As hypothesised, β1STOP failed to enhance I_{Na} when expressed in MDA-MB-231 cells, underlining the importance of β1-ICD in β1-like I_{Na} induction (Figure 6.2). However, β1STOP was able to accelerate channel recovery from inactivation. Mechanistic insight into how β1 accelerates recovery from inactivation is lacking, making this result difficult to explain. However, an α-subunit interaction within the N-terminus has been characterised (McCormick *et al.*, 1999), so potentially there is functional redundancy between the Ig domain and the ICD in regard to α-subunit modulation. Endogenous β-subunits are lowly expressed in MDA-MB-231 cells (Chioni *et al.*, 2009), thus another possibility is that β1-ICD or β1-STOP are imparting their modulatory effect via these subunits. Alternatively, the construct design may be responsible. β1-ICD and β1STOP share a three amino acid overlap in the N-terminus of β1-ICD/ C-terminus of β1STOP, as the original creators of β1STOP observed that maintaining the first three amino acids of β1-ICD was required for correct folding and membrane insertion (McCormick *et al.*, 1998). Similarly, both proteins share the same linker to GFP. Either of these two shared sequences between β1-ICD and β1-STOP may be contributing to inducing channel recovery from inactivation. Despite the recovery from inactivation result, the inability of β1STOP to induce an enlarged I_{Na} verified the hypothesis that β1-ICD is responsible for enlarging I_{Na}, potentially through increased surface expression of α-subunits. No further assays were performed with β1STOP in this thesis, but it would be informative to test TTX sensitivity in β1STOP-expressing cells to verify whether β1STOP is altering the surface expression of TTX-sensitive α-subunits.

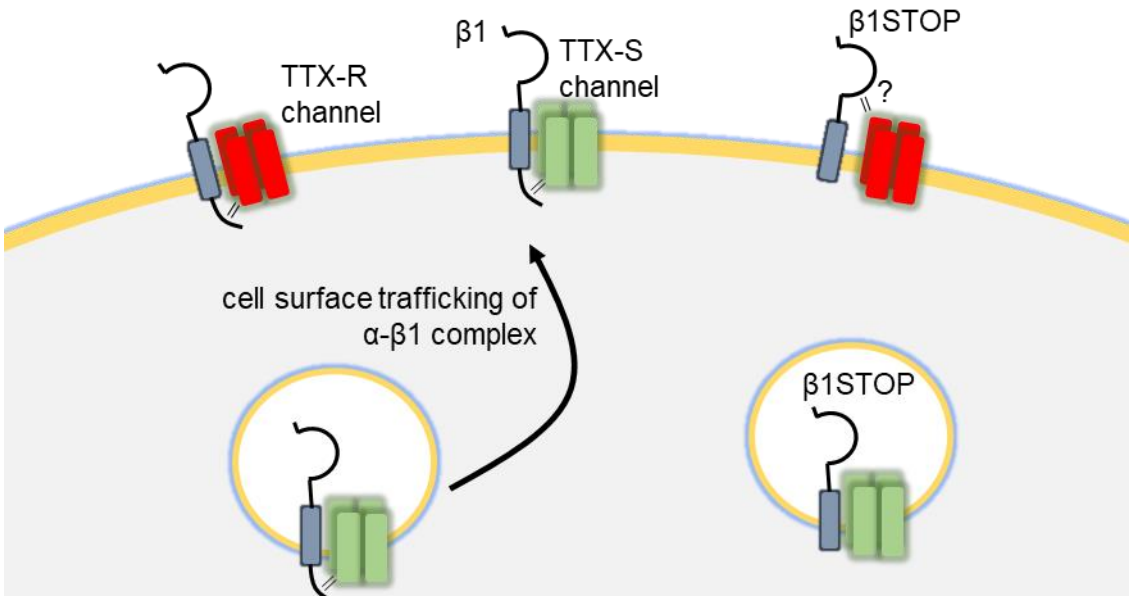

Figure 6.2 β1-mediated regulation of α-subunits

The β1-ICD is required and sufficient to increase I_{Na} current density, presumably through cell surface trafficking of α-subunits, including TTX-sensitive (TTX-S) channels. β1STOP (β1 lacking its ICD sequence) is unable to increase current density, supporting the model. However, β1, β1-ICD and β1STOP are able to accelerate channel recovery from inactivation, suggesting the mechanism to induce this gating effect is more complex than a simple reliance on β1-ICD. β1STOP may potentially be interacting with TTX-resistant (TTX-R) channels, which are present at the plasma membrane independently of β1, via its N-terminus.

How β1-ICD is enhancing I_{Na} is an interesting question. As discussed in chapter 6.1, Tyr181 is a potential regulator of β1 function, by preventing ankyrin binding when phosphorylated (Malhotra *et al.*, 2002). β1 interacts with the tyrosine kinase, Fyn kinase and receptor protein tyrosine phosphatase β, RPTPβ, which are thought to regulate Tyr181 phosphorylation status (Ratcliffe *et al.*, 2000; Brackenbury *et al.*, 2008). Ankyrin already has a documented involvement in regulating VGSCs, as ankyrin also binds α-subunits (Mohler *et al.*, 2004). Ankyrin is an adaptor protein that couples a protein to actin filaments and is involved in facilitating $Na_v1.5$ surface expression in cardiomyocytes and VGSC clustering at axon initial segments (Zhou *et al.*, 1998; Mohler *et al.*, 2004). Additionally, in heterologous CHL cells, $Na_v1.2$ interaction with ankyrin is enhanced following β1 expression, leading to increased surface expression of $Na_v1.2$ (McEwen *et al.*, 2004). This process is dependent on contactin and reversed when a phosphomimetic construct of β1 is used (β1Y181E), suggesting β1 binding to ankyrin is also required (McEwen *et al.*, 2004). Interestingly, β1Y181E still interacts with $Na_v1.2$ but fails to modulate channel activation/inactivation kinetics (McEwen *et al.*, 2004). The importance of the cytoskeleton in $Na_v1.5$ activity has already been reported. Treatment of rat ventricular myocytes with cytochalasin-D, an inhibitor of actin polymerisation, decreases single channel open probability and slows inactivation (Undrovinas *et al.*, 1995). Furthermore, treatment of HEK293 cells expressing $Na_v1.5$ with Taxol, a tubulin polymerising agent decreases current density (Casini *et al.*, 2010). The authors speculated ankyrin-mediated coupling of VGSCs to microtubules facilitates microtubule-dependent internalisation of $Na_v1.5$. Therefore, β1ICD-ankyrin binding may be the mechanism required for surface trafficking of VGSCs in MDA-MB-231 cells. In summary, β1-ICD underpins the β1-induced I_{Na} in MDA-MB-231 cells. Investigating the involvement of Tyr181 phosphorylation would be an informative next step.

6.3 β1-induced metastatic cell behaviour

β1 expression is known to increase the metastatic potential of MDA-MB-231 cells, particularly to the liver and lungs, when implanted into mice (Nelson *et al.*, 2014). The increased metastatic potential is accompanied by decreased apoptosis, increased process outgrowth and increased VEGF secretion *in vivo,* as well as an increase in invasion *in vitro,* when compared to control MDA-MB-231 cells (Nelson *et al.*, 2014). However, the relationship between β-subunits and cancer may be complicated, as β1 expression decreases mobility of MDA-MB-231 cells and cervical cancer cell lines *in vitro* (Chioni *et al.*, 2009; Sanchez-Sandoval & Gomora, 2019). Similarly, β2 is considered oncogenic, as its expression is increased in highly metastatic prostate cancer cell lines and overexpression in prostate cancer LNCaP cells increases migration, invasion and growth *in vitro* and increases perineural invasion in an *ex vivo* assay; yet LNCaP-β2 cells show decreased tumour growth, compared to LNCaP cells, when implanted into mice (Jansson *et al.*, 2012; Jansson *et al.*, 2014). The complexity of the involvement of β-subunits in cancer may reflect a tumour stage-dependency, as LNCaP cells are considered weakly metastatic whereas MDA-MB-231 cells are considered strongly metastatic (Iorns *et al.*, 2012; Jansson *et al.*, 2012). This is supported by patient cohort data that indicates *SCN1B* overexpression is seen in invasive breast tumours, whereas high *SCN1B* expression does not correlate with a change in survival in subtype non-specific breast cancer patients (Nelson *et al.*, 2014). The uncertain contribution of β1 in breast cancer highlights the need for deeper mechanistic understanding of β1 function.

6.3.1 The involvement of β1 in cell adhesion

One explanation for the involvement of β1 in breast cancer could be via cell adhesion. CAMs have a diverse involvement in cancer due to their role in regulating transcellular coordination and communication, with some CAMs, for example glialCAM (Du *et al.*,

2018), being downregulated and others, such as epithelial CAM (Zeng *et al.*, 2019), being upregulated (Farahani *et al.*, 2014). E-cadherin is a CAM with a complex involvement in cancer. E-cadherin is the major CAM involved in maintaining epithelial integrity and loss of E-cadherin is thought to be a prerequisite for tumour invasion, demonstrated by loss of E-cadherin causing pancreatic tumour progression from well differentiated adenoma to invasive carcinoma (Perl *et al.*, 1998). Conversely, E-cadherin expression is increased in distant metastases disseminated from breast tumours (Kowalski *et al.*, 2003). E-cadherin expression is required for formation of secondary tumours, and to prevent apoptosis, in a mouse model of invasive ductal carcinoma, leading the authors to conclude E-cadherin expression is stage-specific (Padmanaban *et al.*, 2019). It is therefore possible β1 may increase the metastatic potential of MDA-MB-231 cells, an already strongly metastatic cell line, through increased transcellular adhesion, necessary for growth of secondary tumours. Whereas weakly metastatic breast cancer MCF-7 cells still maintain characteristics of differentiated epithelial cells, while demonstrating high β1 expression (Chioni *et al.*, 2009), as β1 keeps MCF-7 cells compact at the primary site. In the present study, γ-secretase inhibition increased the transcellular adhesiveness of MDA-MB-231-β1GFP cells, suggesting secretase inhibition may potentiate the β1-mediated cell adhesion process. Consistent with this, SRβ1 expression increased transcellular adhesion compared to GFP, although SRβ1 was not compared to β1. An increase in cell adhesion is likely caused by more β1 Ig loops at the cell surface, however if γ-secretase inhibition increases cell adhesion, there is the possibility that β1-ICD may negatively regulate cell adhesion. However, β1ICD-GFP expression did not affect cell adhesion compared to GFP expression. These data underscore the importance of the Ig loop in β1-mediated cell adhesion and exclude the possibility that β1-ICD is involved in regulating cell adhesion. These data also suggest γ-secretase inhibitor treatment may have negative consequences as an anti-cancer drug, if transcellular adhesion is the mechanism underpinning β1-mediated metastasis.

6.3.2 The involvement of β1 in regulating cell morphology

MDA-MB-231 cells have a biphasic cell morphology when grown in culture. Cells can possess a rounded morphology or an elongated morphology, characteristic of a mesenchymal, polarised cell with lamellipodia at the leading edge and an elongated process at the trailing edge. When β1 is expressed in MDA-MB-231 cells, process elongation and narrowing occurs as the cells adopt a more mesenchymal-like morphology (Chioni *et al.*, 2009). A mesenchymal-like morphology is associated with cell migration and this is supported by experimental data demonstrating that MDA-MB-231 cells cultured in astrocyte-conditioned medium displayed reduced circularity (as the cells elongate), increased velocity and increased displacement (Shumakovich *et al.*, 2017). However, the link between morphology and cell motility may not be that straightforward as β1 reduces lateral motility in MDA-MB-231 cells and β4 similarly induces an elongated cell morphology while preventing migration through RhoA inhibition (Chioni *et al.*, 2009; Bon *et al.*, 2016). β1-induced process outgrowth of MDA-MB-231-β1GFP cells is also observed following skeletal muscle invasion of disseminated cancer cells in mouse xenograft models, suggesting morphology changes may be linked to β1-mediated metastatic cancer cell behaviour (Nelson *et al.*, 2014). In tumour cells, processes extending from the cell body are associated with chemosensing and invasion (Meyer *et al.*, 2012; Williams *et al.*, 2019). In fact, process outgrowth correlates with 3D *in vitro* invasion more robustly than 2D lateral motility does (Meyer *et al.*, 2012), suggesting the β1-induced process may be priming the cell for directed motility/invasion instead of random 2D movement. Interestingly, β1 induces neurite outgrowth in cerebellar granule neurons, raising the possibility of functional recapitulation in breast cancer cells (Brackenbury *et al.*, 2008). Furthermore, β1-induced neurite outgrowth is γ-secretase dependent, implicating a potential role for secretase processing in β1-induced breast cancer cell morphology changes (Brackenbury & Isom, 2011). However, in the present study, SRβ1 expression in MDA-MB-231 cells increased cell length and reduced cell

circularity compared to GFP expression, similar to β1, suggesting secretase processing is not required for these morphology changes. This is supported by the observation that β1-ICD did not induce β1-like morphology changes in MDA-MB-231 cells. These data implicate full-length β1 in β1-induced morphology changes, probably via Ig loop-mediated adhesion. In fact, SRβ1-induced cell elongation was significantly greater than β1-induced cell elongation, possibly through higher SRβ1 membrane expression compared to β1. Results from this study do not necessarily contradict the literature; outgrowth assays performed on MDA-MB-231 cells and cerebellar granule neurons previously have used a co-culture model, employing a monolayer of β1-expressing or β1-null cells to focus on β1-induced, transhomophilic process/neurite outgrowth (Brackenbury *et al.*, 2008; Brackenbury & Isom, 2011). Therefore, the results from the present study suggest the mechanism involved in β1-induced cell elongation in cultured cells is secretase-independent, unlike for β1-mediated neurite outgrowth, and may not be fully representative of *in vivo* conditions. The fact that γ-secretase is required for β1-mediated, trans-homophilic neurite outgrowth is intriguing, as it suggests both the extracellular and intracellular domains are required. Trans-homophilic β1 interactions may represent a co-ordinated, signal transduction response initiated by β1-β1 Ig loop interactions and ending with β1-ICD release. If this is occurring in breast cancer cells expressing β1, and process outgrowth is clinically relevant, it could signify a role for γ-secretase in β1-induced metastasis.

6.3.3 The involvement of β1-induced Na^+ current in tumour progression

The potential contribution of I_{Na} in tumour progression is an emerging, compelling field of research, discussed in detail in chapter 1. In mouse xenograft models of breast cancer, $Na_v1.5$ knockdown or treatment with phenytoin decreases tumour metastasis (Nelson *et al.*, 2015a; Nelson *et al.*, 2015b). This result directly implicated I_{Na} in breast tumour

metastasis, which is intriguing considering β1 expression enhances I_{Na} when expressed in breast cancer cells (Chioni *et al.*, 2009). However, the present study demonstrates that β1-induced I_{Na} is not secretase-dependent, so secretase inhibitors would not be a viable treatment option if β1 is contributing to metastasis through enlargement of I_{Na}. A causal relationship between β1-induced I_{Na} and metastasis seems a likely possibility, however, β4 also enlarges I_{Na} in MDA-MB-231 cells, yet has a tumour suppressive effect when β4-overexpressing cells are implanted into mice (Bon *et al.*, 2016). The inhibitory effect of β4 on breast cancer cell invasion was demonstrated to be I_{Na}-independent and is thought to occur through inhibition of RhoA-mediated migration through intracellular interactions instead (Bon *et al.*, 2016). The present study demonstrated β1 also accelerated channel recovery from inactivation and upregulated TTX-sensitive to the plasma membrane, parameters that were not investigated for β4. Therefore, it is possible that one of these parameters underlies β1-induced metastasis. For instance, $Na_v1.6$ and $Na_v1.7$ transcripts, along with β1 transcripts, are overexpressed in cervical cancer biopsies and inhibition of $Na_v1.6$ in a cervical cancer cell line reduces cell invasive capacity (Diaz *et al.*, 2007; Hernandez-Plata *et al.*, 2012). Additionally, other parameters were not measured in this study that may clarify how the β1-induced I_{Na} contributes to breast cancer metastasis. The persistent I_{Na} is generated following incomplete inactivation of VGSCs and results in a small intracellular flow of Na^+. The persistent I_{Na} has been proposed as the major constituent of the inward I_{Na} in breast cancer cells, as cancer cells do not experience large fluctuations in membrane potential like neurons. Hence, VGSCs in cancer cells are not able to cycle through open, inactivated and closed states as they conventionally do in neurons. As cancer cells possess a relatively depolarised membrane potential, it is thought VGSCs are mostly inactivated, with a fraction of VGSCs carrying a persistent I_{Na} (Yang *et al.*, 2012). A persistent I_{Na}, carried by $Na_v1.5$, is observable in MDA-MB-231 cells (Yang *et al.*, 2012). The contribution of the persistent I_{Na} in breast cancer metastasis has not been directly dissected, yet as it may be the most physiologically relevant component of the cancer associated I_{Na}, it

would be informative to measure in β1-expressing cells. Likewise, membrane potential itself may contribute to tumour progression (Yang & Brackenbury, 2013). Membrane potential is proportional to the sum of the extracellular and intracellular concentrations of all ions present, including Na^+, and their respective permeabilities across the plasma membrane. A depolarised membrane potential is observed in proliferative cells (Yang & Brackenbury, 2013). Likewise, depolarisation of mouse lymphocytes induces cell proliferation, whereas hyperpolarisation of CHO cells induces mitotic arrest (Cone & Tongier, 1973; Kiefer *et al.*, 1980). Membrane potential has been further linked as a regulator of cell migration and differentiation (Sundelacruz *et al.*, 2009; Schwab *et al.*, 2012). A depolarised membrane potential is also observed in tumour cells, suggesting a potential direct link between ion flux and migration, proliferation and differentiation in tumour cells (Yang & Brackenbury, 2013). If the β1-induced enlargement of I_{Na} is contributing to membrane potential depolarisation, it provides another possible mechanism for the involvement of β1 in breast tumour metastasis. In summary, there are several potential ways in which the β1-induced I_{Na} may be contributing to breast tumour metastasis, however this study suggests there is no involvement of secretase cleavage in regulating β1-mediated α-subunit modulation.

6.3.4 The involvement of intracellular domain signalling

The last potential mechanism to explain the involvement of β1 in breast cancer is through ICD signalling. ICDs, generated from γ-secretase cleavage of other substrates, have been implicated in cancer. For example, elevated Notch signalling is observed in over 50 % of T lymphoblastic leukaemia cases and has demonstrated the ability to upregulate *c-Myc* and downregulate *PTEN* (Ellisen *et al.*, 1991; Weng *et al.*, 2004; Palomero *et al.*, 2006; Palomero *et al.*, 2007). The contribution of Notch signalling in tumour progression has garnered so much attention that γ-secretase inhibitors have even progressed to clinical trials to treat various cancers (Kummar *et al.*, 2017; Aung *et al.*, 2018). The ICD

of Epithelial CAM (EpICD) interacts with β-catenin and directs gene transcription (Maetzel *et al.*, 2009). EpICD induces oncogenesis in mice and is observed within the nuclei of patient colon cancer cells, but not in the nuclei of cells in normal tissue (Maetzel *et al.*, 2009). Gene transcription may not be the only oncogenic function of ICDs, as a β4CTF-like protein inhibits RhoA-dependent migration of MDA-MB-231 cells, potentially through intracellular protein-protein interactions (Bon *et al.*, 2016). Preliminary evidence in the present study suggests β1-ICD may be translocating to the nucleus. If β1-ICD is involved in regulating a gene expression network or regulating Rho GTPase function that is contributing to breast cancer metastasis, γ-secretase inhibition may represent a desirable method of clinical intervention.

To summarise, various secretase dependent and independent mechanisms may contribute to β1-induced breast tumour metastasis (Figure 6.3). In this study, most effort was invested into gaining an insight into secretase-dependent β1 function and localisation in MDA-MB-231 cells and not into the effect of secretase processing on β1-induced metastatic cell behaviour. However, various β1 constructs have been produced and characterised that could now be used in a range of *in vitro* cancer behavioural assays and *in vivo* mouse xenograft experiments to thoroughly dissect the involvement of secretase processing and the I_{Na} in β1-induced breast tumour metastasis.

6.4 Translational implications for breast cancer

This study aimed to address the possible viability or consequences of using secretase inhibitors as treatment for breast cancers overexpressing β1. As the mechanistic involvement of β1 in breast tumour metastasis is not known, it is not possible to fully translate the effect of secretase inhibition on β1-induced *in vitro* behaviour to *in vivo*

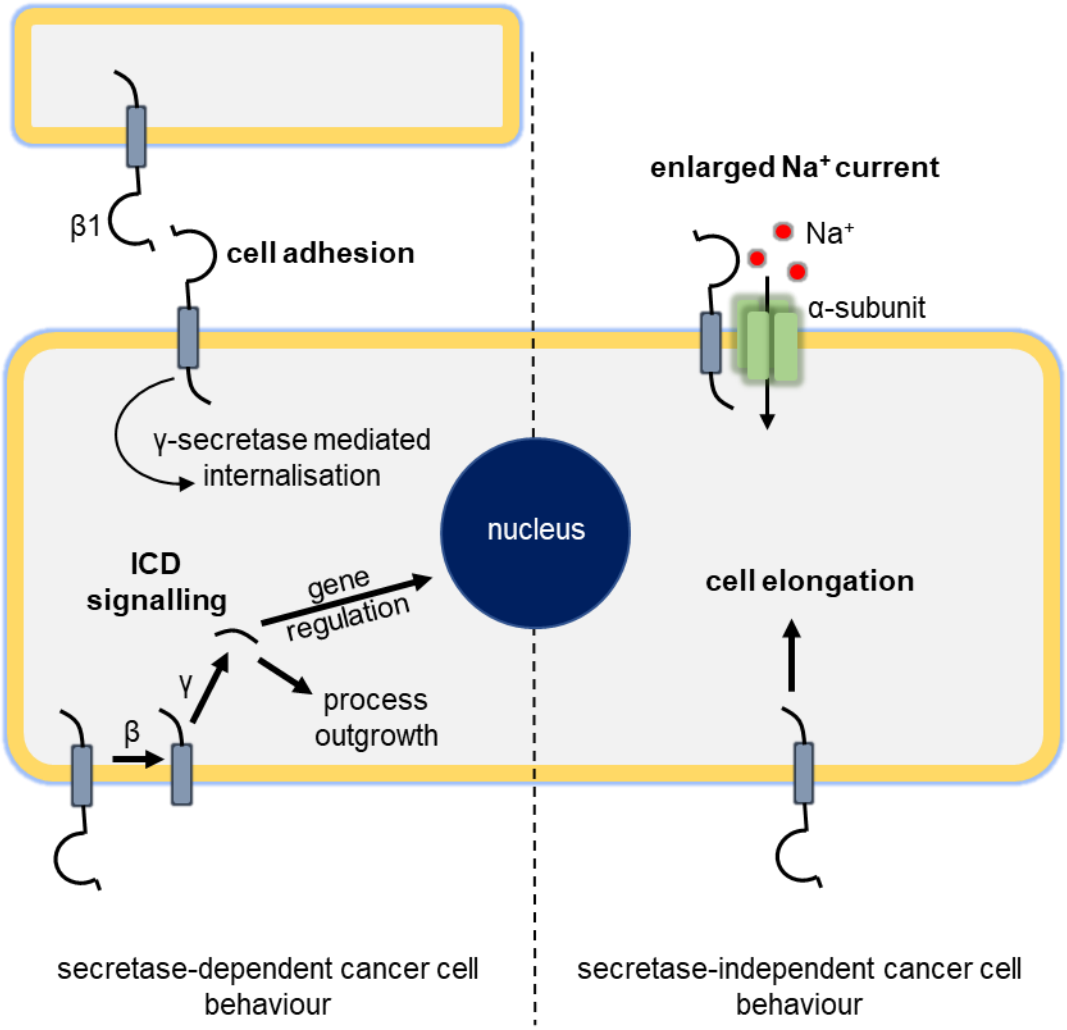

Figure 6.3 Potential secretase-dependent and -independent mechanisms of β1-induced metastatic cancer cell behaviour

In this study, γ-secretase inhibition enhanced β1-induced transcellular adhesion, suggesting secretase cleavage of β1 may regulate cell surface β1 expression. Alternatively, β1-ICD may be involved in various cell signalling pathways. For instance, nuclear localisation and gene regulation underlie the pro-metastatic capacity of Notch-ICD and EpICD (Maetzel *et al.*, 2009; Gokulan & Halagowder, 2014). The requirement of γ-secretase cleavage for β1-induced neurite outgrowth has raised the possibility that the same pathway is recapitulated in breast cancer cells (Brackenbury & Isom, 2011). However, there are secretase-independent pathways that may underlie β1-induced metastasis. For instance, if the β1-induced I_{Na} is implicit, which was shown to be secretase-independent in this study. Or if the cell morphology changes induced by β1 and SRβ1 are associated with cancer cell behaviour.

tumour metastasis, however, it is still possible to make some predictions. This study demonstrated that secretase inhibition had no effect on the β1-induced Na^+ current, suggesting if the enlarged β1-induced Na^+ current is implicit in β1-induced tumour metastasis, then secretase inhibitors will be ineffective. Additionally, secretase cleavage appeared to not be involved in β1-induced cell morphology changes, so if changes in cell morphology are a prerequisite for β1-induced metastasis, then secretase inhibition will also be ineffective. On the other hand, γ-secretase inhibition enhanced β1-induced cell adhesion, which may be a physiologically relevant result, as enhancing primary tumour cell adhesion may reduce dissemination, whereas enhancing metastatic tumour cell adhesion may induce colonisation at secondary sites. Therefore, the effect of secretase inhibition on tumour cell adhesion may have a tumour grade-specific effect.

In summary, this study has yet to fully elucidate the role of secretase cleavage in regulating β1 function, making it difficult to understand the translational impact of secretase cleavage in regulating β1-induced breast tumour metastasis. The following chapter will outline possible future experiments to uncover the role of secretase cleavage in regulating β1-induced breast tumour metastasis.

6.5 Future directions

Further work is required to fully understood the role of β1 in MDA-MB-231 cells and the subsequent involvement of secretase processing. This can be divided into three projects: understanding the subcellular distribution of β1, understanding the electrophysiological properties of β1 and understanding the metastatic cell behaviour induced by β1.

Regarding the subcellular distribution of β1, one of the most intriguing observations was the low abundance of β1 at the plasma membrane. The ability to quantify surface β1 expression would be informative, as it would allow for investigation of whether secretase cleavage impacts β1 dynamics at the plasma membrane. Quantification of surface β1 expression could be achieved through biotinylation and purification of all surface proteins and analysis via western blot. Various imaging techniques also exist to selectively image surface proteins. For instance, extracellularly tagged proteins can be selectively labelled with a fluorophore to prevent fluorescence from intracellular proteins (Bedbrook *et al.*, 2015), which was an issue in this study. Other fluorophores are selectively fluorescent when exposed to the extracellular environment and can be used to selectively image surface proteins, such as phluorin, which has been used to visualise surface APP (Bauereiss *et al.*, 2015). The possibility remains that secretase processing is occurring intracellularly. Subcellular fractionation could be used to assess which cleavage products are present in which compartment. A technique used to assess APP proteolysis involved dual-labelling APP with an extracellular and intracellular fluorophore to determine where the fluorophores dissociate and would provide a spatial profile of β-secretase cleavage (Parenti *et al.*, 2017).

Determining the intracellular fate of β1-ICD may be key to understanding the role of secretase processing of β1. This study uncovered a possible difference in nuclear import between β1ICD-GFP and GFP, using FRAP. Further use of this nuclear import assay could be used to determine if β1ICD-GFP is being actively imported into the nucleus, for instance by decreasing temperature or depleting cellular ATP (Adam *et al.*, 1990). Alternatively, nuclear fractionation is the most common method used to assess nuclear expression and could be used to determine whether β1ICD-GFP is present within the nuclei of MDA-MB-231-β1GFP cells and to verify β1ICD-GFP nuclear localisation is secretase-dependent. If β1-ICD nuclear localisation is confirmed, techniques such as

mass spectrometry of β1ICD-GFP interacting partners could be used to determine if β1ICD-GFP is translocating as part of a complex. Furthermore, qPCR of suspected cDNAs (such as that of α-subunits) or RNAseq could then be used to assess the changes in gene expression elicited by β1-ICD.

Regarding the electrophysiological properties induced by β1 in MDA-MB-231 cells, this study highlights β1-ICD as the responsible domain in enhancing I_{Na}. To fully understand the involvement of β1-ICD, investigating the phosphorylation state of Tyr181 was proposed in chapter 6.2. To investigate this, a range of phosphomimetic and phosphodead mutations have been previously characterised and would be beneficial to use in this study (Malhotra *et al.*, 2002). Alternatively, inhibition of Fyn kinase, the kinase implicated in phosphorylation of Tyr181, in MDA-MB-231-β1GFP cells would also uncover the involvement of Tyr 181 phosphorylation in β1-mediated α-subunit modulation. α-subunit selective toxins could be used to determine the TTX-sensitive channels that are upregulated at the plasma membrane in β1-expressing cells. Lastly, quantification of the surface expression of VGSCs would verify a trafficking effect induced by β1, e.g. through biontinylation, however α-subunits are difficult to quantify due to their low abundance and poor antibodies. If this is the case, α-subunits would have to be overexpressed or an alternate cell system used.

Regarding investigating the mechanistic involvement of β1 in breast tumour metastasis, the β1 constructs designed in this study would be informative. For instance, β1-ICD produces a β1-like I_{Na} and is the final secretase product of β1, however it does not possess the ability to induce cell adhesion or morphology changes. On the other hand, SRβ1 produces a β1-like I_{Na} and is able to induce cell adhesion and morphology changes but lacks ICD production. β1-STOP does not produce a β1-like I_{Na} and does not produce

ICD but may still be able to induce cell adhesion and morphology changes, due to its Ig loop. Use of these constructs can therefore be used to isolate different functions of β1 and test their involvement in β1-induced cancer cell behaviour. *In vitro* assays, such as proliferation, apoptosis, migration and invasion assays, could be used to investigate how β1 induces oncogenic properties in MDA-MB-231 cells. Lastly, the mouse xenograft model of breast cancer, used to implicate β1 in breast cancer metastasis (Nelson *et al.*, 2014), could be repeated for MDA-MB-231-β1ICDGFP, MDA-MB-231-SRβ1GFP or MDA-MB-231-β1STOPGFP cells, to study the involvement of secretase processing in β1-induced breast cancer metastasis.

6.6 Conclusion

This study aimed to understand the involvement of secretase processing in regulating β1 function in breast cancer MDA-MB-231 cells. The most complete set of experiments implicated β1-ICD in the β1-induced I_{Na}, however the involvement of β1-ICD appeared to be secretase-independent. Imaging analysis of β1 demonstrated β1 expression within the ER, Golgi, early endosomes and lysosomes, raising the intriguing observation that β1 is not enriched at the plasma membrane. Locating γ-secretase cleavage in MDA-MB-231 cells was thoroughly investigated with various imaging approaches, however no clear location was found. To date, no thorough investigation into the subcellular distribution of β1 has been reported in the literature and this study has raised many interesting questions, such as: Where is γ-secretase cleavage occurring? What is the fate of β1-ICD? Why is β1 expression at the plasma membrane so low and is plasma membrane expression regulated by secretase cleavage? This study has uncovered a range of interesting *in vitro* results that have explored the mechanism of β1 function in MDA-MB-231 cells but has also established the foundations for potential *in vivo*

experimentation to fully understand the involvement of secretase cleavage in regulating β1-induced breast cancer cell behaviour.

Abbreviations

ADAM: a disintegrin and metalloprotease

AIS: axon initial segment

ALS: amyotrophic lateral sclerosis

AmpR: Ampicillin resistance

ANOVA: analysis of variance

APH-1: anterior pharynx-defective 1

APP: amyloid precursor protein

ATP: adenosine triphosphate

Ava: Avagacestat

BACE: β-amyloid cleaving enzyme

BFA: brefeldin-A

BGH-polyA: bovine growth hormone polyadenylation

BFNIS: benign familial neonatal-infantile seizures

BK_{Ca}: large-conductance Ca^{2+}-activated K^{+}

BPS: BSA, PB, saponin

BRCA1/2: Breast cancer type 1/2 susceptibility protein

BrS: Brugada syndrome

BSA: bovine serum albumin

BSCM: β-secretase cleavage motif

CaM: calmodulin

CAM: cell adhesion molecule

CBF1: C-repeat/DRE binding factor 1

CCD: charge-coupled device

CD: cluster of differentiation

CGN: cerebellar granule neuron

CHO: Chinese hamster ovary

CHL: Chinese hamster lung

CIP: chronic insensitivity to pain

CK2: casein kinase 2

C_m: membrane capacitance

CNS: central nervous system

COS: CV-1 (simian) in Origin, and carrying the SV40 genetic material

CSL: CBF1, suppressor of Hairless, Lag-1

CTF: C-terminal fragment

D_{2D}: diffusion coefficient/ rate of 2D diffusion

DAPI: 4',6-diamidino-2-phenylindole

DAPT: n-[n-(3,5-difluorophenacetyl)-l-alanyl]-s-phenylglycine t-butyl ester

DMEM: Dulbecco's modified eagle medium

DMSO: dimethyl sulfoxide

dNTP: deoxyribonucleotide triphosphate

DRG: dorsal root ganglion

DS: Dravet syndrome

DTT: dithiothreitol

EAE: experiment autoimmune encephalomyelitis

ECD: extracellular domain

EDTA: ethylenediaminetetraacetic acid

EEA1: early endosome antigen 1

EEG: electroencephalogram

EGF: epidermal growth factor

eGFP: enhanced GFP

EGTA: ethylene glycol-bis(β-aminoethyl ether)-N,N,N′,N′-tetraacetic acid

EIEE11: early infantile epileptic encephalopathy 11

EM: electron microscopy

EpICD: epithelialCAM intracellular domain

ER: endoplasmic reticulum

FBS: foetal bovine serum

FDA: food & drug administration

FGF: fibroblast growth factor

FKBP52: FK506-binding protein 4

FRAP: fluorescence recovery after photobleaching

FRET: Förster resonance energy transfer

GABA: γ-aminobutyric acid

GEFS+: generalised epilepsy with febrile seizures plus

GFP: green fluorescent protein

GI: gastrointestinal

GSK3: glycogen synthase kinase 3

GSI: γ-secretase inhibitor

GSM: γ-secretase modifier

HEK: human embryonic kidney

HEPES: 4-(2-hydroxyethyl)-1-piperazineethanesulfonic acid

HF: high fidelity

HRP: horseradish peroxidase

HSP90: heat shock protein 90

hyperPP: hyperkaliaemic periodic paralysis

hypoPP: hypokaliaemic periodic paralysis

ICD: intracellular domain

IFM: isoleucine, phenylalanine, methionine

Ig: immunoglobulin

IL: interleukin

I_{Na}: Na^+ current

$I_{Na}P$: persistent Na^+ current

IPS: intracellular pipette solution

IQR: interquartile range

KChIP: K^+ channel interacting protein

KDa: kilodalton

LAMP1: lysosome associated membrane protein 1

LB: Luria/lysogeny broth

LNCaP: lymph node carcinoma of the prostate

LQTS: long QT syndrome

LRP8: Low-density lipoprotein receptor-related protein 8

MaM: mastermind

MAPK: mitogen-activated protein kinase

MCF-7: Michigan cancer foundation-7

MDA-MB-231: M.D. Anderson metastatic breast cancer 231

MS: multiple sclerosis

Na_V: voltage-gated Na^+ channel

N:C: nuclear: cytoplasmic ratio

NF: neurofascin

NHE1: Na^+-H^+ exchanger 1

NLS: nuclear localisation signal

NPC: neuronal progenitor cell

nrCAM: neuronalCAM

NSAID: non-steroidal anti-inflammatory drug

NTF: N-terminal fragment

NTR: neurotrophic receptor

PB: phosphate buffer

PBTGS: PB, Triton X-100, goat serum

PBS: phosphate-buffered saline

PCC: Pearson's correlation coefficient

PCD: peak current density

pCMV: cytomegalovirus promoter

PCR: polymerase chain reaction

PEN: presenilin enhancer

PEPD: paroxysmal extreme pain disorder

PFA: paraformaldehyde

PKA: protein kinase A

PKC: protein kinase C

PMA: Phorbol 12-myristate 13-acetate

PNS: peripheral nervous system

ProTx-II: protoxin-II

PS: presenilin

PSS: physiological saline solution

PTEN: phosphate and tensin homologue

PY motif: polyproline tyrosine motif

$R_{b(x)}$: background region fluorescence (time *x*)

$R_{C(x)}$: control region fluorescence (time *x*)

RFI: recovery from inactivation

RhoA: Ras homolog gene family, member A

R_n: normalised ROI fluorescence

ROI: region of interest

$R_{p(x)}$: photobleached region fluorescence (time *x*)

RPTP-β: receptor-type protein tyrosine phosphatase-β

SCN(*x*a/b): Na^+ channel type (*x*a/b)

SDF-1: stromal cell derived factor 1

SDS: sodium dodecyl sulphate

SEM: standard error of the mean

SIDS: sudden infantile death syndrome

SR: secretase-resistant

STX: saxitoxin

SUDEP: sudden unexplained death in epilepsy patients

SV40: simian virus 40

T_a: annealing temperature

TBS: tris-buffered saline

TBS-T: TBS-tween

TEMED: Tetramethylethylenediamine

TGN: *trans*-Golgi network

TLL: T-cell leukaemia lymphoma

TMD: transmembrane domain

TNBC: triple negative breast cancer

T_p: time to peak

TSA: tumour-specific antigen

TTX (-S/R): tetrodotoxin (-sensitive/resistant)

$V_{1/2}$: voltage threshold for half-maximal response

V_a: activation voltage

VEGF: vascular endothelial growth factor

VGSC: voltage-gated Na^+ channel

V_h: holding voltage

V_p: voltage at peak

V_s: stimulation voltage

VSD: voltage sensing domain

V_m: membrane voltage/potential

YENTPY motif: tyrosine-glutamic acid-asparagine-threonine-proline-tyrosine motif

YLAI motif: tyrosine-leucine-alanine-isoleucine motif

References

Ackerman MJ, Siu BL, Sturner WQ, Tester DJ, Valdivia CR, Makielski JC & Towbin JA. (2001). Postmortem molecular analysis of SCN5A defects in sudden infant death syndrome. *Jama* **286,** 2264-2269.

Ackerman MJ, Splawski I, Makielski JC, Tester DJ, Will ML, Timothy KW, Keating MT, Jones G, Chadha M, Burrow CR, Stephens JC, Xu C, Judson R & Curran ME. (2004). Spectrum and prevalence of cardiac sodium channel variants among black, white, Asian, and Hispanic individuals: implications for arrhythmogenic susceptibility and Brugada/long QT syndrome genetic testing. *Heart Rhythm* **1,** 600-607.

Adachi K, Toyota M, Sasaki Y, Yamashita T, Ishida S, Ohe-Toyota M, Maruyama R, Hinoda Y, Saito T, Imai K, Kudo R & Tokino T. (2004). Identification of SCN3B as a novel p53-inducible proapoptotic gene. *Oncogene* **23,** 7791-7798.

Adam SA, Marr RS & Gerace L. (1990). Nuclear protein import in permeabilized mammalian cells requires soluble cytoplasmic factors. *J Cell Biol* **111,** 807-816.

Agnew WS, Levinson SR, Brabson JS & Raftery MA. (1978). Purification of the tetrodotoxin-binding component associated with the voltage-sensitive sodium channel from Electrophorus electricus electroplax membranes. *Proc Natl Acad Sci U S A* **75,** 2606-2610.

Ahern CA. (2013). What activates inactivation? *The Journal of general physiology* **142,** 97-100.

Akopian AN, Sivilotti L & Wood JN. (1996). A tetrodotoxin-resistant voltage-gated sodium channel expressed by sensory neurons. *Nature* **379,** 257-262.

Akopian AN, Souslova V, England S, Okuse K, Ogata N, Ure J, Smith A, Kerr BJ, McMahon SB, Boyce S, Hill R, Stanfa LC, Dickenson AH & Wood JN. (1999). The tetrodotoxin-resistant sodium channel SNS has a specialized function in pain pathways. *Nat Neurosci* **2,** 541-548.

Allinquant B, Moya KL, Bouillot C & Prochiantz A. (1994). Amyloid precursor protein in cortical neurons: coexistence of two pools differentially distributed in axons and dendrites and association with cytoskeleton. *J Neurosci* **14,** 6842-6854.

Alsaloum M, Estacion M, Almomani R, Gerrits M, Bonhof G, Ziegler D, Malik R, Ferdousi M, Lauria G, Merkies I, Faber C, Dib-Hajj S & Waxman S. (2019). A gain-of-function sodium channel beta2 subunit mutation in painful diabetic neuropathy. *Molecular pain***,** 1744806919849802.

Altier C, Garcia-Caballero A, Simms B, You H, Chen L, Walcher J, Tedford HW, Hermosilla T & Zamponi GW. (2011). The Cavbeta subunit prevents RFP2-mediated ubiquitination and proteasomal degradation of L-type channels. *Nat Neurosci* **14,** 173-180.

Alzheimer A, Stelzmann RA, Schnitzlein HN & Murtagh FR. (1995). An English translation of Alzheimer's 1907 paper, "Uber eine eigenartige Erkankung der Hirnrinde". *Clinical anatomy (New York, NY)* **8,** 429-431.

An WF, Bowlby MR, Betty M, Cao J, Ling HP, Mendoza G, Hinson JW, Mattsson KI, Strassle BW, Trimmer JS & Rhodes KJ. (2000). Modulation of A-type potassium channels by a family of calcium sensors. *Nature* **403,** 553-556.

Andrikopoulos P, Fraser SP, Patterson L, Ahmad Z, Burcu H, Ottaviani D, Diss JK, Box C, Eccles SA & Djamgoz MB. (2011). Angiogenic functions of voltage-gated Na+ Channels in human endothelial cells: modulation of vascular endothelial growth factor (VEGF) signaling. *J Biol Chem* **286,** 16846-16860.

Angelides KJ, Elmer LW, Loftus D & Elson E. (1988). Distribution and lateral mobility of voltage-dependent sodium channels in neurons. *J Cell Biol* **106,** 1911-1925.

Araki Y, Miyagi N, Kato N, Yoshida T, Wada S, Nishimura M, Komano H, Yamamoto T, De Strooper B, Yamamoto K & Suzuki T. (2004). Coordinated metabolism of Alcadein and amyloid beta-protein precursor regulates FE65-dependent gene transactivation. *J Biol Chem* **279,** 24343-24354.

Area-Gomez E, de Groof AJ, Boldogh I, Bird TD, Gibson GE, Koehler CM, Yu WH, Duff KE, Yaffe MP, Pon LA & Schon EA. (2009). Presenilins are enriched in endoplasmic reticulum membranes associated with mitochondria. *Am J Pathol* **175,** 1810-1816.

Armstrong CM & Bezanilla F. (1973). Currents related to movement of the gating particles of the sodium channels. *Nature* **242,** 459-461.

Armstrong CM & Bezanilla F. (1977). Inactivation of the sodium channel. II. Gating current experiments. *The Journal of general physiology* **70,** 567-590.

Arnestad M, Crotti L, Rognum TO, Insolia R, Pedrazzini M, Ferrandi C, Vege A, Wang DW, Rhodes TE, George AL, Jr. & Schwartz PJ. (2007). Prevalence of long-QT syndrome gene variants in sudden infant death syndrome. *Circulation* **115,** 361-367.

Aster JC, Pear WS & Blacklow SC. (2017). The Varied Roles of Notch in Cancer. *Annual review of pathology* **12,** 245-275.

Atapattu L, Saha N, Chheang C, Eissman MF, Xu K, Vail ME, Hii L, Llerena C, Liu Z, Horvay K, Abud HE, Kusebauch U, Moritz RL, Ding BS, Cao Z, Rafii S, Ernst M, Scott AM, Nikolov DB, Lackmann M & Janes PW. (2016). An activated form of ADAM10 is tumor selective

and regulates cancer stem-like cells and tumor growth. *The Journal of experimental medicine* **213,** 1741-1757.

Aung KL, El-Khoueiry AB, Gelmon K, Tran B, Bajaj G, He B, Chen T, Zhu L, Poojary S, Basak S, Qi Z, Spreafico A, Fischer BS & Desai J. (2018). A multi-arm phase I dose escalating study of an oral NOTCH inhibitor BMS-986115 in patients with advanced solid tumours. *Investigational new drugs* **36,** 1026-1036.

Baek JH, Rubinstein M, Scheuer T & Trimmer JS. (2014). Reciprocal changes in phosphorylation and methylation of mammalian brain sodium channels in response to seizures. *J Biol Chem* **289,** 15363-15373.

Bai XC, Rajendra E, Yang G, Shi Y & Scheres SH. (2015). Sampling the conformational space of the catalytic subunit of human gamma-secretase. *eLife* **4**.

Bailey SJ, Stocksley MA, Buckel A, Young C & Slater CR. (2003). Voltage-gated sodium channels and ankyrinG occupy a different postsynaptic domain from acetylcholine receptors from an early stage of neuromuscular junction maturation in rats. *J Neurosci* **23,** 2102-2111.

Barbosa C, Tan ZY, Wang R, Xie W, Strong JA, Patel RR, Vasko MR, Zhang JM & Cummins TR. (2015). Navbeta4 regulates fast resurgent sodium currents and excitability in sensory neurons. *Molecular pain* **11,** 60.

Barchi RL, Cohen SA & Murphy LE. (1980). Purification from rat sarcolemma of the saxitoxin-binding component of the excitable membrane sodium channel. *Proc Natl Acad Sci U S A* **77,** 1306-1310.

Baron M. (2012). Endocytic routes to Notch activation. *Seminars in cell & developmental biology* **23,** 437-442.

Baroni D, Barbieri R, Picco C & Moran O. (2013). Functional modulation of voltage-dependent sodium channel expression by wild type and mutated C121W-β1 subunit. *J Bioenerg Biomembr* **45,** 353-368.

Batcioglu K, Uyumlu AB, Satilmis B, Yildirim B, Yucel N, Demirtas H, Onkal R, Guzel RM & Djamgoz MB. (2012). Oxidative stress in the in vivo DMBA rat model of breast cancer: suppression by a voltage-gated sodium channel inhibitor (RS100642). *Basic & clinical pharmacology & toxicology* **111,** 137-141.

Bauereiss A, Welzel O, Jung J, Grosse-Holz S, Lelental N, Lewczuk P, Wenzel EM, Kornhuber J & Groemer TW. (2015). Surface Trafficking of APP and BACE in Live Cells. *Traffic* **16,** 655-675.

Baum L, Haerian BS, Ng HK, Wong VC, Ng PW, Lui CH, Sin NC, Zhang C, Tomlinson B, Wong GW, Tan HJ, Raymond AA, Mohamed Z & Kwan P. (2014). Case-control association study of polymorphisms in the voltage-gated sodium channel genes SCN1A, SCN2A, SCN3A, SCN1B, and SCN2B and epilepsy. *Human genetics* **133,** 651-659.

Bedbrook CN, Kato M, Ravindra Kumar S, Lakshmanan A, Nath RD, Sun F, Sternberg PW, Arnold FH & Gradinaru V. (2015). Genetically Encoded Spy Peptide Fusion System to Detect Plasma Membrane-Localized Proteins In Vivo. *Chemistry & biology* **22,** 1108-1121.

Belcher SM, Zerillo CA, Levenson R, Ritchie JM & Howe JR. (1995). Cloning of a sodium channel alpha subunit from rabbit Schwann cells. *Proceedings of the National Academy of Sciences* **92,** 11034-11038.

Belyaev ND, Kellett KA, Beckett C, Makova NZ, Revett TJ, Nalivaeva NN, Hooper NM & Turner AJ. (2010). The transcriptionally active amyloid precursor protein (APP) intracellular domain is preferentially produced from the 695 isoform of APP in a {beta}-secretase-dependent pathway. *J Biol Chem* **285,** 41443-41454.

Beneski DA & Catterall WA. (1980). Covalent labeling of protein components of the sodium channel with a photoactivable derivative of scorpion toxin. *Proc Natl Acad Sci U S A* **77,** 639-643.

Benn SC, Costigan M, Tate S, Fitzgerald M & Woolf CJ. (2001). Developmental expression of the TTX-resistant voltage-gated sodium channels Nav1.8 (SNS) and Nav1.9 (SNS2) in primary sensory neurons. *J Neurosci* **21,** 6077-6085.

Bennett ES, Smith BA & Harper JM. (2004). Voltage-gated Na+ channels confer invasive properties on human prostate cancer cells. *Pflugers Archiv : European journal of physiology* **447,** 908-914.

Bennett PB, Yazawa K, Makita N & George AL, Jr. (1995). Molecular mechanism for an inherited cardiac arrhythmia. *Nature* **376,** 683-685.

Berecki G, Bryson A, Terhag J, Maljevic S, Gazina EV, Hill SL & Petrou S. (2019). SCN1A gain of function in early infantile encephalopathy. *Annals of neurology* **85,** 514-525.

Berwick DC, Diss JK, Budhram-Mahadeo VS & Latchman DS. (2010). A simple technique for the prediction of interacting proteins reveals a direct Brn-3a-androgen receptor interaction. *J Biol Chem* **285,** 15286-15295.

Bhagat TD, Zou Y, Huang S, Park J, Palmer MB, Hu C, Li W, Shenoy N, Giricz O, Choudhary G, Yu Y, Ko YA, Izquierdo MC, Park AS, Vallumsetla N, Laurence R, Lopez R, Suzuki M, Pullman J, Kaner J, Gartrell B, Hakimi AA, Greally JM, Patel B, Benhadji K, Pradhan K, Verma A & Susztak K. (2017). Notch Pathway Is Activated via Genetic and Epigenetic Alterations and Is a Therapeutic Target in Clear Cell Renal Cancer. *J Biol Chem* **292,** 837-846.

Bhattacharyya R, Fenn RH, Barren C, Tanzi RE & Kovacs DM. (2016). Palmitoylated APP Forms Dimers, Cleaved by BACE1. *PLoS One* **11,** e0166400.

Bigan E, Sasidharan Nair S, Lejeune FX, Fragnaud H, Parmentier F, Megret L, Verny M, Aaronson J, Rosinski J & Neri C. (2019). Genetic cooperativity in multi-layer networks implicates cell survival and senescence in the striatum of Huntington's disease mice synchronous to symptoms. *Bioinformatics (Oxford, England)*.

Biki B, Mascha E, Moriarty DC, Fitzpatrick JM, Sessler DI & Buggy DJ. (2008). Anesthetic technique for radical prostatectomy surgery affects cancer recurrence: a retrospective analysis. *Anesthesiology* **109,** 180-187.

Bizzarri R, Cardarelli F, Serresi M & Beltram F. (2012). Fluorescence recovery after photobleaching reveals the biochemistry of nucleocytoplasmic exchange. *Analytical and bioanalytical chemistry* **403,** 2339-2351.

Black JA, Dib-Hajj S, McNabola K, Jeste S, Rizzo MA, Kocsis JD & Waxman SG. (1996). Spinal sensory neurons express multiple sodium channel alpha-subunit mRNAs. *Brain research Molecular brain research* **43,** 117-131.

Blackburn-Munro G & Fleetwood-Walker SM. (1999). The sodium channel auxiliary subunits beta1 and beta2 are differentially expressed in the spinal cord of neuropathic rats. *Neuroscience* **90,** 153-164.

Bon E, Driffort V, Gradek F, Martinez-Caceres C, Anchelin M, Pelegrin P, Cayuela ML, Marionneau-Lambot S, Oullier T, Guibon R, Fromont G, Gutierrez-Pajares JL, Domingo I, Piver E, Moreau A, Burlaud-Gaillard J, Frank PG, Chevalier S, Besson P & Roger S. (2016). SCN4B acts as a metastasis-suppressor gene preventing hyperactivation of cell migration in breast cancer. *Nat Commun* **7,** 13648.

Borg JP, Ooi J, Levy E & Margolis B. (1996). The phosphotyrosine interaction domains of X11 and FE65 bind to distinct sites on the YENPTY motif of amyloid precursor protein. *Molecular and cellular biology* **16,** 6229-6241.

Bosmans F, Martin-Eauclaire MF & Swartz KJ. (2008). Deconstructing voltage sensor function and pharmacology in sodium channels. *Nature* **456,** 202-208.

Boulton ME, Cai J & Grant MB. (2008). gamma-Secretase: a multifaceted regulator of angiogenesis. *J Cell Mol Med* **12,** 781-795.

Boursi B, Lurie I, Mamtani R, Haynes K & Yang YX. (2015). Anti-depressant therapy and cancer risk: a nested case-control study. *European neuropsychopharmacology : the journal of the European College of Neuropsychopharmacology* **25,** 1147-1157.

Bouza AA & Isom LL. (2017). Voltage-Gated Sodium Channel beta Subunits and Their Related Diseases. *Handbook of experimental pharmacology*.

Brackenbury WJ. (2012). Voltage-gated sodium channels and metastatic disease. *Channels (Austin, Tex)* **6,** 352-361.

Brackenbury WJ, Calhoun JD, Chen C, Miyazaki H, Nukina N, Oyama F, Ranscht B & Isom LL. (2010). Functional reciprocity between Na+ channel Nav1.6 and beta1 subunits in the coordinated regulation of excitability and neurite outgrowth. *Proc Natl Acad Sci U S A* **107,** 2283-2288.

Brackenbury WJ, Chioni AM, Diss JK & Djamgoz MB. (2007). The neonatal splice variant of Nav1.5 potentiates in vitro invasive behaviour of MDA-MB-231 human breast cancer cells. *Breast Cancer Res Treat* **101,** 149-160.

Brackenbury WJ, Davis TH, Chen C, Slat EA, Detrow MJ, Dickendesher TL, Ranscht B & Isom LL. (2008). Voltage-gated Na+ channel beta1 subunit-mediated neurite outgrowth requires Fyn kinase and contributes to postnatal CNS development in vivo. *J Neurosci* **28,** 3246-3256.

Brackenbury WJ & Djamgoz MB. (2007). Nerve growth factor enhances voltage-gated Na+ channel activity and Transwell migration in Mat-LyLu rat prostate cancer cell line. *J Cell Physiol* **210,** 602-608.

Brackenbury WJ & Isom LL. (2011). Na Channel β Subunits: Overachievers of the Ion Channel Family. *Front Pharmacol* **2,** 53.

Bradford MM. (1976). A rapid and sensitive method for the quantitation of microgram quantities of protein utilizing the principle of protein-dye binding. *Anal Biochem* **72,** 248-254.

Brisson L, Gillet L, Calaghan S, Besson P, Le Guennec JY, Roger S & Gore J. (2011). Na(V)1.5 enhances breast cancer cell invasiveness by increasing NHE1-dependent H(+) efflux in caveolae. *Oncogene* **30,** 2070-2076.

Buchanan PC, Boylan KL, Walcheck B, Heinze R, Geller MA, Argenta PA & Skubitz AP. (2017). Ectodomain Shedding of the Cell Adhesion Molecule Nectin-4 in Ovarian Cancer is Mediated by ADAM10 and ADAM17. *J Biol Chem*.

Buffington SA & Rasband MN. (2013). Na+ channel-dependent recruitment of Navbeta4 to axon initial segments and nodes of Ranvier. *J Neurosci* **33,** 6191-6202.

Burg VK, Grimm HS, Rothhaar TL, Grosgen S, Hundsdorfer B, Haupenthal VJ, Zimmer VC, Mett J, Weingartner O, Laufs U, Broersen LM, Tanila H, Vanmierlo T, Lutjohann D, Hartmann

T & Grimm MO. (2013). Plant sterols the better cholesterol in Alzheimer's disease? A mechanistical study. *J Neurosci* **33,** 16072-16087.

Burgess DL, Kohrman DC, Galt J, Plummer NW, Jones JM, Spear B & Meisler MH. (1995). Mutation of a new sodium channel gene, Scn8a, in the mouse mutant 'motor endplate disease'. *Nature genetics* **10,** 461-465.

Butler KM, da Silva C, Shafir Y, Weisfeld-Adams JD, Alexander JJ, Hegde M & Escayg A. (2017). De novo and inherited SCN8A epilepsy mutations detected by gene panel analysis. *Epilepsy research* **129,** 17-25.

Cadoo KA, Fornier MN & Morris PG. (2013). Biological subtypes of breast cancer: current concepts and implications for recurrence patterns. *The quarterly journal of nuclear medicine and molecular imaging : official publication of the Italian Association of Nuclear Medicine (AIMN) [and] the International Association of Radiopharmacology (IAR), [and] Section of the So* **57,** 312-321.

Cailleau R, Young R, Olive M & Reeves WJ, Jr. (1974). Breast tumor cell lines from pleural effusions. *Journal of the National Cancer Institute* **53,** 661-674.

Calloe K, Refaat MM, Grubb S, Wojciak J, Campagna J, Thomsen NM, Nussbaum RL, Scheinman MM & Schmitt N. (2013). Characterization and mechanisms of action of novel NaV1.5 channel mutations associated with Brugada syndrome. *Circulation Arrhythmia and electrophysiology* **6,** 177-184.

Calvert PD, Schiesser WE & Pugh EN, Jr. (2010). Diffusion of a soluble protein, photoactivatable GFP, through a sensory cilium. *The Journal of general physiology* **135,** 173-196.

Candenas L, Seda M, Noheda P, Buschmann H, Cintado CG, Martin JD & Pinto FM. (2006). Molecular diversity of voltage-gated sodium channel alpha and beta subunit mRNAs in human tissues. *European journal of pharmacology* **541,** 9-16.

Cao X & Sudhof TC. (2001). A transcriptionally [correction of transcriptively] active complex of APP with Fe65 and histone acetyltransferase Tip60. *Science (New York, NY)* **293,** 115-120.

Capell A, Grunberg J, Pesold B, Diehlmann A, Citron M, Nixon R, Beyreuther K, Selkoe DJ & Haass C. (1998). The proteolytic fragments of the Alzheimer's disease-associated presenilin-1 form heterodimers and occur as a 100-150-kDa molecular mass complex. *J Biol Chem* **273,** 3205-3211.

Capell A, Saffrich R, Olivo JC, Meyn L, Walter J, Grunberg J, Mathews P, Nixon R, Dotti C & Haass C. (1997). Cellular expression and proteolytic processing of presenilin proteins is developmentally regulated during neuronal differentiation. *J Neurochem* **69,** 2432-2440.

Capes DL, Goldschen-Ohm MP, Arcisio-Miranda M, Bezanilla F & Chanda B. (2013). Domain IV voltage-sensor movement is both sufficient and rate limiting for fast inactivation in sodium channels. *The Journal of general physiology* **142,** 101-112.

Caporaso GL, Takei K, Gandy SE, Matteoli M, Mundigl O, Greengard P & De Camilli P. (1994). Morphologic and biochemical analysis of the intracellular trafficking of the Alzheimer beta/A4 amyloid precursor protein. *J Neurosci* **14,** 3122-3138.

Cardarelli F, Serresi M, Bizzarri R, Giacca M & Beltram F. (2007). In vivo study of HIV-1 Tat arginine-rich motif unveils its transport properties. *Molecular therapy : the journal of the American Society of Gene Therapy* **15,** 1313-1322.

Casini S, Tan HL, Demirayak I, Remme CA, Amin AS, Scicluna BP, Chatyan H, Ruijter JM, Bezzina CR, van Ginneken AC & Veldkamp MW. (2010). Tubulin polymerization modifies cardiac sodium channel expression and gating. *Cardiovascular research* **85,** 691-700.

Catterall WA. (2014). Sodium channels, inherited epilepsy, and antiepileptic drugs. *Annu Rev Pharmacol Toxicol* **54,** 317-338.

Catterall WA, Kalume F & Oakley JC. (2010). NaV1.1 channels and epilepsy. *J Physiol* **588,** 1849-1859.

Cestele S, Qu Y, Rogers JC, Rochat H, Scheuer T & Catterall WA. (1998). Voltage sensor-trapping: enhanced activation of sodium channels by beta-scorpion toxin bound to the S3-S4 loop in domain II. *Neuron* **21,** 919-931.

Cestele S, Yarov-Yarovoy V, Qu Y, Sampieri F, Scheuer T & Catterall WA. (2006). Structure and function of the voltage sensor of sodium channels probed by a beta-scorpion toxin. *J Biol Chem* **281,** 21332-21344.

Chanda B & Bezanilla F. (2002). Tracking voltage-dependent conformational changes in skeletal muscle sodium channel during activation. *The Journal of general physiology* **120,** 629-645.

Chen C, Calhoun JD, Zhang Y, Lopez-Santiago L, Zhou N, Davis TH, Salzer JL & Isom LL. (2012). Identification of the cysteine residue responsible for disulfide linkage of Na+ channel alpha and beta2 subunits. *J Biol Chem* **287,** 39061-39069.

Chen C, Westenbroek RE, Xu X, Edwards CA, Sorenson DR, Chen Y, McEwen DP, O'Malley HA, Bharucha V, Meadows LS, Knudsen GA, Vilaythong A, Noebels JL, Saunders TL, Scheuer T, Shrager P, Catterall WA & Isom LL. (2004). Mice lacking sodium channel beta1 subunits display defects in neuronal excitability, sodium channel expression, and nodal architecture. *J Neurosci* **24,** 4030-4042.

Chen Q, Liu X, Xu L, Wang Y, Wang S, Li Q, Huang Y & Liu T. (2016). Long non-coding RNA BACE1-AS is a novel target for anisomycin-mediated suppression of ovarian cancer stem cell proliferation and invasion. *Oncology reports* **35,** 1916-1924.

Chen XB, Li W & Chu AX. (2019). MicroRNA-133a inhibits gastric cancer cells growth, migration, and epithelial-mesenchymal transition process by targeting presenilin 1. *J Cell Biochem* **120,** 470-480.

Cheng HT, Miner JH, Lin M, Tansey MG, Roth K & Kopan R. (2003). Gamma-secretase activity is dispensable for mesenchyme-to-epithelium transition but required for podocyte and proximal tubule formation in developing mouse kidney. *Development (Cambridge, England)* **130,** 5031-5042.

Chioni AM, Brackenbury WJ, Calhoun JD, Isom LL & Djamgoz MB. (2009). A novel adhesion molecule in human breast cancer cells: voltage-gated Na+ channel beta1 subunit. *Int J Biochem Cell Biol* **41,** 1216-1227.

Chow VW, Mattson MP, Wong PC & Gleichmann M. (2010). An overview of APP processing enzymes and products. *Neuromolecular Med* **12,** 1-12.

Choy RW, Cheng Z & Schekman R. (2012). Amyloid precursor protein (APP) traffics from the cell surface via endosomes for amyloid beta (Abeta) production in the trans-Golgi network. *Proc Natl Acad Sci U S A* **109,** E2077-2082.

Chubak J, Bowles EJ, Yu O, Buist DS, Fujii M & Boudreau DM. (2016). Breast cancer recurrence in relation to antidepressant use. *Cancer causes & control : CCC* **27,** 125-136.

Chyung AS, Greenberg BD, Cook DG, Doms RW & Lee VM. (1997). Novel beta-secretase cleavage of beta-amyloid precursor protein in the endoplasmic reticulum/intermediate compartment of NT2N cells. *J Cell Biol* **138,** 671-680.

Chyung JH, Raper DM & Selkoe DJ. (2005). Gamma-secretase exists on the plasma membrane as an intact complex that accepts substrates and effects intramembrane cleavage. *J Biol Chem* **280,** 4383-4392.

Chyung JH & Selkoe DJ. (2003). Inhibition of receptor-mediated endocytosis demonstrates generation of amyloid beta-protein at the cell surface. *J Biol Chem* **278,** 51035-51043.

Clatot J, Hoshi M, Wan X, Liu H, Jain A, Shinlapawittayatorn K, Marionneau C, Ficker E, Ha T & Deschenes I. (2017). Voltage-gated sodium channels assemble and gate as dimers. *Nat Commun* **8,** 2077.

Cohen SA & Barchi RL. (1981). Glycoprotein characteristics of the sodium channel saxitoxin-binding component from mammalian sarcolemma. *Biochim Biophys Acta* **645,** 253-261.

Cone CD, Jr. & Tongier M, Jr. (1973). Contact inhibition of division: involvement of the electrical transmembrane potential. *J Cell Physiol* **82,** 373-386.

Cook N, Basu B, Smith DM, Gopinathan A, Evans J, Steward WP, Palmer D, Propper D, Venugopal B, Hategan M, Anthoney DA, Hampson LV, Nebozhyn M, Tuveson D, Farmer-Hall H, Turner H, McLeod R, Halford S & Jodrell D. (2018). A phase I trial of the gamma-secretase inhibitor MK-0752 in combination with gemcitabine in patients with pancreatic ductal adenocarcinoma. *Br J Cancer* **118,** 793-801.

Copley RR. (2004). Evolutionary convergence of alternative splicing in ion channels. *Trends in genetics : TIG* **20,** 171-176.

Cordy JM, Hussain I, Dingwall C, Hooper NM & Turner AJ. (2003). Exclusively targeting beta-secretase to lipid rafts by GPI-anchor addition up-regulates beta-site processing of the amyloid precursor protein. *Proc Natl Acad Sci U S A* **100,** 11735-11740.

Cortada E, Sr., Brugada R & Verges M. (2019). N-glycosylation of the voltage-gated sodium channel beta2 subunit is required for efficient trafficking of NaV1.5/beta2 to the plasma membrane. *J Biol Chem*.

Cortet M, Bertaut A, Molinie F, Bara S, Beltjens F, Coutant C & Arveux P. (2018). Trends in molecular subtypes of breast cancer: description of incidence rates between 2007 and 2012 from three French registries. *BMC Cancer* **18,** 161.

Coughlan K, Huang X, He X, Chung CH, Li G & Tang J. (2013). Expression and processing of fluorescent fusion proteins of amyloid precursor protein (APP). *Biochim Biophys Acta* **1833,** 1562-1571.

Cox JJ, Reimann F, Nicholas AK, Thornton G, Roberts E, Springell K, Karbani G, Jafri H, Mannan J, Raashid Y, Al-Gazali L, Hamamy H, Valente EM, Gorman S, Williams R, McHale DP, Wood JN, Gribble FM & Woods CG. (2006). An SCN9A channelopathy causes congenital inability to experience pain. *Nature* **444,** 894-898.

Cummins TR, Dib-Hajj SD & Waxman SG. (2004). Electrophysiological properties of mutant Nav1.7 sodium channels in a painful inherited neuropathy. *J Neurosci* **24,** 8232-8236.

Cummins TR, Howe JR & Waxman SG. (1998). Slow closed-state inactivation: a novel mechanism underlying ramp currents in cells expressing the hNE/PN1 sodium channel. *J Neurosci* **18,** 9607-9619.

Cummins TR, Zhou J, Sigworth FJ, Ukomadu C, Stephan M, Ptacek LJ & Agnew WS. (1993). Functional consequences of a Na+ channel mutation causing hyperkalemic periodic paralysis. *Neuron* **10,** 667-678.

Cusdin FS, Nietlispach D, Maman J, Dale TJ, Powell AJ, Clare JJ & Jackson AP. (2010). The sodium channel {beta}3-subunit induces multiphasic gating in NaV1.3 and affects fast inactivation via distinct intracellular regions. *J Biol Chem* **285,** 33404-33412.

Darras N, Ha TK, Rego S, Martin PM, Barroso E, Slavotinek AM & Cilio MR. (2019). Developmental and epileptic encephalopathy in two siblings with a novel, homozygous missense variant in SCN1B. *American journal of medical genetics Part A*.

Das S, Gilchrist J, Bosmans F & Van Petegem F. (2016). Binary architecture of the Nav1.2-beta2 signaling complex. *eLife* **5**.

Davis RL & Turner DL. (2001). Vertebrate hairy and Enhancer of split related proteins: transcriptional repressors regulating cellular differentiation and embryonic patterning. *Oncogene* **20,** 8342-8357.

Davis TH, Chen C & Isom LL. (2004). Sodium channel beta1 subunits promote neurite outgrowth in cerebellar granule neurons. *J Biol Chem* **279,** 51424-51432.

De Jesus-Acosta A, Laheru D, Maitra A, Arcaroli J, Rudek MA, Dasari A, Blatchford PJ, Quackenbush K & Messersmith W. (2014). A phase II study of the gamma secretase inhibitor RO4929097 in patients with previously treated metastatic pancreatic adenocarcinoma. *Investigational new drugs* **32,** 739-745.

De Strooper B, Saftig P, Craessaerts K, Vanderstichele H, Guhde G, Annaert W, Von Figura K & Van Leuven F. (1998). Deficiency of presenilin-1 inhibits the normal cleavage of amyloid precursor protein. *Nature* **391,** 387-390.

Dehury B, Tang N, Blundell TL & Kepp KP. (2019). Structure and dynamics of γ-secretase with presenilin 2 compared to presenilin 1. *RSC Advances* **9,** 20901-20916.

Deschenes I, Armoundas AA, Jones SP & Tomaselli GF. (2008). Post-transcriptional gene silencing of KChIP2 and Navbeta1 in neonatal rat cardiac myocytes reveals a functional association between Na and Ito currents. *Journal of molecular and cellular cardiology* **45,** 336-346.

Deschenes I & Tomaselli GF. (2002). Modulation of Kv4.3 current by accessory subunits. *FEBS Lett* **528,** 183-188.

Diaz-Padilla I, Wilson MK, Clarke BA, Hirte HW, Welch SA, Mackay HJ, Biagi JJ, Reedijk M, Weberpals JI, Fleming GF, Wang L, Liu G, Zhou C, Blattler C, Ivy SP & Oza AM. (2015). A phase II study of single-agent RO4929097, a gamma-secretase inhibitor of Notch signaling, in patients with recurrent platinum-resistant epithelial ovarian cancer: A study of the Princess Margaret, Chicago and California phase II consortia. *Gynecologic oncology* **137,** 216-222.

Diaz D, Delgadillo DM, Hernandez-Gallegos E, Ramirez-Dominguez ME, Hinojosa LM, Ortiz CS, Berumen J, Camacho J & Gomora JC. (2007). Functional expression of voltage-gated sodium channels in primary cultures of human cervical cancer. *J Cell Physiol* **210,** 469-478.

Dib-Hajj SD, Estacion M, Jarecki BW, Tyrrell L, Fischer TZ, Lawden M, Cummins TR & Waxman SG. (2008). Paroxysmal extreme pain disorder M1627K mutation in human Nav1.7 renders DRG neurons hyperexcitable. *Molecular pain* **4,** 37.

Dib-Hajj SD, Tyrrell L, Black JA & Waxman SG. (1998). NaN, a novel voltage-gated Na channel, is expressed preferentially in peripheral sensory neurons and down-regulated after axotomy. *Proc Natl Acad Sci U S A* **95,** 8963-8968.

Ding Y & Djamgoz MB. (2004). Serum concentration modifies amplitude and kinetics of voltage-gated Na+ current in the Mat-LyLu cell line of rat prostate cancer. *Int J Biochem Cell Biol* **36,** 1249-1260.

Diss JK, Archer SN, Hirano J, Fraser SP & Djamgoz MB. (2001). Expression profiles of voltage-gated Na(+) channel alpha-subunit genes in rat and human prostate cancer cell lines. *Prostate* **48,** 165-178.

Diss JK, Stewart D, Pani F, Foster CS, Walker MM, Patel A & Djamgoz MB. (2005). A potential novel marker for human prostate cancer: voltage-gated sodium channel expression in vivo. *Prostate Cancer Prostatic Dis* **8,** 266-273.

Diss JKJ, Fraser SP, Walker MM, Patel A, Latchman DS & Djamgoz MBA. (2008). Beta-subunits of voltage-gated sodium channels in human prostate cancer: quantitative in vitro and in vivo analyses of mRNA expression. *Prostate Cancer Prostatic Dis* **11,** 325-333.

Donnem T, Andersen S, Al-Shibli K, Al-Saad S, Busund LT & Bremnes RM. (2010). Prognostic impact of Notch ligands and receptors in nonsmall cell lung cancer: coexpression of Notch-1 and vascular endothelial growth factor-A predicts poor survival. *Cancer* **116,** 5676-5685.

Donoviel DB, Hadjantonakis AK, Ikeda M, Zheng H, Hyslop PS & Bernstein A. (1999). Mice lacking both presenilin genes exhibit early embryonic patterning defects. *Genes Dev* **13,** 2801-2810.

Du Y, Garden DP, Wang L, Zhorov BS & Dong K. (2011). Identification of new batrachotoxin-sensing residues in segment IIIS6 of the sodium channel. *J Biol Chem* **286,** 13151-13160.

Du Z, Li L, Sun W, Wang X, Zhang Y, Chen Z, Yuan M, Quan Z, Liu N, Hao Y, Li T, Wang J, Luo C & Wu X. (2018). HepaCAM inhibits the malignant behavior of castration-resistant prostate cancer cells by downregulating Notch signaling and PF-3084014 (a gamma-

secretase inhibitor) partly reverses the resistance of refractory prostate cancer to docetaxel and enzalutamide in vitro. *International journal of oncology* **53,** 99-112.

Dulsat G, Palomeras S, Cortada E, Riuro H, Brugada R & Verges M. (2017). Trafficking and localization to the plasma membrane of Nav 1.5 promoted by the beta2 subunit is defective due to a beta2 mutation associated with Brugada syndrome. *Biol Cell*.

Dustrude ET, Wilson SM, Ju W, Xiao Y & Khanna R. (2013). CRMP2 protein SUMOylation modulates NaV1.7 channel trafficking. *J Biol Chem* **288,** 24316-24331.

Eberhardt M, Nakajima J, Klinger AB, Neacsu C, Huhne K, O'Reilly AO, Kist AM, Lampe AK, Fischer K, Gibson J, Nau C, Winterpacht A & Lampert A. (2014). Inherited pain: sodium channel Nav1.7 A1632T mutation causes erythromelalgia due to a shift of fast inactivation. *J Biol Chem* **289,** 1971-1980.

Ebner HL, Blatzer M, Nawaz M & Krumschnabel G. (2007). Activation and nuclear translocation of ERK in response to ligand-dependent and -independent stimuli in liver and gill cells from rainbow trout. *The Journal of experimental biology* **210,** 1036-1045.

Ednie AR, Horton KK, Wu J & Bennett ES. (2013). Expression of the sialyltransferase, ST3Gal4, impacts cardiac voltage-gated sodium channel activity, refractory period and ventricular conduction. *Journal of molecular and cellular cardiology* **59,** 117-127.

Ehehalt R, Keller P, Haass C, Thiele C & Simons K. (2003). Amyloidogenic processing of the Alzheimer beta-amyloid precursor protein depends on lipid rafts. *J Cell Biol* **160,** 113-123.

Ellisen LW, Bird J, West DC, Soreng AL, Reynolds TC, Smith SD & Sklar J. (1991). TAN-1, the human homolog of the Drosophila notch gene, is broken by chromosomal translocations in T lymphoblastic neoplasms. *Cell* **66,** 649-661.

Esch FS, Keim PS, Beattie EC, Blacher RW, Culwell AR, Oltersdorf T, McClure D & Ward PJ. (1990). Cleavage of amyloid beta peptide during constitutive processing of its precursor. *Science (New York, NY)* **248,** 1122-1124.

Esfandi F, Ghafouri-Fard S, Oskooei VK & Taheri M. (2019). beta-Secretase 1 and its Naturally Occurring Anti-Sense RNA are Down-Regulated in Gastric Cancer. *Pathology oncology research : POR* **25,** 1627-1633.

Estacion M, Dib-Hajj SD, Benke PJ, Te Morsche RH, Eastman EM, Macala LJ, Drenth JP & Waxman SG. (2008). NaV1.7 gain-of-function mutations as a continuum: A1632E displays physiological changes associated with erythromelalgia and paroxysmal extreme pain disorder mutations and produces symptoms of both disorders. *J Neurosci* **28,** 11079-11088.

Eto K, Puzon-McLaughlin W, Sheppard D, Sehara-Fujisawa A, Zhang XP & Takada Y. (2000). RGD-independent binding of integrin alpha9beta1 to the ADAM-12 and -15 disintegrin domains mediates cell-cell interaction. *J Biol Chem* **275,** 34922-34930.

Fahmi AI, Patel M, Stevens EB, Fowden AL, John JE, 3rd, Lee K, Pinnock R, Morgan K, Jackson AP & Vandenberg JI. (2001). The sodium channel beta-subunit SCN3b modulates the kinetics of SCN5a and is expressed heterogeneously in sheep heart. *J Physiol* **537,** 693-700.

Farahani E, Patra HK, Jangamreddy JR, Rashedi I, Kawalec M, Rao Pariti RK, Batakis P & Wiechec E. (2014). Cell adhesion molecules and their relation to (cancer) cell stemness. *Carcinogenesis* **35,** 747-759.

Felsher DW & Bishop JM. (1999). Reversible tumorigenesis by MYC in hematopoietic lineages. *Molecular cell* **4,** 199-207.

Felts PA, Yokoyama S, Dib-Hajj S, Black JA & Waxman SG. (1997). Sodium channel alpha-subunit mRNAs I, II, III, NaG, Na6 and hNE (PN1): different expression patterns in developing rat nervous system. *Brain research Molecular brain research* **45,** 71-82.

Feng J, Wang J, Liu Q, Li J, Zhang Q, Zhuang Z, Yao X, Liu C, Li Y, Cao L, Li C, Gong L, Li D, Zhang Y & Gao H. (2019). DAPT, a gamma-Secretase Inhibitor, Suppresses Tumorigenesis, and Progression of Growth Hormone-Producing Adenomas by Targeting Notch Signaling. *Frontiers in oncology* **9,** 809.

Fertleman CR, Baker MD, Parker KA, Moffatt S, Elmslie FV, Abrahamsen B, Ostman J, Klugbauer N, Wood JN, Gardiner RM & Rees M. (2006). SCN9A mutations in paroxysmal extreme pain disorder: allelic variants underlie distinct channel defects and phenotypes. *Neuron* **52,** 767-774.

Fertleman CR, Ferrie CD, Aicardi J, Bednarek NA, Eeg-Olofsson O, Elmslie FV, Griesemer DA, Goutieres F, Kirkpatrick M, Malmros IN, Pollitzer M, Rossiter M, Roulet-Perez E, Schubert R, Smith VV, Testard H, Wong V & Stephenson JB. (2007). Paroxysmal extreme pain disorder (previously familial rectal pain syndrome). *Neurology* **69,** 586-595.

Fischer TZ & Waxman SG. (2010). Familial pain syndromes from mutations of the NaV1.7 sodium channel. *Annals of the New York Academy of Sciences* **1184,** 196-207.

Fotia AB, Ekberg J, Adams DJ, Cook DI, Poronnik P & Kumar S. (2004). Regulation of neuronal voltage-gated sodium channels by the ubiquitin-protein ligases Nedd4 and Nedd4-2. *J Biol Chem* **279,** 28930-28935.

Fox V, Gokhale PJ, Walsh JR, Matin M, Jones M & Andrews PW. (2008). Cell-cell signaling through NOTCH regulates human embryonic stem cell proliferation. *Stem cells (Dayton, Ohio)* **26,** 715-723.

Fraser SP, Diss JK, Chioni AM, Mycielska ME, Pan H, Yamaci RF, Pani F, Siwy Z, Krasowska M, Grzywna Z, Brackenbury WJ, Theodorou D, Koyuturk M, Kaya H, Battaloglu E, De Bella MT, Slade MJ, Tolhurst R, Palmieri C, Jiang J, Latchman DS, Coombes RC & Djamgoz MB. (2005). Voltage-gated sodium channel expression and potentiation of human breast cancer metastasis. *Clin Cancer Res* **11,** 5381-5389.

Fraser SP, Ozerlat-Gunduz I, Brackenbury WJ, Fitzgerald EM, Campbell TM, Coombes RC & Djamgoz MBA. (2014). Regulation of voltage-gated sodium channel expression in cancer: hormones, growth factors and auto-regulation. *Philos Trans R Soc Lond B Biol Sci* **369,** 20130105.

Fraser SP, Salvador V, Manning EA, Mizal J, Altun S, Raza M, Berridge RJ & Djamgoz MB. (2003). Contribution of functional voltage-gated Na+ channel expression to cell behaviors involved in the metastatic cascade in rat prostate cancer: I. Lateral motility. *J Cell Physiol* **195,** 479-487.

Freeman J, Crowley PD, Foley AG, Gallagher HC, Iwasaki M, Ma D & Buggy DJ. (2019). Effect of Perioperative Lidocaine, Propofol and Steroids on Pulmonary Metastasis in a Murine Model of Breast Cancer Surgery. *Cancers* **11**.

Gadadhar A, Marr R & Lazarov O. (2011). Presenilin-1 regulates neural progenitor cell differentiation in the adult brain. *J Neurosci* **31,** 2615-2623.

Gakhar-Koppole N, Hundeshagen P, Mandl C, Weyer SW, Allinquant B, Muller U & Ciccolini F. (2008). Activity requires soluble amyloid precursor protein alpha to promote neurite outgrowth in neural stem cell-derived neurons via activation of the MAPK pathway. *Eur J Neurosci* **28,** 871-882.

Gallo LI, Ghini AA, Piwien Pilipuk G & Galigniana MD. (2007). Differential recruitment of tetratricorpeptide repeat domain immunophilins to the mineralocorticoid receptor influences both heat-shock protein 90-dependent retrotransport and hormone-dependent transcriptional activity. *Biochemistry* **46,** 14044-14057.

Gao R, Shen Y, Cai J, Lei M & Wang Z. (2010). Expression of voltage-gated sodium channel alpha subunit in human ovarian cancer. *Oncology reports* **23,** 1293-1299.

Gardill BR, Rivera-Acevedo RE, Tung CC & Van Petegem F. (2019). Crystal structures of Ca(2+)-calmodulin bound to NaV C-terminal regions suggest role for EF-hand domain in binding and inactivation. *Proc Natl Acad Sci U S A*.

Garver TD, Ren Q, Tuvia S & Bennett V. (1997). Tyrosine phosphorylation at a site highly conserved in the L1 family of cell adhesion molecules abolishes ankyrin binding and increases lateral mobility of neurofascin. *J Cell Biol* **137,** 703-714.

Gasser A, Cheng X, Gilmore ES, Tyrrell L, Waxman SG & Dib-Hajj SD. (2010). Two Nedd4-binding motifs underlie modulation of sodium channel Nav1.6 by p38 MAPK. *J Biol Chem* **285,** 26149-26161.

Gautam V, D'Avanzo C, Hebisch M, Kovacs DM & Kim DY. (2014). BACE1 activity regulates cell surface contactin-2 levels. *Mol Neurodegener* **9,** 4.

Gavert N, Sheffer M, Raveh S, Spaderna S, Shtutman M, Brabletz T, Barany F, Paty P, Notterman D, Domany E & Ben-Ze'ev A. (2007). Expression of L1-CAM and ADAM10 in human colon cancer cells induces metastasis. *Cancer Res* **67,** 7703-7712.

Gellens ME, George AL, Jr., Chen LQ, Chahine M, Horn R, Barchi RL & Kallen RG. (1992). Primary structure and functional expression of the human cardiac tetrodotoxin-insensitive voltage-dependent sodium channel. *Proc Natl Acad Sci U S A* **89,** 554-558.

Gersbacher MT, Goodger ZV, Trutzel A, Bundschuh D, Nitsch RM & Konietzko U. (2013). Turnover of amyloid precursor protein family members determines their nuclear signaling capability. *PLoS One* **8,** e69363.

Gertsik N, Am Ende CW, Geoghegan KF, Nguyen C, Mukherjee P, Mente S, Seneviratne U, Johnson DS & Li YM. (2017). Mapping the Binding Site of BMS-708163 on gamma-Secretase with Cleavable Photoprobes. *Cell chemical biology* **24,** 3-8.

Giacomini A, Stagni F, Trazzi S, Guidi S, Emili M, Brigham E, Ciani E & Bartesaghi R. (2015). Inhibition of APP gamma-secretase restores Sonic Hedgehog signaling and neurogenesis in the Ts65Dn mouse model of Down syndrome. *Neurobiology of disease* **82,** 385-396.

Gianni D, Li A, Tesco G, McKay KM, Moore J, Raygor K, Rota M, Gwathmey JK, Dec GW, Aretz T, Leri A, Semigran MJ, Anversa P, Macgillivray TE, Tanzi RE & del Monte F. (2010). Protein aggregates and novel presenilin gene variants in idiopathic dilated cardiomyopathy. *Circulation* **121,** 1216-1226.

Giebeler N & Zigrino P. (2016). A Disintegrin and Metalloprotease (ADAM): Historical Overview of Their Functions. *Toxins* **8,** 122.

Gilchrist J, Das S, Van Petegem F & Bosmans F. (2013). Crystallographic insights into sodium-channel modulation by the beta4 subunit. *Proc Natl Acad Sci U S A* **110,** E5016-5024.

Gillet L, Roger S, Besson P, Lecaille F, Gore J, Bougnoux P, Lalmanach G & Le Guennec J-Y. (2009). Voltage-gated Sodium Channel Activity Promotes Cysteine Cathepsin-dependent Invasiveness and Colony Growth of Human Cancer Cells. *J Biol Chem* **284,** 8680-8691.

Glenner GG & Wong CW. (1984). Alzheimer's disease: initial report of the purification and characterization of a novel cerebrovascular amyloid protein. *Biochem Biophys Res Commun* **120,** 885-890.

Gokulan R & Halagowder D. (2014). Expression pattern of Notch intracellular domain (NICD) and Hes-1 in preneoplastic and neoplastic human oral squamous epithelium: their correlation with c-Myc, clinicopathological factors and prognosis in Oral cancer. *Medical oncology (Northwood, London, England)* **31,** 126.

Golde TE, Koo EH, Felsenstein KM, Osborne BA & Miele L. (2013). γ-Secretase inhibitors and modulators. *Biochim Biophys Acta* **1828,** 2898-2907.

Goldin AL. (2001). Resurgence of sodium channel research. *Annual review of physiology* **63,** 871-894.

Goldin AL, Snutch T, Lubbert H, Dowsett A, Marshall J, Auld V, Downey W, Fritz LC, Lester HA, Dunn R & et al. (1986). Messenger RNA coding for only the alpha subunit of the rat brain Na channel is sufficient for expression of functional channels in Xenopus oocytes. *Proc Natl Acad Sci U S A* **83,** 7503-7507.

Gong B, Rhodes KJ, Bekele-Arcuri Z & Trimmer JS. (1999). Type I and type II Na(+) channel alpha-subunit polypeptides exhibit distinct spatial and temporal patterning, and association with auxiliary subunits in rat brain. *The Journal of comparative neurology* **412,** 342-352.

Gong Y, Yang J, Wu W, Liu F, Su A, Li Z, Zhu J & Wei T. (2018). Preserved SCN4B expression is an independent indicator of favorable recurrence-free survival in classical papillary thyroid cancer. *PLoS One* **13,** e0197007.

Gonzalez-Gonzalez L, Gonzalez-Ramirez R, Flores A, Avelino-Cruz JE, Felix R & Monjaraz E. (2019). Epidermal Growth Factor Potentiates Migration of MDA-MB 231 Breast Cancer Cells by Increasing NaV1.5 Channel Expression. *Oncology***,** 1-10.

Gosling M, Harley SL, Turner RJ, Carey N & Powell JT. (1998). Human saphenous vein endothelial cells express a tetrodotoxin-resistant, voltage-gated sodium current. *J Biol Chem* **273,** 21084-21090.

Grabher C, von Boehmer H & Look AT. (2006). Notch 1 activation in the molecular pathogenesis of T-cell acute lymphoblastic leukaemia. *Nat Rev Cancer* **6,** 347-359.

Grieco TM, Malhotra JD, Chen C, Isom LL & Raman IM. (2005). Open-channel block by the cytoplasmic tail of sodium channel beta4 as a mechanism for resurgent sodium current. *Neuron* **45,** 233-244.

Grimes JA & Djamgoz MB. (1998). Electrophysiological characterization of voltage-gated Na+ current expressed in the highly metastatic Mat-LyLu cell line of rat prostate cancer. *J Cell Physiol* **175,** 50-58.

Gruninger-Leitch F, Schlatter D, Kung E, Nelbock P & Dobeli H. (2002). Substrate and inhibitor profile of BACE (beta-secretase) and comparison with other mammalian aspartic proteases. *J Biol Chem* **277,** 4687-4693.

Gu Y, Misonou H, Sato T, Dohmae N, Takio K & Ihara Y. (2001). Distinct intramembrane cleavage of the beta-amyloid precursor protein family resembling gamma-secretase-like cleavage of Notch. *J Biol Chem* **276,** 35235-35238.

Guidi S, Stagni F & Bartesaghi R. (2017). Targeting APP/AICD in Down syndrome. *Oncotarget*.

Gura Sadovsky R, Brielle S, Kaganovich D & England JL. (2017). Measurement of Rapid Protein Diffusion in the Cytoplasm by Photo-Converted Intensity Profile Expansion. *Cell Rep* **18,** 2795-2806.

Haapasalo A & Kovacs DM. (2011). The many substrates of presenilin/γ-secretase. *J Alzheimers Dis* **25,** 3-28.

Haass C, Koo EH, Mellon A, Hung AY & Selkoe DJ. (1992). Targeting of cell-surface beta-amyloid precursor protein to lysosomes: alternative processing into amyloid-bearing fragments. *Nature* **357,** 500-503.

Harris B, Pereira I & Parkin E. (2009). Targeting ADAM10 to lipid rafts in neuroblastoma SH-SY5Y cells impairs amyloidogenic processing of the amyloid precursor protein. *Brain Res* **1296,** 203-215.

Hartmann M, Parra LM, Ruschel A, Lindner C, Morrison H, Herrlich A & Herrlich P. (2015). Inside-out Regulation of Ectodomain Cleavage of Cluster-of-Differentiation-44 (CD44) and of Neuregulin-1 Requires Substrate Dimerization. *J Biol Chem* **290,** 17041-17054.

Hartshorne RP & Catterall WA. (1981). Purification of the saxitoxin receptor of the sodium channel from rat brain. *Proc Natl Acad Sci U S A* **78,** 4620-4624.

Hartshorne RP & Catterall WA. (1984). The sodium channel from rat brain. Purification and subunit composition. *J Biol Chem* **259,** 1667-1675.

Hartshorne RP, Keller BU, Talvenheimo JA, Catterall WA & Montal M. (1985). Functional reconstitution of the purified brain sodium channel in planar lipid bilayers. *Proc Natl Acad Sci U S A* **82,** 240-244.

Hartshorne RP, Messner DJ, Coppersmith JC & Catterall WA. (1982). The saxitoxin receptor of the sodium channel from rat brain. Evidence for two nonidentical beta subunits. *J Biol Chem* **257,** 13888-13891.

Haufe V, Camacho JA, Dumaine R, Gunther B, Bollensdorff C, von Banchet GS, Benndorf K & Zimmer T. (2005). Expression pattern of neuronal and skeletal muscle voltage-gated Na+ channels in the developing mouse heart. *J Physiol* **564,** 683-696.

Haworth AS & Brackenbury WJ. (2019). Emerging roles for multifunctional ion channel auxiliary subunits in cancer. *Cell calcium* **80,** 125-140.

He W, Young GT, Zhang B, Cox PJ, Cho LT, John S, Paciga SA, Wood LS, Danziger N, Scollen S & Vangjeli C. (2018). Functional confirmation that the R1488* variant in SCN9A results in complete loss-of-function of Nav1.7. *BMC medical genetics* **19,** 124.

Heinemann SH, Terlau H, Stuhmer W, Imoto K & Numa S. (1992). Calcium channel characteristics conferred on the sodium channel by single mutations. *Nature* **356,** 441-443.

Herms J, Anliker B, Heber S, Ring S, Fuhrmann M, Kretzschmar H, Sisodia S & Muller U. (2004). Cortical dysplasia resembling human type 2 lissencephaly in mice lacking all three APP family members. *Embo j* **23,** 4106-4115.

Hernandez-Plata E, Ortiz CS, Marquina-Castillo B, Medina-Martinez I, Alfaro A, Berumen J, Rivera M & Gomora JC. (2012). Overexpression of NaV 1.6 channels is associated with the invasion capacity of human cervical cancer. *Int J Cancer* **130,** 2013-2023.

Heron SE, Crossland KM, Andermann E, Phillips HA, Hall AJ, Bleasel A, Shevell M, Mercho S, Seni MH, Guiot MC, Mulley JC, Berkovic SF & Scheffer IE. (2002). Sodium-channel defects in benign familial neonatal-infantile seizures. *Lancet (London, England)* **360,** 851-852.

Hien YE, Montersino A, Castets F, Leterrier C, Filhol O, Vacher H & Dargent B. (2014). CK2 accumulation at the axon initial segment depends on sodium channel Nav1. *FEBS Lett* **588,** 3403-3408.

Hille B. (1968). Pharmacological modifications of the sodium channels of frog nerve. *The Journal of general physiology* **51,** 199-219.

Hille B. (1977). Local anesthetics: hydrophilic and hydrophobic pathways for the drug-receptor reaction. *The Journal of general physiology* **69,** 497-515.

Hodgkin AL & Huxley AF. (1952a). The components of membrane conductance in the giant axon of Loligo. *J Physiol* **116,** 473-496.

Hodgkin AL & Huxley AF. (1952b). Currents carried by sodium and potassium ions through the membrane of the giant axon of Loligo. *J Physiol* **116,** 449-472.

Hodgkin AL & Huxley AF. (1952c). The dual effect of membrane potential on sodium conductance in the giant axon of Loligo. *J Physiol* **116,** 497-506.

Hodgkin AL, Huxley AF & Katz B. (1952). Measurement of current-voltage relations in the membrane of the giant axon of Loligo. *J Physiol* **116,** 424-448.

Hodgkin AL & Katz B. (1949). The effect of sodium ions on the electrical activity of giant axon of the squid. *J Physiol* **108,** 37-77.

Hori K, Sen A & Artavanis-Tsakonas S. (2013). Notch signaling at a glance. *J Cell Sci* **126,** 2135-2140.

House CD, Vaske CJ, Schwartz AM, Obias V, Frank B, Luu T, Sarvazyan N, Irby R, Strausberg RL, Hales TG, Stuart JM & Lee NH. (2010). Voltage-gated Na+ channel SCN5A is a key regulator of a gene transcriptional network that controls colon cancer invasion. *Cancer Res* **70,** 6957-6967.

Hu D, Barajas-Martinez H, Medeiros-Domingo A, Crotti L, Veltmann C, Schimpf R, Urrutia J, Alday A, Casis O, Pfeiffer R, Burashnikov E, Caceres G, Tester DJ, Wolpert C, Borggrefe M, Schwartz P, Ackerman MJ & Antzelevitch C. (2012). A novel rare variant in SCN1Bb linked to Brugada syndrome and SIDS by combined modulation of Na(v)1.5 and K(v)4.3 channel currents. *Heart Rhythm* **9,** 760-769.

Hu T, Li SS, Lu MN, Zhang L, Chen B, Mao R, Mei R, Tan YX, Li S & Xiyang YB. (2019). Neuroprotection induced by Navbeta2knockdown in APP/PS1 transgenic neurons is associated with NEP regulation. *Molecular medicine reports*.

Hu T, Xiao Z, Mao R, Chen B, Lu MN, Tong J, Mei R, Li SS, Xiao ZC, Zhang LF & Xiyang YB. (2017). Navbeta2 knockdown improves cognition in APP/PS1 mice by partially inhibiting seizures and APP amyloid processing. *Oncotarget* **8,** 99284-99295.

Huang J, Han C, Estacion M, Vasylyev D, Hoeijmakers JG, Gerrits MM, Tyrrell L, Lauria G, Faber CG, Dib-Hajj SD, Merkies IS & Waxman SG. (2014). Gain-of-function mutations in sodium channel Na(v)1.9 in painful neuropathy. *Brain : a journal of neurology* **137,** 1627-1642.

Huang J, Vanoye CG, Cutts A, Goldberg YP, Dib-Hajj SD, Cohen CJ, Waxman SG & George AL, Jr. (2017). Sodium channel NaV1.9 mutations associated with insensitivity to pain dampen neuronal excitability. *The Journal of clinical investigation* **127,** 2805-2814.

Hudmon A, Choi JS, Tyrrell L, Black JA, Rush AM, Waxman SG & Dib-Hajj SD. (2008). Phosphorylation of sodium channel Na(v)1.8 by p38 mitogen-activated protein kinase increases current density in dorsal root ganglion neurons. *J Neurosci* **28,** 3190-3201.

Huse JT, Pijak DS, Leslie GJ, Lee VM & Doms RW. (2000). Maturation and endosomal targeting of beta-site amyloid precursor protein-cleaving enzyme. The Alzheimer's disease beta-secretase. *J Biol Chem* **275,** 33729-33737.

Huth T, Rittger A, Saftig P & Alzheimer C. (2011). beta-Site APP-cleaving enzyme 1 (BACE1) cleaves cerebellar Na+ channel beta4-subunit and promotes Purkinje cell firing by slowing the decay of resurgent Na+ current. *Pflugers Archiv : European journal of physiology* **461,** 355-371.

Inoue E, Deguchi-Tawarada M, Togawa A, Matsui C, Arita K, Katahira-Tayama S, Sato T, Yamauchi E, Oda Y & Takai Y. (2009). Synaptic activity prompts gamma-secretase-mediated cleavage of EphA4 and dendritic spine formation. *J Cell Biol* **185,** 551-564.

Iorns E, Drews-Elger K, Ward TM, Dean S, Clarke J, Berry D, El Ashry D & Lippman M. (2012). A new mouse model for the study of human breast cancer metastasis. *PLoS One* **7,** e47995.

Isbert S, Wagner K, Eggert S, Schweitzer A, Multhaup G, Weggen S, Kins S & Pietrzik CU. (2012). APP dimer formation is initiated in the endoplasmic reticulum and differs between APP isoforms. *Cell Mol Life Sci* **69,** 1353-1375.

Ishikawa T, Takahashi N, Ohno S, Sakurada H, Nakamura K, On YK, Park JE, Makiyama T, Horie M, Arimura T, Makita N & Kimura A. (2013). Novel SCN3B mutation associated with brugada syndrome affects intracellular trafficking and function of Nav1.5. *Circulation journal : official journal of the Japanese Circulation Society* **77,** 959-967.

Isom LL & Catterall WA. (1996). Na+ channel subunits and Ig domains. *Nature* **383,** 307-308.

Isom LL, De Jongh KS, Patton DE, Reber BF, Offord J, Charbonneau H, Walsh K, Goldin AL & Catterall WA. (1992). Primary structure and functional expression of the beta 1 subunit of the rat brain sodium channel. *Science (New York, NY)* **256,** 839-842.

Isom LL, Ragsdale DS, De Jongh KS, Westenbroek RE, Reber BF, Scheuer T & Catterall WA. (1995). Structure and function of the beta 2 subunit of brain sodium channels, a transmembrane glycoprotein with a CAM motif. *Cell* **83,** 433-442.

James TF, Nenov MN, Wildburger NC, Lichti CF, Luisi J, Vergara F, Panova-Electronova NI, Nilsson CL, Rudra JS, Green TA, Labate D & Laezza F. (2015). The Nav1.2 channel is regulated by GSK3. *Biochim Biophys Acta* **1850,** 832-844.

Jansson K, Lynch J, Lepori-Bui N, Czymmek K, Duncan R & Sikes R. (2012). Overexpression of the VSSC-associated CAM, β-2, enhances LNCaP cell metastasis associated behavior. *The Prostate* **72,** 1080-1092.

Jansson KH, Castillo DG, Morris JW, Boggs ME, Czymmek KJ, Adams EL, Schramm LP & Sikes RA. (2014). Identification of beta-2 as a key cell adhesion molecule in PCa cell neurotropic behavior: a novel ex vivo and biophysical approach. *PLoS One* **9,** e98408.

Jeon YH, Ha M, Kim SW, Kim MJ, Lee CS, Oh CK, Han ME, Oh SO & Kim YH. (2019). Evaluation of the prognostic significances of gamma-secretase genes in pancreatic cancer. *Oncol Lett* **17,** 4614-4620.

Jiang L, Yu G, Meng W, Wang Z, Meng F & Ma W. (2013). Overexpression of amyloid precursor protein in acute myeloid leukemia enhances extramedullary infiltration by MMP-2. *Tumour biology : the journal of the International Society for Oncodevelopmental Biology and Medicine* **34,** 629-636.

Jin J, Gao Y, Zhang J, Wang L, Wang B, Cao J, Shao Z & Wang Z. (2018). Incidence, pattern and prognosis of brain metastases in patients with metastatic triple negative breast cancer. *BMC Cancer* **18,** 446.

Joe EH & Angelides KJ. (1993). Clustering and mobility of voltage-dependent sodium channels during myelination. *J Neurosci* **13,** 2993-3005.

Johnson D, Montpetit ML, Stocker PJ & Bennett ES. (2004). The sialic acid component of the beta1 subunit modulates voltage-gated sodium channel function. *J Biol Chem* **279,** 44303-44310.

Jonsson T, Atwal JK, Steinberg S, Snaedal J, Jonsson PV, Bjornsson S, Stefansson H, Sulem P, Gudbjartsson D, Maloney J, Hoyte K, Gustafson A, Liu Y, Lu Y, Bhangale T, Graham RR, Huttenlocher J, Bjornsdottir G, Andreassen OA, Jonsson EG, Palotie A, Behrens TW, Magnusson OT, Kong A, Thorsteinsdottir U, Watts RJ & Stefansson K. (2012). A mutation in APP protects against Alzheimer's disease and age-related cognitive decline. *Nature* **488,** 96-99.

Jurisch-Yaksi N, Sannerud R & Annaert W. (2013). A fast growing spectrum of biological functions of gamma-secretase in development and disease. *Biochim Biophys Acta* **1828,** 2815-2827.

Kabata R, Okuda H, Noguchi A, Kondo D, Fujiwara M, Hata K, Kato Y, Ishikawa K, Tanaka M, Sekine Y, Hishikawa N, Mizukami T, Ito J, Akasaka M, Sakurai K, Yoshida T, Minoura H, Hayashi T, Inoshita K, Matsuyama M, Kinjo N, Cao Y, Inoue S, Kobayashi H, Harada KH, Youssefian S, Takahashi T & Koizumi A. (2018). Familial episodic limb pain in kindreds with novel Nav1.9 mutations. *PLoS One* **13,** e0208516.

Kakad PP, Penserga T, Davis BP, Henry B, Boerner J, Riso A, Pielage J & Godenschwege TA. (2018). An ankyrin-binding motif regulates nuclear levels of L1-type neuroglian and expression of the oncogene Myc in Drosophila neurons. *J Biol Chem* **293,** 17442-17453.

Kalstrup T & Blunck R. (2018). S4-S5 linker movement during activation and inactivation in voltage-gated K(+) channels. *Proc Natl Acad Sci U S A* **115,** E6751-e6759.

Kamiya K, Kaneda M, Sugawara T, Mazaki E, Okamura N, Montal M, Makita N, Tanaka M, Fukushima K, Fujiwara T, Inoue Y & Yamakawa K. (2004). A nonsense mutation of the sodium channel gene SCN2A in a patient with intractable epilepsy and mental decline. *J Neurosci* **24,** 2690-2698.

Kanellopoulos AH, Koenig J, Huang H, Pyrski M, Millet Q, Lolignier S, Morohashi T, Gossage SJ, Jay M, Linley JE, Baskozos G, Kessler BM, Cox JJ, Dolphin AC, Zufall F, Wood JN & Zhao J. (2018). Mapping protein interactions of sodium channel NaV1.7 using epitope-tagged gene-targeted mice. *Embo j*.

Kang J, Lemaire HG, Unterbeck A, Salbaum JM, Masters CL, Grzeschik KH, Multhaup G, Beyreuther K & Muller-Hill B. (1987). The precursor of Alzheimer's disease amyloid A4 protein resembles a cell-surface receptor. *Nature* **325,** 733-736.

Kaplan MR, Cho MH, Ullian EM, Isom LL, Levinson SR & Barres BA. (2001). Differential control of clustering of the sodium channels Na(v)1.2 and Na(v)1.6 at developing CNS nodes of Ranvier. *Neuron* **30,** 105-119.

Katz E, Stoler O, Scheller A, Khrapunsky Y, Goebbels S, Kirchhoff F, Gutnick MJ, Wolf F & Fleidervish IA. (2018). Role of sodium channel subtype in action potential generation by neocortical pyramidal neurons. *Proc Natl Acad Sci U S A* **115,** E7184-e7192.

Kayano T, Noda M, Flockerzi V, Takahashi H & Numa S. (1988). Primary structure of rat brain sodium channel III deduced from the cDNA sequence. *FEBS Lett* **228,** 187-194.

Kazarinova-Noyes K, Malhotra JD, McEwen DP, Mattei LN, Berglund EO, Ranscht B, Levinson SR, Schachner M, Shrager P, Isom LL & Xiao ZC. (2001). Contactin associates with Na+ channels and increases their functional expression. *J Neurosci* **21,** 7517-7525.

Kazen-Gillespie KA, Ragsdale DS, D'Andrea MR, Mattei LN, Rogers KE & Isom LL. (2000). Cloning, localization, and functional expression of sodium channel beta1A subunits. *J Biol Chem* **275,** 1079-1088.

Kellenberger S, West JW, Catterall WA & Scheuer T. (1997). Molecular analysis of potential hinge residues in the inactivation gate of brain type IIA Na+ channels. *The Journal of general physiology* **109,** 607-617.

Kiaris H, Politi K, Grimm LM, Szabolcs M, Fisher P, Efstratiadis A & Artavanis-Tsakonas S. (2004). Modulation of notch signaling elicits signature tumors and inhibits hras1-induced oncogenesis in the mouse mammary epithelium. *Am J Pathol* **165,** 695-705.

Kiefer H, Blume AJ & Kaback HR. (1980). Membrane potential changes during mitogenic stimulation of mouse spleen lymphocytes. *Proc Natl Acad Sci U S A* **77,** 2200-2204.

Kim DY, Carey BW, Wang H, Ingano LAM, Binshtok AM, Wertz MH, Pettingell WH, He P, Lee VM-Y, Woolf CJ & Kovacs DM. (2007). BACE1 regulates voltage-gated sodium channels and neuronal activity. *Nat Cell Biol* **9,** 755-764.

Kim DY, Gersbacher MT, Inquimbert P & Kovacs DM. (2011). Reduced sodium channel Na(v)1.1 levels in BACE1-null mice. *J Biol Chem* **286,** 8106-8116.

Kim DY, Ingano LAM, Carey BW, Pettingell WH & Kovacs DM. (2005). Presenilin/gamma-secretase-mediated cleavage of the voltage-gated sodium channel beta2-subunit regulates cell adhesion and migration. *J Biol Chem* **280,** 23251-23261.

Kim DY, Wertz MH, Gautam V, D'Avanzo C, Bhattacharyya R & Kovacs DM. (2014). The E280A presenilin mutation reduces voltage-gated sodium channel levels in neuronal cells. *Neuro-degenerative diseases* **13,** 64-68.

Kimberly WT, Zheng JB, Guenette SY & Selkoe DJ. (2001). The intracellular domain of the beta-amyloid precursor protein is stabilized by Fe65 and translocates to the nucleus in a notch-like manner. *J Biol Chem* **276,** 40288-40292.

Kimura N, Nakamura SI, Honda T, Takashima A, Nakayama H, Ono F, Sakakibara I, Doi K, Kawamura S & Yoshikawa Y. (2001). Age-related changes in the localization of presenilin-1 in cynomolgus monkey brain. *Brain Res* **922,** 30-41.

Kleene R, Mzoughi M, Joshi G, Kalus I, Bormann U, Schulze C, Xiao M-F, Dityatev A & Schachner M. (2010). NCAM-induced neurite outgrowth depends on binding of calmodulin to NCAM and on nuclear import of NCAM and fak fragments. *J Neurosci* **30,** 10784-10798.

Knops J, Suomensaari S, Lee M, McConlogue L, Seubert P & Sinha S. (1995). Cell-type and amyloid precursor protein-type specific inhibition of A beta release by bafilomycin A1, a selective inhibitor of vacuolar ATPases. *J Biol Chem* **270,** 2419-2422.

Koh YH, von Arnim CA, Hyman BT, Tanzi RE & Tesco G. (2005). BACE is degraded via the lysosomal pathway. *J Biol Chem* **280,** 32499-32504.

Kohrman DC, Smith MR, Goldin AL, Harris J & Meisler MH. (1996). A missense mutation in the sodium channel Scn8a is responsible for cerebellar ataxia in the mouse mutant jolting. *J Neurosci* **16,** 5993-5999.

Kohutek ZA, diPierro CG, Redpath GT & Hussaini IM. (2009). ADAM-10-mediated N-cadherin cleavage is protein kinase C-alpha dependent and promotes glioblastoma cell migration. *J Neurosci* **29,** 4605-4615.

Kondratyev M, Kreso A, Hallett RM, Girgis-Gabardo A, Barcelon ME, Ilieva D, Ware C, Majumder PK & Hassell JA. (2012). Gamma-secretase inhibitors target tumor-initiating cells in a mouse model of ERBB2 breast cancer. *Oncogene* **31,** 93-103.

Kontis KJ, Rounaghi A & Goldin AL. (1997). Sodium channel activation gating is affected by substitutions of voltage sensor positive charges in all four domains. *The Journal of general physiology* **110,** 391-401.

Korner J, Meents J, Machtens JP & Lampert A. (2018). beta1 subunit stabilises sodium channel Nav1.7 against mechanical stress. *J Physiol*.

Kovacs DM, Gersbacher MT & Kim DY. (2010). Alzheimer's secretases regulate voltage-gated sodium channels. *Neurosci Lett* **486,** 68-72.

Kowalski PJ, Rubin MA & Kleer CG. (2003). E-cadherin expression in primary carcinomas of the breast and its distant metastases. *Breast Cancer Res* **5,** R217-222.

Krafte DS, Goldin AL, Auld VJ, Dunn RJ, Davidson N & Lester HA. (1990). Inactivation of cloned Na channels expressed in Xenopus oocytes. *The Journal of general physiology* **96,** 689-706.

Kruger LC, O'Malley HA, Hull JM, Kleeman A, Patino GA & Isom LL. (2016). beta1-C121W Is Down But Not Out: Epilepsy-Associated Scn1b-C121W Results in a Deleterious Gain-of-Function. *J Neurosci* **36,** 6213-6224.

Kubota T, Correa AM & Bezanilla F. (2017). Mechanism of functional interaction between potassium channel Kv1.3 and sodium channel NavBeta1 subunit. *Sci Rep* **7,** 45310.

Kuhn FJ & Greeff NG. (1999). Movement of voltage sensor S4 in domain 4 is tightly coupled to sodium channel fast inactivation and gating charge immobilization. *The Journal of general physiology* **114,** 167-183.

Kummar S, O'Sullivan Coyne G, Do KT, Turkbey B, Meltzer PS, Polley E, Choyke PL, Meehan R, Vilimas R, Horneffer Y, Juwara L, Lih A, Choudhary A, Mitchell SA, Helman LJ, Doroshow JH & Chen AP. (2017). Clinical Activity of the gamma-Secretase Inhibitor PF-03084014 in Adults With Desmoid Tumors (Aggressive Fibromatosis). *Journal of clinical oncology : official journal of the American Society of Clinical Oncology* **35,** 1561-1569.

Kusumi A, Sako Y & Yamamoto M. (1993). Confined lateral diffusion of membrane receptors as studied by single particle tracking (nanovid microscopy). Effects of calcium-induced differentiation in cultured epithelial cells. *Biophys J* **65,** 2021-2040.

Laedermann CJ, Syam N, Pertin M, Decosterd I & Abriel H. (2013). beta1- and beta3- voltage-gated sodium channel subunits modulate cell surface expression and glycosylation of Nav1.7 in HEK293 cells. *Frontiers in cellular neuroscience* **7,** 137.

Laird FM, Cai H, Savonenko AV, Farah MH, He K, Melnikova T, Wen H, Chiang HC, Xu G, Koliatsos VE, Borchelt DR, Price DL, Lee HK & Wong PC. (2005). BACE1, a major determinant of selective vulnerability of the brain to amyloid-beta amyloidogenesis, is essential for cognitive, emotional, and synaptic functions. *J Neurosci* **25,** 11693-11709.

Laird JM, Souslova V, Wood JN & Cervero F. (2002). Deficits in visceral pain and referred hyperalgesia in Nav1.8 (SNS/PN3)-null mice. *J Neurosci* **22,** 8352-8356.

Lammich S, Kojro E, Postina R, Gilbert S, Pfeiffer R, Jasionowski M, Haass C & Fahrenholz F. (1999). Constitutive and regulated alpha-secretase cleavage of Alzheimer's amyloid precursor protein by a disintegrin metalloprotease. *Proc Natl Acad Sci U S A* **96,** 3922-3927.

Landles C & Bates GP. (2004). Huntingtin and the molecular pathogenesis of Huntington's disease. Fourth in molecular medicine review series. *EMBO reports* **5,** 958-963.

Lassmann H. (2018). Multiple Sclerosis Pathology. *Cold Spring Harbor perspectives in medicine* **8**.

Lee A & Goldin AL. (2009). Role of the terminal domains in sodium channel localization. *Channels (Austin, Tex)* **3,** 171-180.

Lee HW, Kim SJ, Choi IJ, Song J & Chun KH. (2015a). Targeting Notch signaling by gamma-secretase inhibitor I enhances the cytotoxic effect of 5-FU in gastric cancer. *Clinical & experimental metastasis* **32,** 593-603.

Lee MK, Slunt HH, Martin LJ, Thinakaran G, Kim G, Gandy SE, Seeger M, Koo E, Price DL & Sisodia SS. (1996). Expression of presenilin 1 and 2 (PS1 and PS2) in human and murine tissues. *J Neurosci* **16,** 7513-7525.

Lee SM, Moon J, Redman BG, Chidiac T, Flaherty LE, Zha Y, Othus M, Ribas A, Sondak VK, Gajewski TF & Margolin KA. (2015b). Phase 2 study of RO4929097, a gamma-secretase inhibitor, in metastatic melanoma: SWOG 0933. *Cancer* **121,** 432-440.

Lena I & Mantegazza M. (2019). NaV1.2 haploinsufficiency in Scn2a knock-out mice causes an autistic-like phenotype attenuated with age. *Sci Rep* **9,** 12886.

Lerche H, Heine R, Pika U, George AL, Jr., Mitrovic N, Browatzki M, Weiss T, Rivet-Bastide M, Franke C, Lomonaco M & et al. (1993). Human sodium channel myotonia: slowed channel inactivation due to substitutions for a glycine within the III-IV linker. *J Physiol* **470,** 13-22.

Leslie TK, James AD, Zaccagna F, Grist JT, Deen S, Kennerley A, Riemer F, Kaggie JD, Gallagher FA, Gilbert FJ & Brackenbury WJ. (2019). Sodium homeostasis in the tumour microenvironment. *Biochimica et biophysica acta Reviews on cancer* **1872,** 188304.

Li J, Waterhouse RM & Zdobnov EM. (2011). A remarkably stable TipE gene cluster: evolution of insect Para sodium channel auxiliary subunits. *BMC evolutionary biology* **11,** 337.

Li M, West JW, Lai Y, Scheuer T & Catterall WA. (1992). Functional modulation of brain sodium channels by cAMP-dependent phosphorylation. *Neuron* **8,** 1151-1159.

Li M, West JW, Numann R, Murphy BJ, Scheuer T & Catterall WA. (1993). Convergent regulation of sodium channels by protein kinase C and cAMP-dependent protein kinase. *Science (New York, NY)* **261,** 1439-1442.

Li P, Lin X, Zhang JR, Li Y, Lu J, Huang FC, Zheng CH, Xie JW, Wang JB & Huang CM. (2016a). The expression of presenilin 1 enhances carcinogenesis and metastasis in gastric cancer. *Oncotarget* **7,** 10650-10662.

Li S, Wang X, Ma QH, Yang WL, Zhang XG, Dawe GS & Xiao ZC. (2016b). Amyloid precursor protein modulates Nav1.6 sodium channel currents through a Go-coupled JNK pathway. *Sci Rep* **6,** 39320.

Lichtenthaler SF. (2011). alpha-secretase in Alzheimer's disease: molecular identity, regulation and therapeutic potential. *J Neurochem* **116,** 10-21.

Lim S, Yoo BK, Kim HS, Gilmore HL, Lee Y, Lee HP, Kim SJ, Letterio J & Lee HG. (2014). Amyloid-beta precursor protein promotes cell proliferation and motility of advanced breast cancer. *BMC Cancer* **14,** 928.

Lin X, O'Malley H, Chen C, Auerbach D, Foster M, Shekhar A, Zhang M, Coetzee W, Jalife J, Fishman GI, Isom L & Delmar M. (2015). Scn1b deletion leads to increased tetrodotoxin-sensitive sodium current, altered intracellular calcium homeostasis and arrhythmias in murine hearts. *J Physiol* **593,** 1389-1407.

Linde N & Stick R. (2010). Intranuclear membranes induced by lipidated proteins are derived from the nuclear envelope. *Nucleus (Austin, Tex)* **1,** 343-353.

Lipkind GM & Fozzard HA. (2010). Molecular model of anticonvulsant drug binding to the voltage-gated sodium channel inner pore. *Molecular pharmacology* **78,** 631-638.

Liu Q, Jin Y, Wang K, Meng XX, Yang Y, Yang Z, Zhao YS, Zhao MY & Zhang JH. (2014). Study of the residues involved in the binding of beta1 to beta3 subunits in the sodium channel. *Comptes rendus biologies* **337,** 73-77.

Lo AC, Black JA & Waxman SG. (2002). Neuroprotection of axons with phenytoin in experimental allergic encephalomyelitis. *Neuroreport* **13,** 1909-1912.

Loechel F, Overgaard MT, Oxvig C, Albrechtsen R & Wewer UM. (1999). Regulation of human ADAM 12 protease by the prodomain. Evidence for a functional cysteine switch. *J Biol Chem* **274,** 13427-13433.

Lombet A & Lazdunski M. (1984). Characterization, solubilization, affinity labeling and purification of the cardiac Na+ channel using Tityus toxin gamma. *Eur J Biochem* **141,** 651-660.

Lopez-Charcas O, Espinosa AM, Alfaro A, Herrera-Carrillo Z, Ramirez-Cordero BE, Cortes-Reynosa P, Perez Salazar E, Berumen J & Gomora JC. (2018). The invasiveness of human cervical cancer associated to the function of NaV1.6 channels is mediated by MMP-2 activity. *Sci Rep* **8,** 12995.

Lopez-Santiago LF, Brackenbury WJ, Chen C & Isom LL. (2011). Na+ channel Scn1b gene regulates dorsal root ganglion nociceptor excitability in vivo. *J Biol Chem* **286,** 22913-22923.

Lopez-Santiago LF, Meadows LS, Ernst SJ, Chen C, Malhotra JD, McEwen DP, Speelman A, Noebels JL, Maier SK, Lopatin AN & Isom LL. (2007). Sodium channel Scn1b null mice exhibit prolonged QT and RR intervals. *Journal of molecular and cellular cardiology* **43,** 636-647.

Lorenzen A, Samosh J, Vandewark K, Anborgh PH, Seah C, Magalhaes AC, Cregan SP, Ferguson SS & Pasternak SH. (2010). Rapid and direct transport of cell surface APP to the lysosome defines a novel selective pathway. *Mol Brain* **3,** 11.

Lossin C, Rhodes TH, Desai RR, Vanoye CG, Wang D, Carniciu S, Devinsky O & George AL, Jr. (2003). Epilepsy-associated dysfunction in the voltage-gated neuronal sodium channel SCN1A. *J Neurosci* **23,** 11289-11295.

Lossin C, Wang DW, Rhodes TH, Vanoye CG & George AL, Jr. (2002). Molecular basis of an inherited epilepsy. *Neuron* **34,** 877-884.

Lowell S, Benchoua A, Heavey B & Smith AG. (2006). Notch promotes neural lineage entry by pluripotent embryonic stem cells. *PLoS Biol* **4,** e121.

Lu CM, Han J, Rado TA & Brown GB. (1992). Differential expression of two sodium channel subtypes in human brain. *FEBS Lett* **303,** 53-58.

Lu Y, Yu W, Xi Z, Xiao Z, Kou X & Wang XF. (2010). Mutational analysis of SCN2B, SCN3B and SCN4B in a large Chinese Han family with generalized tonic-clonic seizure. *Neurological sciences : official journal of the Italian Neurological Society and of the Italian Society of Clinical Neurophysiology* **31,** 675-677.

Lusk CP, Blobel G & King MC. (2007). Highway to the inner nuclear membrane: rules for the road. *Nat Rev Mol Cell Biol* **8,** 414-420.

Maekawa K, Saito Y, Ozawa S, Adachi-Akahane S, Kawamoto M, Komamura K, Shimizu W, Ueno K, Kamakura S, Kamatani N, Kitakaze M & Sawada J. (2005). Genetic polymorphisms and haplotypes of the human cardiac sodium channel alpha subunit gene (SCN5A) in Japanese and their association with arrhythmia. *Annals of human genetics* **69,** 413-428.

Maetzel D, Denzel S, Mack B, Canis M, Went P, Benk M, Kieu C, Papior P, Baeuerle PA, Munz M & Gires O. (2009). Nuclear signalling by tumour-associated antigen EpCAM. *Nat Cell Biol* **11,** 162-171.

Maier SK, Westenbroek RE, McCormick KA, Curtis R, Scheuer T & Catterall WA. (2004). Distinct subcellular localization of different sodium channel alpha and beta subunits in single ventricular myocytes from mouse heart. *Circulation* **109,** 1421-1427.

Makita N, Bennett PB & George AL, Jr. (1996). Molecular determinants of beta 1 subunit-induced gating modulation in voltage-dependent Na+ channels. *J Neurosci* **16,** 7117-7127.

Makita N, Bennett PB, Jr. & George AL, Jr. (1994a). Voltage-gated Na+ channel beta 1 subunit mRNA expressed in adult human skeletal muscle, heart, and brain is encoded by a single gene. *J Biol Chem* **269,** 7571-7578.

Makita N, Sloan-Brown K, Weghuis DO, Ropers HH & George AL, Jr. (1994b). Genomic organization and chromosomal assignment of the human voltage-gated Na+ channel beta 1 subunit gene (SCN1B). *Genomics* **23,** 628-634.

Malhotra JD, Kazen-Gillespie K, Hortsch M & Isom LL. (2000). Sodium channel beta subunits mediate homophilic cell adhesion and recruit ankyrin to points of cell-cell contact. *J Biol Chem* **275,** 11383-11388.

Malhotra JD, Koopmann MC, Kazen-Gillespie KA, Fettman N, Hortsch M & Isom LL. (2002). Structural requirements for interaction of sodium channel beta 1 subunits with ankyrin. *J Biol Chem* **277,** 26681-26688.

Malhotra JD, Thyagarajan V, Chen C & Isom LL. (2004). Tyrosine-phosphorylated and nonphosphorylated sodium channel beta1 subunits are differentially localized in cardiac myocytes. *J Biol Chem* **279,** 40748-40754.

Maltsev VA, Kyle JW & Undrovinas A. (2009). Late Na+ current produced by human cardiac Na+ channel isoform Nav1.5 is modulated by its beta1 subunit. *The journal of physiological sciences : JPS* **59,** 217-225.

Malykhina AP, Lei Q, Erickson CS, Epstein ML, Saban MR, Davis CA & Saban R. (2012). VEGF induces sensory and motor peripheral plasticity, alters bladder function, and promotes visceral sensitivity. *BMC physiology* **12,** 15.

Mao L, Zhao ZL, Yu GT, Wu L, Deng WW, Li YC, Liu JF, Bu LL, Liu B, Kulkarni AB, Zhang WF, Zhang L & Sun ZJ. (2018). gamma-Secretase inhibitor reduces immunosuppressive cells and enhances tumour immunity in head and neck squamous cell carcinoma. *Int J Cancer* **142,** 999-1009.

Marchi M, Provitera V, Nolano M, Romano M, Maccora S, D'Amato I, Salvi E, Gerrits M, Santoro L & Lauria G. (2018). A novel SCN9A splicing mutation in a compound heterozygous girl with congenital insensitivity to pain, hyposmia and hypogeusia. *Journal of the peripheral nervous system : JPNS* **23,** 202-206.

Marionneau C, Carrasquillo Y, Norris AJ, Townsend RR, Isom LL, Link AJ & Nerbonne JM. (2012). The sodium channel accessory subunit Navbeta1 regulates neuronal excitability through modulation of repolarizing voltage-gated K(+) channels. *J Neurosci* **32,** 5716-5727.

Maschietto M, Girardi S, Dal Maschio M, Scorzeto M & Vassanelli S. (2013). Sodium channel beta2 subunit promotes filopodia-like processes and expansion of the dendritic tree in developing rat hippocampal neurons. *Frontiers in cellular neuroscience* **7,** 2.

Masters JR, Thomson JA, Daly-Burns B, Reid YA, Dirks WG, Packer P, Toji LH, Ohno T, Tanabe H, Arlett CF, Kelland LR, Harrison M, Virmani A, Ward TH, Ayres KL & Debenham PG. (2001). Short tandem repeat profiling provides an international reference standard for human cell lines. *Proc Natl Acad Sci U S A* **98,** 8012-8017.

Matsumoto M, Hiyama TY, Kuboyama K, Suzuki R, Fujikawa A & Noda M. (2015). Channel properties of Nax expressed in neurons. *PLoS One* **10,** e0126109.

Matsumura H, Nakano Y, Ochi H, Onohara Y, Sairaku A, Tokuyama T, Tomomori S, Motoda C, Amioka M, Hironobe N, Toshishige M, Takahashi S, Imai K, Sueda T, Chayama K & Kihara Y. (2017). H558R, a common SCN5A polymorphism, modifies the clinical phenotype of Brugada syndrome by modulating DNA methylation of SCN5A promoters. *Journal of biomedical science* **24,** 91.

Mattson MP, Cheng B, Culwell AR, Esch FS, Lieberburg I & Rydel RE. (1993). Evidence for excitoprotective and intraneuronal calcium-regulating roles for secreted forms of the beta-amyloid precursor protein. *Neuron* **10,** 243-254.

Mauthe M, Orhon I, Rocchi C, Zhou X, Luhr M, Hijlkema KJ, Coppes RP, Engedal N, Mari M & Reggiori F. (2018). Chloroquine inhibits autophagic flux by decreasing autophagosome-lysosome fusion. *Autophagy* **14,** 1435-1455.

McCormick KA, Isom LL, Ragsdale D, Smith D, Scheuer T & Catterall WA. (1998). Molecular determinants of Na+ channel function in the extracellular domain of the beta1 subunit. *J Biol Chem* **273,** 3954-3962.

McCormick KA, Srinivasan J, White K, Scheuer T & Catterall WA. (1999). The extracellular domain of the beta1 subunit is both necessary and sufficient for beta1-like modulation of sodium channel gating. *J Biol Chem* **274,** 32638-32646.

McCulloch DR, Akl P, Samaratunga H, Herington AC & Odorico DM. (2004). Expression of the disintegrin metalloprotease, ADAM-10, in prostate cancer and its regulation by dihydrotestosterone, insulin-like growth factor I, and epidermal growth factor in the prostate cancer cell model LNCaP. *Clin Cancer Res* **10,** 314-323.

McEwen DP, Chen C, Meadows LS, Lopez-Santiago L & Isom LL. (2009). The voltage-gated Na+ channel beta3 subunit does not mediate trans homophilic cell adhesion or associate with the cell adhesion molecule contactin. *Neurosci Lett* **462,** 272-275.

McEwen DP & Isom LL. (2004). Heterophilic interactions of sodium channel beta1 subunits with axonal and glial cell adhesion molecules. *J Biol Chem* **279,** 52744-52752.

McEwen DP, Meadows LS, Chen C, Thyagarajan V & Isom LL. (2004). Sodium channel beta1 subunit-mediated modulation of Nav1.2 currents and cell surface density is dependent on interactions with contactin and ankyrin. *J Biol Chem* **279,** 16044-16049.

McFarlane S, Coulter JA, Tibbits P, O'Grady A, McFarlane C, Montgomery N, Hill A, McCarthy HO, Young LS, Kay EW, Isacke CM & Waugh DJ. (2015). CD44 increases the efficiency of distant metastasis of breast cancer. *Oncotarget* **6,** 11465-11476.

McKinney BC, Chow CY, Meisler MH & Murphy GG. (2008). Exaggerated emotional behavior in mice heterozygous null for the sodium channel Scn8a (Nav1.6). *Genes, brain, and behavior* **7,** 629-638.

Meadows L, Malhotra JD, Stetzer A, Isom LL & Ragsdale DS. (2001). The intracellular segment of the sodium channel beta 1 subunit is required for its efficient association with the channel alpha subunit. *J Neurochem* **76,** 1871-1878.

Meadows LS, Malhotra J, Loukas A, Thyagarajan V, Kazen-Gillespie KA, Koopman MC, Kriegler S, Isom LL & Ragsdale DS. (2002). Functional and biochemical analysis of a sodium channel beta1 subunit mutation responsible for generalized epilepsy with febrile seizures plus type 1. *J Neurosci* **22,** 10699-10709.

Medeiros-Domingo A, Kaku T, Tester DJ, Iturralde-Torres P, Itty A, Ye B, Valdivia C, Ueda K, Canizales-Quinteros S, Tusie-Luna MT, Makielski JC & Ackerman MJ. (2007). SCN4B-encoded sodium channel beta4 subunit in congenital long-QT syndrome. *Circulation* **116,** 134-142.

Meisler MH & Kearney JA. (2005). Sodium channel mutations in epilepsy and other neurological disorders. *The Journal of clinical investigation* **115,** 2010-2017.

Merrick EC, Kalmar CL, Snyder SL, Cusdin FS, Yu EJ, Sando JJ, Isakson BE, Jackson AP & Patel MK. (2010). The importance of serine 161 in the sodium channel beta3 subunit for modulation of Na(V)1.2 gating. *Pflugers Archiv : European journal of physiology* **460,** 743-753.

Meyer AS, Hughes-Alford SK, Kay JE, Castillo A, Wells A, Gertler FB & Lauffenburger DA. (2012). 2D protrusion but not motility predicts growth factor-induced cancer cell migration in 3D collagen. *J Cell Biol* **197,** 721-729.

Mishra S, Undrovinas NA, Maltsev VA, Reznikov V, Sabbah HN & Undrovinas A. (2011). Post-transcriptional silencing of SCN1B and SCN2B genes modulates late sodium current in cardiac myocytes from normal dogs and dogs with chronic heart failure. *Am J Physiol Heart Circ Physiol* **301,** H1596-1605.

Miyazaki H, Oyama F, Wong HK, Kaneko K, Sakurai T, Tamaoka A & Nukina N. (2007). BACE1 modulates filopodia-like protrusions induced by sodium channel beta4 subunit. *Biochem Biophys Res Commun* **361,** 43-48.

Mohler PJ, Rivolta I, Napolitano C, LeMaillet G, Lambert S, Priori SG & Bennett V. (2004). Nav1.5 E1053K mutation causing Brugada syndrome blocks binding to ankyrin-G and expression of Nav1.5 on the surface of cardiomyocytes. *Proc Natl Acad Sci U S A* **101,** 17533-17538.

Mojica SA, Hovis KM, Frieman MB, Tran B, Hsia RC, Ravel J, Jenkins-Houk C, Wilson KL & Bavoil PM. (2015). SINC, a type III secreted protein of Chlamydia psittaci, targets the inner nuclear membrane of infected cells and uninfected neighbors. *Mol Biol Cell* **26,** 1918-1934.

Molinarolo S, Lee S, Leisle L, Lueck JD, Granata D, Carnevale V & Ahern CA. (2018). Cross-kingdom auxiliary subunit modulation of a voltage-gated sodium channel. *J Biol Chem* **293,** 4981-4992.

Morgan K, Stevens EB, Shah B, Cox PJ, Dixon AK, Lee K, Pinnock RD, Hughes J, Richardson PJ, Mizuguchi K & Jackson AP. (2000). beta 3: an additional auxiliary subunit of the voltage-sensitive sodium channel that modulates channel gating with distinct kinetics. *Proc Natl Acad Sci U S A* **97,** 2308-2313.

Morgan KM, Fischer BS, Lee FY, Shah JJ, Bertino JR, Rosenfeld J, Singh A, Khiabanian H & Pine SR. (2017). Gamma Secretase Inhibition by BMS-906024 Enhances Efficacy of Paclitaxel in Lung Adenocarcinoma. *Molecular cancer therapeutics* **16,** 2759-2769.

Morohashi Y, Kan T, Tominari Y, Fuwa H, Okamura Y, Watanabe N, Sato C, Natsugari H, Fukuyama T, Iwatsubo T & Tomita T. (2006). C-terminal fragment of presenilin is the molecular target of a dipeptidic gamma-secretase-specific inhibitor DAPT (N-[N-(3,5-difluorophenacetyl)-L-alanyl]-S-phenylglycine t-butyl ester). *J Biol Chem* **281,** 14670-14676.

Morris PG, Murphy CG, Mallam D, Accordino M, Patil S, Howard J, Omuro A, Beal K, Seidman AD, Hudis CA & Fornier MN. (2012). Limited overall survival in patients with brain metastases from triple negative breast cancer. *The breast journal* **18,** 345-350.

Muller P, Draguhn A & Egorov AV. (2018). Persistent sodium current modulates axonal excitability in CA1 pyramidal neurons. *J Neurochem* **146,** 446-458.

Mullooly M, McGowan PM, Kennedy SA, Madden SF, Crown J, O' Donovan N & Duffy MJ. (2015). ADAM10: a new player in breast cancer progression? *Br J Cancer* **113,** 945-951.

Mumm JS, Schroeter EH, Saxena MT, Griesemer A, Tian X, Pan DJ, Ray WJ & Kopan R. (2000). A ligand-induced extracellular cleavage regulates gamma-secretase-like proteolytic activation of Notch1. *Molecular cell* **5,** 197-206.

Murphy MP & LeVine H, 3rd. (2010). Alzheimer's disease and the amyloid-beta peptide. *J Alzheimers Dis* **19,** 311-323.

Murthy A, Shao YW, Narala SR, Molyneux SD, Zuniga-Pflucker JC & Khokha R. (2012). Notch activation by the metalloproteinase ADAM17 regulates myeloproliferation and atopic barrier immunity by suppressing epithelial cytokine synthesis. *Immunity* **36,** 105-119.

Musarella M, Alcaraz G, Caillol G, Boudier JL, Couraud F & Autillo-Touati A. (2006). Expression of Nav1.6 sodium channels by Schwann cells at neuromuscular junctions: role in the motor endplate disease phenotype. *Glia* **53,** 13-23.

Myers KA, Shevell MI & Sebire G. (2019). Sudden unexpected death in GEFS+ families with sodium channel pathogenic variants. *Epilepsy research* **150,** 66-69.

Nakajima M, Moriizumi E, Koseki H & Shirasawa T. (2004). Presenilin 1 is essential for cardiac morphogenesis. *Developmental dynamics : an official publication of the American Association of Anatomists* **230,** 795-799.

Nakajima T, Kaneko Y, Dharmawan T & Kurabayashi M. (2019). Role of the voltage sensor module in Nav domain on fast inactivation in sodium channelopathies: The implication of closed-state inactivation. *Channels (Austin, Tex)*.

Nakamura Y, Nakajima S & Grundfest H. (1965). The action of tetrodotoxin on electrogenic components of squid giant axons. *The Journal of general physiology* **48,** 975-996.

Namadurai S, Balasuriya D, Rajappa R, Wiemhöfer M, Stott K, Klingauf J, Edwardson JM, Chirgadze DY & Jackson AP. (2014). Crystal structure and molecular imaging of the Nav channel β3 subunit indicates a trimeric assembly. *J Biol Chem* **289,** 10797-10811.

Narahashi T, Moore JW & Scott WR. (1964). Tetrodotoxin blockage of sodium conductance increase in lobster giant axons. *The Journal of general physiology* **47,** 965-974.

Nassar MA, Stirling LC, Forlani G, Baker MD, Matthews EA, Dickenson AH & Wood JN. (2004). Nociceptor-specific gene deletion reveals a major role for Nav1.7 (PN1) in acute and inflammatory pain. *Proc Natl Acad Sci U S A* **101,** 12706-12711.

Nelson M, Millican-Slater R, Forrest LC & Brackenbury WJ. (2014). The sodium channel β1 subunit mediates outgrowth of neurite-like processes on breast cancer cells and promotes tumour growth and metastasis. *Int J Cancer* **135,** 2338-2351.

Nelson M, Yang M, Dowle AA, Thomas JR & Brackenbury WJ. (2015a). The sodium channel-blocking antiepileptic drug phenytoin inhibits breast tumour growth and metastasis. *Mol Cancer* **14,** 13.

Nelson M, Yang M, Millican-Slater R & Brackenbury WJ. (2015b). Nav1.5 regulates breast tumor growth and metastatic dissemination in vivo. *Oncotarget* **6,** 32914-32929.

Nemoto T, Yanagita T, Kanai T & Wada A. (2009). Drug development targeting the glycogen synthase kinase-3beta (GSK-3beta)-mediated signal transduction pathway: the role of GSK-3beta in the maintenance of steady-state levels of insulin receptor signaling molecules and Na(v)1.7 sodium channel in adrenal chromaffin cells. *Journal of pharmacological sciences* **109,** 157-161.

Nguyen HM, Miyazaki H, Hoshi N, Smith BJ, Nukina N, Goldin AL & Chandy KG. (2012). Modulation of voltage-gated K+ channels by the sodium channel beta1 subunit. *Proc Natl Acad Sci U S A* **109,** 18577-18582.

Nguyen PT, DeMarco KR, Vorobyov I, Clancy CE & Yarov-Yarovoy V. (2019). Structural basis for antiarrhythmic drug interactions with the human cardiac sodium channel. *Proc Natl Acad Sci U S A* **116,** 2945-2954.

Nikolaev A, McLaughlin T, O'Leary DD & Tessier-Lavigne M. (2009). APP binds DR6 to trigger axon pruning and neuron death via distinct caspases. *Nature* **457,** 981-989.

Noda M & Hiyama TY. (2015). The Na(x) Channel: What It Is and What It Does. *Neuroscientist* **21,** 399-412.

Noda M, Ikeda T, Kayano T, Suzuki H, Takeshima H, Kurasaki M, Takahashi H & Numa S. (1986). Existence of distinct sodium channel messenger RNAs in rat brain. *Nature* **320,** 188-192.

Noda M, Shimizu S, Tanabe T, Takai T, Kayano T, Ikeda T, Takahashi H, Nakayama H, Kanaoka Y, Minamino N & et al. (1984). Primary structure of Electrophorus electricus sodium channel deduced from cDNA sequence. *Nature* **312,** 121-127.

Nof E, Vysochek L, Meisel E, Burashnikov E, Antzelevitch C, Clatot J, Beinart R, Luria D, Glikson M & Oz S. (2019). Mutations in NaV1.5 Reveal Calcium-Calmodulin Regulation of Sodium Channel. *Front Physiol* **10,** 700.

Noursadeghi M, Tsang J, Haustein T, Miller RF, Chain BM & Katz DR. (2008). Quantitative imaging assay for NF-kappaB nuclear translocation in primary human macrophages. *Journal of immunological methods* **329,** 194-200.

Nutini M, Spalloni A, Florenzano F, Westenbroek RE, Marini C, Catterall WA, Bernardi G & Longone P. (2011). Increased expression of the beta3 subunit of voltage-gated Na+ channels in the spinal cord of the SOD1G93A mouse. *Mol Cell Neurosci* **47,** 108-118.

O'Malley HA, Hull JM, Clawson BC, Chen C, Owens-Fiestan G, Jameson MB, Aton SJ, Parent JM & Isom LL. (2019). Scn1b deletion in adult mice results in seizures and SUDEP. *Annals of clinical and translational neurology* **6,** 1121-1126.

O'Malley HA, Shreiner AB, Chen GH, Huffnagle GB & Isom LL. (2009). Loss of Na+ channel beta2 subunits is neuroprotective in a mouse model of multiple sclerosis. *Mol Cell Neurosci* **40,** 143-155.

Ogiwara I, Ito K, Sawaishi Y, Osaka H, Mazaki E, Inoue I, Montal M, Hashikawa T, Shike T, Fujiwara T, Inoue Y, Kaneda M & Yamakawa K. (2009). De novo mutations of voltage-gated sodium channel alphaII gene SCN2A in intractable epilepsies. *Neurology* **73,** 1046-1053.

Ogiwara I, Miyamoto H, Morita N, Atapour N, Mazaki E, Inoue I, Takeuchi T, Itohara S, Yanagawa Y, Obata K, Furuichi T, Hensch TK & Yamakawa K. (2007). Nav1.1 localizes to

axons of parvalbumin-positive inhibitory interneurons: a circuit basis for epileptic seizures in mice carrying an Scn1a gene mutation. *J Neurosci* **27,** 5903-5914.

Okamoto I, Kawano Y, Murakami D, Sasayama T, Araki N, Miki T, Wong AJ & Saya H. (2001). Proteolytic release of CD44 intracellular domain and its role in the CD44 signaling pathway. *J Cell Biol* **155,** 755-762.

Okamoto M. (2012). Immunoreactivity of the amino-terminal portion of the amyloid-beta precursor protein in the nucleolus. *Neurosci Lett* **521,** 82-87.

Olesen MS, Holst AG, Svendsen JH, Haunso S & Tfelt-Hansen J. (2012). SCN1Bb R214Q found in 3 patients: 1 with Brugada syndrome and 2 with lone atrial fibrillation. *Heart Rhythm* **9,** 770-773.

Onganer PU & Djamgoz MB. (2005). Small-cell lung cancer (human): potentiation of endocytic membrane activity by voltage-gated Na(+) channel expression in vitro. *The Journal of membrane biology* **204,** 67-75.

Onkal R, Mattis JH, Fraser SP, Diss JK, Shao D, Okuse K & Djamgoz MB. (2008). Alternative splicing of Nav1.5: an electrophysiological comparison of 'neonatal' and 'adult' isoforms and critical involvement of a lysine residue. *J Cell Physiol* **216,** 716-726.

Onwuli DO & Beltran-Alvarez P. (2016). An update on transcriptional and post-translational regulation of brain voltage-gated sodium channels. *Amino acids* **48,** 641-651.

Onwuli DO, Yanez-Bisbe L, Pinsach-Abuin M, Tarradas A, Brugada R, Greenman J, Pagans S & Beltran-Alvarez P. (2017). Do sodium channel proteolytic fragments regulate sodium channel expression? *Channels (Austin, Tex)***,** 0.

Oyama F, Miyazaki H, Sakamoto N, Becquet C, Machida Y, Kaneko K, Uchikawa C, Suzuki T, Kurosawa M, Ikeda T, Tamaoka A, Sakurai T & Nukina N. (2006). Sodium channel beta4 subunit: down-regulation and possible involvement in neuritic degeneration in Huntington's disease transgenic mice. *J Neurochem* **98,** 518-529.

Pablo JL, Wang C, Presby MM & Pitt GS. (2016). Polarized localization of voltage-gated Na+ channels is regulated by concerted FGF13 and FGF14 action. *Proc Natl Acad Sci U S A* **113,** E2665-2674.

Padmanaban V, Krol I, Suhail Y, Szczerba BM, Aceto N, Bader JS & Ewald AJ. (2019). E-cadherin is required for metastasis in multiple models of breast cancer. *Nature*.

Palomero T, Lim WK, Odom DT, Sulis ML, Real PJ, Margolin A, Barnes KC, O'Neil J, Neuberg D, Weng AP, Aster JC, Sigaux F, Soulier J, Look AT, Young RA, Califano A & Ferrando AA. (2006). NOTCH1 directly regulates c-MYC and activates a feed-forward-loop

transcriptional network promoting leukemic cell growth. *Proc Natl Acad Sci U S A* **103,** 18261-18266.

Palomero T, Sulis ML, Cortina M, Real PJ, Barnes K, Ciofani M, Caparros E, Buteau J, Brown K, Perkins SL, Bhagat G, Agarwal AM, Basso G, Castillo M, Nagase S, Cordon-Cardo C, Parsons R, Zuniga-Pflucker JC, Dominguez M & Ferrando AA. (2007). Mutational loss of PTEN induces resistance to NOTCH1 inhibition in T-cell leukemia. *Nature medicine* **13,** 1203-1210.

Pandey P, Sliker B, Peters HL, Tuli A, Herskovitz J, Smits K, Purohit A, Singh RK, Dong J, Batra SK, Coulter DW & Solheim JC. (2016). Amyloid precursor protein and amyloid precursor-like protein 2 in cancer. *Oncotarget* **7,** 19430-19444.

Pandis D & Scarmeas N. (2012). Seizures in Alzheimer disease: clinical and epidemiological data. *Epilepsy currents* **12,** 184-187.

Pant S, Jones SF, Kurkjian CD, Infante JR, Moore KN, Burris HA, McMeekin DS, Benhadji KA, Patel BKR, Frenzel MJ, Kursar JD, Zamek-Gliszczynski MJ, Yuen ESM, Chan EM & Bendell JC. (2016). A first-in-human phase I study of the oral Notch inhibitor, LY900009, in patients with advanced cancer. *Eur J Cancer* **56,** 1-9.

Papale LA, Paul KN, Sawyer NT, Manns JR, Tufik S & Escayg A. (2010). Dysfunction of the Scn8a voltage-gated sodium channel alters sleep architecture, reduces diurnal corticosterone levels, and enhances spatial memory. *J Biol Chem* **285,** 16553-16561.

Pardossi-Piquard R & Checler F. (2012). The physiology of the β-amyloid precursor protein intracellular domain AICD. *J Neurochem* **120 Suppl 1,** 109-124.

Pardossi-Piquard R, Petit A, Kawarai T, Sunyach C, Alves da Costa C, Vincent B, Ring S, D'Adamio L, Shen J, Muller U, St George Hyslop P & Checler F. (2005). Presenilin-dependent transcriptional control of the Abeta-degrading enzyme neprilysin by intracellular domains of betaAPP and APLP. *Neuron* **46,** 541-554.

Parenti N, Del Grosso A, Antoni C, Cecchini M, Corradetti R, Pavone FS & Calamai M. (2017). Direct imaging of APP proteolysis in living cells. *PeerJ* **5,** e3086.

Parkhurst CN, Zampieri N & Chao MV. (2010). Nuclear localization of the p75 neurotrophin receptor intracellular domain. *J Biol Chem* **285,** 5361-5368.

Parks AL, Klueg KM, Stout JR & Muskavitch MA. (2000). Ligand endocytosis drives receptor dissociation and activation in the Notch pathway. *Development (Cambridge, England)* **127,** 1373-1385.

Pasternak SH, Bagshaw RD, Guiral M, Zhang S, Ackerley CA, Pak BJ, Callahan JW & Mahuran DJ. (2003). Presenilin-1, nicastrin, amyloid precursor protein, and gamma-secretase activity are co-localized in the lysosomal membrane. *J Biol Chem* **278,** 26687-26694.

Patel F & Brackenbury WJ. (2015). Dual roles of voltage-gated sodium channels in development and cancer. *Int J Dev Biol*.

Patino GA, Brackenbury WJ, Bao Y, Lopez-Santiago LF, O'Malley HA, Chen C, Calhoun JD, Lafrenière RG, Cossette P, Rouleau GA & Isom LL. (2011). Voltage-gated Na+ channel β1B: a secreted cell adhesion molecule involved in human epilepsy. *J Neurosci* **31,** 14577-14591.

Patino GA, Claes LR, Lopez-Santiago LF, Slat EA, Dondeti RS, Chen C, O'Malley HA, Gray CB, Miyazaki H, Nukina N, Oyama F, De Jonghe P & Isom LL. (2009). A functional null mutation of SCN1B in a patient with Dravet syndrome. *J Neurosci* **29,** 10764-10778.

Payandeh J, Scheuer T, Zheng N & Catterall WA. (2011). The crystal structure of a voltage-gated sodium channel. *Nature* **475,** 353-358.

Peng J, Ou Q, Wu X, Zhang R, Zhao Q, Jiang W, Lu Z, Wan D, Pan Z & Fang Y. (2017). Expression of voltage-gated sodium channel Nav1.5 in non-metastatic colon cancer and its associations with estrogen receptor (ER)-beta expression and clinical outcomes. *Chinese journal of cancer* **36,** 89.

Perl AK, Wilgenbus P, Dahl U, Semb H & Christofori G. (1998). A causal role for E-cadherin in the transition from adenoma to carcinoma. *Nature* **392,** 190-193.

Pertin M, Ji RR, Berta T, Powell AJ, Karchewski L, Tate SN, Isom LL, Woolf CJ, Gilliard N, Spahn DR & Decosterd I. (2005). Upregulation of the voltage-gated sodium channel beta2 subunit in neuropathic pain models: characterization of expression in injured and non-injured primary sensory neurons. *J Neurosci* **25,** 10970-10980.

Phair RD, Gorski SA & Misteli T. (2004). Measurement of dynamic protein binding to chromatin in vivo, using photobleaching microscopy. *Methods Enzymol* **375,** 393-414.

Pieri M, Carunchio I, Curcio L, Mercuri NB & Zona C. (2009). Increased persistent sodium current determines cortical hyperexcitability in a genetic model of amyotrophic lateral sclerosis. *Experimental neurology* **215,** 368-379.

Plummer NW & Meisler MH. (1999). Evolution and diversity of mammalian sodium channel genes. *Genomics* **57,** 323-331.

Pocobelli G, Yu O, Ziebell RA, Aiello Bowles EJ, Fujii MM, Sterrett AT, Boggs JM, Chen L, Boudreau DM, Ritzwoller DP, Hubbard RA & Chubak J. (2019). Use of antidepressants after colon cancer diagnosis and risk of recurrence. *Psycho-oncology* **28,** 750-758.

Pragnell M, De Waard M, Mori Y, Tanabe T, Snutch TP & Campbell KP. (1994). Calcium channel beta-subunit binds to a conserved motif in the I-II cytoplasmic linker of the alpha 1-subunit. *Nature* **368,** 67-70.

Pryce KD, Powell R, Agwa D, Evely KM, Sheehan GD, Nip A, Tomasello DL, Gururaj S & Bhattacharjee A. (2019). Magi-1 scaffolds NaV1.8 and Slack KNa channels in dorsal root ganglion neurons regulating excitability and pain. *Faseb j* **33,** 7315-7330.

Qin N, D'Andrea MR, Lubin ML, Shafaee N, Codd EE & Correa AM. (2003). Molecular cloning and functional expression of the human sodium channel beta1B subunit, a novel splicing variant of the beta1 subunit. *Eur J Biochem* **270,** 4762-4770.

Qu Y, Curtis R, Lawson D, Gilbride K, Ge P, DiStefano PS, Silos-Santiago I, Catterall WA & Scheuer T. (2001). Differential modulation of sodium channel gating and persistent sodium currents by the beta1, beta2, and beta3 subunits. *Mol Cell Neurosci* **18,** 570-580.

Ran Y, Ladd GZ, Ceballos-Diaz C, Jung JI, Greenbaum D, Felsenstein KM & Golde TE. (2015). Differential Inhibition of Signal Peptide Peptidase Family Members by Established gamma-Secretase Inhibitors. *PLoS One* **10,** e0128619.

Ratcliffe CF, Qu Y, McCormick KA, Tibbs VC, Dixon JE, Scheuer T & Catterall WA. (2000). A sodium channel signaling complex: modulation by associated receptor protein tyrosine phosphatase beta. *Nat Neurosci* **3,** 437-444.

Ratcliffe CF, Westenbroek RE, Curtis R & Catterall WA. (2001). Sodium channel beta1 and beta3 subunits associate with neurofascin through their extracellular immunoglobulin-like domain. *J Cell Biol* **154,** 427-434.

Reedijk M, Odorcic S, Chang L, Zhang H, Miller N, McCready DR, Lockwood G & Egan SE. (2005). High-level coexpression of JAG1 and NOTCH1 is observed in human breast cancer and is associated with poor overall survival. *Cancer Res* **65,** 8530-8537.

Reinhard C, Borgers M, David G & De Strooper B. (2013). Soluble amyloid-beta precursor protein binds its cell surface receptor in a cooperative fashion with glypican and syndecan proteoglycans. *J Cell Sci* **126,** 4856-4861.

Remme CA & Bezzina CR. (2010). Sodium channel (dys)function and cardiac arrhythmias. *Cardiovascular therapeutics* **28,** 287-294.

Remme CA, Verkerk AO, Hoogaars WM, Aanhaanen WT, Scicluna BP, Annink C, van den Hoff MJ, Wilde AA, van Veen TA, Veldkamp MW, de Bakker JM, Christoffels VM & Bezzina CR. (2009). The cardiac sodium channel displays differential distribution in the conduction system and transmural heterogeneity in the murine ventricular myocardium. *Basic research in cardiology* **104,** 511-522.

Rice HC, de Malmazet D, Schreurs A, Frere S, Van Molle I, Volkov AN, Creemers E, Vertkin I, Nys J, Ranaivoson FM, Comoletti D, Savas JN, Remaut H, Balschun D, Wierda KD, Slutsky I, Farrow K, De Strooper B & de Wit J. (2019). Secreted amyloid-beta precursor protein functions as a GABABR1a ligand to modulate synaptic transmission. *Science (New York, NY)* **363**.

Riuro H, Beltran-Alvarez P, Tarradas A, Selga E, Campuzano O, Verges M, Pagans S, Iglesias A, Brugada J, Brugada P, Vazquez FM, Perez GJ, Scornik FS & Brugada R. (2013). A missense mutation in the sodium channel beta2 subunit reveals SCN2B as a new candidate gene for Brugada syndrome. *Human mutation* **34,** 961-966.

Riuro H, Campuzano O, Arbelo E, Iglesias A, Batlle M, Perez-Villa F, Brugada J, Perez GJ, Scornik FS & Brugada R. (2014). A missense mutation in the sodium channel beta1b subunit reveals SCN1B as a susceptibility gene underlying long QT syndrome. *Heart Rhythm* **11,** 1202-1209.

Rivolta I, Abriel H, Tateyama M, Liu H, Memmi M, Vardas P, Napolitano C, Priori SG & Kass RS. (2001). Inherited Brugada and long QT-3 syndrome mutations of a single residue of the cardiac sodium channel confer distinct channel and clinical phenotypes. *J Biol Chem* **276,** 30623-30630.

Roch JM, Masliah E, Roch-Levecq AC, Sundsmo MP, Otero DA, Veinbergs I & Saitoh T. (1994). Increase of synaptic density and memory retention by a peptide representing the trophic domain of the amyloid beta/A4 protein precursor. *Proc Natl Acad Sci U S A* **91,** 7450-7454.

Rofe AP, Davis LJ, Whittingham JL, Latimer-Bowman EC, Wilkinson AJ & Pryor PR. (2017). The Rhodococcus equi virulence protein VapA disrupts endolysosome function and stimulates lysosome biogenesis. *MicrobiologyOpen* **6**.

Roger S, Gillet L, Le Guennec J-Y & Besson P. (2015). Voltage-gated sodium channels and cancer: is excitability their primary role? *Front Pharmacol* **6,** 152.

Rogers JC, Qu Y, Tanada TN, Scheuer T & Catterall WA. (1996). Molecular determinants of high affinity binding of alpha-scorpion toxin and sea anemone toxin in the S3-S4 extracellular loop in domain IV of the Na+ channel alpha subunit. *J Biol Chem* **271,** 15950-15962.

Rougier JS, van Bemmelen MX, Bruce MC, Jespersen T, Gavillet B, Apotheloz F, Cordonier S, Staub O, Rotin D & Abriel H. (2005). Molecular determinants of voltage-gated sodium channel regulation by the Nedd4/Nedd4-like proteins. *American journal of physiology Cell physiology* **288,** C692-701.

Rubinstein M, Patowary A, Stanaway IB, McCord E, Nesbitt RR, Archer M, Scheuer T, Nickerson D, Raskind WH, Wijsman EM, Bernier R, Catterall WA & Brkanac Z. (2018). Association

of rare missense variants in the second intracellular loop of NaV1.7 sodium channels with familial autism. *Molecular psychiatry* **23,** 231-239.

Rush AM, Craner MJ, Kageyama T, Dib-Hajj SD, Waxman SG & Ranscht B. (2005). Contactin regulates the current density and axonal expression of tetrodotoxin-resistant but not tetrodotoxin-sensitive sodium channels in DRG neurons. *Eur J Neurosci* **22,** 39-49.

Sachan N, Mishra AK, Mutsuddi M & Mukherjee A. (2013). The Drosophila importin-alpha3 is required for nuclear import of notch in vivo and it displays synergistic effects with notch receptor on cell proliferation. *PLoS One* **8,** e68247.

Sakuta H, Nishihara E, Hiyama TY, Lin CH & Noda M. (2016). Nax signaling evoked by an increase in [Na+] in CSF induces water intake via EET-mediated TRPV4 activation. *American journal of physiology Regulatory, integrative and comparative physiology* **311,** R299-306.

Sanchez-Sandoval AL & Gomora JC. (2019). Contribution of voltage-gated sodium channel beta-subunits to cervical cancer cells metastatic behavior. *Cancer cell international* **19,** 35.

Sangameswaran L, Fish LM, Koch BD, Rabert DK, Delgado SG, Ilnicka M, Jakeman LB, Novakovic S, Wong K, Sze P, Tzoumaka E, Stewart GR, Herman RC, Chan H, Eglen RM & Hunter JC. (1997). A novel tetrodotoxin-sensitive, voltage-gated sodium channel expressed in rat and human dorsal root ganglia. *J Biol Chem* **272,** 14805-14809.

Sato C, Ueno Y, Asai K, Takahashi K, Sato M, Engel A & Fujiyoshi Y. (2001). The voltage-sensitive sodium channel is a bell-shaped molecule with several cavities. *Nature* **409,** 1047-1051.

Sato T, Ananda K, Cheng CI, Suh EJ, Narayanan S & Wolfe MS. (2008). Distinct pharmacological effects of inhibitors of signal peptide peptidase and gamma-secretase. *J Biol Chem* **283,** 33287-33295.

Schaller KL, Krzemien DM, Yarowsky PJ, Krueger BK & Caldwell JH. (1995). A novel, abundant sodium channel expressed in neurons and glia. *J Neurosci* **15,** 3231-3242.

Schattling B, Fazeli W, Engeland B, Liu Y, Lerche H, Isbrandt D & Friese MA. (2016). Activity of NaV1.2 promotes neurodegeneration in an animal model of multiple sclerosis. *JCI insight* **1,** e89810.

Scheuner D, Eckman C, Jensen M, Song X, Citron M, Suzuki N, Bird TD, Hardy J, Hutton M, Kukull W, Larson E, Levy-Lahad E, Viitanen M, Peskind E, Poorkaj P, Schellenberg G, Tanzi R, Wasco W, Lannfelt L, Selkoe D & Younkin S. (1996). Secreted amyloid beta-protein similar to that in the senile plaques of Alzheimer's disease is increased in vivo by the presenilin 1 and 2 and APP mutations linked to familial Alzheimer's disease. *Nature medicine* **2,** 864-870.

Schlachter K, Gruber-Sedlmayr U, Stogmann E, Lausecker M, Hotzy C, Balzar J, Schuh E, Baumgartner C, Mueller JC, Illig T, Wichmann HE, Lichtner P, Meitinger T, Strom TM, Zimprich A & Zimprich F. (2009). A splice site variant in the sodium channel gene SCN1A confers risk of febrile seizures. *Neurology* **72,** 974-978.

Schmadeka R, Harmon BE & Singh M. (2014). Triple-negative breast carcinoma: current and emerging concepts. *American journal of clinical pathology* **141,** 462-477.

Schmalhofer WA, Calhoun J, Burrows R, Bailey T, Kohler MG, Weinglass AB, Kaczorowski GJ, Garcia ML, Koltzenburg M & Priest BT. (2008). ProTx-II, a selective inhibitor of NaV1.7 sodium channels, blocks action potential propagation in nociceptors. *Molecular pharmacology* **74,** 1476-1484.

Schmidt J, Rossie S & Catterall WA. (1985). A large intracellular pool of inactive Na channel alpha subunits in developing rat brain. *Proc Natl Acad Sci U S A* **82,** 4847-4851.

Schmidt JW & Catterall WA. (1986). Biosynthesis and processing of the alpha subunit of the voltage-sensitive sodium channel in rat brain neurons. *Cell* **46,** 437-444.

Schmidt JW & Catterall WA. (1987). Palmitylation, sulfation, and glycosylation of the alpha subunit of the sodium channel. Role of post-translational modifications in channel assembly. *J Biol Chem* **262,** 13713-13723.

Schott AF, Landis MD, Dontu G, Griffith KA, Layman RM, Krop I, Paskett LA, Wong H, Dobrolecki LE, Lewis MT, Froehlich AM, Paranilam J, Hayes DF, Wicha MS & Chang JC. (2013). Preclinical and clinical studies of gamma secretase inhibitors with docetaxel on human breast tumors. *Clin Cancer Res* **19,** 1512-1524.

Schrey M, Codina C, Kraft R, Beetz C, Kalff R, Wolfl S & Patt S. (2002). Molecular characterization of voltage-gated sodium channels in human gliomas. *Neuroreport* **13,** 2493-2498.

Schroeter EH, Kisslinger JA & Kopan R. (1998). Notch-1 signalling requires ligand-induced proteolytic release of intracellular domain. *Nature* **393,** 382-386.

Schwab A, Fabian A, Hanley PJ & Stock C. (2012). Role of ion channels and transporters in cell migration. *Physiological reviews* **92,** 1865-1913.

Schwartz PJ, Stramba-Badiale M, Segantini A, Austoni P, Bosi G, Giorgetti R, Grancini F, Marni ED, Perticone F, Rosti D & Salice P. (1998). Prolongation of the QT interval and the sudden infant death syndrome. *The New England journal of medicine* **338,** 1709-1714.

Sehrawat A, Sakao K & Singh SV. (2014). Notch2 activation is protective against anticancer effects of zerumbone in human breast cancer cells. *Breast Cancer Res Treat* **146,** 543-555.

Senechal Y, Kelly PH & Dev KK. (2008). Amyloid precursor protein knockout mice show age-dependent deficits in passive avoidance learning. *Behavioural brain research* **186,** 126-132.

Sepult C, Bellefroid M, Rocks N, Donati K, Gerard C, Gilles C, Ludwig A, Duysinx B, Noel A & Cataldo D. (2019). ADAM10 mediates malignant pleural mesothelioma invasiveness. *Oncogene* **38,** 3521-3534.

Shah BS, Rush AM, Liu S, Tyrrell L, Black JA, Dib-Hajj SD & Waxman SG. (2004). Contactin associates with sodium channel Nav1.3 in native tissues and increases channel density at the cell surface. *J Neurosci* **24,** 7387-7399.

Shah BS, Stevens EB, Pinnock RD, Dixon AK & Lee K. (2001). Developmental expression of the novel voltage-gated sodium channel auxiliary subunit beta3, in rat CNS. *J Physiol* **534,** 763-776.

Sheets MF, Fozzard HA & Hanck DA. (2015). Important Role of Asparagines in Coupling the Pore and Votage-Sensor Domain in Voltage-Gated Sodium Channels. *Biophys J* **109,** 2277-2286.

Shen H, Liu D, Wu K, Lei J & Yan N. (2019). Structures of human Nav1.7 channel in complex with auxiliary subunits and animal toxins. *Science (New York, NY)*.

Shen H, Zhou Q, Pan X, Li Z, Wu J & Yan N. (2017). Structure of a eukaryotic voltage-gated sodium channel at near-atomic resolution. *Science (New York, NY)* **355**.

Shen J, Bronson RT, Chen DF, Xia W, Selkoe DJ & Tonegawa S. (1997). Skeletal and CNS defects in Presenilin-1-deficient mice. *Cell* **89,** 629-639.

Shi JM, Lv JM, Gao BX, Zhang L & Ji SR. (2019). Endosomal pH favors shedding of membrane-inserted amyloid-beta peptide. *Protein science : a publication of the Protein Society*.

Shi X, Yasumoto S, Kurahashi H, Nakagawa E, Fukasawa T, Uchiya S & Hirose S. (2012). Clinical spectrum of SCN2A mutations. *Brain & development* **34,** 541-545.

Shih YL, Chou HM, Chou HC, Lu HF, Chu YL, Shang HS & Chung JG. (2017). Casticin impairs cell migration and invasion of mouse melanoma B16F10 cells via PI3K/AKT and NF-kappaB signaling pathways. *Environmental toxicology*.

Shin W, Kweon H, Kang R, Kim D, Kim K, Kang M, Kim SY, Hwang SN, Kim JY, Yang E, Kim H & Kim E. (2019). Scn2a Haploinsufficiency in Mice Suppresses Hippocampal Neuronal Excitability, Excitatory Synaptic Drive, and Long-Term Potentiation, and Spatial Learning and Memory. *Frontiers in molecular neuroscience* **12,** 145.

Shorer Z, Wajsbrot E, Liran TH, Levy J & Parvari R. (2014). A novel mutation in SCN9A in a child with congenital insensitivity to pain. *Pediatric neurology* **50,** 73-76.

Shumakovich MA, Mencio CP, Siglin JS, Moriarty RA, Geller HM & Stroka KM. (2017). Astrocytes from the brain microenvironment alter migration and morphology of metastatic breast cancer cells. *Faseb j*.

Siegel RL, Miller KD & Jemal A. (2018). Cancer statistics, 2018. *CA: a cancer journal for clinicians* **68,** 7-30.

Smith MR & Goldin AL. (1999). A mutation that causes ataxia shifts the voltage-dependence of the Scn8a sodium channel. *Neuroreport* **10,** 3027-3031.

Smolarkiewicz M, Skrzypczak T & Wojtaszek P. (2013). The very many faces of presenilins and the gamma-secretase complex. *Protoplasma* **250,** 997-1011.

Soderholm JF, Bird SL, Kalab P, Sampathkumar Y, Hasegawa K, Uehara-Bingen M, Weis K & Heald R. (2011). Importazole, a small molecule inhibitor of the transport receptor importin-beta. *ACS chemical biology* **6,** 700-708.

Sokolov MV, Henrich-Noack P, Raynoschek C, Franzen B, Larsson O, Main M & Dabrowski M. (2018). Co-expression of beta Subunits with the Voltage-Gated Sodium Channel NaV1.7: the Importance of Subunit Association and Phosphorylation and Their Effects on Channel Pharmacology and Biophysics. *Journal of molecular neuroscience : MN*.

Sokolov S, Scheuer T & Catterall WA. (2008). Depolarization-activated gating pore current conducted by mutant sodium channels in potassium-sensitive normokalemic periodic paralysis. *Proc Natl Acad Sci U S A* **105,** 19980-19985.

Sorlie T, Perou CM, Tibshirani R, Aas T, Geisler S, Johnsen H, Hastie T, Eisen MB, van de Rijn M, Jeffrey SS, Thorsen T, Quist H, Matese JC, Brown PO, Botstein D, Lonning PE & Borresen-Dale AL. (2001). Gene expression patterns of breast carcinomas distinguish tumor subclasses with clinical implications. *Proc Natl Acad Sci U S A* **98,** 10869-10874.

Soule HD, Vazguez J, Long A, Albert S & Brennan M. (1973). A human cell line from a pleural effusion derived from a breast carcinoma. *Journal of the National Cancer Institute* **51,** 1409-1416.

Spampanato J, Kearney JA, de Haan G, McEwen DP, Escayg A, Aradi I, MacDonald BT, Levin SI, Soltesz I, Benna P, Montalenti E, Isom LL, Goldin AL & Meisler MH. (2004). A novel

epilepsy mutation in the sodium channel SCN1A identifies a cytoplasmic domain for beta subunit interaction. *J Neurosci* **24,** 10022-10034.

Spratt PWE, Ben-Shalom R, Keeshen CM, Burke KJ, Jr., Clarkson RL, Sanders SJ & Bender KJ. (2019). The Autism-Associated Gene Scn2a Contributes to Dendritic Excitability and Synaptic Function in the Prefrontal Cortex. *Neuron*.

Srinivasan J, Schachner M & Catterall WA. (1998). Interaction of voltage-gated sodium channels with the extracellular matrix molecules tenascin-C and tenascin-R. *Proc Natl Acad Sci U S A* **95,** 15753-15757.

Stafstrom CE. (2007). Persistent sodium current and its role in epilepsy. *Epilepsy currents* **7,** 15-22.

Stein RE, Kaplan JS, Li J & Catterall WA. (2019). Hippocampal deletion of NaV1.1 channels in mice causes thermal seizures and cognitive deficit characteristic of Dravet Syndrome. *Proc Natl Acad Sci U S A*.

Sternberg D, Maisonobe T, Jurkat-Rott K, Nicole S, Launay E, Chauveau D, Tabti N, Lehmann-Horn F, Hainque B & Fontaine B. (2001). Hypokalaemic periodic paralysis type 2 caused by mutations at codon 672 in the muscle sodium channel gene SCN4A. *Brain : a journal of neurology* **124,** 1091-1099.

Stevens M, Peigneur S & Tytgat J. (2011). Neurotoxins and their binding areas on voltage-gated sodium channels. *Front Pharmacol* **2,** 71.

Stoeck A, Lejnine S, Truong A, Pan L, Wang H, Zang C, Yuan J, Ware C, MacLean J, Garrett-Engele PW, Kluk M, Laskey J, Haines BB, Moskaluk C, Zawel L, Fawell S, Gilliland G, Zhang T, Kremer BE, Knoechel B, Bernstein BE, Pear WS, Liu XS, Aster JC & Sathyanarayanan S. (2014). Discovery of biomarkers predictive of GSI response in triple-negative breast cancer and adenoid cystic carcinoma. *Cancer discovery* **4,** 1154-1167.

Strege PR, Mercado-Perez A, Mazzone A, Saito YA, Bernard CE, Farrugia G & Beyder A. (2019). SCN5A mutation G615E results in NaV1.5 voltage-gated sodium channels with normal voltage-dependent function yet loss of mechanosensitivity. *Channels (Austin, Tex)* **13,** 287-298.

Strege PR, Ou Y, Sha L, Rich A, Gibbons SJ, Szurszewski JH, Sarr MG & Farrugia G. (2003). Sodium current in human intestinal interstitial cells of Cajal. *American journal of physiology Gastrointestinal and liver physiology* **285,** G1111-1121.

Strosberg JR, Yeatman T, Weber J, Coppola D, Schell MJ, Han G, Almhanna K, Kim R, Valone T, Jump H & Sullivan D. (2012). A phase II study of RO4929097 in metastatic colorectal cancer. *Eur J Cancer* **48,** 997-1003.

Struyk AF, Scoggan KA, Bulman DE & Cannon SC. (2000). The human skeletal muscle Na channel mutation R669H associated with hypokalemic periodic paralysis enhances slow inactivation. *J Neurosci* **20,** 8610-8617.

Strydom A, Coppus A, Blesa R, Danek A, Fortea J, Hardy J, Levin J, Nuebling G, Rebillat AS, Ritchie C, van Duijn C, Zaman S & Zetterberg H. (2018). Alzheimer's disease in Down syndrome: An overlooked population for prevention trials. *Alzheimer's & dementia (New York, N Y)* **4,** 703-713.

Stuhmer W, Conti F, Suzuki H, Wang XD, Noda M, Yahagi N, Kubo H & Numa S. (1989). Structural parts involved in activation and inactivation of the sodium channel. *Nature* **339,** 597-603.

Sundelacruz S, Levin M & Kaplan DL. (2009). Role of membrane potential in the regulation of cell proliferation and differentiation. *Stem cell reviews and reports* **5,** 231-246.

Sunn KL, Eisman JA, Gardiner EM & Jans DA. (2005). FRAP analysis of nucleocytoplasmic dynamics of the vitamin D receptor splice variant VDRB1: preferential targeting to nuclear speckles. *Biochem J* **388,** 509-514.

Suzuki K, Hayashi Y, Nakahara S, Kumazaki H, Prox J, Horiuchi K, Zeng M, Tanimura S, Nishiyama Y, Osawa S, Sehara-Fujisawa A, Saftig P, Yokoshima S, Fukuyama T, Matsuki N, Koyama R, Tomita T & Iwatsubo T. (2012). Activity-dependent proteolytic cleavage of neuroligin-1. *Neuron* **76,** 410-422.

Swaminathan R, Hoang CP & Verkman AS. (1997). Photobleaching recovery and anisotropy decay of green fluorescent protein GFP-S65T in solution and cells: cytoplasmic viscosity probed by green fluorescent protein translational and rotational diffusion. *Biophys J* **72,** 1900-1907.

Tabarean IV, Juranka P & Morris CE. (1999). Membrane stretch affects gating modes of a skeletal muscle sodium channel. *Biophys J* **77,** 758-774.

Tackenberg C & Nitsch RM. (2019). The secreted APP ectodomain sAPPalpha, but not sAPPbeta, protects neurons against Abeta oligomer-induced dendritic spine loss and increased tau phosphorylation. *Mol Brain* **12,** 27.

Talvenheimo JA, Tamkun MM & Catterall WA. (1982). Reconstitution of neurotoxin-stimulated sodium transport by the voltage-sensitive sodium channel purified from rat brain. *J Biol Chem* **257,** 11868-11871.

Tam JH & Pasternak SH. (2015). Imaging the Intracellular Trafficking of APP with Photoactivatable GFP. *Journal of visualized experiments : JoVE***,** e53153.

Tam JH, Seah C & Pasternak SH. (2014). The Amyloid Precursor Protein is rapidly transported from the Golgi apparatus to the lysosome and where it is processed into beta-amyloid. *Mol Brain* **7,** 54.

Tamkun MM, Talvenheimo JA & Catterall WA. (1984). The sodium channel from rat brain. Reconstitution of neurotoxin-activated ion flux and scorpion toxin binding from purified components. *J Biol Chem* **259,** 1676-1688.

Tan BH, Pundi KN, Van Norstrand DW, Valdivia CR, Tester DJ, Medeiros-Domingo A, Makielski JC & Ackerman MJ. (2010). Sudden infant death syndrome-associated mutations in the sodium channel beta subunits. *Heart Rhythm* **7,** 771-778.

Tan HL, Kupershmidt S, Zhang R, Stepanovic S, Roden DM, Wilde AA, Anderson ME & Balser JR. (2002). A calcium sensor in the sodium channel modulates cardiac excitability. *Nature* **415,** 442-447.

Tan JZA & Gleeson PA. (2019). The trans-Golgi network is a major site for alpha-secretase processing of amyloid precursor protein in primary neurons. *J Biol Chem* **294,** 1618-1631.

Tang CE, Guan YJ, Yi B, Li XH, Liang K, Zou HY, Yi H, Li MY, Zhang PF, Li C, Peng F, Chen ZC, Yao KT & Xiao ZQ. (2010). Identification of the amyloid beta-protein precursor and cystatin C as novel epidermal growth factor receptor regulated secretory proteins in nasopharyngeal carcinoma by proteomics. *Journal of proteome research* **9,** 6101-6111.

Telese F, Ma Q, Perez PM, Notani D, Oh S, Li W, Comoletti D, Ohgi KA, Taylor H & Rosenfeld MG. (2015). LRP8-Reelin-Regulated Neuronal Enhancer Signature Underlying Learning and Memory Formation. *Neuron* **86,** 696-710.

Terlau H, Heinemann SH, Stuhmer W, Pusch M, Conti F, Imoto K & Numa S. (1991). Mapping the site of block by tetrodotoxin and saxitoxin of sodium channel II. *FEBS Lett* **293,** 93-96.

Tikhonov DB & Zhorov BS. (2005). Sodium channel activators: model of binding inside the pore and a possible mechanism of action. *FEBS Lett* **579,** 4207-4212.

Tikhonov DB & Zhorov BS. (2017). Mechanism of sodium channel block by local anesthetics, antiarrhythmics, and anticonvulsants. *The Journal of general physiology* **149,** 465-481.

Timney BL, Raveh B, Mironska R, Trivedi JM, Kim SJ, Russel D, Wente SR, Sali A & Rout MP. (2016). Simple rules for passive diffusion through the nuclear pore complex. *J Cell Biol* **215,** 57-76.

Toh WH, Tan JZ, Zulkefli KL, Houghton FJ & Gleeson PA. (2017). Amyloid precursor protein traffics from the Golgi directly to early endosomes in an Arl5b- and AP4-dependent pathway. *Traffic* **18,** 159-175.

Tomita S, Kirino Y & Suzuki T. (1998). Cleavage of Alzheimer's amyloid precursor protein (APP) by secretases occurs after O-glycosylation of APP in the protein secretory pathway. Identification of intracellular compartments in which APP cleavage occurs without using toxic agents that interfere with protein metabolism. *J Biol Chem* **273,** 6277-6284.

Torre LA, Islami F, Siegel RL, Ward EM & Jemal A. (2017). Global Cancer in Women: Burden and Trends. *Cancer epidemiology, biomarkers & prevention : a publication of the American Association for Cancer Research, cosponsored by the American Society of Preventive Oncology* **26,** 444-457.

Tournoy J, Bossuyt X, Snellinx A, Regent M, Garmyn M, Serneels L, Saftig P, Craessaerts K, De Strooper B & Hartmann D. (2004). Partial loss of presenilins causes seborrheic keratosis and autoimmune disease in mice. *Human molecular genetics* **13,** 1321-1331.

Trainer VL, Baden DG & Catterall WA. (1994). Identification of peptide components of the brevetoxin receptor site of rat brain sodium channels. *J Biol Chem* **269,** 19904-19909.

Trazzi S, Mitrugno VM, Valli E, Fuchs C, Rizzi S, Guidi S, Perini G, Bartesaghi R & Ciani E. (2011). APP-dependent up-regulation of Ptch1 underlies proliferation impairment of neural precursors in Down syndrome. *Human molecular genetics* **20,** 1560-1573.

Trudeau MM, Dalton JC, Day JW, Ranum LP & Meisler MH. (2006). Heterozygosity for a protein truncation mutation of sodium channel SCN8A in a patient with cerebellar atrophy, ataxia, and mental retardation. *Journal of medical genetics* **43,** 527-530.

Tsang JYS, Lee MA, Chan TH, Li J, Ni YB, Shao Y, Chan SK, Cheungc SY, Lau KF & Tse GMK. (2018). Proteolytic cleavage of amyloid precursor protein by ADAM10 mediates proliferation and migration in breast cancer. *EBioMedicine* **38,** 89-99.

Tyrrell L, Renganathan M, Dib-Hajj SD & Waxman SG. (2001). Glycosylation alters steady-state inactivation of sodium channel Nav1.9/NaN in dorsal root ganglion neurons and is developmentally regulated. *J Neurosci* **21,** 9629-9637.

Undrovinas AI, Shander GS & Makielski JC. (1995). Cytoskeleton modulates gating of voltage-dependent sodium channel in heart. *The American journal of physiology* **269,** H203-214.

Vaccari T, Lu H, Kanwar R, Fortini ME & Bilder D. (2008). Endosomal entry regulates Notch receptor activation in Drosophila melanogaster. *J Cell Biol* **180,** 755-762.

Valdivia CR, Medeiros-Domingo A, Ye B, Shen WK, Algiers TJ, Ackerman MJ & Makielski JC. (2010). Loss-of-function mutation of the SCN3B-encoded sodium channel {beta}3 subunit associated with a case of idiopathic ventricular fibrillation. *Cardiovascular research* **86,** 392-400.

van Genderen PJ, Michiels JJ & Drenth JP. (1993). Hereditary erythermalgia and acquired erythromelalgia. *American journal of medical genetics* **45,** 530-532.

Van Wart A & Matthews G. (2006). Expression of sodium channels Nav1.2 and Nav1.6 during postnatal development of the retina. *Neurosci Lett* **403,** 315-317.

Vasquez-Del Carpio R, Kaplan FM, Weaver KL, VanWye JD, Alves-Guerra MC, Robbins DJ & Capobianco AJ. (2011). Assembly of a Notch transcriptional activation complex requires multimerization. *Molecular and cellular biology* **31,** 1396-1408.

Vassar R, Bennett BD, Babu-Khan S, Kahn S, Mendiaz EA, Denis P, Teplow DB, Ross S, Amarante P, Loeloff R, Luo Y, Fisher S, Fuller J, Edenson S, Lile J, Jarosinski MA, Biere AL, Curran E, Burgess T, Louis JC, Collins F, Treanor J, Rogers G & Citron M. (1999). Beta-secretase cleavage of Alzheimer's amyloid precursor protein by the transmembrane aspartic protease BACE. *Science (New York, NY)* **286,** 735-741.

Veeraraghavan R, Hoeker GS, Alvarez-Laviada A, Hoagland D, Wan X, King DR, Sanchez-Alonso J, Chen C, Jourdan J, Isom LL, Deschenes I, Smyth J, Gorelik J, Poelzing S & Gourdie RG. (2018). The adhesion function of the sodium channel beta subunit (beta1) contributes to cardiac action potential propagation. *eLife* **7**.

Venkataramani V, Rossner C, Iffland L, Schweyer S, Tamboli IY, Walter J, Wirths O & Bayer TA. (2010). Histone deacetylase inhibitor valproic acid inhibits cancer cell proliferation via down-regulation of the alzheimer amyloid precursor protein. *J Biol Chem* **285,** 10678-10689.

Venugopal C, Demos CM, Rao KS, Pappolla MA & Sambamurti K. (2008). Beta-secretase: structure, function, and evolution. *CNS & neurological disorders drug targets* **7,** 278-294.

Vetrivel KS, Cheng H, Lin W, Sakurai T, Li T, Nukina N, Wong PC, Xu H & Thinakaran G. (2004). Association of gamma-secretase with lipid rafts in post-Golgi and endosome membranes. *J Biol Chem* **279,** 44945-44954.

Villa JC, Chiu D, Brandes AH, Escorcia FE, Villa CH, Maguire WF, Hu CJ, de Stanchina E, Simon MC, Sisodia SS, Scheinberg DA & Li YM. (2014). Nontranscriptional role of Hif-1alpha in activation of gamma-secretase and notch signaling in breast cancer. *Cell Rep* **8,** 1077-1092.

Villalobos VM, Hall F, Jimeno A, Gore L, Kern K, Cesari R, Huang B, Schowinsky JT, Blatchford PJ, Hoffner B, Elias A & Messersmith W. (2018). Long-Term Follow-Up of Desmoid

Fibromatosis Treated with PF-03084014, an Oral Gamma Secretase Inhibitor. *Annals of surgical oncology* **25,** 768-775.

von Reyn CR, Spaethling JM, Mesfin MN, Ma M, Neumar RW, Smith DH, Siman R & Meaney DF. (2009). Calpain mediates proteolysis of the voltage-gated sodium channel alpha-subunit. *J Neurosci* **29,** 10350-10356.

von Rotz RC, Kohli BM, Bosset J, Meier M, Suzuki T, Nitsch RM & Konietzko U. (2004). The APP intracellular domain forms nuclear multiprotein complexes and regulates the transcription of its own precursor. *J Cell Sci* **117,** 4435-4448.

Vorobyeva AG, Lee R, Miller S, Longen C, Sharoni M, Kandelwal PJ, Kim FJ, Marenda DR & Saunders AJ. (2014). Cyclopamine modulates gamma-secretase-mediated cleavage of amyloid precursor protein by altering its subcellular trafficking and lysosomal degradation. *J Biol Chem* **289,** 33258-33274.

Vucic S, Nicholson GA & Kiernan MC. (2008). Cortical hyperexcitability may precede the onset of familial amyotrophic lateral sclerosis. *Brain : a journal of neurology* **131,** 1540-1550.

Vysokov N, McMahon SB & Raouf R. (2019). The role of NaV channels in synaptic transmission after axotomy in a microfluidic culture platform. *Sci Rep* **9,** 12915.

Walker AJ, Card T, Bates TE & Muir K. (2011). Tricyclic antidepressants and the incidence of certain cancers: a study using the GPRD. *Br J Cancer* **104,** 193-197.

Walker AJ, Grainge M, Bates TE & Card TR. (2012). Survival of glioma and colorectal cancer patients using tricyclic antidepressants post-diagnosis. *Cancer causes & control : CCC* **23,** 1959-1964.

Walkiewicz K, Nowakowska-Zajdel E, Strzelczyk J, Dziegielewska-Gesiak S & Muc-Wierzgon M. (2017). Serum levels of ADAM10, ADAM12, ADAM17 AND ADAM28 in colorectal cancer patients. *Journal of biological regulators and homeostatic agents* **31,** 929-934.

Wallace RH, Wang DW, Singh R, Scheffer IE, George AL, Jr., Phillips HA, Saar K, Reis A, Johnson EW, Sutherland GR, Berkovic SF & Mulley JC. (1998). Febrile seizures and generalized epilepsy associated with a mutation in the Na+-channel beta1 subunit gene SCN1B. *Nature genetics* **19,** 366-370.

Wang J, Ou SW, Bai YF, Wang YJ, Xu ZD & Luan GM. (2017). Multiple Nav1.5 isoforms are functionally expressed in the brain and present distinct expression patterns compared with cardiac Nav1.5. *Molecular medicine reports*.

Wang JZ, Rojas CV, Zhou JH, Schwartz LS, Nicholas H & Hoffman EP. (1992). Sequence and genomic structure of the human adult skeletal muscle sodium channel alpha subunit gene on 17q. *Biochem Biophys Res Commun* **182,** 794-801.

Wang R & Brattain MG. (2007). The maximal size of protein to diffuse through the nuclear pore is larger than 60kDa. *FEBS Lett* **581,** 3164-3170.

Wang Y, Zhang J, Li X, Ji J, Yang F, Wan C, Feng G, Wan P, He L & He G. (2008). SCN8A as a novel candidate gene associated with bipolar disorder in the Han Chinese population. *Progress in neuro-psychopharmacology & biological psychiatry* **32,** 1902-1904.

Wang Z, Lin Y, Liu W, Kuang P, Lao W, Ji Y & Zhu H. (2019). Voltage-Gated Sodium Channels Are Involved in Cognitive Impairments in Parkinson's Disease- like Rats. *Neuroscience*.

Wasserman D, Geijer T, Rozanov V & Wasserman J. (2005). Suicide attempt and basic mechanisms in neural conduction: relationships to the SCN8A and VAMP4 genes. *American journal of medical genetics Part B, Neuropsychiatric genetics : the official publication of the International Society of Psychiatric Genetics* **133b,** 116-119.

Watanabe E, Fujikawa A, Matsunaga H, Yasoshima Y, Sako N, Yamamoto T, Saegusa C & Noda M. (2000). Nav2/NaG channel is involved in control of salt-intake behavior in the CNS. *J Neurosci* **20,** 7743-7751.

Watanabe H, Darbar D, Kaiser DW, Jiramongkolchai K, Chopra S, Donahue BS, Kannankeril PJ & Roden DM. (2009). Mutations in sodium channel beta1- and beta2-subunits associated with atrial fibrillation. *Circulation Arrhythmia and electrophysiology* **2,** 268-275.

Watanabe H, Koopmann TT, Le Scouarnec S, Yang T, Ingram CR, Schott JJ, Demolombe S, Probst V, Anselme F, Escande D, Wiesfeld AC, Pfeufer A, Kaab S, Wichmann HE, Hasdemir C, Aizawa Y, Wilde AA, Roden DM & Bezzina CR. (2008). Sodium channel beta1 subunit mutations associated with Brugada syndrome and cardiac conduction disease in humans. *The Journal of clinical investigation* **118,** 2260-2268.

Wedekind H, Smits JP, Schulze-Bahr E, Arnold R, Veldkamp MW, Bajanowski T, Borggrefe M, Brinkmann B, Warnecke I, Funke H, Bhuiyan ZA, Wilde AA, Breithardt G & Haverkamp W. (2001). De novo mutation in the SCN5A gene associated with early onset of sudden infant death. *Circulation* **104,** 1158-1164.

Weiss LA, Escayg A, Kearney JA, Trudeau M, MacDonald BT, Mori M, Reichert J, Buxbaum JD & Meisler MH. (2003). Sodium channels SCN1A, SCN2A and SCN3A in familial autism. *Molecular psychiatry* **8,** 186-194.

Weng AP, Ferrando AA, Lee W, Morris JPt, Silverman LB, Sanchez-Irizarry C, Blacklow SC, Look AT & Aster JC. (2004). Activating mutations of NOTCH1 in human T cell acute lymphoblastic leukemia. *Science (New York, NY)* **306,** 269-271.

Weng AP, Millholland JM, Yashiro-Ohtani Y, Arcangeli ML, Lau A, Wai C, Del Bianco C, Rodriguez CG, Sai H, Tobias J, Li Y, Wolfe MS, Shachaf C, Felsher D, Blacklow SC, Pear

WS & Aster JC. (2006). c-Myc is an important direct target of Notch1 in T-cell acute lymphoblastic leukemia/lymphoma. *Genes Dev* **20,** 2096-2109.

West JW, Patton DE, Scheuer T, Wang Y, Goldin AL & Catterall WA. (1992). A cluster of hydrophobic amino acid residues required for fast Na(+)-channel inactivation. *Proc Natl Acad Sci U S A* **89,** 10910-10914.

Whitaker WR, Faull RL, Waldvogel HJ, Plumpton CJ, Emson PC & Clare JJ. (2001). Comparative distribution of voltage-gated sodium channel proteins in human brain. *Brain research Molecular brain research* **88,** 37-53.

Willem M, Tahirovic S, Busche MA, Ovsepian SV, Chafai M, Kootar S, Hornburg D, Evans LDB, Moore S, Daria A, Hampel H, Müller V, Giudici C, Nuscher B, Wenninger-Weinzierl A, Kremmer E, Heneka MT, Thal DR, Giedraitis V, Lannfelt L, Müller U, Livesey FJ, Meissner F, Herms J, Konnerth A, Marie H & Haass C. (2015). η-Secretase processing of APP inhibits neuronal activity in the hippocampus. *Nature* **526,** 443-447.

Williams KC, Cepeda MA, Javed S, Searle K, Parkins KM, Makela AV, Hamilton AM, Soukhtehzari S, Kim Y, Tuck AB, Ronald JA, Foster PJ, Chambers AF & Leong HS. (2019). Invadopodia are chemosensing protrusions that guide cancer cell extravasation to promote brain tropism in metastasis. *Oncogene*.

Wimmer VC, Reid CA, Mitchell S, Richards KL, Scaf BB, Leaw BT, Hill EL, Royeck M, Horstmann MT, Cromer BA, Davies PJ, Xu R, Lerche H, Berkovic SF, Beck H & Petrou S. (2010). Axon initial segment dysfunction in a mouse model of genetic epilepsy with febrile seizures plus. *The Journal of clinical investigation* **120,** 2661-2671.

Winters JJ & Isom LL. (2016). Developmental and Regulatory Functions of Na(+) Channel Non-pore-forming beta Subunits. *Current topics in membranes* **78,** 315-351.

Wisedchaisri G, Tonggu L, McCord E, Gamal El-Din TM, Wang L, Zheng N & Catterall WA. (2019). Resting-State Structure and Gating Mechanism of a Voltage-Gated Sodium Channel. *Cell*.

Wolfe MS, Xia W, Ostaszewski BL, Diehl TS, Kimberly WT & Selkoe DJ. (1999). Two transmembrane aspartates in presenilin-1 required for presenilin endoproteolysis and gamma-secretase activity. *Nature* **398,** 513-517.

Wong H-K, Sakurai T, Oyama F, Kaneko K, Wada K, Miyazaki H, Kurosawa M, De Strooper B, Saftig P & Nukina N. (2005). beta Subunits of voltage-gated sodium channels are novel substrates of beta-site amyloid precursor protein-cleaving enzyme (BACE1) and gamma-secretase. *J Biol Chem* **280,** 23009-23017.

Wong MH & Filbin MT. (1996). Dominant-negative effect on adhesion by myelin Po protein truncated in its cytoplasmic domain. *J Cell Biol* **134,** 1531-1541.

Woods NK & Padmanabhan J. (2013). Inhibition of amyloid precursor protein processing enhances gemcitabine-mediated cytotoxicity in pancreatic cancer cells. *J Biol Chem* **288,** 30114-30124.

Wu Y, Cain-Hom C, Choy L, Hagenbeek TJ, de Leon GP, Chen Y, Finkle D, Venook R, Wu X, Ridgway J, Schahin-Reed D, Dow GJ, Shelton A, Stawicki S, Watts RJ, Zhang J, Choy R, Howard P, Kadyk L, Yan M, Zha J, Callahan CA, Hymowitz SG & Siebel CW. (2010). Therapeutic antibody targeting of individual Notch receptors. *Nature* **464,** 1052-1057.

Xia W, Zhang J, Ostaszewski BL, Kimberly WT, Seubert P, Koo EH, Shen J & Selkoe DJ. (1998). Presenilin 1 regulates the processing of beta-amyloid precursor protein C-terminal fragments and the generation of amyloid beta-protein in endoplasmic reticulum and Golgi. *Biochemistry* **37,** 16465-16471.

Xiao Y, Barbosa C, Pei Z, Xie W, Strong JA, Zhang JM & Cummins TR. (2019). Increased Resurgent Sodium Currents in Nav1.8 Contribute to Nociceptive Sensory Neuron Hyperexcitability Associated with Peripheral Neuropathies. *J Neurosci* **39,** 1539-1550.

Xiao Y, Blumenthal K, Jackson JO, 2nd, Liang S & Cummins TR. (2010). The tarantula toxins ProTx-II and huwentoxin-IV differentially interact with human Nav1.7 voltage sensors to inhibit channel activation and inactivation. *Molecular pharmacology* **78,** 1124-1134.

Xiao ZC, Ragsdale DS, Malhotra JD, Mattei LN, Braun PE, Schachner M & Isom LL. (1999). Tenascin-R is a functional modulator of sodium channel beta subunits. *J Biol Chem* **274,** 26511-26517.

Xiong H, Yang Q, Zhang X, Wang P, Chen F, Liu Y, Wang P, Zhao Y, Li S, Huang Y, Chen S, Wang X, Zhang H, Yu D, Tan C, Fang C, Huang Y, Wu G, Wu Y, Cheng X, Liao Y, Zhang R, Yang Y, Ke T, Ren X, Li H, Tu X, Xia Y, Xu C, Chen Q & Wang QK. (2019). Significant association of rare variant p.Gly8Ser in cardiac sodium channel beta4-subunit SCN4B with atrial fibrillation. *Annals of human genetics*.

Xu H, Li T, Rohou A, Arthur CP, Tzakoniati F, Wong E, Estevez A, Kugel C, Franke Y, Chen J, Ciferri C, Hackos DH, Koth CM & Payandeh J. (2019). Structural Basis of Nav1.7 Inhibition by a Gating-Modifier Spider Toxin. *Cell*.

Xu TH, Yan Y, Kang Y, Jiang Y, Melcher K & Xu HE. (2016). Alzheimer's disease-associated mutations increase amyloid precursor protein resistance to gamma-secretase cleavage and the Abeta42/Abeta40 ratio. *Cell discovery* **2,** 16026.

Yaghoobi H, Azizi H, Banitalebi-Dehkordi M, Mohammad Rezaei F, Arsang-Jnag S, Taheri M & Ghafouri-Fard S. (2019). Beta-Secretase 1 (BACE1) Is Down-Regulated in Invasive Ductal Carcinoma of Breast. *Reports of biochemistry & molecular biology* **8,** 200-207.

Yamaci RF, Fraser SP, Battaloglu E, Kaya H, Erguler K, Foster CS & Djamgoz MBA. (2017). Neonatal Nav1.5 protein expression in normal adult human tissues and breast cancer. *Pathology, research and practice*.

Yan Z, Zhou Q, Wang L, Wu J, Zhao Y, Huang G, Peng W, Shen H, Lei J & Yan N. (2017). Structure of the Nav1.4-beta1 Complex from Electric Eel. *Cell* **170,** 470-482.e411.

Yanagita T, Satoh S, Uezono Y, Matsuo K, Nemoto T, Maruta T, Yoshikawa N, Iwakiri T, Minami K & Murakami M. (2011). Transcriptional up-regulation of cell surface Na V 1.7 sodium channels by insulin-like growth factor-1 via inhibition of glycogen synthase kinase-3beta in adrenal chromaffin cells: enhancement of 22Na+ influx, 45Ca2+ influx and catecholamine secretion. *Neuropharmacology* **61,** 1265-1274.

Yang EK, Alvira MR, Levitan ES & Takimoto K. (2001). Kvbeta subunits increase expression of Kv4.3 channels by interacting with their C termini. *J Biol Chem* **276,** 4839-4844.

Yang M & Brackenbury WJ. (2013). Membrane potential and cancer progression. *Front Physiol* **4,** 185.

Yang M, Kozminski DJ, Wold LA, Modak R, Calhoun JD, Isom LL & Brackenbury WJ. (2012). Therapeutic potential for phenytoin: targeting Na(v)1.5 sodium channels to reduce migration and invasion in metastatic breast cancer. *Breast Cancer Res Treat* **134,** 603-615.

Yang N, George AL, Jr. & Horn R. (1996). Molecular basis of charge movement in voltage-gated sodium channels. *Neuron* **16,** 113-122.

Yang Q, Xiong H, Xu C, Huang Y, Tu X, Wu G, Fu F, Wang Z, Wang L, Zhao Y, Li S, Huang Y, Wang C, Wang D, Yao Y, Wang F, Wang Y, Xue Y, Wang P, Chen Q, Pu J & Wang QK. (2019). Identification of rare variants in cardiac sodium channel beta4-subunit gene SCN4B associated with ventricular tachycardia. *Molecular genetics and genomics : MGG* **294,** 1059-1071.

Yang Y, Huang J, Mis MA, Estacion M, Macala L, Shah P, Schulman BR, Horton DB, Dib-Hajj SD & Waxman SG. (2016). Nav1.7-A1632G Mutation from a Family with Inherited Erythromelalgia: Enhanced Firing of Dorsal Root Ganglia Neurons Evoked by Thermal Stimuli. *J Neurosci* **36,** 7511-7522.

Yang Y, Wang Y, Li S, Xu Z, Li H, Ma L, Fan J, Bu D, Liu B, Fan Z, Wu G, Jin J, Ding B, Zhu X & Shen Y. (2004). Mutations in SCN9A, encoding a sodium channel alpha subunit, in patients with primary erythermalgia. *Journal of medical genetics* **41,** 171-174.

Yao H, Fan J, Cheng YJ, Chen XM, Ji CC, Liu LJ, Zheng ZH & Wu SH. (2018). SCN1Bbeta mutations that affect their association with Kv4.3 underlie early repolarization syndrome. *J Cell Mol Med* **22,** 5639-5647.

Yarov-Yarovoy V, DeCaen PG, Westenbroek RE, Pan CY, Scheuer T, Baker D & Catterall WA. (2012). Structural basis for gating charge movement in the voltage sensor of a sodium channel. *Proc Natl Acad Sci U S A* **109,** E93-102.

Ye B, Valdivia CR, Ackerman MJ & Makielski JC. (2003). A common human SCN5A polymorphism modifies expression of an arrhythmia causing mutation. *Physiological genomics* **12,** 187-193.

Yip D, Le MN, Chan JL, Lee JH, Mehnert JA, Yudd A, Kempf J, Shih WJ, Chen S & Goydos JS. (2009). A phase 0 trial of riluzole in patients with resectable stage III and IV melanoma. *Clin Cancer Res* **15,** 3896-3902.

Yoneyama T, Gorry M, Sobo-Vujanovic A, Lin Y, Vujanovic L, Gaither-Davis A, Moss ML, Miller MA, Griffith LG, Lauffenburger DA, Stabile LP, Herman J & Vujanovic NL. (2018). ADAM10 Sheddase Activity is a Potential Lung-Cancer Biomarker. *Journal of Cancer* **9,** 2559-2570.

Young-Pearse TL, Bai J, Chang R, Zheng JB, LoTurco JJ & Selkoe DJ. (2007). A critical function for beta-amyloid precursor protein in neuronal migration revealed by in utero RNA interference. *J Neurosci* **27,** 14459-14469.

Yu FH & Catterall WA. (2003). Overview of the voltage-gated sodium channel family. *Genome Biol* **4,** 207.

Yu FH, Mantegazza M, Westenbroek RE, Robbins CA, Kalume F, Burton KA, Spain WJ, McKnight GS, Scheuer T & Catterall WA. (2006). Reduced sodium current in GABAergic interneurons in a mouse model of severe myoclonic epilepsy in infancy. *Nat Neurosci* **9,** 1142-1149.

Yu FH, Westenbroek RE, Silos-Santiago I, McCormick KA, Lawson D, Ge P, Ferriera H, Lilly J, DiStefano PS, Catterall WA, Scheuer T & Curtis R. (2003). Sodium channel beta4, a new disulfide-linked auxiliary subunit with similarity to beta2. *J Neurosci* **23,** 7577-7585.

Zaklyazminskaya E & Dzemeshkevich S. (2016). The role of mutations in the SCN5A gene in cardiomyopathies. *Biochim Biophys Acta* **1863,** 1799-1805.

Zeng L, Deng X, Zhong J, Yuan L, Tao X, Zhang S, Zeng Y, He G, Tan P & Tao Y. (2019). Prognostic value of biomarkers EpCAM and alphaB-crystallin associated with lymphatic metastasis in breast cancer by iTRAQ analysis. *BMC Cancer* **19,** 831.

Zhang B, Deng Z, Zeng B, Yang S, Chen X, Xu X & Wu J. (2018a). In-vitro effects of the FS50 protein from salivary glands of Xenopsylla cheopis on voltage-gated sodium channel activity and motility of MDA-MB-231 human breast cancer cells. *Anti-cancer drugs* **29,** 880-889.

Zhang D, Zhou C, Li Y, Gao L, Pang Z, Yin G & Shi B. (2018b). Amyloid precursor protein is overexpressed in bladder cancer and contributes to the malignant bladder cancer cell behaviors. *International journal of urology : official journal of the Japanese Urological Association* **25,** 808-816.

Zhang J, Kang DE, Xia W, Okochi M, Mori H, Selkoe DJ & Koo EH. (1998). Subcellular distribution and turnover of presenilins in transfected cells. *J Biol Chem* **273,** 12436-12442.

Zhang LI & Poo MM. (2001). Electrical activity and development of neural circuits. *Nat Neurosci* **4 Suppl,** 1207-1214.

Zhang XY, Wen J, Yang W, Wang C, Gao L, Zheng LH, Wang T, Ran K, Li Y, Li X, Xu M, Luo J, Feng S, Ma X, Ma H, Chai Z, Zhou Z, Yao J, Zhang X & Liu JY. (2013). Gain-of-function mutations in SCN11A cause familial episodic pain. *American journal of human genetics* **93,** 957-966.

Zhang Z, Song M, Liu X, Su Kang S, Duong DM, Seyfried NT, Cao X, Cheng L, Sun YE, Ping Yu S, Jia J, Levey AI & Ye K. (2015). Delta-secretase cleaves amyloid precursor protein and regulates the pathogenesis in Alzheimer's disease. *Nat Commun* **6,** 8762.

Zhang ZN, Li Q, Liu C, Wang HB, Wang Q & Bao L. (2008). The voltage-gated Na+ channel Nav1.8 contains an ER-retention/retrieval signal antagonized by the beta3 subunit. *J Cell Sci* **121,** 3243-3252.

Zhao G, Mao G, Tan J, Dong Y, Cui MZ, Kim SH & Xu X. (2004). Identification of a new presenilin-dependent zeta-cleavage site within the transmembrane domain of amyloid precursor protein. *J Biol Chem* **279,** 50647-50650.

Zhao J, O'Leary ME & Chahine M. (2011). Regulation of Nav1.6 and Nav1.8 peripheral nerve Na+ channels by auxiliary beta-subunits. *Journal of neurophysiology* **106,** 608-619.

Zheng X, Jiang F, Katakowski M, Zhang ZG, Lu QE & Chopp M. (2009). ADAM17 promotes breast cancer cell malignant phenotype through EGFR-PI3K-AKT activation. *Cancer biology & therapy* **8,** 1045-1054.

Zhou D, Lambert S, Malen PL, Carpenter S, Boland LM & Bennett V. (1998). AnkyrinG is required for clustering of voltage-gated Na channels at axon initial segments and for normal action potential firing. *J Cell Biol* **143,** 1295-1304.

Zhou J, Shin HG, Yi J, Shen W, Williams CP & Murray KT. (2002). Phosphorylation and putative ER retention signals are required for protein kinase A-mediated potentiation of cardiac sodium current. *Circulation research* **91,** 540-546.

Zhou TT, Zhang ZW, Liu J, Zhang JP & Jiao BH. (2012). Glycosylation of the sodium channel beta4 subunit is developmentally regulated and involves in neuritic degeneration. *International journal of biological sciences* **8,** 630-639.

Zhou Y, Xia C, Yin M, Wang X, Wu H & Ji Y. (2019). Distribution and Functional Characteristics of Voltage-Gated Sodium Channels in Immature Cochlear Hair Cells. *Neuroscience bulletin*.

Zhu W, Voelker TL, Varga Z, Schubert AR, Nerbonne JM & Silva JR. (2017). Mechanisms of noncovalent beta subunit regulation of NaV channel gating. *The Journal of general physiology*.

Zubeldia-Brenner L, De Winne C, Perrone S, Rodriguez-Segui SA, Willems C, Ornstein AM, Lacau-Mengido I, Vankelecom H, Cristina C & Becu-Villalobos D. (2019). Inhibition of Notch signaling attenuates pituitary adenoma growth in Nude mice. *Endocrine-related cancer* **26,** 13-29.